

CE 383T

Plasticity in Structural Concrete

Class Notes
Research Report 1127-3F-Project 0-1127

Dr. John E. Breen
Spring 2008

The University of Texas at Austin
Department of Civil, Architectural and Environmental Engineering

CE 383T

Plasticity in Structural Concrete

Class Notes
Research Report 1127-3F – Project 0-1127

Dr. John E. Breen
Fall 2000

The University of Texas at Austin
Department of Civil Engineering

1. Report No. <i>FHW/TX-93+1127-3F</i>		2. Government Accession No.		3. Recipient's Catalog No.	
4. Title and Subtitle <i>DETAILING FOR STRUCTURAL CONCRETE</i>				5. Report Date <i>May 1993</i>	
				6. Performing Organization Code	
7. Author(s) <i>K. Bergmeister, J. E. Breen, J. O. Jirsa, and M. E. Kreger</i>				8. Performing Organization Report No. <i>Research Report 1127-3F</i>	
9. Performing Organization Name and Address <i>Center for Transportation Research The University of Texas at Austin 3208 Red River, Suite 200 Austin, Texas 78705-2650</i>				10. Work Unit No. (TRAIIS)	
				11. Contract or Grant No. <i>Research Study 3-5-87/9-1127</i>	
12. Sponsoring Agency Name and Address <i>Texas Department of Transportation Research and Technology Transfer Office P. O. Box 5080 Austin, Texas 78763-5080</i>				13. Type of Report and Period Covered <i>Final</i>	
				14. Sponsoring Agency Code	
15. Supplementary Notes <i>Study conducted in cooperation with the U.S. Department of Transportation, Federal Highway Administration. Research Study Title: "Reinforcement Detail Design in Structural Concrete"</i>					
16. Abstract <p><i>This report is the final report in a series which investigates the applications of strut-and-tie modelling for typical details in structural concrete bridges. It summarizes the state of the art of strut-and-tie modelling and presents specific recommendations for choosing the critical dimensions and carrying out detailed computations using such strut-and-tie models. Separate sections treat the overall modelling and detailing process, checking compression struts, detailing tension ties, evaluating TTT, CCC, CCT and CTT nodes, and incorporating prestressing forces. The report includes a series of examples showing application of strut-and-tie models in detailing deep beams, corbels, anchorage zones, dapped ends, openings, and pretensioned beams. In addition, a number of detailing aids are included in an appendix.</i></p>					
17. Key Words <i>strut-and-tie modelling, details, structural concrete bridges, critical dimensions, compression struts, tension ties, anchorage zones, beams, corbels</i>			18. Distribution Statement <i>No restrictions. This document is available to the public through the National Technical Information Service, Springfield, Virginia 22161.</i>		
19. Security Classif. (of this report) <i>Unclassified</i>		20. Security Classif. (of this page) <i>Unclassified</i>		21. No. of Pages <i>316</i>	22. Price

DETAILING IN STRUCTURAL CONCRETE

by

**K. Bergmeister
J. E. Breen
J. O. Jirsa
M. E. Kreger**

Research Report Number 1127-3F

Research Project 3-5-87/9-1127

"Reinforcement Detail Design in Structural Concrete"

conducted for the

Texas Department of Transportation

in cooperation with the

U.S. Department of Transportation
Federal Highway Administration

by the

CENTER FOR TRANSPORTATION RESEARCH
Bureau of Engineering Research
THE UNIVERSITY OF TEXAS AT AUSTIN

May 1993

Intentions of Paper

1. Explain details of Schlaich
2. Look for experimental verification
3. Present example problems
not based on current code provisions
(didn't exist at the time)

IMPLEMENTATION STATEMENT

This report provides detailed background, specific recommendations and comprehensive examples to illustrate applications of strut-and-tie models for detailing structural concrete. It outlines the basis for detailing complex and unusual structural applications and provides a practical way of extending results of sophisticated analyses (such as finite element results) to determining practical construction details. A series of specific recommendations are provided for determining node dimensions for typical node applications as well as determining limiting node stresses considering confinement present. The report is aimed at improving the ability of design engineers to provide proper reinforcement and anchorage details in complex and/or unfamiliar design applications. Usage of these procedures should improve the behavior of concrete structures, allow more efficient use of reinforcement and result in lower maintenance and repair expenditures. A series of design examples are presented to illustrate typical applications. Study of these examples should greatly improve familiarity of design personnel with strut-and-tie models for detailing structural concrete.

Prepared in cooperation with the Texas Department of Transportation
and the U.S. Department of Transportation,
Federal Highway Administration

The contents of this report reflect the views of the authors, who are responsible for the facts and the accuracy of the data presented herein. The contents do not necessarily reflect the official views or policies of the Federal Highway Administration. This report does not constitute a standard, specification, or regulation.

There was no invention or discovery conceived or first actually reduced to practice in the course of or under this contract, including any art, method, process, machine, manufacturer, design or composition of matter, or any new and useful improvement thereof, or any variety of plant which is or may be patentable under the patent laws of the United States of America or any foreign country.

**NOT INTENDED FOR CONSTRUCTION,
PERMIT, OR BIDDING PURPOSES**

J. E. Breen, P.E. (Texas No. 18479)

J. O. Jirsa, P.E. (Texas No. 31360)

M. E. Kreger, P. E. (Texas No. 65541)

Research Supervisors

PREFACE

This is the final report in a series of three reports which investigated applications of strut-and-tie modelling for typical details of structural concrete bridges. Research Report 1127-1 looked more specifically at the problems of shear and diagonal tension in the negative moment regions of precast girders for use with drop-in spans. Research Report 1127-2 summarized a series of tests of typical details used with dapped beams and several different types of nodes. This report (1127-3F) presents a summary of the basis for strut-and-tie model use in detailing structural concrete and includes a series of illustrative examples.

This work is part of Research Project 3-5-87/9-1127 entitled "Reinforcement Detail Design in Structural Concrete." The research was conducted by the Phil M. Ferguson Structural Engineering Laboratory as part of the overall research programs of the Center for Transportation Research at The University of Texas at Austin. The work was sponsored jointly by the Texas Department of Transportation and the Federal Highway Administration.

Liaison with the Texas Department of Transportation was maintained through the contact representative, Ms. Mary Lou Ralls, who was extremely helpful in providing typical current details from a wide variety of projects. Mr. Eric Munley was the contact representative from the Federal Highway Administration.

This portion of the overall study was directed by John E. Breen, who holds the Nasser I. Al-Rashid Chair in Civil Engineering. He was assisted by co-principal investigators James O. Jirsa, Professor of Civil Engineering (who had primary responsibility for directing the nodal and dapped beam tests) and Michael E. Kreger, Associate Professor of Civil Engineering (who had primary responsibility for directing the negative moment test series). The synthesis of ideas and the development of the initial draft of this final report were the direct responsibility of Dr. Konrad Bergmeister, Visiting Engineer from the University of Innsbruck.

TABLE OF CONTENTS

Chapter 1	Introduction	1
1.1	General Introduction	1
1.2	Summary of the History of Detailing	5
1.3	Objectives	24
1.4	Scope	27
Chapter 2	Background	29
2.1	Concept Background	29
2.2	Isolate Discontinuity or Detail Region: D - Region	33
2.3	Elasticity Analysis Method as Load Path Method	38
2.4	Strut Background	41
2.4.1	Concrete Compressive Strength Limitation for Struts	45
2.4.1.1	Effective concrete strength in compression diagonals	63
2.4.1.2	Two- and three-dimensional concrete strength ...	69
2.4.1.3	Confined concrete strength	71
2.5	Tie Background	84
2.5.1	Prestressing Forces	88
2.6	Node Background	105
2.6.1	CCC - Nodes	107
2.6.2	CCT - Nodes	112
2.6.3	CTT - Nodes	119
2.6.4	TTT - Nodes	124
2.6.5	Anchorage Requirements in the Nodal Zone	128
2.7	Model Optimization	133
2.8	Concrete Efficiency Factors for Design	135
2.8.1	Unconfined Nodes and Undisturbed Concrete Struts	135
2.8.2	Compression Diagonals	136
2.8.3	Confined Nodes	136
2.9	Anchorage Requirements for Design	139
Chapter 3	Procedures	141
3.1	General Analysis – Structural Analysis	141
3.2	Checking and Dimensioning Concrete Compression	143
3.3	Checking and Dimensioning Tensile Ties	147

Chapter 3	Procedures (continued)	
3.4	Checking and Dimensioning Nodes:	
	Determining Anchorage Requirements	149
3.4.1	Checking and Dimensioning CCC - nodes	150
3.4.2	Checking and Dimensioning CCT - nodes	151
3.4.3	Checking and Dimensioning CTT - nodes	157
3.4.4	Checking and Dimensioning TTT - nodes	160
3.4.5	Curved Tensile Ties	162
Chapter 4	Design Aids	165
4.1	Detailing Aids	165
4.2	Types	168
4.3	Typical Examples of Detailing Aids	169
4.3.1	Load Near Support	171
4.3.2	Corbel Projecting from a Column	189
4.3.3	Deep Beam with a Hole	205
4.3.4	Dapped Beam	226
4.3.5	Anchorage Zone	243
4.3.6	Pretensioned Beam with Eccentricity	257
Chapter 5	Conclusions and Recommendations	271
References	273
Appendix A: Detailing Aids	285

LIST OF FIGURES

<i>Figure</i>		<i>Page</i>
1.1	Typical examples of strut-and-tie models	3
1.2	Examples of flow of forces and the strut-and-tie model	4
1.3	Details of special concern that may exist in actual structures	6
1.4	Truss action in a cracked reinforced concrete beam	8
1.5	Lower and upper bound solution	13
1.6	Truss model and tied-arch model	15
1.7	Truss model for the force transfer between the concrete and the steel	19
1.8	Basic truss-model cube	20
1.9	Tension and dowel force, and hoop stress close to a bar	20
1.10	Two-phase model for aggregate interlock	21
1.11	Semi-continuous members with dapped end	23
2.1	The principle of Saint Venant	34
2.2	Subdivision of structures into B and D regions using Saint Venant's principle	35
2.3	Suggested subdivision of structure	37
2.4	Load path method with "u-turn"	40
2.5	Planar stresses in prism under compression	42
2.6	The basic compression fields	43
2.7(a)	Fan region at beam support	44
2.7(b)	Bottle shaped struts	44
2.8	Stress-strain curves for low, medium and high strength concrete	47
2.9	Relationship of diagonal concrete strut efficiency factor versus concrete strength	49
2.10	Distortional effect	51
2.11	Forces acting on edge members of parabolic arches	51
2.12	Mean crack strain	53
2.13	Relationship between the mean crack strain and the strains in the reinforcement for different angles of inclination of the diagonal strut	53
2.14	Varying strut angle versus efficiency factor for concrete compression strength	55

2.15	Mohr's circle	58
2.16	Proposed strut-and-tie model for shear behavior	66
2.17	Comparison of test results with the theoretical approach of predicting the diagonal compression strength	68
2.18	Two-dimensional compressive strength	70
2.19	Typical geometrical data for confined core	71
2.20	Experimental stress-strain curves of 4 x 16 in. normal weight spiral columns	74
2.21(a)	Strip load dimensions	76
2.21(b)	Variable dimensions for geometry of the bearing and loaded plate ...	77
2.22	Bearing stresses versus concrete strength	78
2.23	Comparison of test results with theoretical approaches for predicting confined concrete strength	83
2.24	Various approaches for the tensile strength of concrete	86
2.25	Crack width versus tensile strength reduction factor	86
2.26	The biaxial compressive-tensile strength of concrete	87
2.27	Pretensioned beam	91
2.28	Frictional loss along circular curve	93
2.29	Bond stress distribution at the end of a bond anchorage of a pretensioned wire	96
2.30	Strut-and-tie models for prestressed concrete	99
	(a) Pretensioning force transfer	99
	(b) Overall model	99
	(c) Eccentric pretension force	100
	(d) Fully plastic strut-and-tie model	100
	(e) Strut-and-tie model for the end "D" region	100
2.31	Strut-and-tie model for prestressed concrete beam with curved tendon	101
2.32	Approximation for radial compression component of curved tendon ..	103
2.33	Prestressed beam with parabolic tendon	104
2.34	Width of the compression-and-tension chord	104
2.35	Types of nodes	106
2.36	CCC nodes	108
	(a) CCC node with unequal pressure	108
	(b) Struts created by hydrostatically dimensioned node	108
2.37	Dimensions for hydrostatic stress check in CCC node	109

2.38	CCC node	110
2.39	Comparison of the horizontal compression strut width	111
2.40	Anchorage detail for CCT node: Anchorage of reinforcement with anchor plate	113
2.41	Anchorage detail for CCT node with directly anchored bars	113
2.42	Equivalent concrete area approach to define the tie width	114
2.43	Proposed tie width by CEB-MC – Draft 1990	115
2.44	General information about the tested CCT nodes	116
2.45	Comparison of test results with the concrete efficiency factor of $v_e = 0.8$	117
2.46	Dependency of the efficiency factors for CCT node	118
2.47	Comparison of design rationale used for nodal region of strut-and-tie model and joint of steel truss	120
2.48	Geometrical approach to define the strut width for CTT node	121
2.49	Dependency of the compression strut width for CTT node	124
2.50	Tensile strength of concrete implicitly utilized	125
2.51	Conservative starting point for computing development length	126
2.52	Positive and development length anchorage details	127
2.53	Lateral pressure on reinforcement bar	130
2.54	Lateral pressure and the distance “e” to the reinforcing bar	131
2.55	Comparison of a theoretical approach and test results for the development length of straight bars with confinement from bearing plates	132
2.56	Design approach for concrete efficiency factor	138
3.1	Design procedure for concrete structures	142
3.2	Compression fields and strut-and-tie model	143
3.3	Comparison of various diffusion angles	146
3.4	Proposed diffusion angle for design	146
3.5	Width of the reinforcing tie	147
3.6	Assumption for the biaxial compressive-tensile strength	148
3.7	Strut width for smeared node	149
3.8	Geometrical relation for CCC node for dimensioning process	152
3.9	Geometrical relation for CCC node with borders not parallel to the compression strut	153
3.10	CCT node with single straight reinforcement bar	154
3.11	CCT node with hooked bar	155

3.12	CCT node with multiple reinforcement bar layers	156
3.13	CCT node with single reinforcement bar layer	158
3.14	CCT node with multiple reinforcement bar layers	159
3.15	Special anchorage devices	160
3.16	TTT node with looped bar	161
3.17	Dimensions for curved tensile ties	163
4.1	Types of nodes	169
4.2	Examples to be presented in detail	170
4.3	Elastic finite element analysis: principal stresses	173
4.4	Strut-and-tie model for load near a support	174
4.5	Node <u>a</u> – CCT node	183
4.6	Node <u>b</u> – CCC node	187
4.7	Reinforcement layout	188
4.8	Typical cracking patterns of corbels	189
4.9	Possible failures of corbels	191
4.10	Stress trajectories in a homogeneous elastic corbel	192
4.11	Diagonally reinforced corbels	193
4.12	Failure mechanism in corbels	193
4.13	Strut-and-tie model for corbel	194
4.14	Corbel strut-and-tie model	195
4.15	Strut-and-tie model results compared with test results	196
4.16	Strut-and-tie model for corbel projecting from a column	199
4.17	Anchorage detail for corbel design	203
4.18	Reinforcement layout	204
4.19	Geometry for determining stress concentration factors	206
4.20	Principal tension trajectories and reinforcement for corner in tension	207
4.21	Strut-and-tie models for deep beam with a hole	211
	(a) Example 4.3 dimensions	211
	(b) Finite element analysis contours for similar structure with load placed farther to right	212
	(c) Model 1, left side	213
	(d) Model 2, left side	214
	(e) Model 1 – 50% of load (left)	215
	(f) Model 2 – 50% of load (left)	216

4.21	Strut-and-tie models for deep beam with a hole (continued)	
	(g) Model 3 – 100% of load (right)	217
	(h) Combined strut-and-tie models	218
4.22	Reinforcement layout for deep beam with a hole	225
4.23	Reinforcement layout for strut-and-tie model ST1	227
4.24	Reinforcement layout for PCI detail	227
4.25	Reinforcement layout for Menon/Furlong – detail	228
4.26	Reinforcement layout for modified strut-and-tie model ST2	228
4.27	Orthogonal strut-and-tie model	230
4.28	Diagonal strut-and-tie model	230
4.29	Proposed strut-and-tie model for dapped end beam	231
4.30	Proposed strut-and-tie angle for dapped end beam	232
4.31	Comparison with the proposed strut-and-tie model using test results	233
4.32	Strut-and-tie model for example: dapped end beam	236
4.33	Reinforcement layout for dapped end beam	242
4.34	Possible configuration for single anchor	245
4.35	Concentric single anchor: geometry	246
4.36	Comparison of finite element analysis with results from Guyon	247
4.37	Comparison of two different strut-and-tie models with principal stress vectors	249
4.38	Proposed strut-and-tie model for anchorage zone	250
4.39	Strut-and-tie model for example: anchorage zone	253
4.40	Reinforcement layout for anchorage zone	256
4.41	Pretensioned beam: geometry	260
4.42	Strut-and-tie model for prestressed concrete	261
	(a) Transfer length forces	261
	(b) Model with tendon eccentricity effects	261
	(c) “D” region at end	262
4.43	Reinforcement layout for pretensioned beam	269

LIST OF TABLES

<i>Table</i>		<i>Page</i>
1.1	Statistical data from comparison with different models	16
2.1	Analysis usage	32
2.2	Statistical parameter for shear tests	57
2.3	Efficiency factor proposed in the CSA and by Macgregor	60
2.4	Efficiency factors proposed by Schlaich et al. and CEB	62
2.5	Values for τ_{RD} according to CEB MC – Draft 1990	64
2.6	Comparison with the proposed strut-and-tie model and test data	67
2.7	Statistical data of the comparison in Figure 2.17	68
2.8	Strength ratio for three-dimensional concrete compressive strength	69
2.9	Statistical data from Figure 2.18	70
2.10	(Number inadvertently skipped – Table 2.11 is next following Table 2.9)	—
2.11	Statistical data for confined concrete strength with various test data ...	81
2.12	Statistical data from Figure 2.23 for confined concrete with an efficiency factor $v_e = 0.5 + 15/(f_c)^{0.5}$	82
2.13	Statistical data for confined concrete with an efficiency factor $v_e = 0.5 + 20/(f_c)^{0.5}$	82
2.14	Friction and wobble coefficient	93
2.15	Loss of prestress	94
2.16	Design steps for 'B' regions of prestressed beams using the strut-and-tie method	102
2.17	Statistical data from Figure 2.45 (CCT node)	118
2.18	General information about the tested CTT nodes	122
2.19	Statistical data from comparison in Figure 2.55	131
4.1	Statistical analysis from Figure 4.15 omitting unreinforced specimen ..	196
4.2	Statistical data from Figure 4.31	233

SUMMARY

This report is the final report in a series which investigates the applications of strut-and-tie modelling for typical details in structural concrete bridges. It summarizes the state of the art of strut-and-tie modelling and presents specific recommendations for choosing the critical dimensions and carrying out detailed computations using such strut-and-tie models. Separate sections treat the overall modelling and detailing process, checking compression struts, detailing tension ties, evaluating TTT, CCC, CCT and CTT nodes, and incorporating prestressing forces. The report includes a series of examples showing application of strut-and-tie models in detailing deep beams, corbels, anchorage zones, dapped ends, openings, and pretensioned beams. In addition, a number of detailing aids are included in an appendix.

CHAPTER 1. INTRODUCTION

1.1 General Introduction

A structure must be safe, serviceable and durable during its lifetime. In addition, a designer must always be aware that a structure should be practical and economical to construct and should fulfill not only functional but also aesthetic needs.

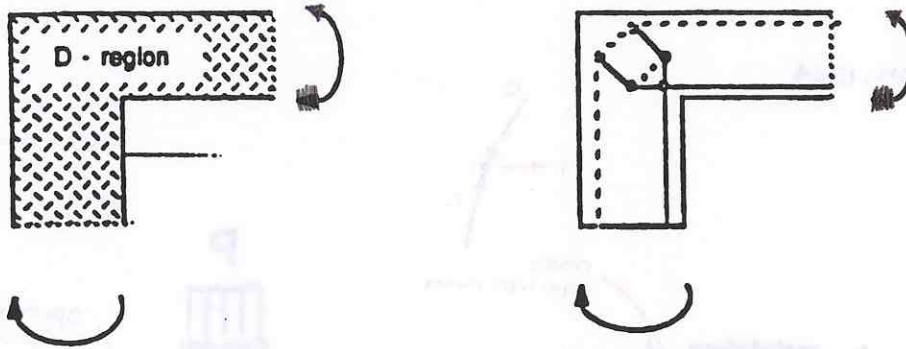
S&T considers only strength; need to go back and make other checks

Concrete structure construction is marked by increasingly versatile applications. The wide spectrum includes precast and cast-in-place concrete with conventional pretensioned and /or post-tensioned reinforcement. The term structural concrete is used to define the global spectrum for the different concrete structures and covers all loadbearing concrete, including reinforced, prestressed and also plain unreinforced concrete, if the latter is part of a concrete structure. This definition purposely eliminates traditional expressions such as "reinforced concrete", "prestressed concrete" and "partially prestressed concrete". It was chosen to emphasize that a traditional "prestressed concrete" beam in fact may have "active" or "prestressed" reinforcement for a portion of the flexural resistance, "passive" or "non prestressed" reinforcement for the remainder of the flexural resistance and for local crack control as well as for shear - diagonal tension resistance, and additional "passive" reinforcement for anchorage zone resistance to bursting and spalling stresses. The basic design principles for selection of these various reinforcements are essentially identical at the ultimate limit state and can be consistently treated by well recognized similar analysis techniques at the serviceability limit state. It will greatly reduce confusion and possible error if a consistent treatment can be developed for

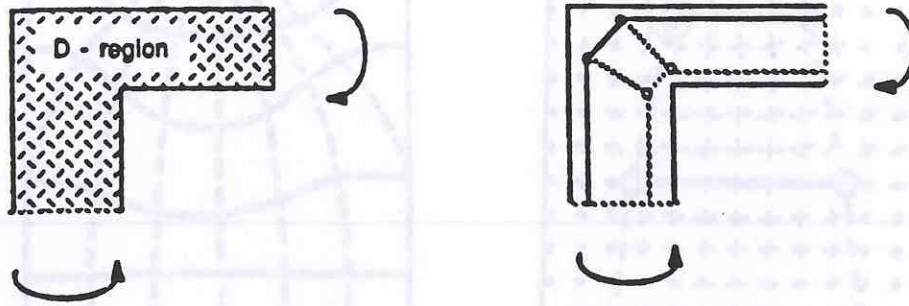
determination of the internal forces in the members of the selected structural system. The action forces (external forces) on a structure must be in equilibrium with the resisting forces (internal forces). Most structural analyses use an elastic system which combines equilibrium, geometric constraints and continuity to determine the action forces. These analytical models condense linear structural members along their centerlines and condense slabs and shells in their middle plane. Modern computer methods provide rapid and efficient solutions for these action forces (including support reactions) as well as the determination of sectional resistance forces such as axial load, shear, bending moment and torsional moment acting on a specified cross section. Both linear elastic analysis and simplified plastic analysis procedures have been widely accepted for such determination. However, to reasonably dimension a concrete structure, choose cross-section dimensions and specify reinforcement quantities and patterns, further knowledge of material properties and internal force distributions are required. For a better understanding of the distribution of internal forces in a concrete structure, applications of strut-and-tie models are helpful [1]. Struts and ties condense the real stress-fields and internal forces of a structure along straight or curved lines and concentrate the curvatures of the force paths in nodes, as shown in Fig. 1.1. In these examples dashed internal lines indicate the compressive struts while solid internal lines indicate the tension ties. The small circles represent the nodes where the struts and ties intersect. Because the strut-and-tie model is a conceptual model, it enables the designer to visualize the flow of forces within the structure (Fig. 1.2) and is of particularly great assistance in proportioning reinforcing.

A consistent design approach for a structure is attained when its tension members, compression members, and the interconnecting nodes with their specific joining requirements are designed with proper regard to ensure safety, serviceability and durability.

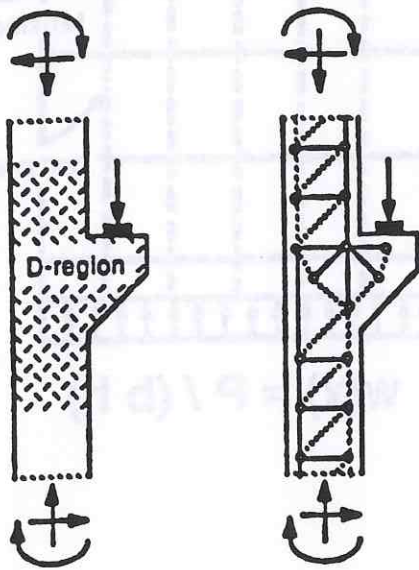
a. Moment Opening Corner



b. Moment Closing Corner



c. Corbel



d. Deep Beam

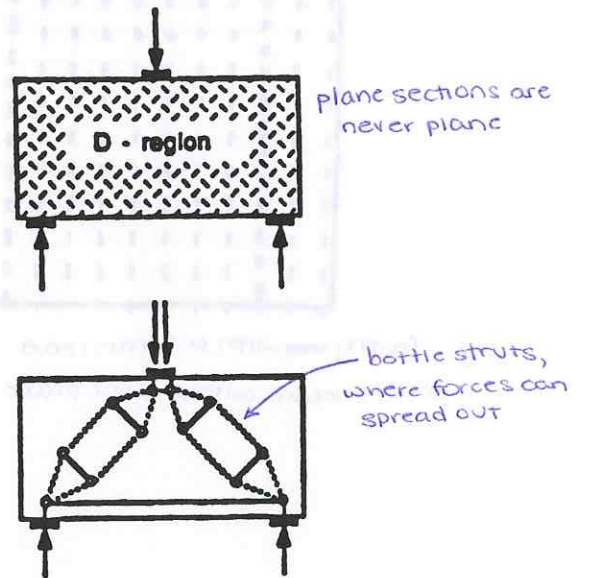


Figure 1.1: Typical examples of strut- and tie- models (from Ref. [2])

From Mörsch, 1924

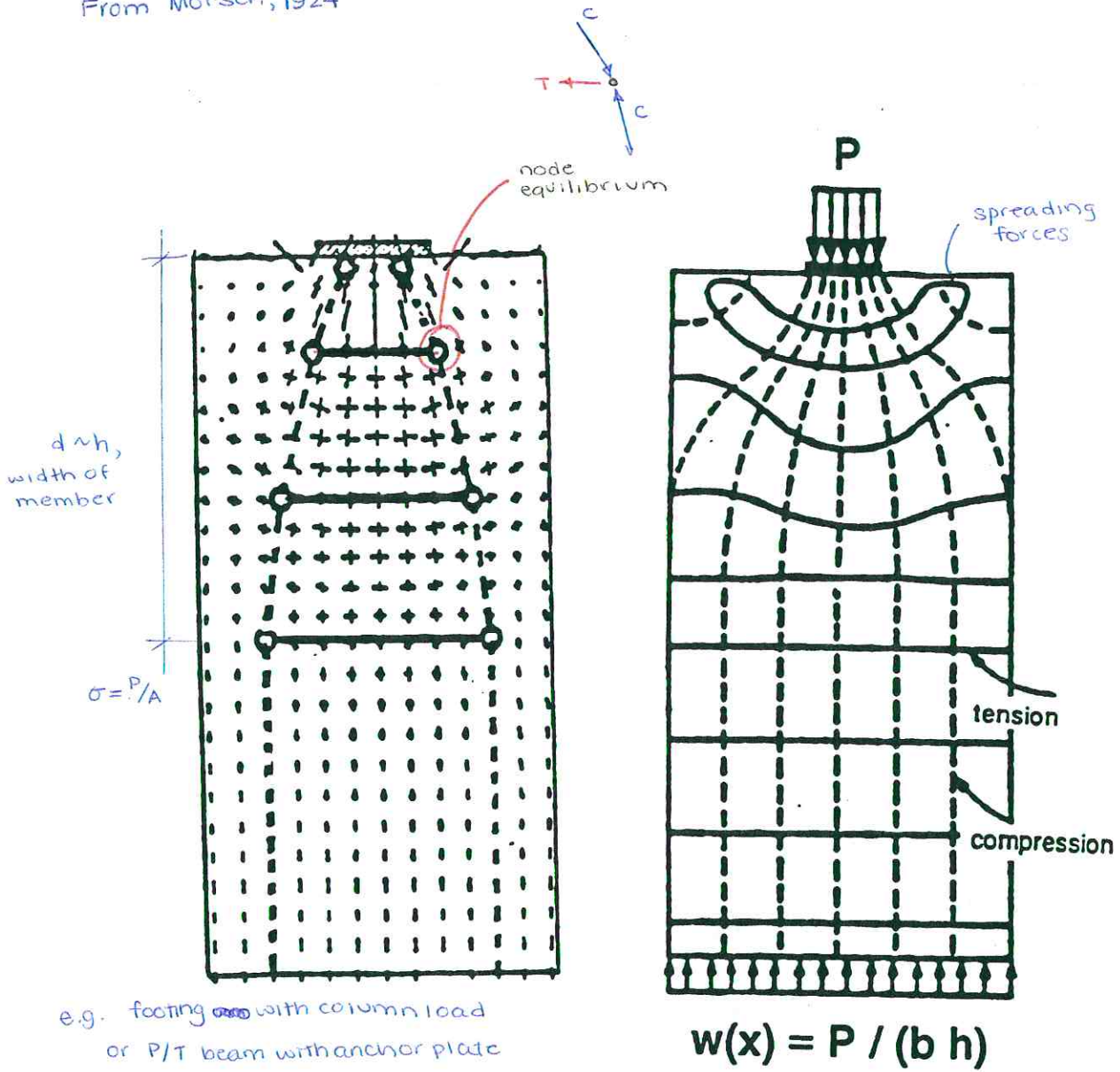


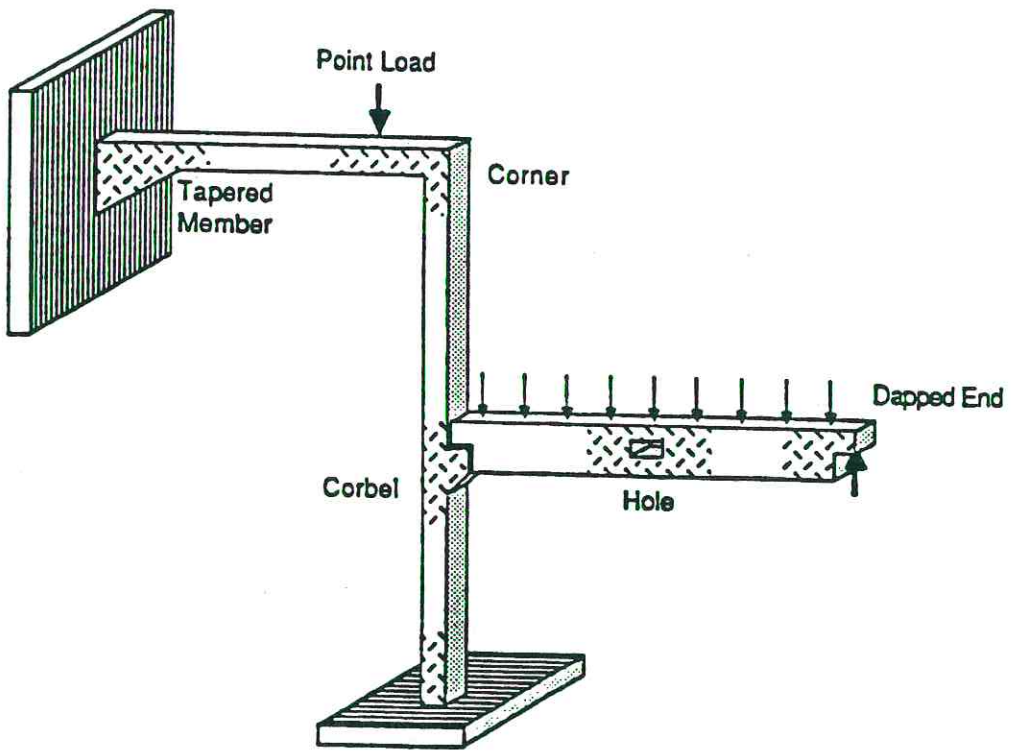
Figure 1.2: Examples of flow of forces and the strut- and- tie- model

1.2 Summary of the History of Detailing

Design of a concrete structure is a step by step procedure beginning with estimation of the loads acting on the structural system, preliminary proportioning of relative stiffnesses of the structural system, carrying out a detailed and often iterative general structural analysis, followed by the sizing or proportioning of members and concluding with the detailing process. In concrete structures, detailing would encompass:

- preparation of drawings showing the size and location of structural elements and reinforcement, and specifying the required concrete strength
- specification of bar details such as anchorage provisions and locations of splices and overlaps
- specification of time dependent quality control requirements

In detailing a concrete structure particular attention must be paid to the statical or geometrical discontinuities, shown in Fig. 1.3, such as concentrated loads (statical) or frame corners, corbels, recesses, holes and other openings (geometrical). The proper detailing for such areas of special concern is essential to overall structural integrity. While engineers are usually well trained in analysis procedures and the basic mechanics of structural concrete, there is not a general methodology for detailing. This often presents the designer with numerous difficulties. The different codes and standards (AASHTO [3], ACI 318-89 [4]) propose empirical recommendations for some specific applications. However, the design standards cannot include the innumerable details that may arise. Most text books emphasize the basic mechanics and are vague or illusory regarding details for irregular members.



From Schlaich

Figure 1.3: Details of special concern that may exist in actual structures

Since all parts of a structure including the discontinuity regions are of similar importance, an acceptable design concept must be based on a physical model with a logical understanding. Truss models, because of their transparency and adaptability to many design situations, are seen as attractive alternatives to empirical approaches for detailing structural concrete. Truss models for shear design of reinforced concrete beams were introduced by Wilhelm Ritter [5] in 1899. Ritter introduced his model to dispel the idea that the main function of the stirrups was to resist horizontal shearing stresses by a dowel-type action for which vertical wooden pegs were used in timber beams. Mörsch [6] in 1902 presented the truss analogy for the design of web reinforcement based on laboratory tests. In the truss model for shear, the reinforced concrete beam is represented by an analogous truss. A typical reinforcement scheme in a cracked reinforced concrete beam will mobilize the truss action as shown in Fig. 1.4(b). The flexural concrete compression zone is thought of as the top chord of the truss while the tensile reinforcing forms the bottom chord. The top and bottom chords are connected by stirrups acting as vertical tension hangers and pieces of concrete between diagonal tension cracks acting as compression struts.

In 1906 Withey [8] introduced Ritter's equation into the American literature. He found that this equation gave tensile stresses in the stirrups which were too high when compared with values obtained from actual test results. Withey indicated that the concrete of the compression zone may carry considerable shear even after the web below the neutral axis is cracked in diagonal tension. He also indicated a possible vertical shear transfer by dowel action of the longitudinal reinforcement.

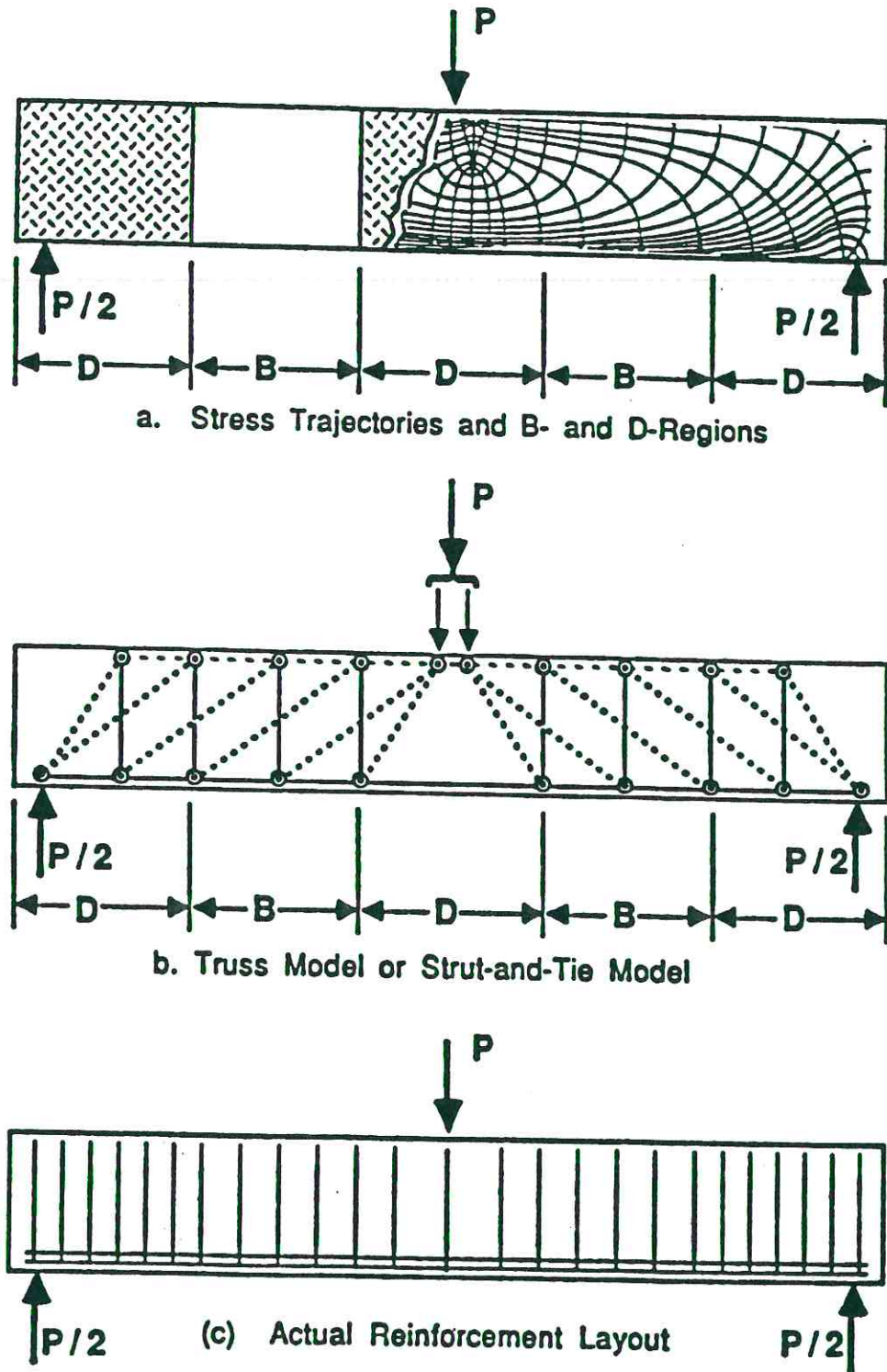


Figure 1.4 : Truss action in a cracked reinforced concrete beam (from Ref. [7])

In 1909, Talbot [9] presented a study of web stresses, including tests of 188 beams. The conclusions of this report are indeed important. In particular, the conclusion referring to beams with stirrups said:

Stirrup stresses computed by Ritter's equation appear too high. It is therefore recommended that stirrups be dimensioned for two-thirds of the external shear, the remaining one-third being carried by the concrete in the compression zone. It will be found that the value of nominal shearing stress will vary with the amount of reinforcement, with other factors which affect the stiffness of the beam.

The stiffer the beam the larger the vertical stresses which may be developed. Short, deep beams give higher results than long slender ones, and beams with high percentage of reinforcement than beams with a small amount of metal ... In beams without web reinforcement, web resistance depends upon the quality and strength of the concrete ...

Unfortunately Talbot's findings were not expressed in mathematical terms, and became lost as far as design equations were concerned. The National Association of Cement Users, the forerunner of the present American Concrete Institute, published its first code recommendations in 1908 [10]. This report was essentially based on what has later become known as ultimate strength design. The various sections were dimensioned on an ultimate basis for a load four times the total working load.

In 1927, Richart [11] expressed the shear capacity of concrete beams with vertical stirrups by an equation of the form:

$$v = C + r f_v$$

where

- v = nominal unit shearing stress in concrete
- r = $a_v / (s b)$
- a_v = cross sectional area of web reinforcement
- s = spacing of web reinforcing bars, measured at right angles to their direction
- b = width of beam
- f_v = tensile unit stress in web reinforcement
- C = factor which varies between 90 and 200 psi (depends upon the the percentage of web reinforcement used and also on the quality of the concrete).

This expression indicates that the computed stresses from the truss model were lower than the measured stresses. The factor "C" was included to express the additional mechanism for shear behavior, like aggregate interlock (friction), dowel action etc. These basic ideas found wide use in American design standards throughout the Twentieth Century. Since the majority of members designed were subjected to only low or moderate shear levels, an empirical "C" or concrete contribution (V_c) was introduced to supplement the truss model capacity (V_s). The present US expressions [3, 4] for shear capacity are of the pattern:

$$V_u \leq \phi V_n = \phi (V_c + V_s)$$

Continued use of the supplementary " V_c " term in US practice was encouraged by more contemporary leaders such as Hognestad [12] who stated in 1951 that if designs are made on an ultimate limit state basis the truss model will not result in safe and *economic* structures under all conditions met in practice.

Kupfer [13] in 1964 developed an expansion of Morsch's truss analogy by application of the principle of minimum strain energy.

For the last 25 years, researchers in Europe and North America have been working with the goal of developing a conceptual model to properly represent the behavior of concrete members subjected to torsion and shear. The main objectives were to rationalize and at the same time simplify the design procedures in these areas. Lampert and Thürlimann [14] developed a conceptual model based on theory of plasticity. The theory of plasticity provides a mathematical basis for collapse load calculations. Using a yield condition, a mathematical description for the ultimate stresses can be developed. Given a set of generalized stresses, $\sigma_1, \sigma_2, \dots, \sigma_n$ the yield condition is a function $f(\sigma_1, \sigma_2, \dots, \sigma_n) = 0$. The yield condition can be visualized as a surface in n-dimensional space.

If $f < 0$, the point determined by the generalized stresses lies within the surface and does not give yielding. The condition $f > 0$ implies a point outside the yield surface which corresponds to stresses that cannot occur. The flow law is a second major concept in plasticity. The flow law is defined as

$$\begin{aligned} \varepsilon_i &= f / (\lambda \sigma_i) & i &= 1, 2, \dots, n \\ \varepsilon_i &= \text{generalized strain corresponding to } \sigma_i \\ \lambda &= \text{positive constant} \end{aligned}$$

Starting from the yield condition and flow rules it is possible to derive the theorems of limit analysis. The lower bound theorem states (see Fig. 1.5 (a)):

$$\lambda_1 \sigma_i \leq \lambda_u \sigma_i$$

A load system based on a statically allowable stress field which does not violate the yield condition is a lower bound of the ultimate load.

The statically allowable stress distribution must satisfy the equilibrium equations and the statical boundary conditions. From this it follows that the strut- and tie- model is a lower bound solution. Use of the lower bound theorem will in all cases be conservative. The upper bound theorem states (see Fig. 1.5 (b)):

A load system which is in equilibrium with a kinematically allowable mechanism and compatible with the geometrical boundary conditions is an upper bound of the ultimate load.

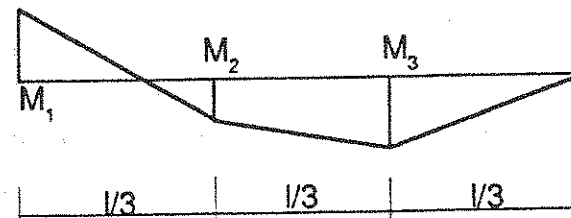
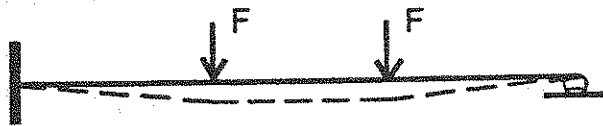
Solutions for the upper bounds are derived by equating the external work done to the internal energy dissipation for the assumed mechanism. Upper bound solutions are generally unconservative. The theory of plasticity states that there is a unique and exact solution such that both the upper and lower bound theorems are satisfied. The quality of a plastic analysis is dependent on the constitutive equations used. These constitutive models of material behavior define the yield condition which determines failure of the plastic model. The way constitutive equations (most are empirically derived) are handled by the models will be discussed in Chapter 2.

Various researchers, including Leonhardt [15], Rüschi [16], Lampert [17], Grob [18], Lüchinger (space truss) [19], Müller (optimum inclination of the diagonal members) [20], Neilsen et al. [21], Mitchell and Collins [22], Ramirez and Breen [23] have worked to refine and expand the method so it is applicable

$$M_1 = -F l / 3$$

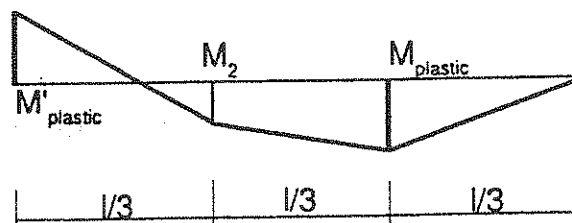
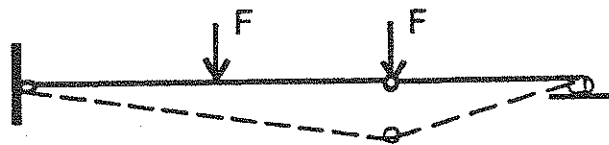
$$M_2 = +F l / 9$$

$$M_3 = +2F l / 9$$



(a) lower bound solution

$$F_u = (3 M_{pl} + M'_{pl}) / l$$



(a) upper bound solution

Figure 1.5: Lower- and upper bound solution

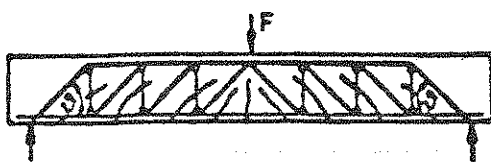
to shear, torsion, and the interaction of these actions, as well as bending. The space strut - and- tie-model with variable angle of inclination of the compression diagonals departs from the traditional truss model with 45 degree angle diagonals. The angle is chosen such that in the field where failure occurs, both the longitudinal and transversal (stirrups) reinforcement will reach their yield strength. In this case a sufficient shear transfer by aggregate interlock across the initial inclined cracks is assumed so that the concrete diagonals can reach their final inclination under ultimate load. Due to the fact that such shear transfer across a crack decreases with increasing crack widths (rough crack model [24, 25]), additional considerations become necessary. Hence, limits on the inclination of the concrete diagonals must be introduced. The model is valid in the complete range of interaction between general bending, normal force, shear force, and torsion. However, limits must be set in some fashion to preclude initial compression failures. Recently, MacGregor and Gergely [26], Marti [27], Schlaich et al. [28], Schlaich and Schäfer [2] have published refined methods for detailing structures using strut- and- tie- models. In the Canadian CSA-Standard [29] the compression field theory, an idea somewhat similar to the strut- and- tie-model, was introduced in 1984. Cook and Mitchell [30] published studies on regions near discontinuities. The strut- and- tie- models were compared with a nonlinear finite element study and test results.

The "Design and Construction Specifications for Segmental Concrete Bridges" [31] introduces also the strut-and-tie-model as a design tool for areas where the strain distribution is non-linear.

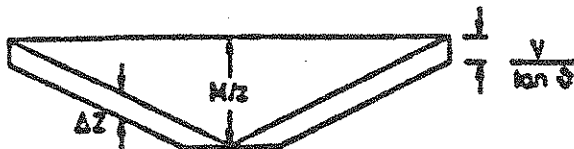
For prestressed beams with unbonded tendons, Kordina et al. [32] compared their test results with the truss- model (Fig. 1.6(a)) and also with a tied-arch model (Fig. 1.6(b)). According to the truss model, the shear-carrying capacity increases approximately linearly with the amount of web reinforcement, whereas with the tied-arch model the shear-carrying capacity depends only on the load-carrying capacity of the arch or the tension chord. The comparison of the

test results with the truss model (45-deg truss was assumed) showed that the shear capacity could be predicted best for unbonded prestressed beams. Conversely, for a tied-arch model, an insufficient agreement with the test results was obtained; only the compression-arch failure was considered as a failure mode. Measurements indicated that the stirrup stresses in beams with unbonded prestressing do not differ in principle from comparable beams with bonded prestress reinforcement, as far as the shear-carrying system is concerned.

Idealized crack pattern



Tension force within the tension chord



Forces acting of a truss joint



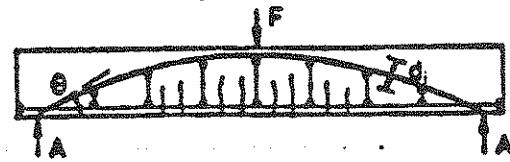
D = compression strut force

Z_s , Z_s = stirrup force

ΔZ = differential force in the longitudinal reinforcement according to the truss analogy

M/z = tension force according to the beam theory

Idealized crack pattern



Tension force within the tension chord



Forces acting of the support



D = compression force within the arch

Z = tension force within the tension chord

A = bearing force of the support

(a) Truss model

(b) Tied-arch model

Figure 1.6 : Truss model and tied-arch model (from Ref. [32])

Similar to the case of bonded prestress, the stirrup forces are reduced by a part of the shear force carried by the concrete, including parts of the shear force carried by aggregate interlock, the compression zone, and the dowel action of the longitudinal reinforcement.

Recent studies by Hartmann, Breen and Kreger [33] compared the truss model with test results for prestressed concrete girders using concrete strength in the range of 12,000 psi. The 45 degree truss model gave very conservative results when using a concrete efficiency factor of 0.5. Table 1.1 contains the statistical comparison of the analysis with different models.

Table 1.1: Statistical data from comparison with different models

Method	Experiment/theory: mean	standard deviation
ACI [2]	1.18	0.18
CSA [28]	1.74	0.78
Truss: $v_e = 30 / (f'_c)^{0.5}$	1.72	0.26
Truss: $v_e = 0.5 (f'_c)$	1.38	0.32

It is interesting that the traditional ACI - AASHTO shear expressions [3,4] provide the closest agreement, once again indicating that the use of a supplementary " V_c " term is important for economy in beams with carefully controlled loading. Presence of precracking of the webs due to other loading patterns would greatly affect and could substantially diminish any V_c contribution. One of the problems in evaluating test data and comparing it with the truss model is to define the strut width, strut angle and the efficiency factor of the concrete.

Powers [34] studied prestressed girders with high strength concrete. Evaluation of the test results and the comparison with the strut-and-tie-model show that even for prestressed girders with high strength concrete, failure can be predicted on the basis of a strut-and-tie-model. For the web-crushing failure the limitation of the efficiency factor of the concrete is highly important.

Schäefer [35] and Castrodale [36] have shown that there is good agreement between the truss model and observed test results in both reinforced and prestressed concrete beams subjected to different loading combinations of bending and shear which extensively precrack the girders. Experimental results of the behavior of reinforced concrete beams with various arrangements of stirrups were compared with the strut- and-tie model by Kotsovos [37]. He concluded that in general the strut- and-tie- model does not provide any detailed information with regard to the strength and deformation of concrete.

Related work on this project by Barton [7] studied the application of a strut- and- tie- model to beams with dapped ends. The various singular nodes that may occur in the strut- and- tie- models were studied by Anderson [38] and Bouadi [39]. Their detailed observations are summarized in the accompanying report 1127-1.

Noguchi and Watanabe [40] applied the strut- and-tie- model based on a finite element study for the shear resistance mechanisms to beam-column joints under reversed cyclic loading. The strut-and- tie- model gave good agreement with the shear stress distribution model for all test specimens. Breen and Stone [41], Burdet [42] and Sanders [43] investigated strut-and-tie-model approaches based on elastic finite element studies and experimental tests, for the design of post-tensioned girder anchorage zones.

The approaches of the various authors cited differ in the treatment of the prediction of ultimate load and the satisfaction of serviceability requirements. Schlaich et al. [28] proposed in general to treat the ultimate limit state and serviceability in the cracked state by using the same model. This was to be done by orienting the geometry of the strut- and- tie- model based on elastic stress fields and by analyzing the resulting strut-and-tie-model structure following the theory of plasticity. A computer based design approach based on these ideas was developed by M. Schlaich [44].

The concept of a strut- and- tie- model can be used not only for statical or geometrical discontinuities but also for other load transfer mechanisms like anchorage provisions, dowel action and force transfer between concrete and steel. Yankelevsky [45] described a truss model for the force transfer between the concrete and the steel by using static equilibrium and compatibility to relate the forces. By knowing the axial force in the steel (a differential equation was solved for the axial force in the steel), the bond shear stress was predicted and was of an exponentially decaying form, maximum at the bar's ends and minimum at the specimen's midspan (see Fig. 1.7). Another application of strut- and- tie- models to details is the three dimensional truss model suggested for the fracture behavior of concrete. Rode [46] used a three dimensional truss model cube (Fig. 1.8) for a computer simulation to study crack opening and crack growth. The model conception is based on a 1941 idea of Hrennikoff [47] for the solution of linear elastic continuum problems by a three dimensional framework method. This model allows simulations on micro- and macro levels without altering the number of elements. The basic cell is a truss cube with edge struts, surface diagonal struts and space diagonal struts. The struts themselves behave linearly elastic up to given strain rates. On exceeding the maximum tensile or compressive strain, the affected struts are removed from the system, representing cracks. A

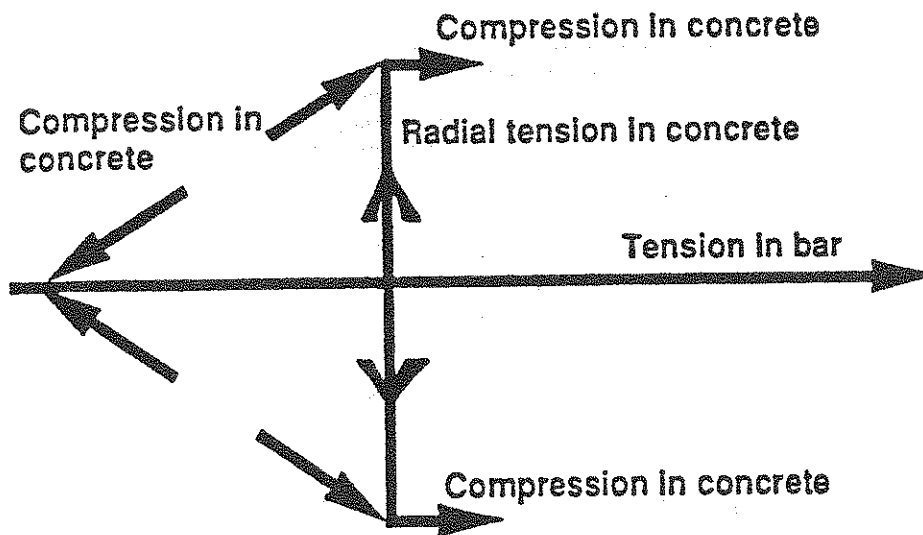
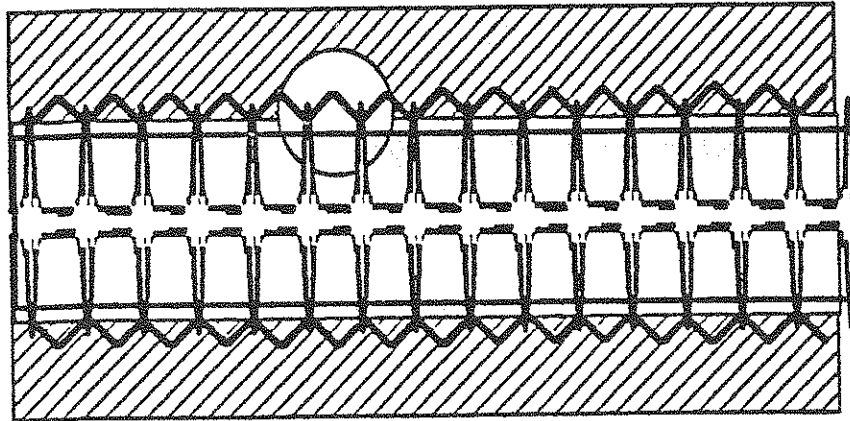


Figure 1.7: Truss model for the force transfer between the concrete and the steel (from Ref. [45])

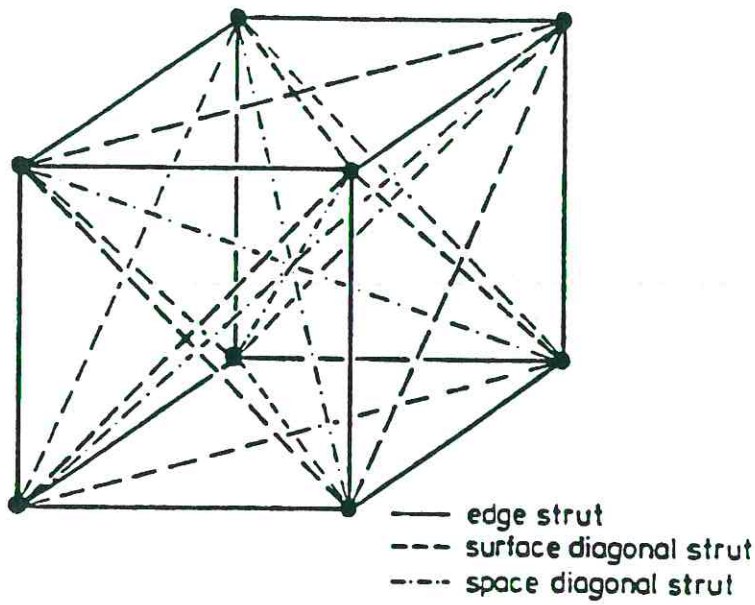


Figure 1.8: Basic truss-model cube (from Ref. [46])

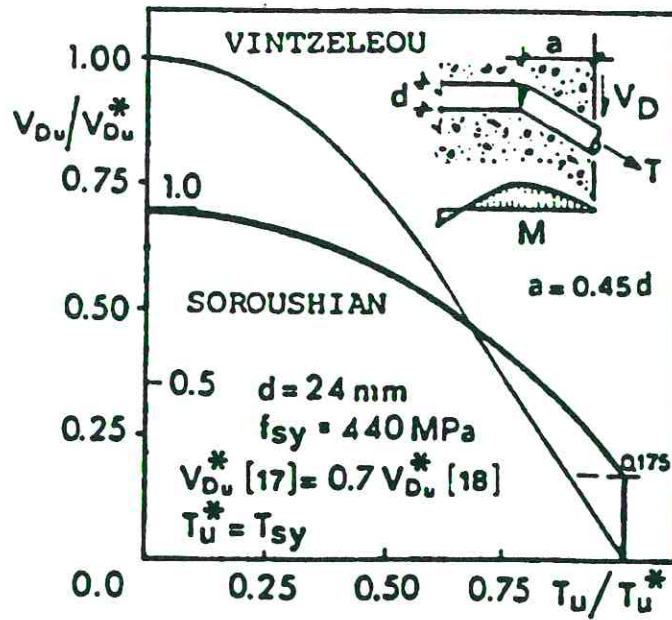
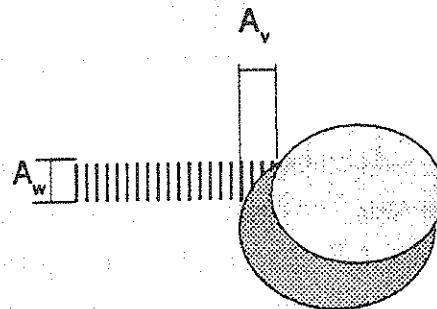


Figure 1.9: Tension and dowel force, and hoop stress close to a bar (from Ref. [48])

single strut represents the stress flow mainly through an aggregate particle, another one represents the flow mainly through the mortar matrix, and a third one is affected by the bond between matrix and aggregate. The strut parameters are stochastically endowed with values by a computerized random number process. All quantities of the strut parameters are normally distributed with a variance of 50%.

Soroushian et al. [48] and Vintzeleou [49] studied the dowel action with regard to bond, tensile strength of concrete, and bar- to- stirrup interaction with stirrup tension stiffening (see Fig. 1.9).

Different studies were done to investigate the shear transfer mechanism based on aggregate interlock (Bazant and Gamabarova [50], Divakar, Fafitis and Shah [51]). The two-phase model (Walraven [52]) has a rational formulation based on a few assumptions. (See Fig. 1.10.)



$$\begin{aligned} \sigma_{wv} &= \sigma_{mc} (A_w + \mu A_v) \\ \sigma_{vw} &= \sigma_{mc} (A_v - \mu A_w) \\ \sigma_{mc} &= 0.394 f_c^{0.56} \text{ (matrix compressive strength)} \\ \mu &\approx 0.4 \text{ (friction coefficient)} \end{aligned}$$

Figure 1.10: Two-phase model for aggregate interlock

The principal factors affecting the aggregate interlock are:

- quality of the concrete. Usually the top part of a member, because of the particle sedimentation and water gain under the coarse aggregate, will contain weaker concrete.
- the size of the crack width. Smaller crack widths lead to larger shear stresses, but also to more sudden failures.

Based on the interface shear transfer tests conducted by Walraven [52], an approximate expression to limit the shear stress along the crack was given by Cook and Mitchell [30]:

$$V_{\max} = 2.168 (f'_c)^{0.5} / (0.31 + 24 w / (d_a + 0.63))$$

$$V_{\max} = \text{max shear stress [psi]}$$

$$w = \text{crack width [in.]}$$

$$d_a = \text{maximum aggregate size [in.]}$$

Gamabarova [53] compared the truss model with test data and found that for thin-webbed I beams the truss-model is a quite conservative approach. Therefore, more realistically the aggregate interlock should be taken into account for shear design. This conclusion reemphasizes the findings of Talbot [9] and Richart et al. [54] in the 20's and Hognestad [12] in the 50's that a concrete term was needed to amplify the truss model for economical design of lightly loaded members. Also Brandtzaeg [54] concluded in his theoretical "analysis of stresses in a material composed of non-isotropic elements" that the limiting value of shearing stress is the sum of the shearing strength of the material and the coefficient of internal friction times the normal stress.

There are several additional load-carrying mechanisms that can supplement the basic truss model:

- dowel action of the longitudinal bars (vertical)
- aggregate interlock transfer forces across a crack (vertical and normal)
- component of inclined prestressing tendons (vertical)

These components of force transfer must either be neglected or treated indirectly in the strut- and- tie- model. In lightly loaded members with low levels of shear, such components are significant and some supplementary design mechanism continues to be necessary for economy [55]. Current design codes and standards work satisfactorily for typical "traditional" members such as uniform depth beams with well distributed loading. Empirical solutions at supports have been developed to give good designer guidance for such cases. However when irregular members are used, such guidance is limited. For example, the increased usage of concrete bridge substructures and superstructures in highly congested urban areas has caused increasing complexity in bent cap geometry, the introduction of new cross section shapes and the increasing usage of precast, prestressed beams cantilevered over a support to a hinge away from the support. Simply supported drop-in beams are placed from one hinge to another hinge at the other end of the drop-in beam. (See Fig. 1.11.)



Figure 1.11: Semi-continuous members with dapped end

This generally necessitates large notches or "daps" being used at the cantilever span end and the ends of the drop-in span. The many unusual bent configurations in congested urban areas result in many highly loaded short bracket and corbel applications in reinforced and post-tensioned concrete members. The increasing usage of pretensioned concrete in unusual long span situations as well as in massive bent caps creates a host of new applications of reinforced, pretensioned and post-tensioned members and assemblages. Traditional code rules and simple reinforcement patterns based on the simple span test specimens utilized for experimental determination of so many of the ACI [3] and AASHTO [4] design provisions do not provide guidance and are not applicable to many of these new applications.

In order to avoid potentially serious strength or serviceability problems, better guidelines for proportioning and locating reinforcement are needed. Such guidelines should consider the full range of reinforcement from the passive action of nonprestressed bars to the active action of prestressing tendons, as well as the case of mixed reinforcement (active and passive) which is becoming widely found in post-tensioned concrete. Comprehensive detailing methodology and guides are needed in practical detailing.

1.3 Objectives

The general practice in detailing structural concrete has been based on experience, rules of thumb or highly specific standard details. Most of these methods do not incorporate conceptual models to assist the designer. The lack of a consistent, rational method for detailing may lead to problems when unique situations are encountered. Strut- and- tie models serve to provide a rational framework for a detailing method which may be applied to a variety of structural components and loading conditions. Restriction of the use of such models to

zones or regions where traditional approaches incorporating a concrete contribution are inappropriate or uncertain will eliminate the economic penalty occurring in general usage of strut-and-tie-models with lightly loaded members. In the strut-and-tie model, the actual stress distribution within a structure is idealized as a static force system consisting of the following basic elements:

- struts: representing concrete compression stress fields
- ties: representing concrete tension stress fields or bonded reinforcement or bonded prestressing steel (unbonded tendons are individual members of the structure and should be treated correspondingly in the structural analysis)
- nodes: representing the intersection area of struts and ties in which the internal forces are redirected

The quantification of the strut- and- tie model as a comprehensive design tool for structural concrete details is a relatively new undertaking. The focus of this study is on design of details for which no rational design method currently exist. Therefore traditionally well defined applications such as uniform depth beams, columns, and slabs with uniform loading patterns are only briefly addressed. This study has as a basic objective the development of a consistent methodology and an accompanying comprehensive detailing guide for structural concrete based on use of refined strut- and- tie- models. It is hoped that the methodology and the illustrative guide will help designers develop a clearer understanding of the functioning of reinforcement and anchorage details in a wide variety of details in concrete structures. It is envisioned that the designer will approach the detailing of a concrete structure using strut-and- tie- models which may be based on an equilibrium analysis of load paths, on detailed results from a linear finite element analysis, or by analogy with a steel design procedure. After isolating the geometrical and/or statical discontinuities regions, the designer has to develop

a suitable strut- and- tie- model to carry the applied loads and meet the given boundary conditions. After selecting and analyzing a strut- and- tie- model, a major concern are the nodal zones where inclined compression struts, vertical stirrups, and longitudinal reinforcement intersect. The actual patterns of the nodes and the limiting stresses in the nodes must be quantified before practical implementation. Similarly, the allowable or effective compressive stresses in inclined compressive struts must be carefully evaluated.

The specific objectives of this overall study are:

- (1) To determine the state of the art in structural concrete detailing as reflected by research conducted and reported in Europe and North America
- (2) To specifically investigate experimentally the applicability of current AASHTO provisions for shear in the negative moment zones of pretensioned and post-tensioned composite beams.
- (3) To test selected structural concrete details experimentally, such as beams with dapped ends and node regions
- (4) To use the experimental results to refine the strut- and-tie model especially in terms of nodal zones, material characteristics, and member continuity
- (5) To develop a detailing guide which provides simple models for designing complex details in structural concrete

Objectives (2) and (3) have been reported in detailed in Reports 1127-1 and 1127-2. This report summarizes the efforts to meet objectives (1) and (4) and presents the detailing guide of objective (5). The guide should lead to more consistent, constructible, economical and reliable details.

1.4 Scope

The existing state of knowledge is not sufficient for complete application of the strut-and-tie-model to complex detailing situations. Therefore, the scope of this study was to develop a relatively simple approach to show how a designer can develop a strut- and-tie- model for different applications, to provide some ideas about model optimization in order to be economical and to provide some in-depth understanding of the behavior of singular nodes as affected by their reinforcing and anchorage details. The experimental tests in the accompanying studies (1127-1, 1127-2) included different concrete strengths, degrees of confinement, strut width, reinforcement anchorage details, and strut angles. Also full-sized dapped beams were studied and compared with the possible use of the strut- and tie- model.

Chapters 2 and 3 explain the basis for the strut- and- tie- model used for detailing structural concrete. They present an overview of the proposals developed by various researchers. In particular this study was aimed at providing information about:

- length of the discontinuity zone (D-region)
- model optimization
- dimensioning the nodes
- configuration of the stress field
- allowable concrete stresses or efficiency factor of the nodes
- detailing considerations

Chapter 2 and 3 discuss general principles, components, and modeling techniques as well as dimensioning of the struts, ties and nodes to illustrate the method and facilitate its use. Recent studies about high strength concrete were also included and design provisions evaluated. Suggested Design Specification

language to implement these procedures are provided. Illustrative design aids and design examples are presented in Chapters 4 and in Appendix A.

Chapter 5 summarizes the work and presents conclusions and recommendations. The guide should provide support to the structural designer in an area where current codes and design specifications provide little information.

CHAPTER 2 BACKGROUND

2.1 Concept Background

The strut- and- tie model is a limit analysis approach to the design of structural concrete. More specifically, the strut- and- tie model is a static or lower bound plasticity solution. Marti [27] explains that strut- and tie models represent a possible equilibrium system of forces within a structure at its ultimate load. While the plasticity theory behind the strut- and- tie model is quite complex [56], it is primarily used to establish a rational basis for the method. For most practical applications, it is only necessary to understand that a properly chosen and dimensioned strut - and- tie model represents a lower bound (or conservative) estimate of the true capacity of a structural element assuming other brittle failures such as stability or local crushing are precluded

Although development of detailed mathematical verification for the strut- and- tie- method is unnecessary to understand its application, awareness of the assumptions is important. The most important of these assumptions are:

1. Failure is due to the formation of a mechanism resulting from yielding of one or more ties
2. Crushing of the concrete struts should not occur prior to yielding of the ties. This is prevented by limiting the stress levels in the concrete.
3. Only uniaxial forces are present in the struts and ties
4. All external loads including post- and pretensioning forces are applied at the nodes of the strut- and- tie model. In the case of distributed loads and pretensioned strand loads, the model must be adequately formulated to realistically represent the load distribution
5. The reinforcement is properly detailed so as to prevent local bond or anchorage failure

While strut-and-tie-models can be used in detailing any element of a concrete structure, it generally is more efficient to use traditional methods based on cross-section analysis for proportioning axial, flexural and web reinforcement in constant depth beam, column or slab type structures subject to distributed loading. Irregular shaped zones or zones subject to heavy concentrated loads are logically targets for the application of strut-and-tie-models. For a successful implementation of the strut- and- tie model a classification of concrete structures with respect to their geometry and their load bearing behavior is required. Any concrete structure may be classified by subdividing it (by application of Saint Venant's principle) into D- (Discontinuity) and B- (Bending) regions [28]. (See Fig. 1.4.)

Those specific areas for which the Jakob Bernoulli-hypothesis that a plane section before bending remains plane after bending (linear strain profile or plane strain) applies with sufficient accuracy are identified as B-regions. In the B-regions the elastic principal stresses may be determined directly from the axial, flexural and shear stresses acting on the member.

Any general region in which the strain distribution in the cross-section is substantially nonlinear due to statical and/ or geometrical discontinuities is defined as a D-region.

The following classifications can be made with regard to geometry and loading and used in taking into account the division of B- and D-regions.

- (1) Linear structures are structures with two dimensions considerably smaller than the third (beams, frames). If they are essentially uniformly loaded, they will consist in substantial part of B-regions.
- (2) Plates or deep beams are plane structures with two dimensions considerably larger than the third with loads acting in their plane (walls, thin webs of box girders).

3. Slabs and shells are structures with two dimensions considerably larger than the third with loads acting transverse to their plane or curved middle plane. If they are predominantly uniformly loaded, they will essentially consist of B-regions. Strips taken along the principal moment directions behave and can be treated therefore as linear structures.

If a structure contains B-regions in substantial part, it is usually more convenient to first determine its sectional load effects (M_B , M_T , V , N) by use of conventional elastic analysis.

For uncracked B-regions the internal stresses then can be determined from the sectional load effects by use of cross-sectional values A , I_B , I_T , and the usual laws of mechanics (bending theory). In the case of high compressive stresses the linear analysis of internal stresses may have to be modified by replacing Hooke's law with one of the nonlinear material laws. For cracked B-regions the internal forces are generally determined from the cross-sectional load effects by application of the standard truss or ordinary cracked reinforced concrete theory. In B-regions the use of truss models or of strut- and- tie- models will often be more complex than required.

The forcepaths or the struts and ties of the D-regions can be determined from the loads applied to the D-regions by equilibrium analysis. If a structure or member consists of only one D-region, the analysis of sectional effects by a conventional structural analysis may be omitted and the internal forces or stresses may be directly determined from the applied loads. If the structure is externally statically indeterminate, the internal compatibility of stresses should be considered by first orienting the geometry of the model to the pattern of forces indicated by the results from a conventional elastic analysis and then possibly reorienting it thereafter according to the major design intent: emphasis on ultimate load capacity or on serviceability under working loads.

Table 2.1 summarizes the above statements.

Table 2.1: Analysis usage

	B-regions	D-regions
analysis	sectional analysis	direct
material behavior	linear or nonlinear	nonlinear
state I = uncracked	sectional values	elastic stress analysis
state II = cracked	conventional reinforced concrete analysis or truss model	strut- and- tie- model or nonlinear analysis

It is usually most convenient to orient the geometry of the strut- and- tie models to the general pattern of load paths traced by the forces passing through the member. These load paths can be determined from intuition, experience, or in unusual cases by examining the elastic stress fields indicated by a finite element analysis. Design of B-regions is accomplished by ordinary cracked reinforced concrete theory or by using a special type of strut- and- tie model which is generally termed the truss analogy. In the truss model for a simply supported beam the upper horizontal chord represents the concrete compression zone. The lower horizontal chord represents the main tension reinforcement. The stirrups of the beam are lumped together as the truss vertical members. Inclined compression struts are used to represent the continuous inclined compression fields in the web of the beam. The strut- and- tie model is proposed as a generalization of the truss analogy applicable to a variety of design situations.

The truss analogy is a specialized form of the strut- and- tie model and can be used exclusively in the design of B-regions. Other types of models which apply to the wide range of D-regions occurring in the structure are then lumped under the more general category of strut- and- tie- models.

2.2 Isolate Discontinuity or Detail Region: D-region

For the majority of structures it would be unreasonable and inefficient to model the entire structure with a strut and tie model. Rather, it is a more convenient and common practice to first carry out a general structural analysis. The general elastic analysis of linear structures results in determination of external support reactions. Then, from equilibrium methods, sectional effects (bending moment M_B , normal forces N , shear forces V , and torsional moments M_T) can be determined at any desired section.

It is advantageous to subdivide the given structure into B-regions and D-regions. In order to roughly find the division lines between B- and D-regions, the following procedure was proposed by Schlaich et al. [2]. It utilizes the well known principle of Saint Venant which localizes the effect of concentrated forces as shown in Fig. 2.1. This procedure is illustrated in the examples of Fig. 2.2.

1. Replace the real structure (a) by the fictitious structure (b) which is loaded in such a way that it complies with the Jakob Bernoulli hypothesis and satisfies equilibrium with the sectional forces. Thus, (b) consists entirely of one or several B-regions. It usually violates the actual boundary conditions.
2. Select a self-equilibrating state of stress (c) which, if superimposed on (b), satisfies the real boundary conditions of (a).

d = distance between the self-equilibrating forces

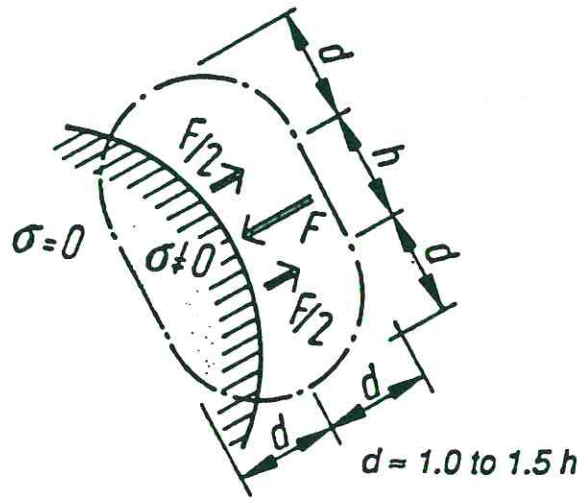


Figure 2.1: The principle of Saint Venant (from Ref. [28])

Column

Beam

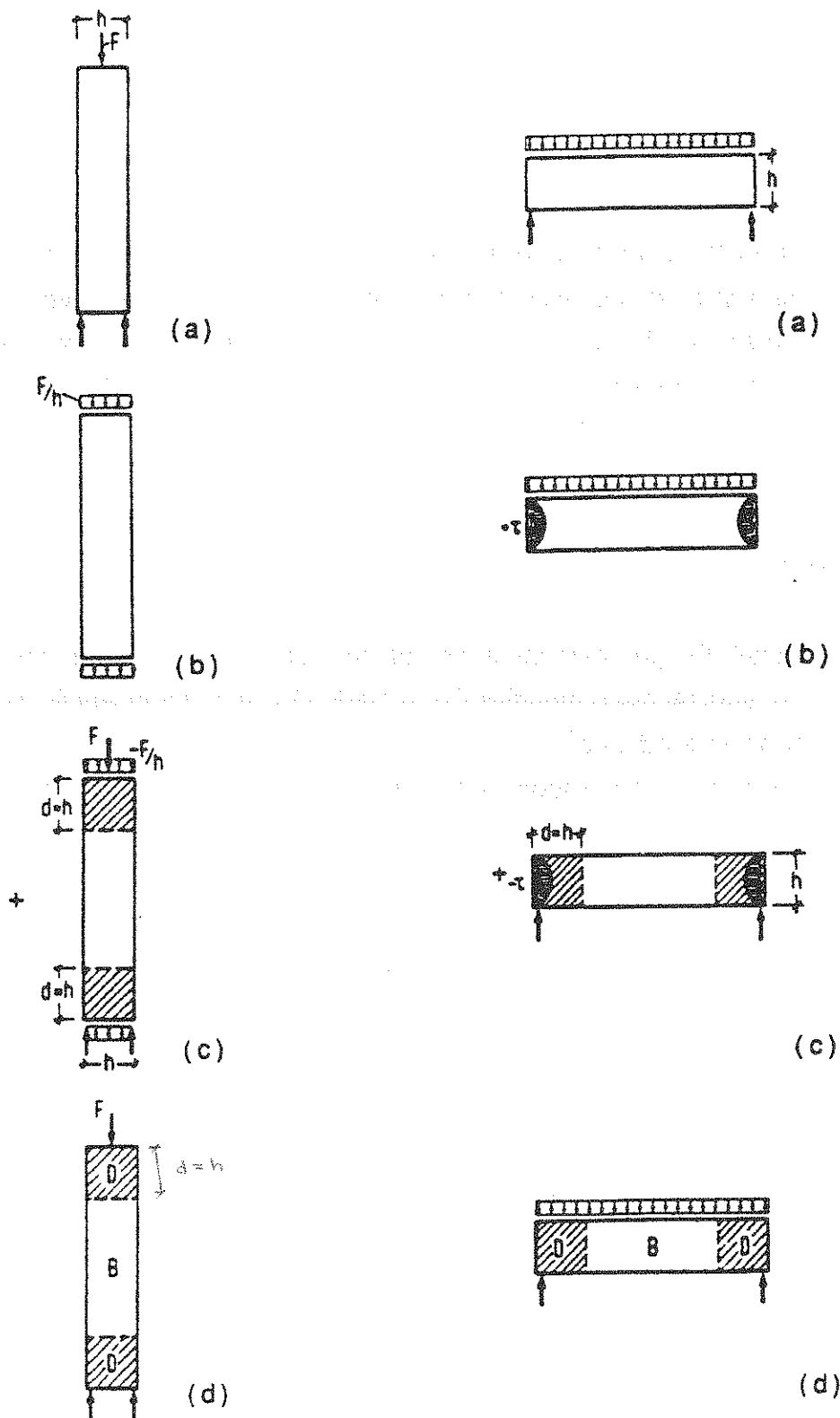


Figure 2.2 Subdivision of structures into B and D regions using Saint Venant's principle (from Ref. [28])

3. Apply the principle of Saint-Venant to (c) so that the local stresses may be assumed negligible at a distance "d" from the equilibrating forces, which is approximately equal to 1.0 to 1.5 of the maximum distance between the equilibrating forces themselves. This distance defines the range of the D-region (d).

For practical applications the following approaches illustrated in Fig. 2.3 are suggested:

- (1) Isolate the geometrical or the statical discontinuity regions (zone 1)
For statical discontinuities this is basically the point of application of concentrated loads
For geometrical discontinuities these are the end points of the irregular zones: end of an opening, corner line, etc.
- (2) Combine overlapping areas of the statical and geometrical discontinuities (zone 1 in Fig. 2.3)

- (3) Add additional lengths (zone 2) equal to $1.5 h$ or h' on both sides of the previously isolated discontinuity zone
- (4) Assume that the total area of zone 2 + zone 1 + zone 2 is the effective D-region

The discontinuity region boundaries may also be determined by the use of stress trajectories (contours of principal stress). For theoretical purposes, the D-regions end where the stresses introduced by the discontinuities are negligible or where the strain distribution is linear. Between the D-regions the stress distribution is essentially uniform and regular. The linear strain profile assumption of Jakob Bernoulli is applicable (B-region).

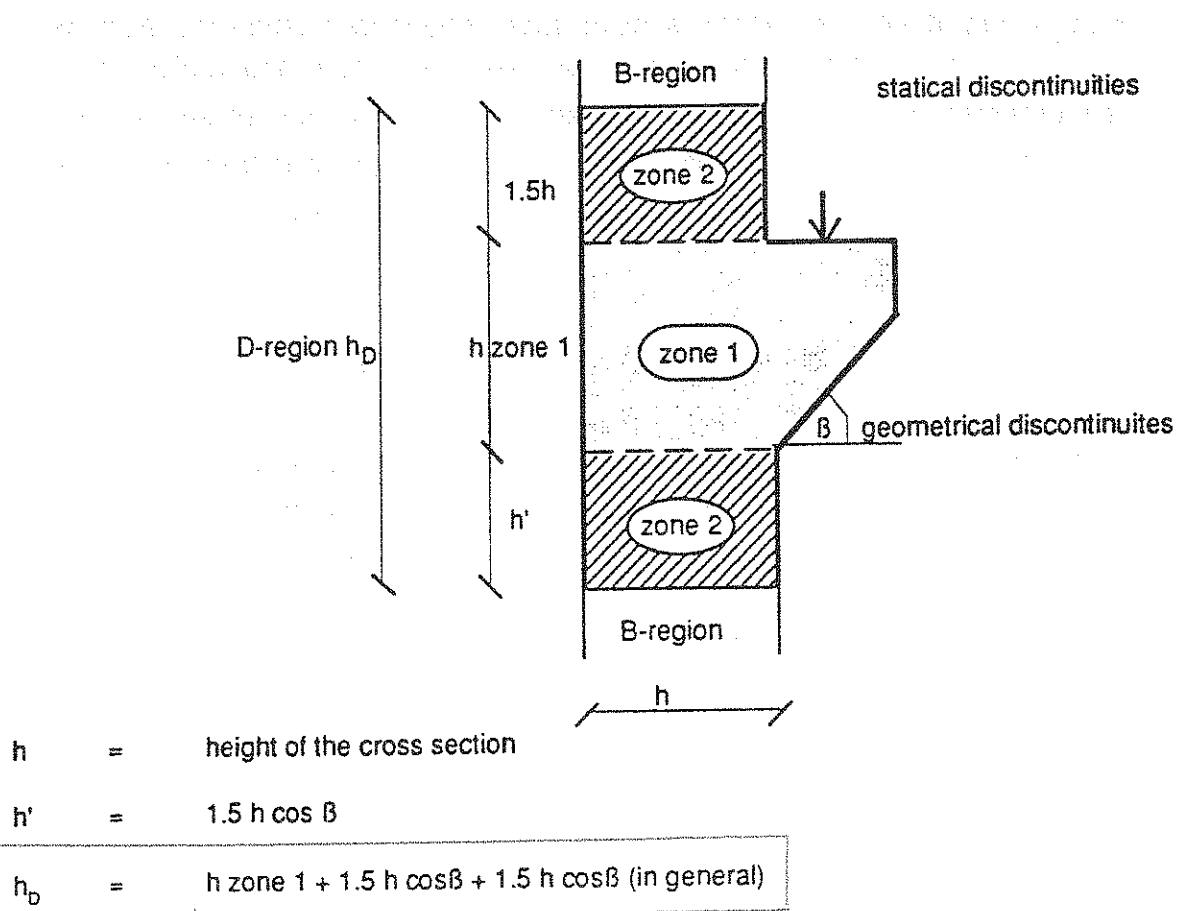


Figure 2.3: Suggested subdivision of structure

2.3 Elasticity Analysis Method vs. Load Path Method

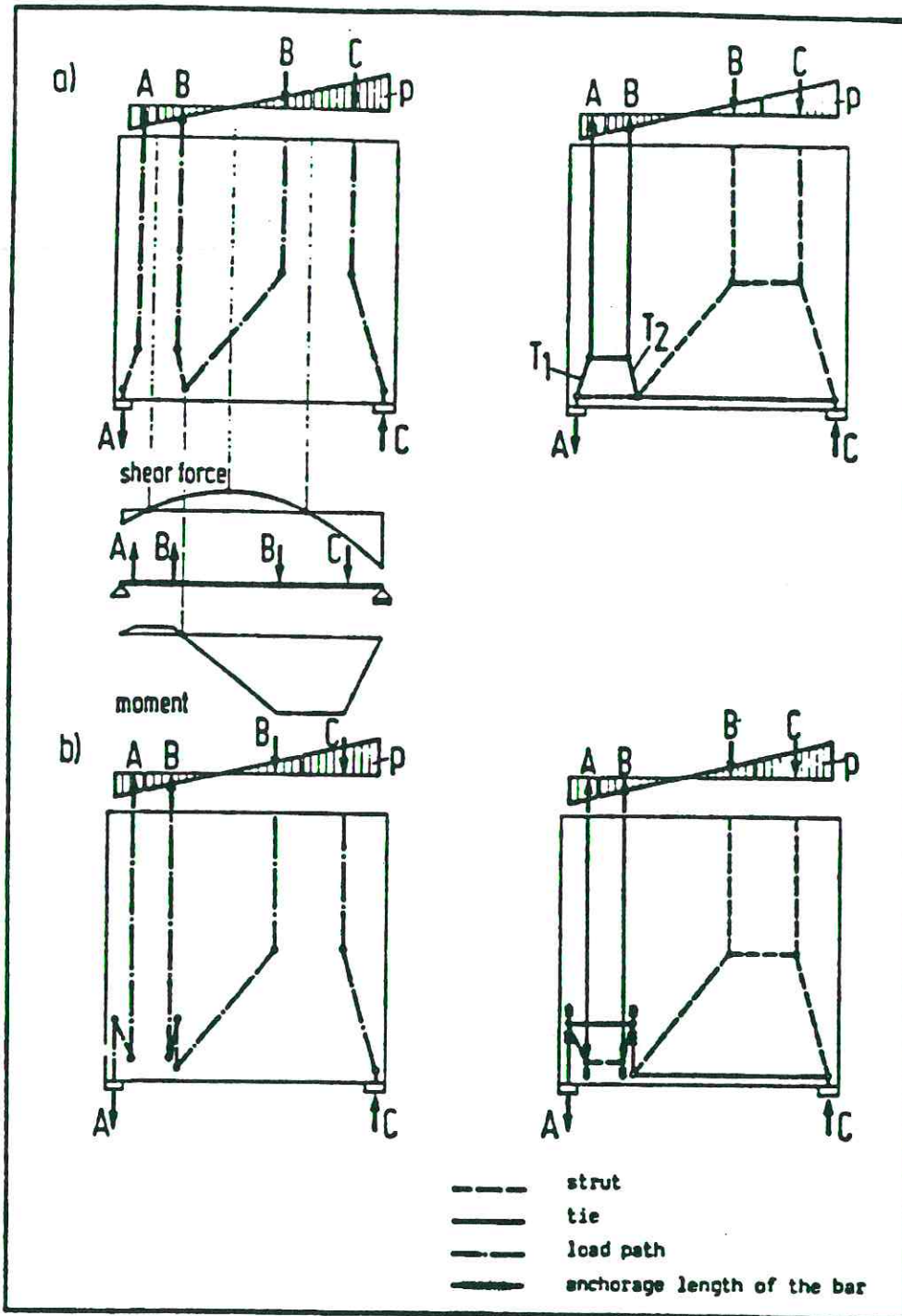
For the D-regions it is necessary to develop an individual strut- and- tie- model for each application. For very unusual configurations as well as to ensure good crack control behavior at service stress levels, it is recommended that the model should be generally based on the principal stress pattern as determined from an elastic analysis . For unusual cases such an elastic analysis with the principal stress direction can be computed with an elastic finite element program. The directions of the struts and ties can be located at the center of gravity of the corresponding stress fields. It usually makes it more convenient if the principal stresses are converted to stresses parallel to the structural member borders (σ_x , σ_y , τ_{xy}). A strut- and- tie- model based on such orthogonal elastic stresses chosen parallel to the concrete surface generally leads to more economical straight reinforcement layouts. As a general approach, the reinforcement should be arranged parallel and/or normal to the concrete surface and take into account the requirements of controlling possible inclined crack propagations by inclined bars when needed.

If such elastic analyses are inconvenient or when the general form of the solution is known from experience, the strut- and- tie- model can also be formulated by tracing the so called "load paths". The outer equilibrium of the D-region must be satisfied by previously determining all the loads and reactions acting on it. For a boundary adjacent to a B-region, the loads on the D-region are taken from the B-region analysis. The following approach can be used in order to determine the load paths (see Fig. 2.4).

- (1) Compute the elastic stress resultants or ordinary cracked reinforced concrete forces for the B-region and apply the equivalent forces to the D-region.

- (2) Subdivide the discontinuity zone into regions in such a way that the loads on one side of the discontinuity zone are in unique regions with their counterpart on the other side of the discontinuity zone. These regions are the load paths connecting the opposite sides and tend to take the shortest possible streamlined way across.
The load paths must be single lines and must not cross each other.
- (3) If the applied forces are not completely equilibrated with the obvious load paths, then the resulting loads must follow a U-path as shown for B-B in Fig. 2.4.
- (4) Sketch all load paths (including possible U-paths) and replace them by polygons made up of compression struts and tension ties.
- (5) Add further struts and ties as required for equilibrium at the nodes.
- (6) If necessary rearrange the struts and ties with consideration of practicality of the reinforcement layout.

For very complicated cases, the finite element analysis results can also be combined with the load path method.



Two models for the same case: (a) requiring oblique reinforcement; (b) for orthogonal reinforcement.

Figure 2.4: Load path method with "u-turn" (from Ref. [28])

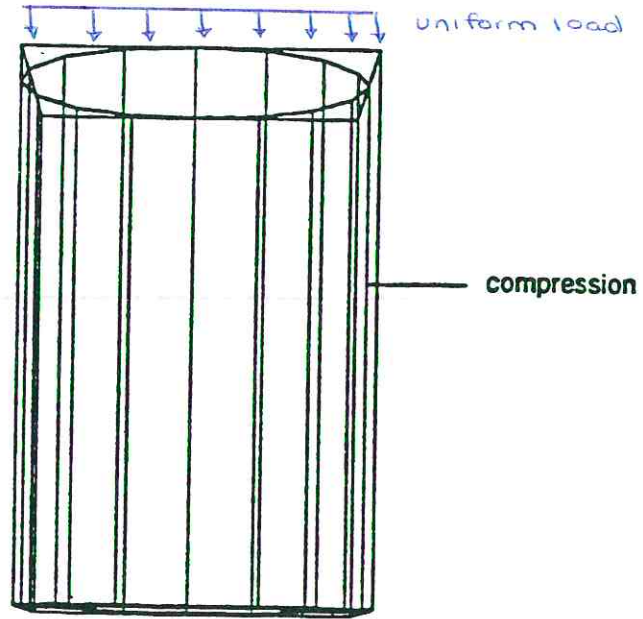
2.4 Strut Background

The struts transfer internal compression forces from node to node. In general this transfer is via three-dimensional stress fields in the concrete. Due to compatibility requirements the stress fields tend to spread out between the nodes and fill the available space. This results in transverse tensile and compressive stresses which must be considered in the evaluation of a strut's strength and which may require provision of local reinforcement (see Fig. 2.5). However, well tied compression reinforcement will also resist compressive forces as long as it is restrained from buckling. While all concrete structures must be built and reinforced in three dimensional space, it is usually sufficient to determine reinforcement separately in two orthogonal planes. This leads to consideration of two dimensional or planar struts.

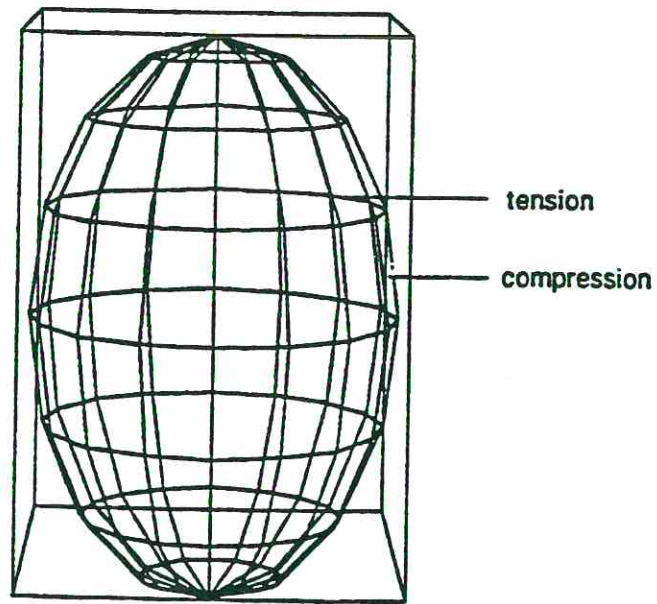
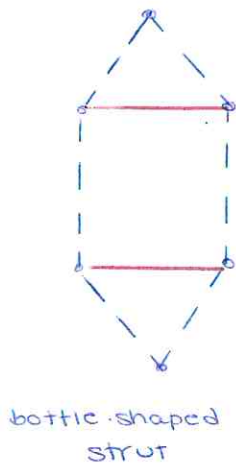
Four typical configurations of two dimensional compression fields are presented in Fig. 2.6. Generally it is safe to determine the strength of compression struts using one of the four simplified types of stress fields shown in Fig. 2.6 (a) to (d).

A prismatic strut as shown in Fig. 2.6 (a) is the simplest idealization of a compressive stress field. The prism is uniform in geometry and has a constant stress along its length. Prisms are generally used to model stress fields having uniform parallel stress trajectories.

The fan shaped stress fields shown in Fig. 2.6 (b) are developed at points of concentrated loading or at supports. Fig. 2.7(a) illustrates a fan region incorporating a series of trapezoidal struts which act to distribute force to several stirrups.

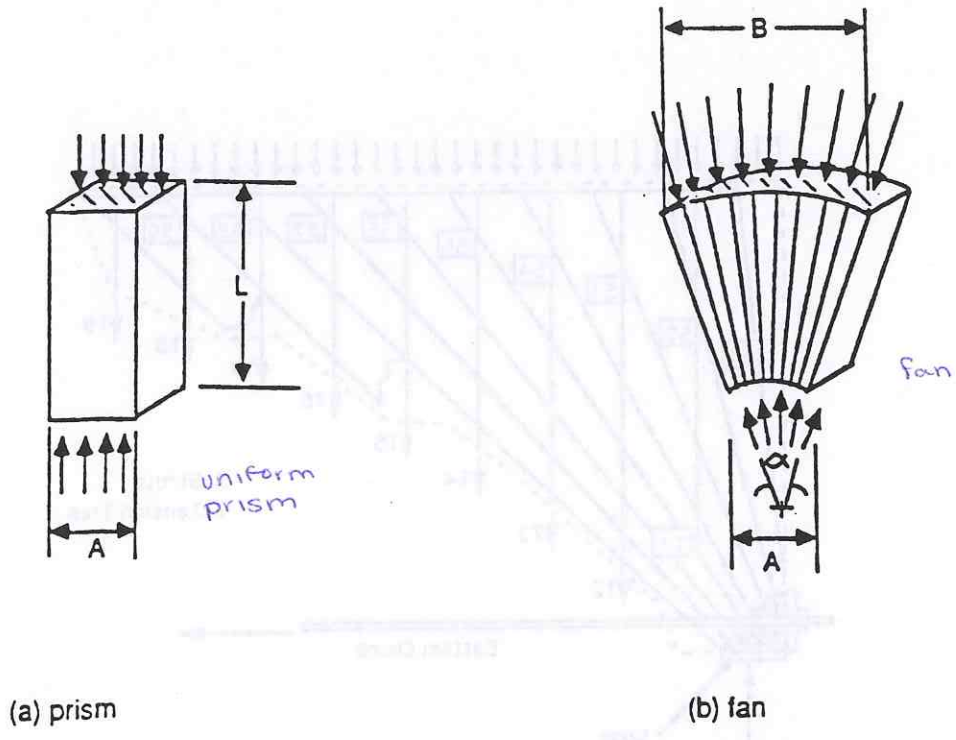


(a) compression only



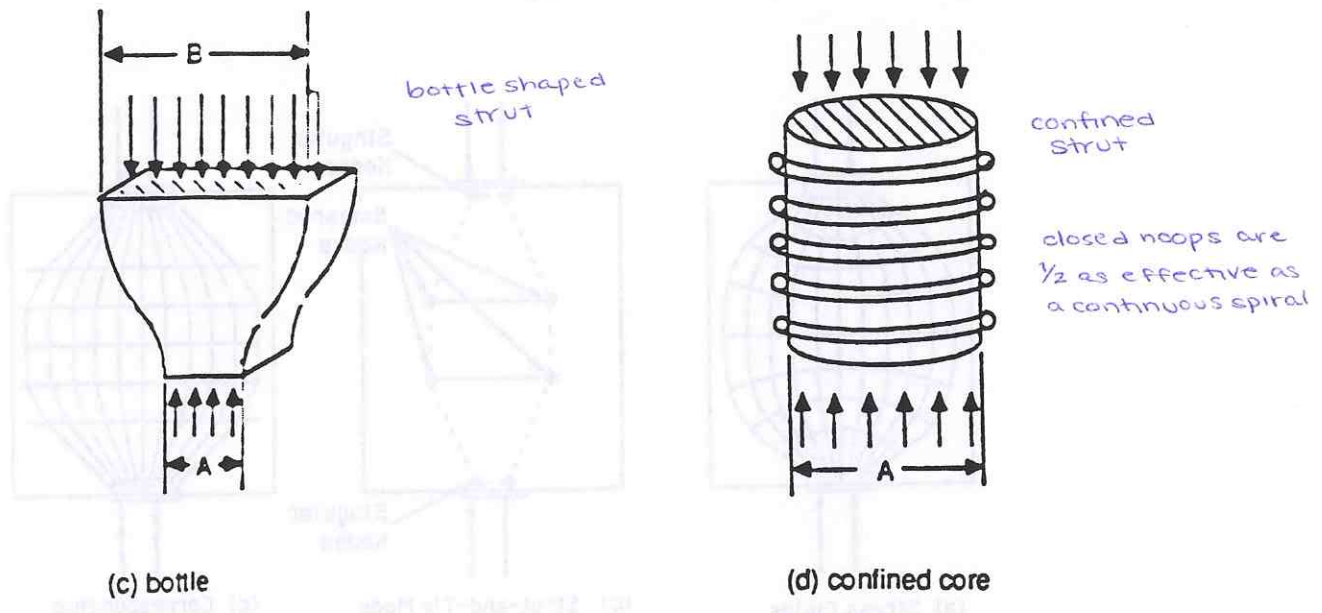
(b) real state of stress: compression and tension

Figure 2.5: Planar stresses in prism under compression



(a) prism

(b) fan



(c) bottle

(d) confined core

Figure 2.6: The basic compression fields (from [2])

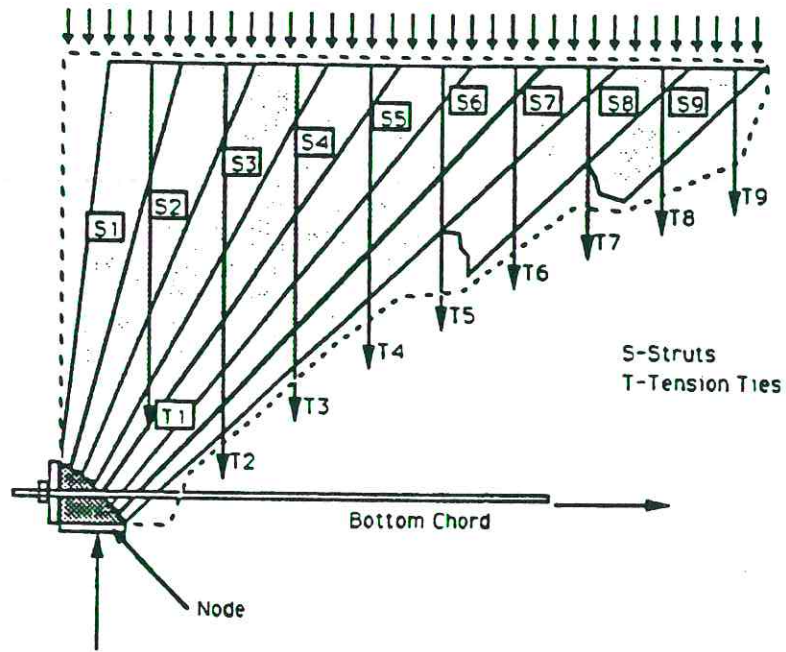


Figure 2.7(a): Fan region at beam support

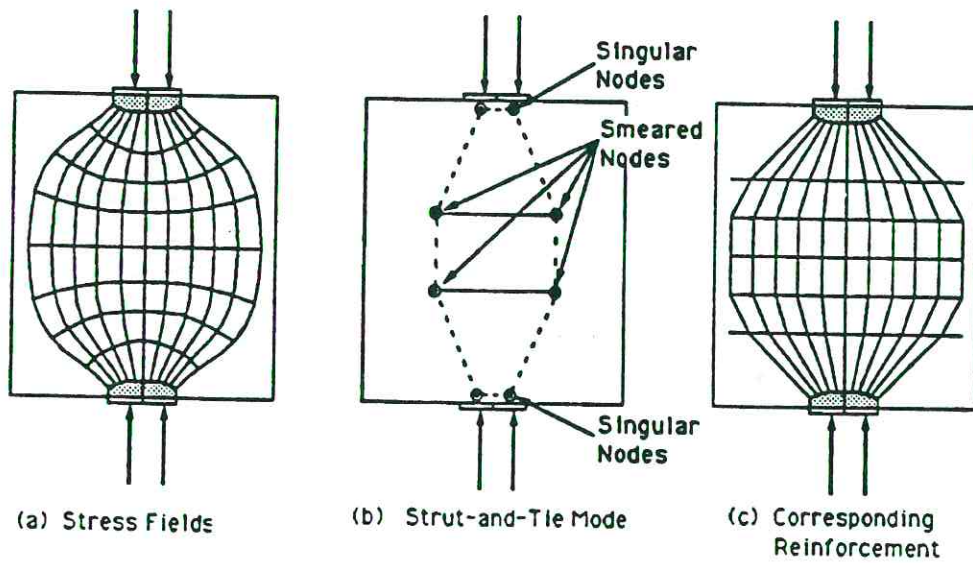


Figure 2.7(b): Bottle shaped struts

In some cases, as a corollary to the trend of stress fields widening between loads, a stress field may tend to narrow near points of application of concentrated loads or at supports. This can be modelled by using a bottle shaped strut (Fig. 2.6(c)). The increase in strut width induces tensile stresses normal to the longitudinal axis of the strut. This tensile stress must either be resisted by transverse reinforcement or by the tensile strength of the concrete in order to prevent cracking. Fig. 2.7(b) shows a bottle shaped strut represented by a secondary strut- and- tie model for the analysis and provided with local transverse reinforcement to properly develop the required tie forces. The confined core of Fig. 2.6 (d) is a transversally reinforced core or prism with a special behavior. The reinforcement can be spirals, closed stirrups or steel pipe. The reinforced core develops under load a three dimensional state of stress, which is controlled by the behavior and the form of the reinforcement and the transversal contraction of the concrete. It is generally restricted to points of application of very large magnitude forces or relatively small areas as when post-tensioned tendons are anchored or when extremely large loads are applied by columns bearing on a transfer girder.

2.4.1 Concrete compressive strength limitation for struts

In recent years the useful range of concrete compressive strengths in highway applications has exceeded 12000 psi. Most empirical equations for concrete structures now in standards such as the AASHTO Specifications [3] were derived using results from tests having concrete compressive strengths less than 6000 psi. Extrapolating such empirical equations for concretes with twice the compressive strength of those used in the original formulation can be dangerous or uneconomical. In this study the proposed efficiency factors for concrete compressive strength should be applicable to values up to 12000 psi. Many different test results of high strength concrete specimens were included in the study. For background a brief literature review on pertinent information concerning high strength concrete is included.

High strength concrete requires extreme care in all steps of the production process. It has become common practice to specify high strength concrete strengths at 7, 28, 56, or 90 days [57, 58]. Economically it is important to know at the outset of high strength concrete production specifically what strength one needs and when one needs it. High strength concrete requires a very low water to cement ratio ($\approx 0.25 - 0.45$). Therefore, inaccurate estimation of the aggregates water content, which affects the quantity of additional water added at batching, can result in either balling of the concrete due to lack of mixing water or in too high a slump. Mixing is critically important as well. For satisfactory performance all the materials, especially admixtures, must be thoroughly mixed. Curing becomes more critical in high strength concrete production and proper hydration must be allowed to prevent shrinkage cracking.

The tensile strength is significantly linked to the curing conditions. The following relations (concrete compressive strength between 7310 and 10040 psi) were given in Ref. [33] with a 10% coefficient of variation:

$$f_{ct} = 13.3 (f'_c)^{0.5} \quad \text{moist cured}$$

$$f_{ct} = 7.9 (f'_c)^{0.5} \quad \text{dry cured}$$

The compressive strength of the aggregate has a major effect on the strength of high strength concrete. The aggregate must be sufficiently strong to allow higher concrete strength. Tests reported in [33] indicated that the failure breaks were going through the aggregate without bond failure. This proved that the coarse aggregate has a major effect on the strength of high concrete strength. The physical properties of high strength concrete tend to be somewhat different than for normal strength concrete. The slope of the stress-strain curve is steeper and more linear up to about 80% of ultimate capacity (see Fig. 2.8). The descending branch of the high strength concrete stress-strain curve is steeper.

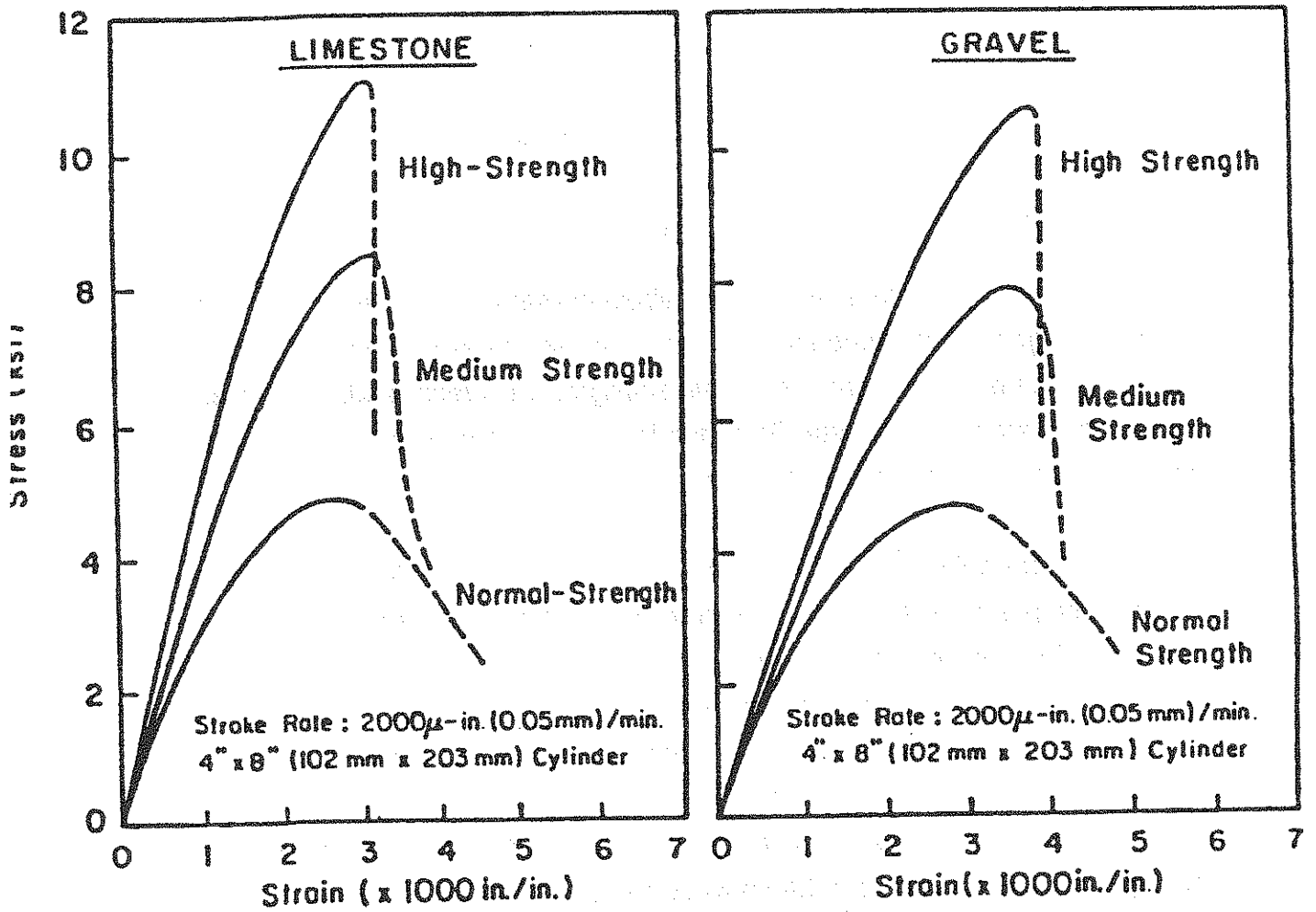


Figure 2.8: Stress-strain curves for low, medium and high strength concrete (from Ref. [59])

It has been stated that the descending branch becomes almost a vertical line. The ultimate strain at failure is lower than for moderate strength concretes. The steeper stress-strain curve for high strength concrete means the modulus of elasticity is higher. The following equation for the modulus of elasticity has been proposed [59]:

$$E_c = (40000) (f'_c)^{0.5} + 1.0 \times 10^6 (w/145)^{1.5}$$

w = unit weight of concrete (≈ 145 pcf)

The total shrinkage at later ages is about the same as for medium strength concrete. High strength concrete does, however, see more of its total shrinkage at early ages than does normal concrete strength. Unit creep tends to be much lower in high strength concrete. Given the fact that it is stressed to higher stress levels, total creep stays about the same.

Considerable research has been conducted in effort to determine the limiting compressive stress for concrete in compression struts in structural members. Because of cracking, aspect ratios other than the value of 2 found in standard cylinder tests, and the presence of strain gradients, the value of compressive strength found in a cylinder test may not be appropriate for the compressive strut in a structural member. Much of this work has focused on thin webs of beams which is a critical case. Empirical relations for the compressive strength of concrete struts in beam webs as suggested by, Nielsen et al. [21], Ramirez and Breen [23], Thürlimann [60], Collins and Mitchell [61] and MacGregor [62] are summarized in Fig. 2.9.

Several factors influence the value of the effective concrete strength in a diagonal concrete strut. Due to the fact that the stirrups cross the diagonal tension cracked concrete, the diagonal concrete strut is then in a biaxial state of stress (Compression-Tension) which reduces its compressive strength. Another

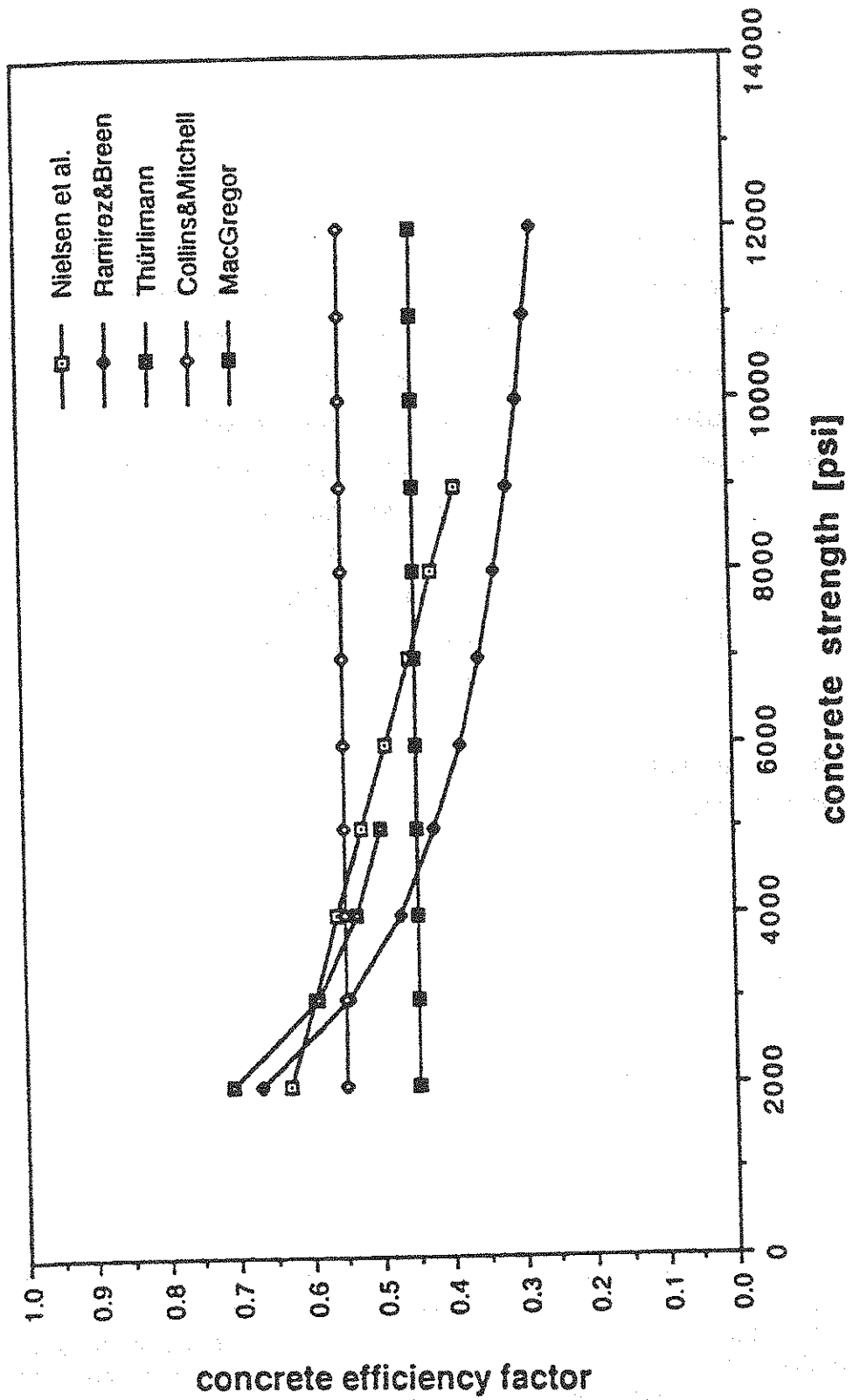


Figure 2.9: Relationship of diagonal concrete strut efficiency factor versus concrete strength

factor is that the redistribution of forces in the member due to the different ratios of longitudinal to transverse reinforcement may cause the failure crack and the compressive struts between them to be at an inclination other than the 45 degree angle corresponding to initial diagonal tension cracking of the concrete. Thus the strut may be crossing previously cracked concrete. Another important factor is the need to select a very conservative value due to the undesirability of a failure due to crushing of the concrete in the web because of its brittle nature. In general, the effective concrete strength available for use in the struts is chosen as some portion of the concrete compressive strength f'_c . The effective strength f'_c is the product of an efficiency factor v_e and the 28 day cylinder compressive strength. The efficiency factor should take into account the following parameters:

- multiaxial state of stress
- disturbances from cracks
- disturbances from reinforcement
- confining reinforcement
- friction forces
- aggregate interlock after cracking
- dowel forces
- time dependence

$$f'_{ce} = v_e f'_c$$

Various proposals for the efficiency " v_e " factor have been presented. They are usually based on tests of continuous compression fields either in rather thin web beams or rather thin shear panels although some seem to be based largely on engineering judgement. Very little experimental verification exists for effective compressive stress efficiency factors for use in model analysis or for use in large panels where shear is not a major concern. Many of the various proposals for the efficiency factor are summarized in this section. They basically correspond to the product of a basic efficiency factor and a modifier to make them applicable to thin webs although this distinction is not always shown by the various authors. Another factor considered by some authors was the fact that in the case of torsion the twisting of the beam induces an additional compression stress into the diagonal. Lampert and Thurlimann [14] stated that the increase in the diagonal compression test was due to a distortional effect in the walls of the cross

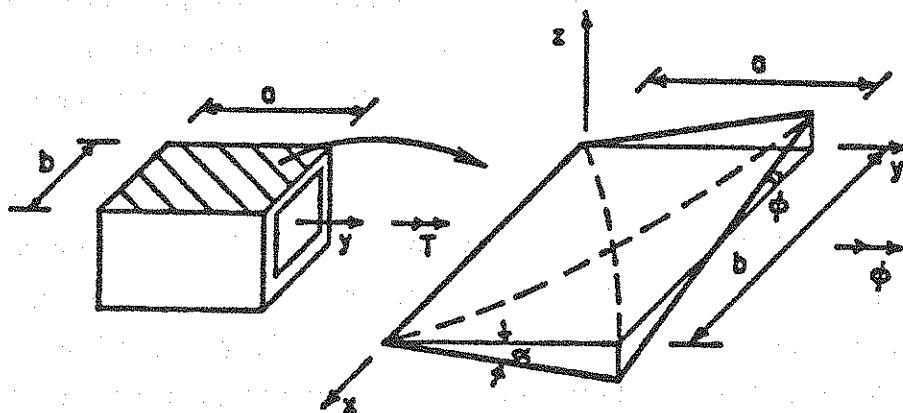


Figure 2.10: Distortional effect (from Ref.[23])

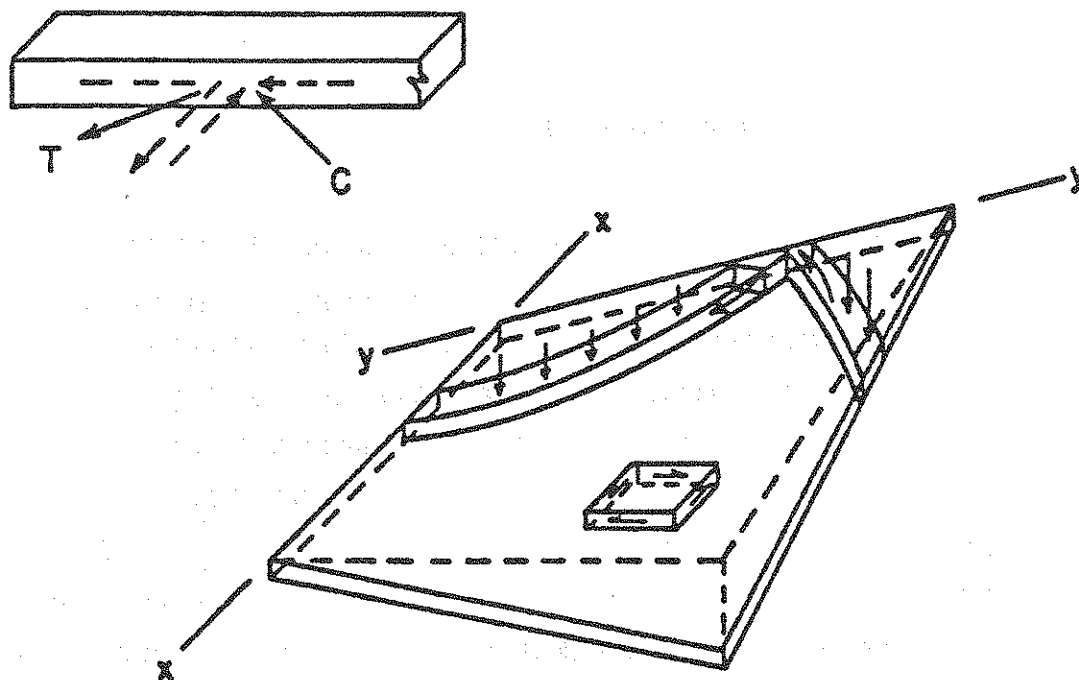


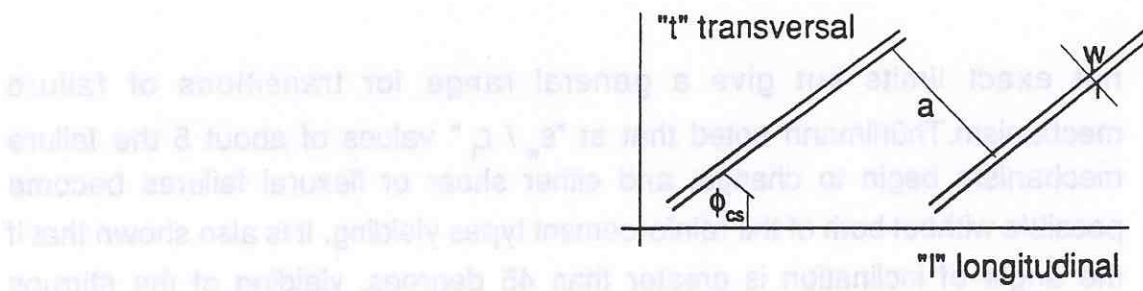
Figure 2.11: Forces acting on edge members of parabolic arches (from Ref. [23])

section. Through twisting, the originally plane walls of the section are distorted to hyperbolic paraboloids (Fig. 2.10) limited by four straight edges. The distorted wall then constitutes a hyperbolic paraboloid shell subjected to a uniform shear flow. The entire shell when loaded in this fashion is subjected solely to pure shear stresses of constant intensity (see Fig. 2.11). These edge shears require edge members. In the case of truss models these edge members are provided by the longitudinal chords which are thereby loaded axially. The additional compressive stresses on the outer surface of the diagonal due to wall distortion must be added to those obtained from the actual shear flow. As a result Thürlimann [60] suggests that the maximum value of the compression strength in diagonal compression struts used be approximately 2400 psi, corresponding to f'_c of about 4800 psi. Thürlimann [60] on the basis of test evidence proposed that the allowable efficiency factor for the compression stress be:

$$v_e = 0.36 + 696 / f'_c \text{ [psi]} \quad f'_c \leq 4800 \text{ psi}$$

This upper limit should prevent a premature failure.

Additionally a limit is placed on the inclination of the concrete compression strut " ϕ_{cs} ", and thereby on the amount of redistribution of internal forces. The flow rule or failure mechanism is uniaxial yielding of the reinforcement opening up the final cracks perpendicular to the crack direction (see Fig. 2.12). Finally the reinforcement is assumed to be properly detailed so that no local failures are possible. As shown in [56], within the limits for the angle of inclination of the diagonal compression strut ($26.5^\circ \leq \phi_{cs} \leq 63.5^\circ$ see Fig. 2.13), the average diagonal compression stress can be controlled by limiting the nominal shear stress independently of the inclination ϕ_{cs} of the compression diagonals. From Fig. 2.13, it can be seen that if the compression struts are inclined at 45 degrees, the mean crack strain and hence the mean crack width are at the minimum value for yielding of both the longitudinal and transverse reinforcement. The values are



$$w = a \epsilon_w$$

$$\epsilon_w = \epsilon_l (1 + \tan^2 \phi_{cs}) \text{ (yielding of transversal reinforcement)}$$

$$\epsilon_w = \epsilon_l (1 + \cot^2 \phi_{cs}) \text{ (yielding of longitudinal reinforcement)}$$

Figure 2.12: Mean crack strain (from Ref. [56])

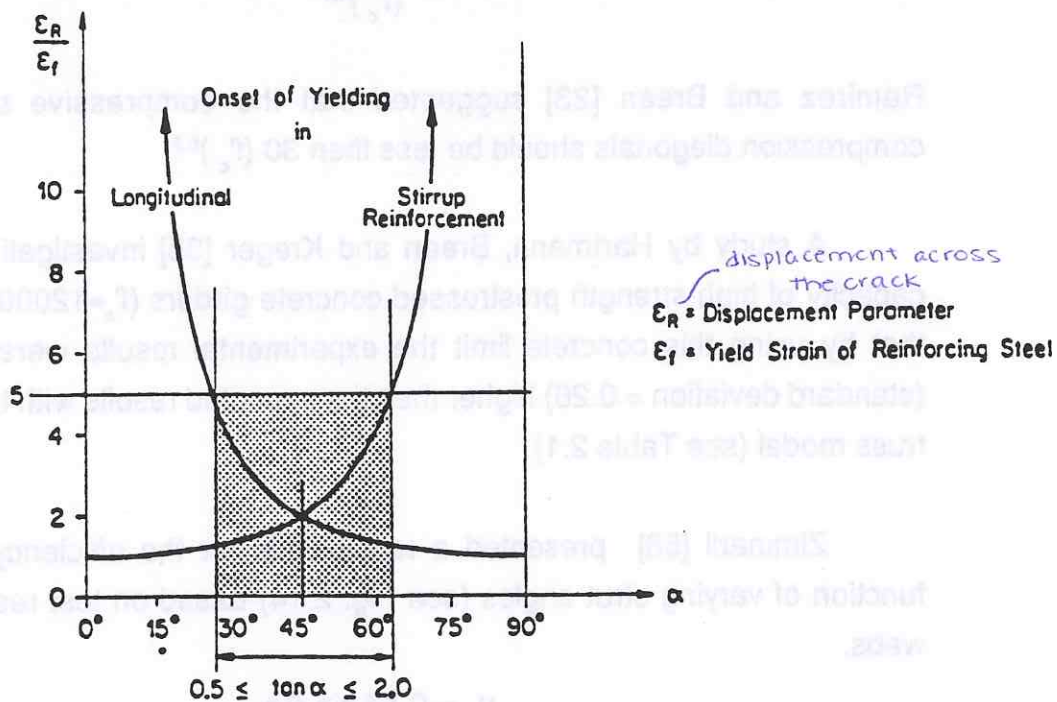


Figure 2.13: Relationship between the mean crack strain and the strains in the reinforcement for different angles of inclination of the diagonal strut (from Ref. [61])

not exact limits but give a general range for transitions of failure mechanism. Thürlimann noted that at " ϵ_w / ϵ_1 " values of about 5 the failure mechanism begin to change, and either shear or flexural failures become possible without both of the reinforcement types yielding. It is also shown that if the angle of inclination is greater than 45 degrees, yielding of the stirrups demands larger mean crack strains. Conversely, for angles less than 45 degrees, yielding of the longitudinal reinforcement requires increasingly larger crack openings.

A best fit curve of the form $k (f'_c)^{0.5}$ to approximate the equation proposed by Thürlimann resulted in the relation [23]):

$$v_e = \frac{34}{(f'_c)^{0.5}} \quad [\text{psi}]$$

Ramirez and Breen [23] suggested that the compressive stress in the compression diagonals should be less than $30 (f'_c)^{0.5}$.

A study by Hartmann, Breen and Kreger [33] investigating the shear capacity of high strength prestressed concrete girders ($f'_c \approx 12000$ psi) showed that by using this concrete limit the experimental results were 1.72 times (standard deviation = 0.26) higher than the expected results with the 45 degree truss model (see Table 2.1).

Zimmerli [56] presented a relationship for the efficiency factor as a function of varying strut angles (see Fig. 2.14) based on test results of beam webs.

$$v_e = 0.83 \sin 2 \phi_{cs}$$

ϕ_{cs} = angle between the tie and the strut
 f'_c = $0.7 f'_{cc,5\%}$ (5% fractile cube compressive strength)

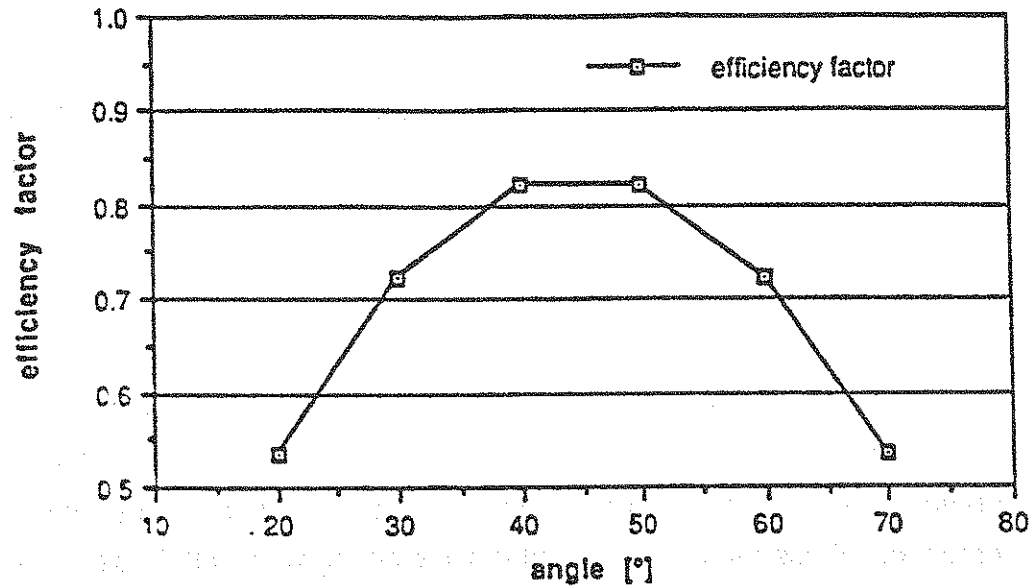


Figure 2.14: Varying strut angle versus efficiency factor for concrete compression strength

It was assumed that for an inclination of 45 degrees the effective concrete strength for the principal compression strut would be $5/6$ of the normal concrete strength (f_c). The decrease of the efficiency factor for other angles is based on the changed angle between the compression strut and the principal stress direction.

Collins and Mitchell [61] suggested that the limiting value of the average principal compressive stress in the diagonal concrete strut is governed not as much by the compression strength of the uncracked portions of the strut as by the capacity of the interface shear transfer mechanisms, such as aggregate interlock, to transmit the required shear stress across previously existing cracks.

The principal factors affecting the aggregate interlock are:

- quality of the concrete. Usually the top part of a member, because of the particle sedimentation and water gain under the coarse aggregate will contain weaker concrete
- crack width
- aggregate strength

Tests by Paulay and Loeber [63], in which the crack width increased proportionally with the applied load, verified that the stiffness of the aggregate interlock mechanism gradually decreased as the shear across the interface increased. Since the aggregate interlock disintegrates with large crack widths, and the mechanism of shear transfer in the diagonally cracked concrete is largely dependent on the aggregate interlock, it is apparent that the maximum compressive stress that the diagonal strut can take will be a function of the angle ϕ_{cs} .

Nielsen et al. [21] at the Technical University of Denmark applied a rigid plastic model for the concrete based on the modified Coulomb failure criteria. With the assumption of only plane stresses the model gives a square yield locus with a compressive yield stress of f'_c and zero tensile capacity. Based on experimental results an effectiveness parameter for concrete strength in the webs was suggested. Nielsen et al. [21] described the experimental facts by means of an empirical formula of the type

$$v_e = f_1(\sigma_c) f_2(h) f_3(\mu) f_4(a/h)$$

$$f_1(\sigma_c) = 42 / (\sigma_c)^{0.5} \quad 725 \leq \sigma_c \leq 8700 \text{ psi}$$

$$f_2(h) = 10.6 (1 + 0.16 / (h)^{0.5}) \quad 3 \text{ in.} \leq h \leq 27.5 \text{ in.}$$

$$f_3(\mu) = 0.15 \mu + 0.58 \quad \mu \leq 4.5\%$$

$$f_4(a) = 1.0 + 0.17 (a/h - 2.6)^2 \quad a/h \leq 5.5$$

$$f_5(\sigma_{\text{eff}}/\sigma_{0.2}) = 1.1 (1.0 + 0.81 (\sigma_{\text{eff}}/\sigma_{0.2})) \quad \text{for prestressing}$$

σ_c = compressive stress in concrete

$\sigma_{0.2}$ = steel stress at 2000 micro-strain in the prestressing bar

σ_{eff} = effective prestress stress

a = length of shear span

h = depth of beam

μ = $A_s / (b h)$

A_s = longitudinal reinforcement

b = web width of beam

The analysis included 186 test results from normal reinforced rectangular beams and 19 rectangular prestressed beams without shear reinforcement. The statistical parameters of the ratio between the experimental and the calculated v_e - values are presented in Table 2.2.

Table 2.2: Statistical parameter for shear tests from [21]

	mean value	coefficient of variation
normal reinforced	1.0	14.5%
prestressed	1.0	8.6%

For design Nielsen et al. [21] recommended the use of the conservative straight line expression

$$v_e = 0.7 - f'_c / (28997) \quad [\text{psi}] \quad f'_c \leq 8700 \text{ psi}$$

Limits are also placed on the angle of assumed strut inclination to prevent too large a deviation from elastic behavior.

$21.8^\circ < \phi_{cs} < 45^\circ$: beams with constant longitudinal reinforcement

$26.5^\circ < \phi_{cs} < 45^\circ$: beams with curtailed reinforcement

Mitchell and Collins [19] and the Canadian CSA-Standard A 23.3-M84 [29] presented a more detailed method for determining the limiting stress in compression struts based on results of tests on shear panels. (See Fig. 2.15.)

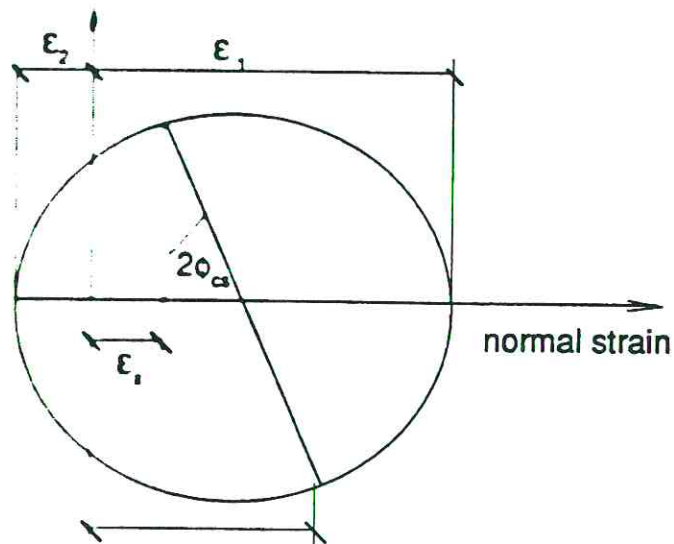


Figure 2.15: Mohr's circle

The principal strain may be determined based on Mohr's circle of strain using the strut angle, principal compressive strain and the strain parallel to the beam axis. The efficiency factor is related to the principal tensile strength along with the cylinder compressive strength.

$$v_e = \frac{1}{(0.8 + 170 \epsilon_1)}$$

ϵ_1 = principal tensile strain normal to the principal compressive stress

Mitchell and Collins [61] assumed that the principal compressive strain (ϵ_2) in the strut is generally - 0.002 and the principal strain direction is assumed to coincide with the principal stress direction. The principal tensile strain in the tie ϵ_1 can be computed by compatibility as follows:

$$\epsilon_1 = \epsilon_x + (\epsilon_x + 0.002) / \tan^2 \phi_{cs}$$

ϕ_{cs} = angle between the tie and the strut

The strain ϵ_x for the reinforcing bar can be conservatively taken as f_y / E_s . Table 2.3 summarizes the recommendations for the efficiency factor from CSA (see also [61])[29] and [62]

$$f_{ce} = v_e f'_c 0.6$$

f'_c = specified compressive strength

f_{ce} = the factored concrete strengths used in checking ultimate limit state

0.6 = partial safety factor = $\frac{1}{1.667}$

(somewhat similar to the ACI and AASHTO ϕ factor)

Table 2.3: Efficiency factor proposed in the CSA [29] and by Macgregor [62]

Structural member	v_e [29]	v_e [62]
Truss nodes:		
Joints bounded by compressive struts and bearing areas	0.85	0.85
Joints anchoring one tension tie	0.75	0.65
Joints anchoring tension ties in more than one direction	0.6	0.50
If the tie reinforcement is anchored by bearing against metal plates at the back of the nodal zone, then	0.85	/
Isolated compression strut in deep beams or D-region	/	0.50
Severely cracked webs or slender beams with $\epsilon_s=0.002$ ϕ_{cs} = angle between tension tie and strut		
$\phi_{cs} = 30^\circ$	0.31	0.25
$\phi_{cs} = 45^\circ$	0.55	0.45

For buildings of normal importance the load factors for dead load and live load are $D = 1.25$ (except that if dead load resists overturning, uplift or stress reversal, then $D = 0.85$) and $L = 1.5$ respectively.

Relating to the Canadian CSA - Standard [29] the CEB-MC - Draft 1990 [64] gives the following formula for plane stress fields with closely spaced cracks and no major geometrical disturbance:

$$v_e = \frac{1}{(0.85 + 0.27 \varepsilon_t / \varepsilon_c)} \leq 1.0$$

- f'_c = cylinder compressive strength
 ε_c = longitudinal compressive strain (absolute value)
 ε_t = average transverse tensile strain perpendicular to the compression direction

In the CEB Code-Draft [64], $\phi = 1.0$ in all cases and the load factors for dead and live load are 1.35 and 1.5, respectively.

Major skew cracks are not likely, if the theory of elasticity is followed sufficiently closely during modelling. This means that the angle between struts and ties entering a singular node should not be too small. However, skew cracks may also be left over from a previous loading case with different stress situations (creep, shrinkage, temperature etc.)

The CEB proposed efficiency factors are related to specified safety factors which are different from those in North America. The following equation will be used in Europe to compute the effective concrete strength:

$$f_{ce} = v_e f'_c c / 1.5$$

- f_{ce} = $v_e f'_c 0.667$ for short duration load
 f_{ce} = $v_e f'_c 0.567$ for sustained load

- f'_c = specified compressive strength
 c = coefficient for sustained load = 0.85
 coefficient for short duration load = 1.0
 1.5 = partial safety factor for the concrete in compression

Table 2.4 gives the efficiency factors proposed by Schlaich et al [28] and CEB - MC 1990 [64]:

Table 2.4: Efficiency factors proposed by Schlaich et al. [28] and CEB [64]

State of stress and/or reinforcement layout for strut	v_e
For undisturbed uniaxially state of compressive stress	1.0
If tensile strains in the cross direction or tensile reinforcement in the cross direction may cause cracking parallel to the strut with normal crack widths	0.8
For skew cracking or skew reinforcement	0.6
For skew cracks with extraordinary crack width Such cracks must be expected, if modelling of the struts departs extremely from the theory of elasticity's flow of internal forces.	0.4

In the following subsections, some test results are analyzed with the strut- and-tie-model in order to evaluate the efficiency factor for compression struts in cracked webs.

2.4.1.1 Effective concrete strength in compression diagonals

Shear capacity can be analyzed with different models. A number of empirical and conceptual models have been presented over the course of time. Given all of this effort, however, a completely satisfactory solution has not been attained. The design concepts of the ACI [3] and AASHTO [3] - recommendations and those in the CEB-MC - Draft 1990 [64] have in principle the same structure. The general basis is

$$V_u = \phi (V_c + V_s + V_p)$$

V_u	=	factored shear force at a section
V_c	=	nominal shear strength provided by concrete
V_s	=	nominal shear strength provided by shear reinforcement
V_p	=	vertical component of effective prestress force at section
ϕ	=	strength reduction factor = 0.85 for shear

For reinforced concrete there are two equations for V_c under normal loading conditions. One equation is [3]

V_c	=	$\{1.9 (f'_c)^{0.5} + 2500 (A_s / (d b_w)) [V_u d / M_u]\} b_w d \leq 3.5 (f'_c)^{0.5} d b_w$
A_s	=	area of longitudinal reinforcement
M_u	=	factored moment at section
b_w	=	web width
d	=	distance from extreme compression fiber to centroid of longitudinal tension reinforcement

The second equation for V_c in reinforced concrete is

$$V_c = 2 b_w d (f'_c)^{0.5}$$

For the concrete contribution in prestressed members the equation is

$$2 b_w d (f'_c)^{0.5} \leq V_c = (0.6 (f'_c)^{0.5} + 700 [V_u d / M_u]) b_w d \leq 5 (f'_c)^{0.5} d b_w$$

however, $V_u d / M_u \leq 1.0$

In both reinforced and prestressed concrete,

$$V_s = A_v f_y d / s$$

In prestressed concrete with inclined tendons,

$$V_p = N_p \sin \alpha$$

According to CEB [64] the concrete contribution is given as follow

$$V_c = 2.5 \tau_{RD} b_w d \beta$$

$$\beta = 1 + M_c / M_u$$

Values for τ_{RD} for different concrete strengths are given in Table 2.5.

Table 2.5: Values for τ_{RD} according to CEB MC - Draft 1990 [64]

f'_c	1740	2320	2900	3625	4350	5075	5800	6525	7250
τ_{RD}	26.1	31.9	37.7	43.5	49.3	55.2	60.9	66.7	72.5

Kordina and Hegger [32] present another formulation for the concrete contribution in prestressed concrete girders.

$$V_c = \{2.5 (f'_c)^{0.5} [A_{sl} / (b_w d)]^{0.5} f_y + 0.15 \sigma_{cp}\} (d b_w)$$

$$\sigma_{cp} = N / (A_c) \leq 0.4 f'_c$$

N = longitudinal force or prestressing force

A_{sl} = longitudinal reinforcement

An excellent approach is given by Vecchio and Collins [65] to predict the response of reinforced concrete beams subjected to shear using the modified compression field theory. Strain softening and tension stiffening effects are taken into account in the theoretical model.

The strut- and-tie-model for shear design is based on some assumptions. Yielding of both the longitudinal and transverse reinforcement is required. This requires an upper limit on the diagonal concrete stresses to prevent crushing. The reinforcement can only resist axial loads. The reinforcement is properly detailed so that local crushing and bond failures are prevented. The angle of inclination for the compression diagonals differ as proposed by different authors.

$$25^\circ \leq \phi_{cs} \leq 65^\circ \text{ (Ramirez, Breen [23])}$$

$$15^\circ \leq \phi_{cs} \leq 60^\circ \text{ (Mitchell, Collins [22])}$$

The compressive stress in the compression diagonals, f_d can be computed

$$f_d = V (b_w z \cos \phi_{cs} \sin \phi_{cs})$$

z = distance between stringers

The orientation of the diagonal compression strut and the width of the strut are the most important factors for a strut-and-tie-model. Fig. 2.16 shows the strut-and-tie-model based on the idea of a "design zone" for the ultimate behavior under shear and bending proposed by Kaufmann and Ramirez [66]. A new formulation of the compression width is given here and the proposed model is compared with test results. To obtain this strut-and-tie-model, the beam is first divided into design zones. A vertical tension tie is placed at the location of the resultant force of the web reinforcement in each design zone. The tension chord is located at the centroid of the flexural tension reinforcement and the compression chord is located at the centroid of the flexural compression block. Diagonal concrete members are then placed to complete static equilibrium of the model.

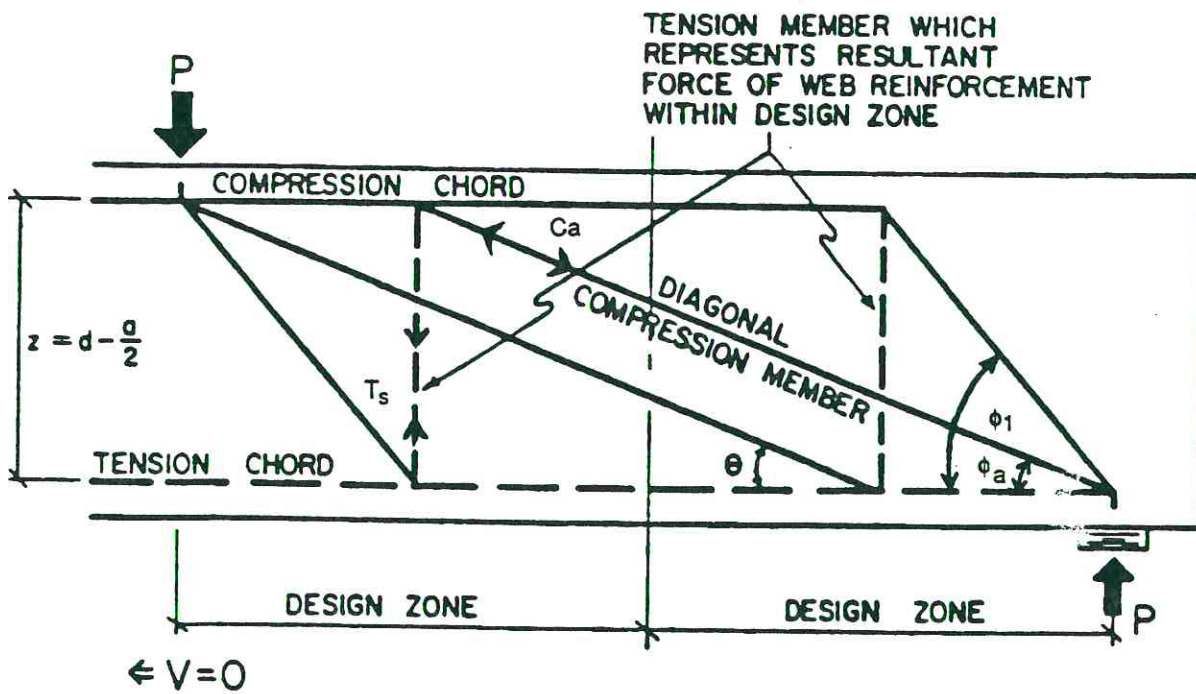


Figure 2.16: Proposed strut-and-tie-model for shear behavior (from Ref. [66])

In this behavioral model, the strength and angle of inclination of the diagonal compression members represent the concrete contribution to the ultimate shear strength. The selection of the angle value is important because it directly affects the number of design zones in the member and the relative amount of transverse and longitudinal reinforcement, as well as concrete stresses in the diagonal strut.

Table 2.6 contains the geometrical data and the concrete efficiency factor obtained by using the proposed model for different test results by Kaufmann and Ramirez [66], Johnson and Ramirez [67]. Symbols are illustrated in Fig. 2.16.

Table 2.6: Comparison with the proposed strut- and-tie-model and test data

Ref.	f'_c	Ca	ϕ_a	ϕ_t	z	b	T_s	v
[67]	5.28	111.9	15.3	28.7	18	6	20.5	0.435
[67]	7.44	161.2	15.3	28.7	18	6	20.5	0.44
[67]	7.44	142.2	15.3	28.7	18	6	20.5	0.39
[67]	8.1	170.8	15.3	28.7	18	6	40.9	0.43
[66]	8.34	287.4	21.8	34.8	24	6	39.3	0.67*
[67]	10.49	191.5	15.3	28.7	18	6	20.5	0.375

* I-beam, all the other had rectangular cross sections

The following equation for the concrete efficiency factor in diagonal compression struts is proposed (see also section 2.4.1.2 confined concrete strength). As can be seen in the next section the

same equation without the 0.6 reduction factor is used for the basic efficiency factor for confined concrete strength and for the compression strength in the nodal zone. The reduction factor 0.6 (in actuality a judgement factor "3/5") reflects the lower effective concrete strength for severely cracked webs of slender beams. A differentiation between the higher effective concrete strength in nodal zones and isolated concrete struts as compared to more uniformly stressed webs is also made by MacGregor [62] as reflected in Table 2.3. MacGregor and most of those proposing efficiency factors do not consider reductions for high strength concretes.

$$v_{ed} = 0.6 v_e = 0.6 [0.5 + 15 / (f'_c)^{0.5}]$$

The statistical data from the comparison are given in Table 2.7 and shown in Fig. 2.17.

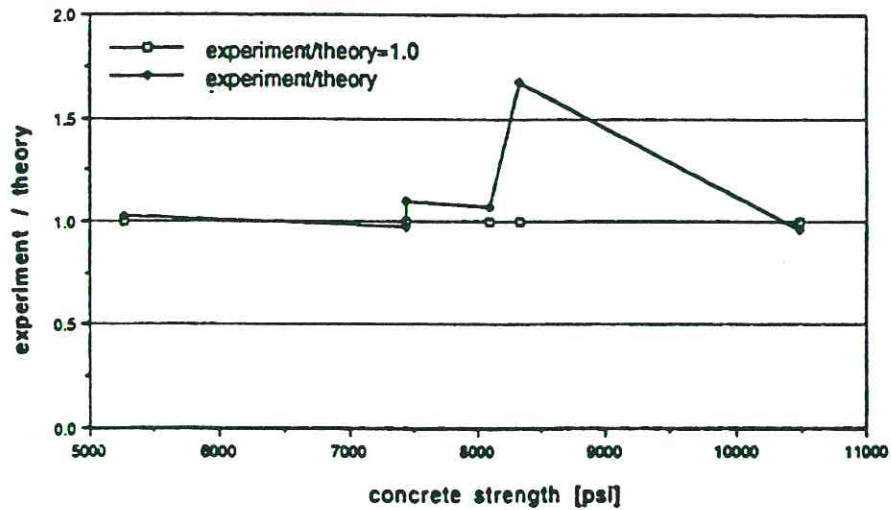


Figure 2.17: Comparison of test results with the theoretical approach of predicting the diagonal compression strength

X1: Column 1					
Mean:	Std. Dev.:	Std. Error:	Variance:	Coef. Var.:	Count
1.136	.272	.111	.074	23.938	6
Minimum:	Maximum:	Range:	Sum:	Sum of Sqr.:	# Missing:
.967	1.68	.713	6.815	8.11	4

Table 2.7: Statistical data of the comparison in Figure 2.17

2.4.1.2 Two- and threedimensional concrete strength

Test results from Kupfer [68] showing the two-dimensional compression strength are summarized in Fig. 2.18. The maximum efficiency factor "v" was 1.498 and was obtained from tests with solid bearing plates ($f'_c = 4480$ psi). It should be kept in mind, that this apparent increase in strength is only due to the quite artificial restraint of the specimen. The other test data indicate that the strength of concrete under two-dimensional state of stress, $\sigma_1 = \sigma_2$, is only 17.8% larger than under uniaxial compression. For the three-dimensional state of stress the test results from Linse [69] with a compressive strength between 4480 and 3620 psi are presented for different stress ratios in Table 2.8. The results show that the efficiency factor depends to a large extent on the triaxial stress ratio and the difference between the three stresses.

The CEB-MC Draft - 1990 [64] proposes that the multidimensional compressive strength have the following values:

two dimensional compressive strength	=	$1.1 f'_c$
efficiency factor	v_{e2}	= 1.1
threedimensional compressive strength	=	$3.0 f'_c$ (confined = $3.3 f'_c$)
efficiency factor	v_{e3}	= 3.0

Table 2.8: Strength ratio for three-dimensional concrete compressive strength

$\sigma_1 / \sigma_2 / \sigma_3$	strength ratios
-1.0 / -1.0 / 0.	1.1
-1.0 / -0.93 / -0.18	= 6
-1.0 / -0.49 / -0.14	3.5
-1.0 / -0.50 / -0.25	≈8
-1.0 / -0.26 / -0.09	3.3
-1.0 / -0.25 / -0.12	6.0
-1.0 / -0.16 / -0.08	2.6
-1.0 / -0.14 / -0.14	4.4
-1.0 / -0.26 / -0.09	3.3
-1.0 / -0.1 / -0.05	1.8

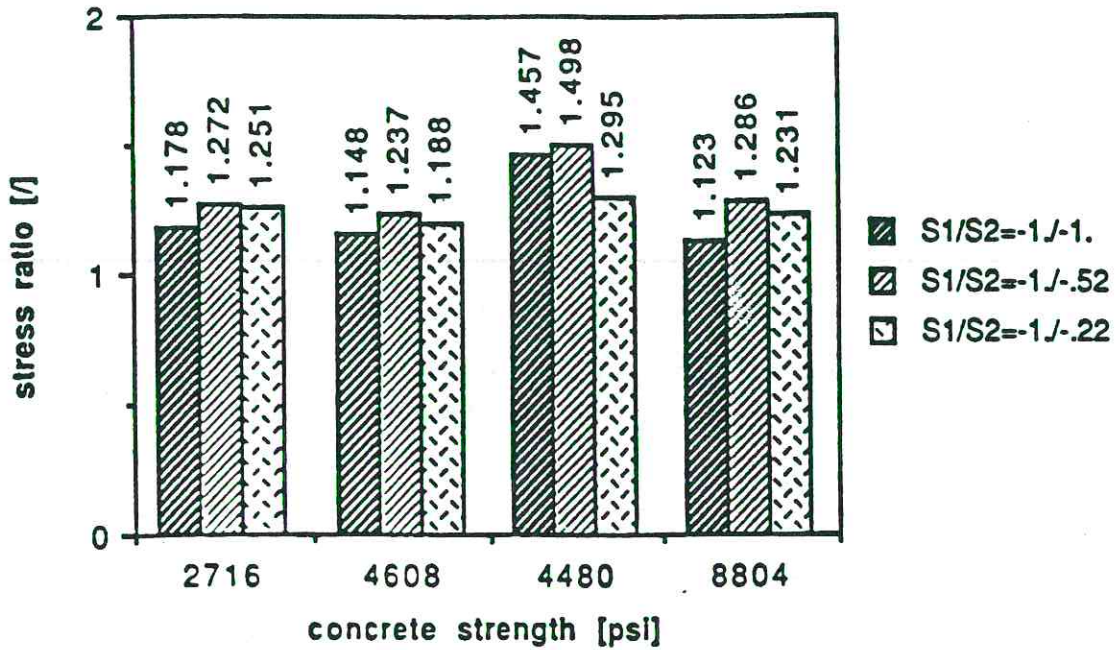


Figure 2.18: Two-dimensional compressive strength

Table 2.9: Statistical data from Figure 2.18

X1: Column 1					
Mean:	Std. Dev.:	Std. Error:	Variance:	Coef. Var.:	Count:
1.264	.114	.033	.013	8.991	12
Minimum:	Maximum:	Range:	Sum:	Sum Squared:	# Missing:
1.123	1.498	.375	15.164	19.304	0

For the two- or three dimensional state of stress, a large number of theoretical investigations have been carried out in recent years and various models have been proposed to characterize the multiaxial stress-strain behavior of concrete . A brief review of some previous recommendations is given here. The Cauchy model (nonlinear elastic) by Kotsovos [70], the hypoelastic material law by Stankowski and Gerstle [71], the elasto-plastic constitutive law by Han and Chen [72] and the bounding surface model developed by Meschke et al [73] and by Fardis, Alibe, Tassoulas [74] represent typical constitutive models for description of the material behavior for multiaxially loaded concrete structures.

2.4.1.3 Confined concrete strength

In many applications substantial confining reinforcement may be present so as to greatly increase the efficiency factor for concrete in compression. If such triaxial concrete strength increase from confining reinforcement is taken into account, then the unconfined concrete portions such as the concrete cover over the confining steel have to be disregarded in the evaluation of the strut strength. For triaxially confined concrete strength, Richart, Brandtzaeg and Brown [75] based the following formula on 112 test results (see Fig. 2.19):

$$f_{e3} = f'_c + 4.1 f_{lat}$$

$$f_{lat} = 2 A_s f_y / (d s)$$

$$A_s = \text{confining reinforcement area}$$

$$f_y = \text{confining reinforcement yield strength}$$

$$d = \text{diameter of entire concrete section}$$

$$d_b = \text{diameter of bearing area}$$

$$A = \pi d^2 / 4$$

$$A_b = \pi d_b^2 / 4$$

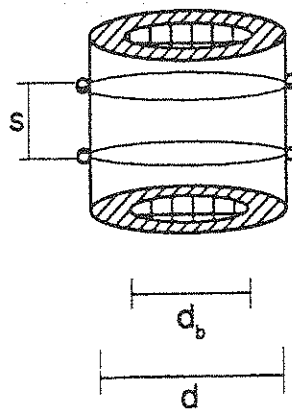


Figure 2. 19: Typical geometrical data for confined core

For square compression struts, with longitudinal reinforcement at the corners as well as at intermediate points, and with closed ties arranged so that sufficient lateral support is provided to longitudinal bars, the lateral pressure is reduced from that of spiral confinement and can be computed by assuming an equivalent circular compression strut with effective diameter " d_e " equal to the side of the confined square core [76] and a substantially reduced confining effect as

$$f_{lat} = A_{st} f_y / (d_e s)$$

A_{st} = total cross sectional area of the stirrups and ties (cross tie included)

If the square compression strut has no longitudinal reinforcement and the lateral reinforcement consists of square ties, the effective confinement was found by Fafitis and Shah [76] to be about 40% of the confinement pressure for a square compression strut with longitudinal reinforcement.

Recent work by Ahmad and Shah [77] has shown that spiral reinforcement is less effective for compression struts of higher strength concrete. The authors also found that the stress in the steel spiral at peak load for high-strength concrete is often significantly less than the yield strength. These conclusions are consistent with results of experimental research at Cornell University. In the study by Martinez, Nilson and Slate [78], an effective confinement stress " $f_s(1 - s/d)$ " was used in evaluating results, where " f_s " is the actual stress in the spiral. The term " $(1 - s/d)$ " reflects the reduction in effectiveness of the spiral associated with increasing spacing of the spiral wires.

$$f_{e3} = f'_c (A/A_b)^{0.5} + 4.0 f_{lat}^{act}$$

$$f_{lat}^{act} = f_s (1 - s/d) 2 A_s / (d s)$$

$$f_s = C \mu 2 s / (\pi d A_s) \leq f_y$$

C = compression load

μ = poisson ratio ($\approx 0.16 - 0.3$ up to 12,500 psi)

There is not a general agreement on the effectiveness of spiral steel for improving the ductility of high strength concrete compression struts, that is, for increasing the strain limit and flattening the negative slope of the stress-strain curve past the point of peak stress. The paper by Ahmad and Shah [77] indicates that confining spirals are about as effective in flattening the negative slope of the stress-strain curve for high -strength concrete as for normal-concrete. However, the study by Martinez, Nilson and Slate [78] showed significant differences. Fig. 2.20 shows experimental stress-strain curves for different strengths of normal weight concrete columns with varying spiral reinforcement. Three groups of curves are identified by the three concrete strength levels studied. Each of these groups consists of three sets of curves corresponding to three different amounts of lateral reinforcement. Different behavior for comparable confinement stress is evident. Not only is the strain at peak stress much less for high-strength concrete, but the stress falls off sharply just past the peak value. This is seen to be true even for compression strut "NC169" with a very high confinement stress of 2500 psi. Caution must be used when applying the results to very high strength concretes.

The basis for design of ACI 318-83 is the following equation

$$f_{e3} \leq \phi 0.85 f_c A$$

$$\begin{aligned} \phi &= 0.7 && \text{for ties} \\ \phi &= 0.75 && \text{for spirals} \end{aligned}$$

When the supporting surface is wider on all sides than the loaded area (A_b), design bearing strength on the loaded area may be multiplied by $(A / A_b)^{0.5}$, but not more than 2.

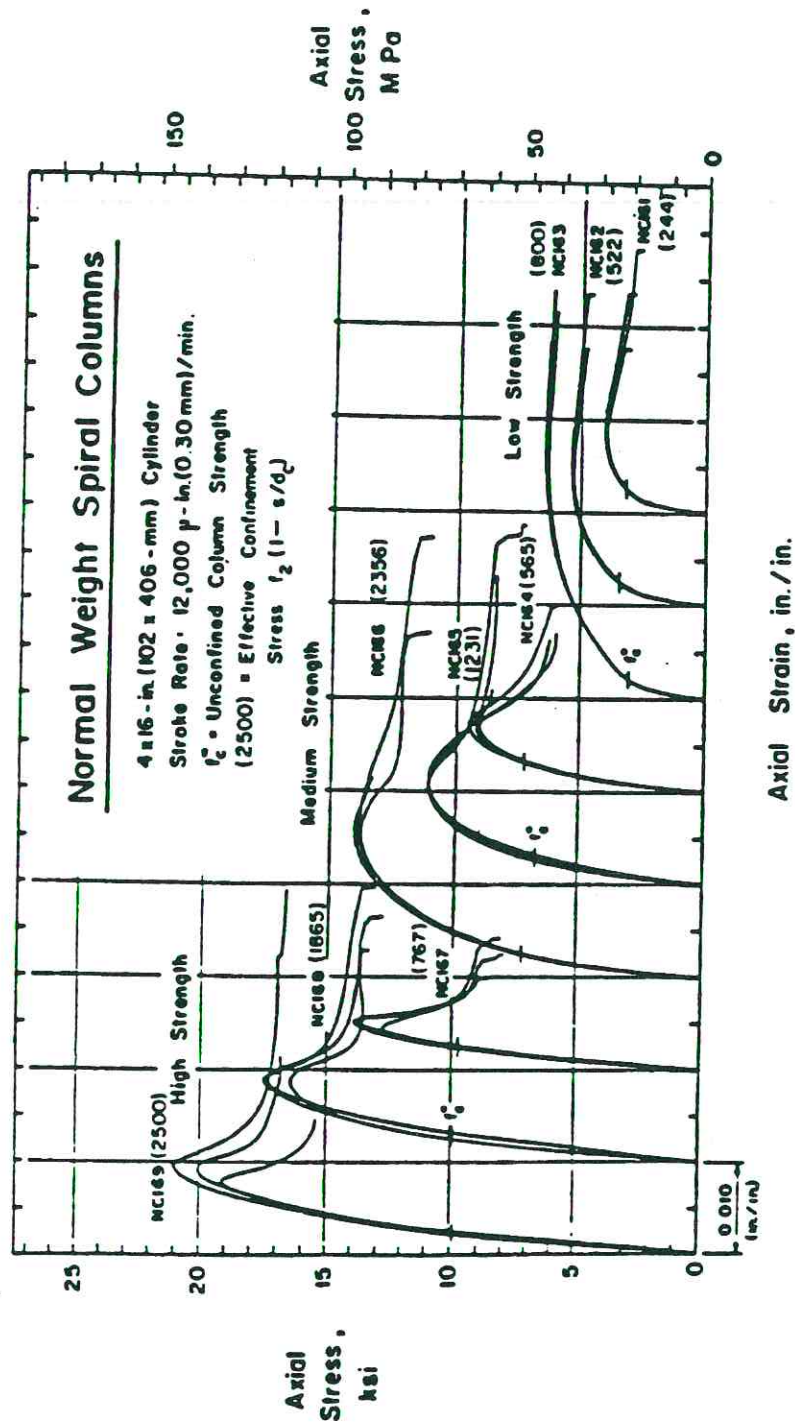


Figure 2.20: Experimental stress-strain curves of 4 x 16 in. normal weight spiral columns (from Ref. [79])

Based upon a number of tests of cylinders loaded through rigid bearing plates, in 1948 Billig [80] developed the following formula for permissible bearing stresses:

$$f_{c3} = 0.6 f'_c (A/A_b)^{1/3} \leq f'_c$$

In 1952 Komendant [81] published the same formula with the exception that the cube root was replaced by the square root. This was based on a substantial number of tests using, again, cylinders loaded through bearing plates. Four substantial studies performed under the direction of Middendorf [82] were carried out in 1960. Using both rectangular blocks as well as cylinders ranging from 6 in. to 16 in. in diameter, Middendorf reaffirmed the recommendations of Komendant, and recommended the following formula:

$$f_{c3} = 0.6 f'_c (A/A_b)^{0.5} \leq f'_c$$

He further recommended that the restriction $f_{c3} \leq f'_c$ be dropped and the value be increased to a multiple of f'_c , probably $3 f'_c$. Middendorf [82] concluded that the recommendations are applicable to concrete with f'_c ranging from 4000 to 6000 psi.

Approximate expressions were developed by Hawkins [83] for the bearing strength of concrete members loaded through rigid plates.

$$f_{c3} = f'_c \{1 + K / (2 (f'_c)^{0.5} [c/b (3-a/b) - 1])\}$$

- K = function of aggregates internal coefficient of friction
 = 50 - 65
 a = length of shorter side of a rectangular plate or side of square plate
 b = length of longer side of a rectangular plate or side of square plate
 c = side length of a square block

For $a=b=c$ and $K=50$ the increase of the bearing stresses is a function of the square root of the concrete strength. The author proposed for design purpose a K equal to 50 (see Fig. 2.22). The results for block length equal to the plate dimensions are shown in Fig. 2. 22.

In 1971, based upon further tests, Hawkins [84] recommended the following formula for strip loading of concrete through rigid plates:

$$f_{cs} = 18.5 (f'_c)^{0.5} (d/(2 w))^{0.3}$$

- $d/2$ = distance from the block edge to the centerline of the plate
 w = width of the plate (see Fig. 2.21(a))

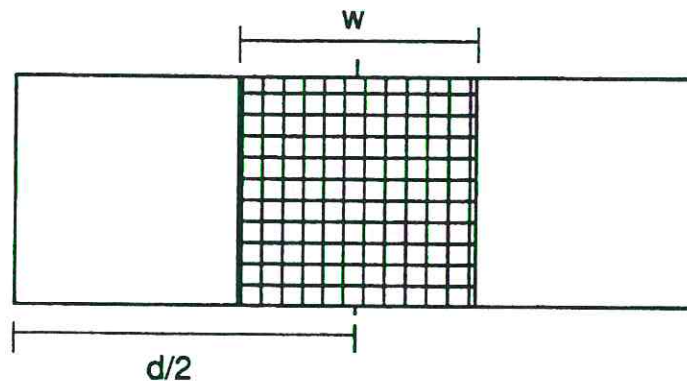


Figure 2.21(a): Strip load dimensions

Niyogi [85] discussed the problems associated with the calculation of the allowable stresses and the probable mechanics of failure. The primary parameters were the geometry of the bearing plate related to the loaded surface and the plate geometry. Square, rectangular and strip loadings were considered. He postulated the following formula:

$$f_{cs} = f'_c \{ 0.42 (a/a' + a/b') - 0.29 [(a/a' - a/b')^2 + 5.06]^{0.5} \}$$

Dimensions and definitions are shown in Fig. 2.21(b). According to Niyogi, the bearing strength decreased for increasing height and eccentricity of the load.

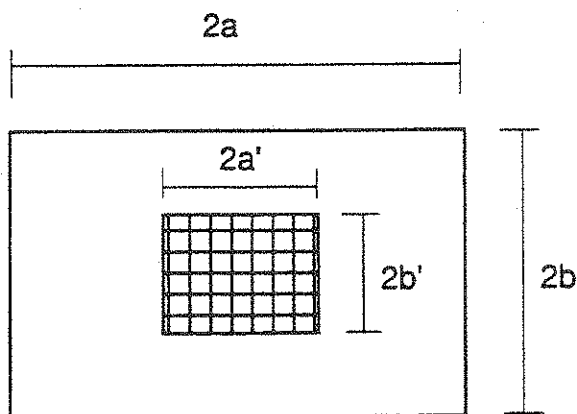


Figure 2.21(b): Variable definitions for geometry of the bearing and loaded plate (from Ref. [85])

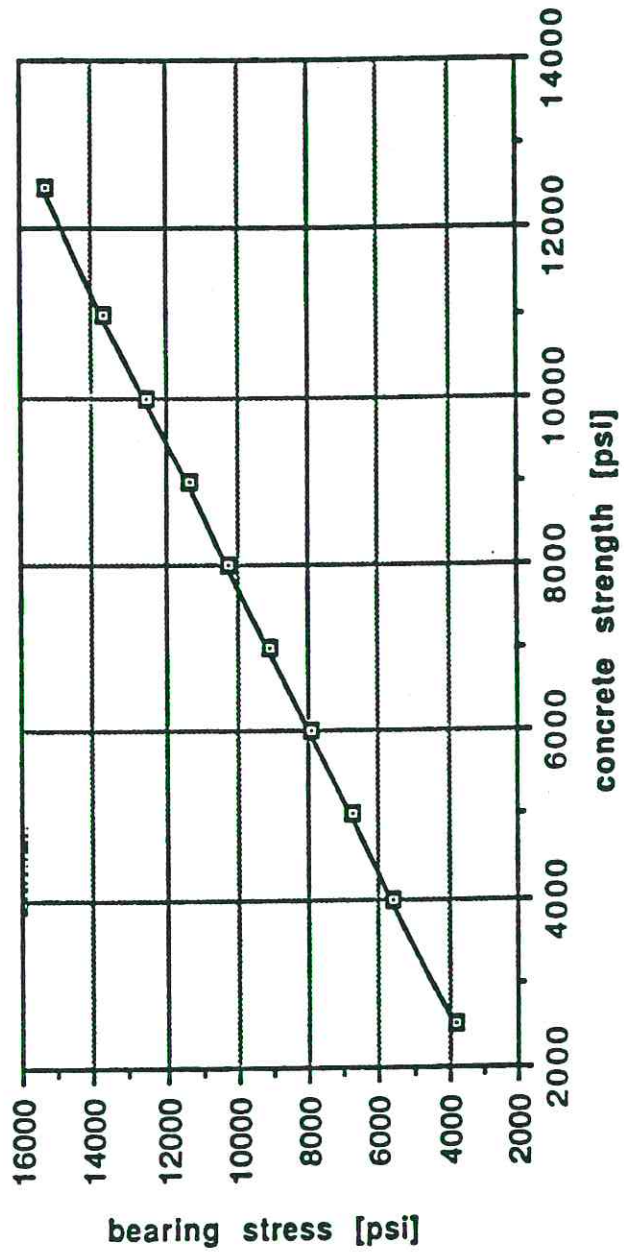


Figure 2.22: Bearing stresses versus concrete strength (from Ref. [83])

In another study Niyogi [86] studied various forms of lateral reinforcement. Among the various forms used, single large diameter spirals gave the highest efficiency for the same percentage of steel. Provision of reinforcement had some beneficial effect on the resistance of specimens against initial cracking, depending on the form and amount of reinforcement and the relative size of the bearing plate. The cracking load, particularly for specimens reinforced with large spirals, and for small relative loaded areas increased with increasing percentage of steel. Niyogi also suggested that the concrete efficiency of spirally reinforced concrete be expressed relative to that of plain concrete by a linear relationship depending on the percentage of steel.

Fafitis and Shah [76] presented an analytical expression for the stress-strain curves of confined high strength concrete based on several sets of experimental data. The peak stress (f_{c3}) and the corresponding strain (ϵ_{c3}) are given by the following equations.

$$f_{c3} = \Omega [f'_c + (1.15 + 3048 / f'_c) f_{lat}]$$

$$\begin{aligned} \epsilon_{c3} &= 1.027 \cdot 10^{-7} f'_c + 0.0296 \Omega f_{lat} / f'_c + 0.00195 \\ \Omega &= 1 + 15 (f_{lat} / f'_c)^3 \end{aligned}$$

In general the following stress-strain relationships are proposed:

$$\begin{aligned} f &= f_{c3} [1 - (1 - \epsilon / \epsilon_{c3})^A] && \text{for } \epsilon \leq \epsilon_{c3} \\ f &= f_{c3} \exp[-k (\epsilon - \epsilon_{c3})^{1.15}] && \text{for } \epsilon \geq \epsilon_{c3} \end{aligned}$$

$$\begin{aligned} A &= E_c \epsilon_{c3} / f_{c3} \\ E_c &= 33 w^{1.5} (f'_c)^{0.5} \\ w &= \text{weight of concrete [lbs / ft.}^3\text{]} \\ k &= 0.17 f'_c \exp(-0.01 f_{lat} / \Omega_1) \\ \Omega_1 &= 1 + 25 f_{lat} / f'_c [1 - \exp(-f'_c / 6500)]^9 \end{aligned}$$

The analytically predicted values of peak stress compared to the test results (with concrete strength of the specimens from about 3000 psi to about 10,000 psi and the confinement pressure from about 250 psi to about 3000 psi) gave differences from 3.5 to 26.5%.

Schlaich et. al. [2] propose the following equation to compute the confined strength for spiral confining reinforcement:

$$f_{c3} = 1.1 f'_c (A/A_b)^{0.5} + 5.2 A_s f_y / (s d) \leq 3.3 f'_c$$

For square compression struts and square confinement reinforcement the lateral pressure can be computed by reducing the equivalent circular compression strength by 50%

$$f_{c3} = 1.1 f'_c (A/A_b)^{0.5} + 2.6 A_s f_y / (s d).$$

d = equivalent diameter = side length of confined square core

Roberts [89] tested local anchorage zone specimens with spiral confining reinforcement. Test results of five different authors were compared with theoretical approaches to determine the best fit function. For the basic concrete efficiency factor the same term was used as shown in 2.4.1.1 for concrete strength in compression diagonals. The following approach is used for the comparison

$$f_{e3} = [0.5 + 15/(f'_c)^{0.5}] f'_c (A/A_b)^{0.5} + 4 (A_{core} / A_b) f_{lat} (1 - s/d)$$

A = the area of confined concrete concentric with and geometrically similar to the bearing plate

A_b = effective area of bearing plate (Roberts imposed a stiffness requirement on the plates)

A_{core} = $d_{core}^2 \pi / 4$

f_{lat} = $2 A_s f_y / (s d)$

For square confining reinforcement with no longitudinal reinforcement and with lateral reinforcement consisting of square ties (ineffectiveness of ties without longitudinal reinforcement, was studied by Sheikh [87]) the following approach was used (for the test results by Muguruma, et al [88]).

$$f_{e3} = [0.5 + 15/(f'_c)^{0.5}] f'_c (A/A_b)^{1/2} + 1.0 (A_{core} / A_b) f_{lat} (1 - s/d)$$

Table 2.11 gives the results from the statistical analysis:

Table 2.11: Statistical data for confined concrete strength with various test data

author	specimens	experiment/theory	
		mean	standard deviation
Roberts [89]:	28	0.95	0.15
Wurm & Daschner [90]:	29	1.05	0.06
Niyogi [85]:	39	1.07	0.19
Muguruma [88]:	25	1.38	0.22
Martinez [78]	11	1.31	0.09
Total	122	1.125	0.24

Different sensitivity analyses have shown that the reduction factor $(1 - s/d)$ for the confinement strength has a significant influence. In the following approaches the squared reduction factor $(1 - s/d)^2$ is used for the comparison. For practical application the reduction factor forces the designer to use smaller spacings for confinement reinforcement.

The term "(1 - s/d)" reflects the reduction in effectiveness of spiral associated with increasing spacing of the spiral wires. For a better correlation with test data the second term in the equation was changed. The following approaches were used:

$$f_{e3} = [0.5 + 15/(f'_c)^{0.5}] f'_c (A/A_b)^{0.5} + 4.0 (A_{core} / A_b) f_{lat} (1 - s/d)^2$$

Comparison with the test results (see Fig. 2.23 and Table 2.12) shows that the proposed equation with the effective confinement strength is a generally conservative and safe approach. The 95 percent limits ($\bar{x} - 2\sigma$) would be 0.65 which is also the minimum actual test result.

Table 2.12: Statistical data from Figure 2.23 for confined concrete with an efficiency factor " $v_e = 0.5 + 15/(f'_c)^{0.5}$ "

X ₁ : Column 1					
Mean:	Std. Dev.	Std. Error:	Variance:	Coef. Var.:	Count:
1.124	.230	.022	.057	21.184	120
Minimum:	Maximum:	Range:	Sum:	Sum of Sqr.:	# Missing:
.654	2.128	1.474	134.851	158.285	0

By using a higher concrete efficiency factor " $v = 0.5 + 20/(f'_c)^{0.5}$ " the statistical mean of the comparison is 1.05 (see Table 2.13). The 95 percent limits become 0.61 with the minimum actual test result 0.62. Either of these efficiency factors could be used in practice.

Table 2.13: Statistical data for confined concrete with an efficiency factor " $v_e = 0.5 + 20/(f'_c)^{0.5}$ "

X ₁ : Column 1					
Mean:	Std. Dev.	Std. Error:	Variance:	Coef. Var.:	Count:
1.054	.221	.02	.049	20.952	120
Minimum:	Maximum:	Range:	Sum:	Sum of Sqr.:	# Missing:
.621	2	1.379	126.46	139.069	0

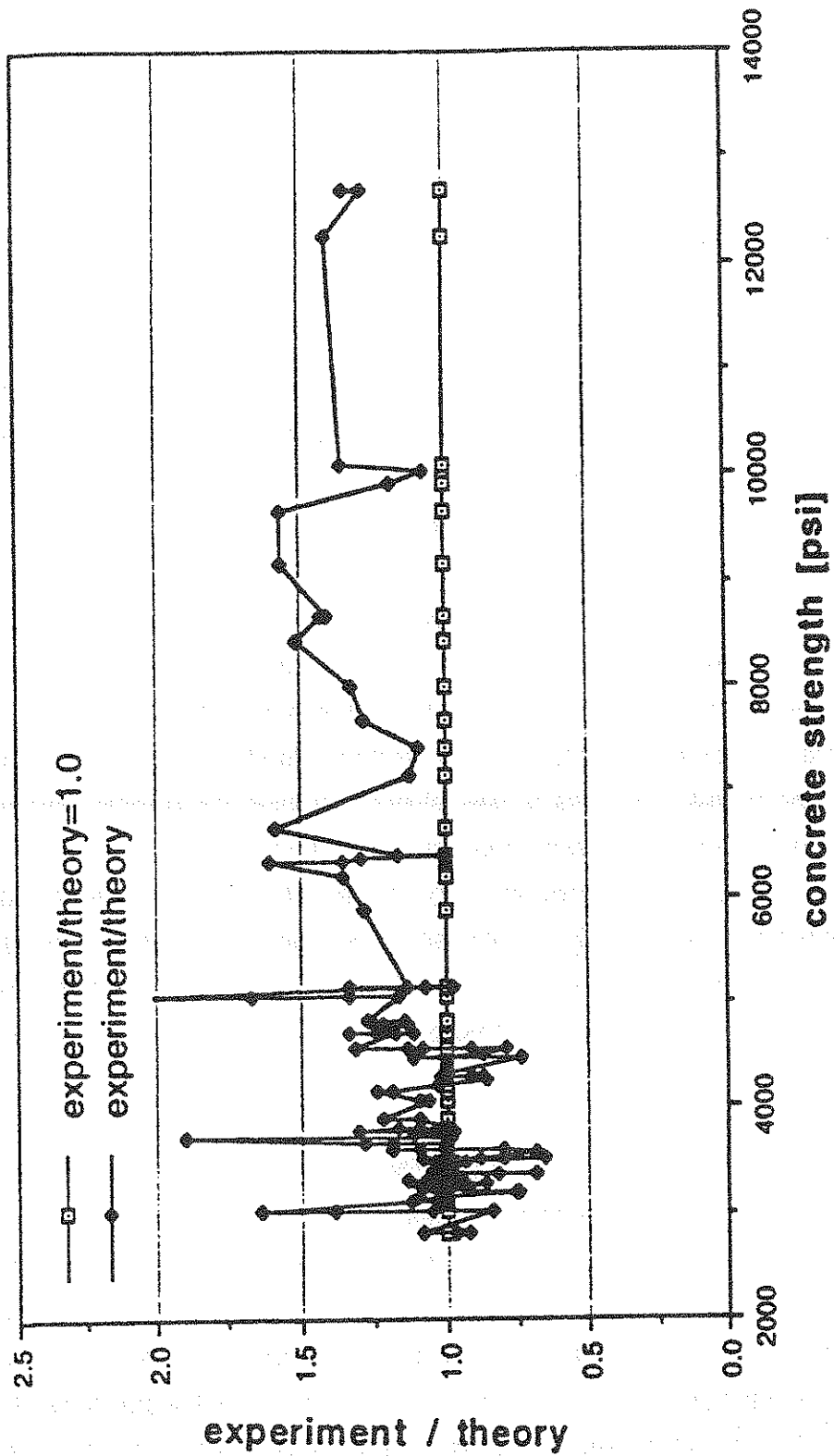


Figure 2.23: Comparison of test results with theoretical approaches for predicting confined concrete strength

2.5 Tie Background

The ties in a strut- and- tie model have to be provided either by reinforcement or by the concrete tensile strength. Availability of the concrete tensile strength to resist loadings depends to a large extent on the restraint forces in the concrete and its load history. Microcracks from other former load cases, thermal stresses or shrinkage may reduce the concrete tensile strength locally to zero. Considering these circumstances individually in each case, dependence on the concrete tensile strength has to be chosen very cautiously. The dependable tensile strength contribution is usually assumed as zero or as only a small fraction of the theoretical computed tensile strength. For most practical detailing problems, concrete tensile strength should be ignored. However, in certain cases such as massive wall sections, such discounting of the tensile strength contribution may produce very conservative designs. Dependence on tensile strength should only be utilized for equilibrium forces in those cases where no progressive failure is possible. If such dependence is made, restraint forces and microcracks due to shrinkage and temperature have to be taken into account.

Because of the great incompatibility of their strains at peak values, the tensile strength of concrete and the yield strength of reinforcement cannot be counted on jointly for carrying internal forces. However, in those regions where the tensile strength of concrete is counted on for strength purposes, nominal reinforcement improves the reliability of the concrete's tensile strength and thereby contributes to the overall strength and safety of the structure. Although it is difficult to develop design criteria for this case, it would be even worse to maintain the formalistic view that the tensile strength of concrete cannot and therefore must not be utilized. Following the flow of forces in a gap free and consistent manner with strut- and- tie- models will inevitably show that equilibrium can frequently only be satisfied if ties or tensile forces can be accepted in places where, for practical reasons, reinforcement cannot be provided.

Some examples which demonstrate that in fact certain types of members presently depend on the tensile strength of the concrete:

- plain or unreinforced concrete members such as pedestals
- slabs without stirrups or other vertical reinforcement yet carrying shear
- bond strength and lap splices in reinforcement
- concrete joining and fastening elements (anchor bolts, expansion- and adhesive anchors)

Representative design values for tensile strength obtained from tests and measurements vary greatly as shown in Fig. 2.24 [91].

The full tensile strength should never be counted since restraint forces and microcracks have to be taken into account, even in uncracked and unloaded concrete. In many important cases, the engineer has to deal with larger crack widths than microcracks (0.002 in.). Although the tensile strength at a section with an open crack is certainly limited, still sizeable shear forces can be transferred across large cracked interfaces. Figure 2. 25 shows some test results. If the tensile strength in concrete structures is used for the analysis, then the stress peaks at outer fibres or at failure zones may be averaged over a length of approximately 2 in., but not more than 3 times the largest aggregate size [28]. The design engineer will have to decide if, and to what degree the tensile strength can be depended on for carrying load. Although design standards frequently require that the tensile strength of concrete be neglected, such restrictions are usually qualified as in ACI Building Code Section 10.2.5 by insertion of the wording "in flexural calculations of reinforced concrete." [4] Thus, these limitations do not apply to strut-and-tie models at discontinuity regions, per se.

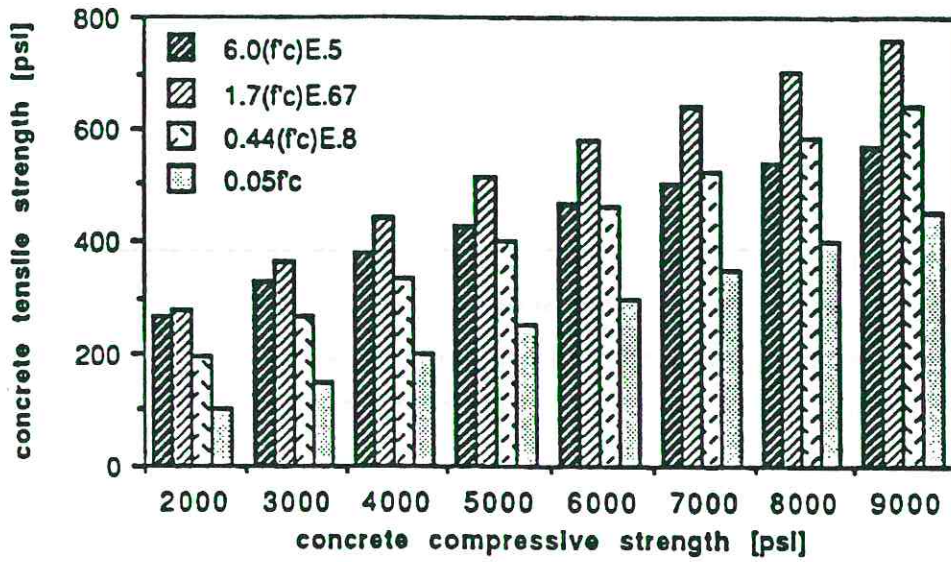


Figure 2.24: Various approaches for the tensile strength of concrete [91]

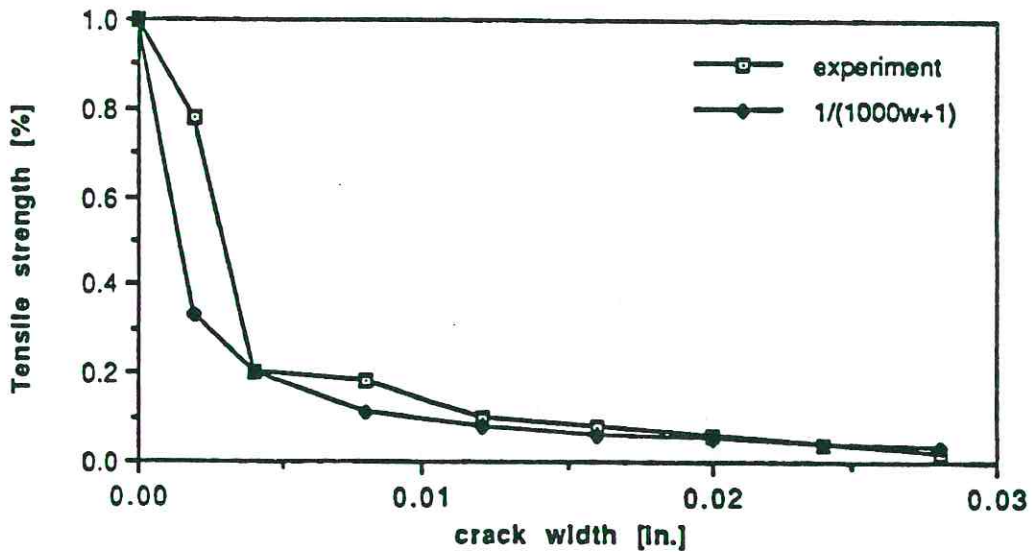


Figure 2.25: Crack width versus tensile strength reduction factor (from Ref. [53])

If the tensile stress field is crossed by a compression field, the reduced biaxial strength must be considered. Fig. 2.26 provides a safe assumption based on test results [68]. Usually, tie forces are resisted by reinforcement placed symmetrically about the line of action of the force. The reinforcement must extend the entire length of the tie and should be properly anchored at the nodes. The amount of reinforcement must extend the entire length of the tie although the amount may vary from one set of nodes to the next set of nodes as bars are cut off or bent. Reinforcement should be proportioned so that at the ultimate design load it will just reach yield. In order to ensure a ductile failure mode, sufficient yielding must occur to allow the formation of a mechanism prior to crushing of the concrete. Tie reinforcement may consist of single or multiple bars or of prestressing bars or strands. However, in many cases it is not readily apparent whether ties should consist of a few large reinforcing bars or a large number of smaller bars. A more theoretical approach indicates reinforcement within a tie should undergo similar strains in order to act as a unit or a single tie. A practical advice in this matter is to use normal diameter bars, normal spacings for the bars and take care to provide sufficient concrete cover. In addition the concrete curing and quality control during the hydration process plays an important role for development of efficient concrete tensile strength.

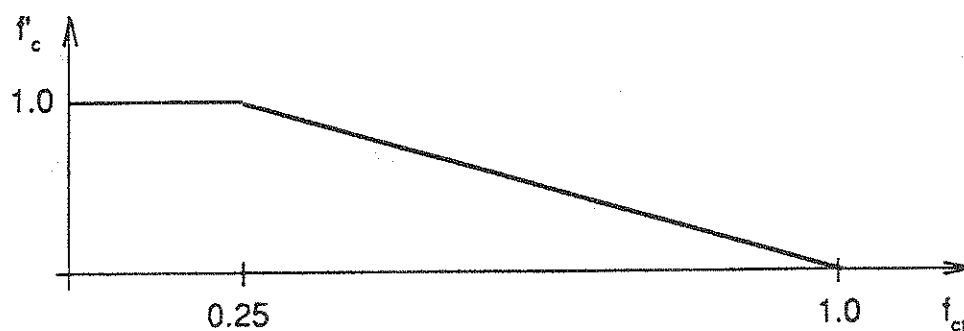


Figure 2.26: The biaxial compressive -tensile strength of concrete

2.5.1 Prestressing forces

Intensive research work has been done to develop procedures for the calculation of the flexural strength of prestressed concrete structures. Also a large number of prestressed concrete specimens have been tested to determine their strength in resisting shear, or combined moment and shear, with or without web reinforcement [91].

Prestressed concrete members pose a somewhat different challenge in detailing. The computation of the ultimate strength of such members is generally very similar to that of non-prestressed members when appropriate assumptions and calculations are made to determine the stress level in the tendons at failure. This stress level depends principally on whether the tendons have been effectively bonded to the concrete. Required quantities of non-prestressed reinforcement to resist anchorage force concentrations, to distribute support reactions, and to counteract similar concentrated load effects can be effectively determined using strut- and- tie models for these D or discontinuity zones. Use of such models actually gives superior understanding and very good guidance for the special reinforcement required. However, while they can be used if desired, strut- and- tie models applied to the B zones tend to be time-consuming and somewhat unwieldy in application.

Since strut- and- tie modelling is a plasticity approach, it is quite inefficient and artificial to use if for checking elastic stresses such as allowable stresses at service load levels. Such checks are important in prestressed concrete members in which it may be desirable to prevent or severely limit crack formation at the service load limit state. It is possible to make such calculations using a type of strut- and- tie model for B zones, but it does not appear very efficient to do so. In order to illustrate the nature of the computations, a type of model adaptable to allowable stress calculations will be shown in this section and used in Example 4.6. Examination of the actual calculations will indicate the general impracticality

of such an approach in B regions which are efficiently treated by ordinary procedures.

For the efficient use of strut- and- tie models in prestressed concrete, the humanly controlled prestressing forces are applied in the same manner as other loads to the strut- and- tie models. This requires knowledge of their magnitude and of the effective points of application of both horizontal and vertical components. Subsequent changes in the prestressing forces in the tendons due to other load effects are treated as internal forces or tie forces.

In order to apply the strut- tie- model to a prestressed member some basic information has to be known. First and foremost is an accurate estimate of the actual prestressing forces, both initially and after time dependent losses. In the pretension process the first step is to stretch high strength wires or strands between end piers of a prestressing bed. After placing the member forms and casting the concrete, the wires or strands are cut between members. The resulting release of wire tension P_i is equivalent to applying P_i as an external compressive force. The strands are usually eccentric and the prestressing force introduces a moment as well. Because of P_i and the accompanying eccentricity, rather large calculated tensile stresses develop on the top beam fibers. Except near the ends, those need not be considered dangerous because nearer midspan these stresses never exist without the counteracting compression from dead load moment [55] (see. Fig. 2.27). The stress levels do need checking; shrinkage of concrete, creep under the applied prestressing forces, relaxation of steel and loss-of-steel stress from elastic shortening reduce the applied prestressing force to an effective prestress P_{se} .

Shrinkage of concrete is influenced by many factors, such as volume-to-surface ratio, relative humidity, and time from end of moist curing to application of prestress. Since shrinkage is time dependent, about 80% will occur in the first

year [92]. The loss of prestress due to shrinkage is the product of the effective shrinkage " ϵ_{sh} " and the modulus of elasticity of prestressing steel.

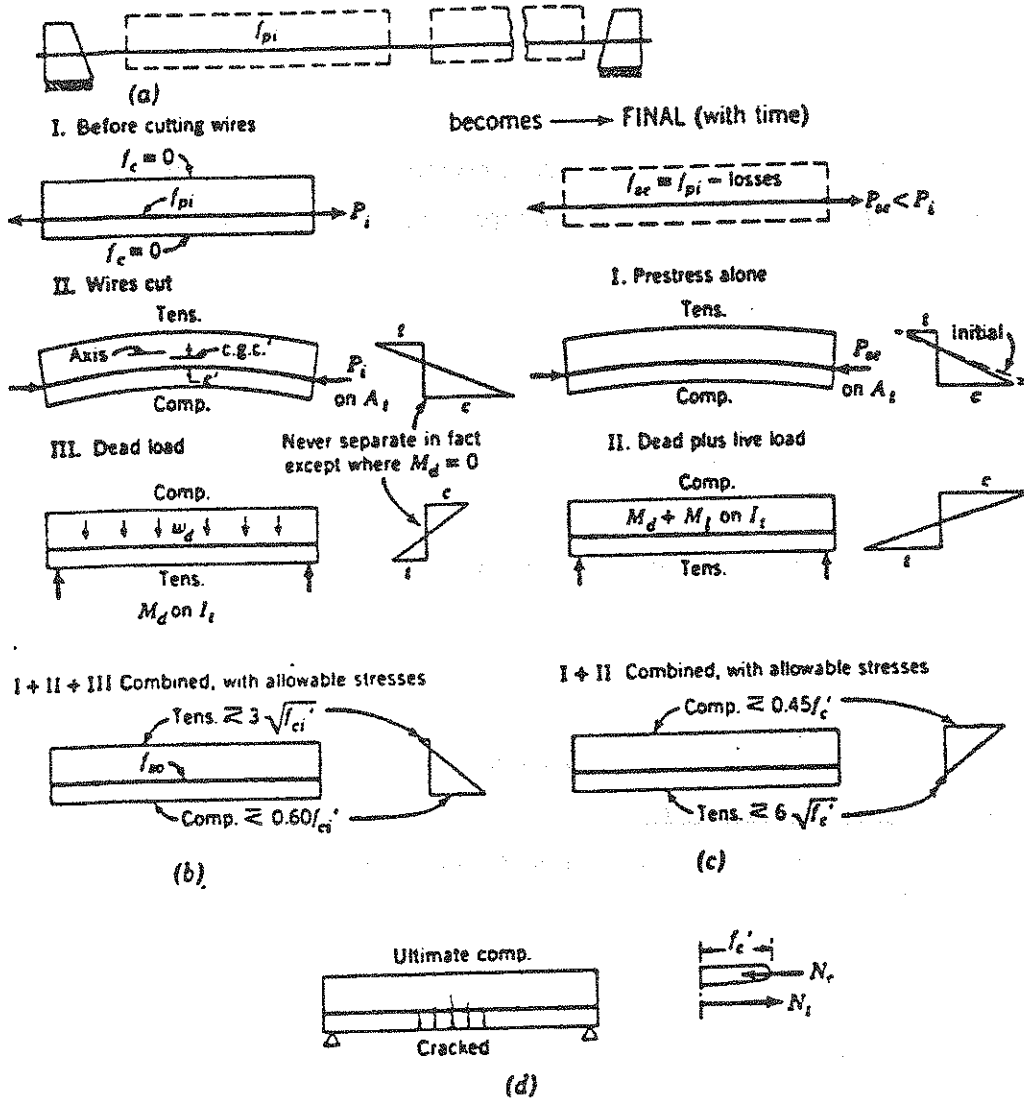
$$\epsilon_{sh} = 8.2 \cdot 10^{-6} (1 - 0.06 V/S) (100 - RH)$$

RH = relative humidity

V/S = volume-to-surface ratio

$$P_{lsh} = \epsilon_{sh} E_p$$

E_p = modulus of elasticity of prestressing steel



- (a) prestressing wire stretched between casting yard abutments
- (b) initial stresses at midspan
- (c) stresses at midspan under full service load
- (d) ultimate strength conditions

Figure 2.27: Pretensioned beam (from Ref. [55])

Creep is assumed to occur with the superimposed permanent dead load added to the member after it has been prestressed. Loss of prestress due to creep is computed for bonded members from the following expression:

$$P_{lcr} = K_{cr} E_s / E_c (f_{cir} - f_{od})$$

- K_{cr} = 2.0 for pretensioned members
 K_{cr} = 1.6 for post-tensioned members
 E_c = modulus of elasticity of concrete at 28 days
 f_{cir} = stress in the concrete at level of steel due to prestress force
 f_{cir} = $P / A + P e^2 / I - M_w e / I$
 e = eccentricity
 I = moment of inertia of the section
 A = cross section area
 M_w = moment acting due to only its own weight

$$P_{lcr} = K_{cr} (E_s / E_c) f_{cp}$$

- f_{cp} = average compressive stress in the concrete along the member length at the center of gravity of the tendon

For unbonded tendons the average compressive stress is used to evaluate losses due to elastic shortening and creep of concrete losses.

The loss of prestress force strands in a duct due to friction and wobble within a duct according to the "Design and Construction Specifications for Segmental Bridges" [31] shall be calculated using the equation:

$$P_{lfr} = P_{lfr,x} e^{(\mu \alpha + k l)}$$

- α = angle from the curved tendon
 k = wobble coefficient
 μ = friction coefficient
 l = length over curved tendon (see Fig. 2.28)

The proposed friction - " μ " and wobble coefficient " α " are shown in Table 2.14 [31]:

Table 2.14: Friction - and wobble coefficient (from Ref. [31])

Type of strand	Friction coefficient μ [/]	Wobble coefficient α [k/ft]
wire or strand in galvanized metal sheathing:	0.15-0.25*	0.0002
high strength bars in galvanized metal sheathing:	0.15	0.0002
wire or strand in internal polyethylene duct:	0.23	0.0002
wire or strand in straight polyethylene duct (external to concrete):	0.00	0.00
rigid steel pipe deviators:	0.25*	0.0002

* lubrication will probably be required

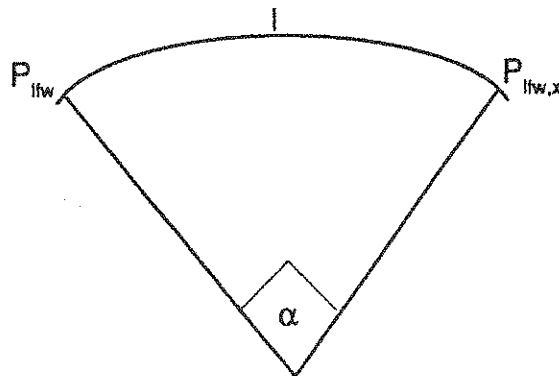


Figure 2.28: Frictional loss along circular curve (from Ref. [92])

Loss of prestress due to steel relaxation over the time interval t_1 to t may be estimated as follows for ordinary stress relieved strand::

$$P_{ls} = [\log (24 t - \log 24 t_1) / 10] \times f_{st} / (0.85 f_y) - 0.55$$

$$f_{st} / (0.85 f_y) - 0.55 \geq 0$$

f_{st} = steel stress level at beginning of time interval t_1

As proposed in [31] for low relaxation steel a different expression can be used:

$$P_{ls} = [\log (24 t - \log 24 t_1) / 45] \times f_{st} / (0.9 f_y) - 0.55$$

$$f_{st} / (0.9 f_y) - 0.55 \geq 0$$

The value for t_1 at the time of anchorage of the prestressing steel shall be taken as 1/24 of a day so that $\log t_1$ at this times equals zero.

It is difficult to generalize the amount of loss of prestress, because it is dependent on so many factors. For average steel and concrete properties, cured under average air conditions, the tabulated percentages of Table 2.15 may be taken as representative of the average losses [92].

Table 2.15: Loss of prestress (from Ref. [92])

type of loss	pretensioning [%]	post-tensioning [%]
elastic shortening	4	1
creep of concrete	6	5
shrinkage of concrete	7	6
steel relaxation	8	8
Total loss	25	20

After an accurate estimate of the prestressed forces is obtained, the spread of the highly concentrated forces into the member must be approximated in the strut- and- tie models. Based on comprehensive finite element analyses by Burdet (42) and comparison with experimental values by Sanders (43) a conservative values of the diffusion angle was chosen. The proposed compression strut diffusion angle is 12° . It is the first term from the more comprehensive expression for the diffusion angle for a compression strut given in Section 3.4.

In post-tensioned concrete the point of application of the major or initial force is relatively clear. Except for frictional and radial forces in curved tendons, the post-tensioning forces are applied at the anchorages. However, in pretensioned concrete, the initial prestressing forces are distributed over longer lengths. With both bonded post-tensioned tendons and bonded pretensioned tendons, subsequent stress changes can be induced by flexural actions.

The development length of the prestressing strands is another important factor. Two types of bond strength must be considered. The first of these is referred to as "transfer bond stress" and has the function of transferring the force in a pre-tensioned tendon to the concrete. Transfer bond stresses come into existence when the prestressing force in the tendons is transferred from the prestressing beds to the concrete section. The second type of bond is termed "flexural bond stress" and comes into existence in pre-tensioned and bonded post-tensioned members when the members are subjected to external loads [93]. After cracking, the increase in steel stress above effective prestress develops flexural bond stress between the steel and the concrete. Flexural bond stress does not exist in unbonded, post-tensioned members. Transfer bond involves the Hoyer effect. When a prestressing tendon is stressed, the elongation of the tendon is accompanied by a reduction in the diameter due to Poissons' effect [94]. Hoyer [95] pointed out that, on release of the wire from its temporary anchorage on the prestressing bed, the end of the wire swells as a result of the recovery of the lateral contraction and develops a wedge effect because the prestressing force must diminish to zero at the end of the wire. The stress in the wire is zero at the extreme end and is at a maximum value at some distance called the "transmission length" from the end of the member (see Fig. 2.29). The length over which the prestress transfer bond exists is termed the prestress transfer length, and depends mainly on the amount of prestress, surface condition of the strand and the concrete strength. Three factors which contribute to bond performance are adhesion between concrete and steel, friction between concrete and steel and mechanical resistance [96]. Libby [93] pointed out that under normal conditions, the transmission length for clean seven-wire strands can be assumed to be equal to 50 times the diameter of the strand. The transmission length of tendons can be expected to increase from 5 to 20% within one year after release as a result of relaxation.

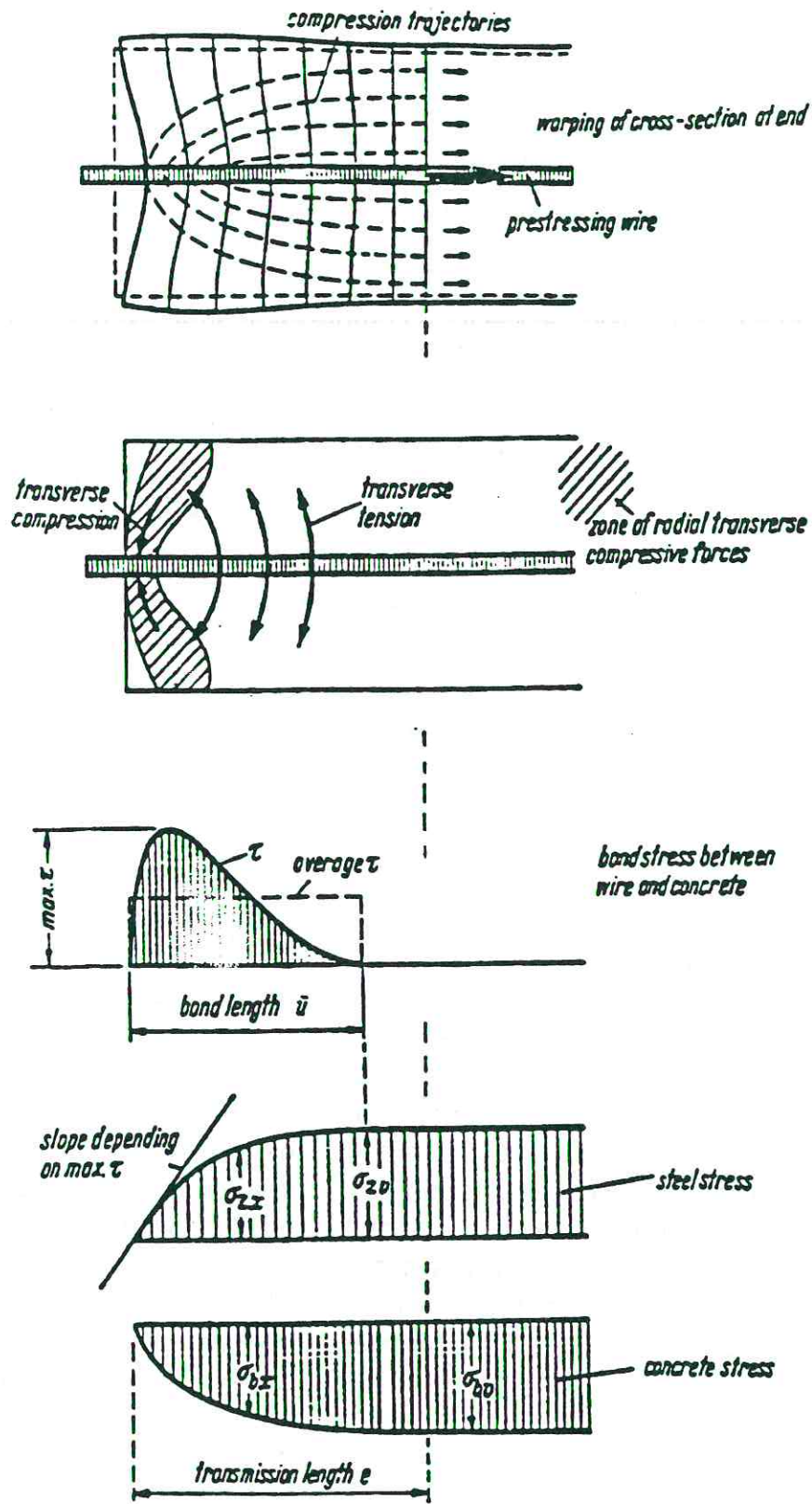


Figure 2.29: Bond stress distribution at the end of a bond anchorage of a pre-tensioned wire [94]

In order to apply the strut- and- tie- model to pretensioned concrete a model has to be developed for the force transfer into the concrete over the transmission length. Such a transfer length model is shown in Fig. 2.30(a). Use of such a model will indicate special lateral and vertical reinforcement is required in the transmission zones to resist the splitting tensile components T_p . A second model can be developed for the internal forces induced through the eccentricity of the applied prestressing forces. Figure 2.30(b) shows a suggested model which can be used to compute effects of various load cases for prestressed members.. The internal force combined load action case shown in Fig. 2.30(b) is the sum of the strut-and- tie-forces developed by external loading w (dead- and live load) and the prestressing forces. As mentioned by Schlaich et al. [28] the prestressing steel will serve as regular reinforcement, if it is bonded with the concrete. The remaining force in the tension chord T can be taken by the reserve capacity of the prestressing steel " T_p " and the capacity of any additional non-prestressed regular reinforcement " T_s ".

$$T = T_p + T_s$$

The reserve capacity " T_p " of the prestressing steel which is still available for use as a tensile chord after prestressing is equal to its yield force (under ultimate load the prestressing steel is strained beyond its yield strength) minus the prestressing force which is applied to the member as a load

$$T_p = A_p f_{py} - P$$

- P = prestressing force = $A_p f_{pi}$
 f_{pi} = effective prestress level in the prestressing steel
 f_{py} = yield strength of the prestressed steel
 A_p = area of the prestressed steel

A major problem in the calculation of "elastic stresses" using the strut- and- tie models is that the fully plastic strut- and- tie model does not adequately represent

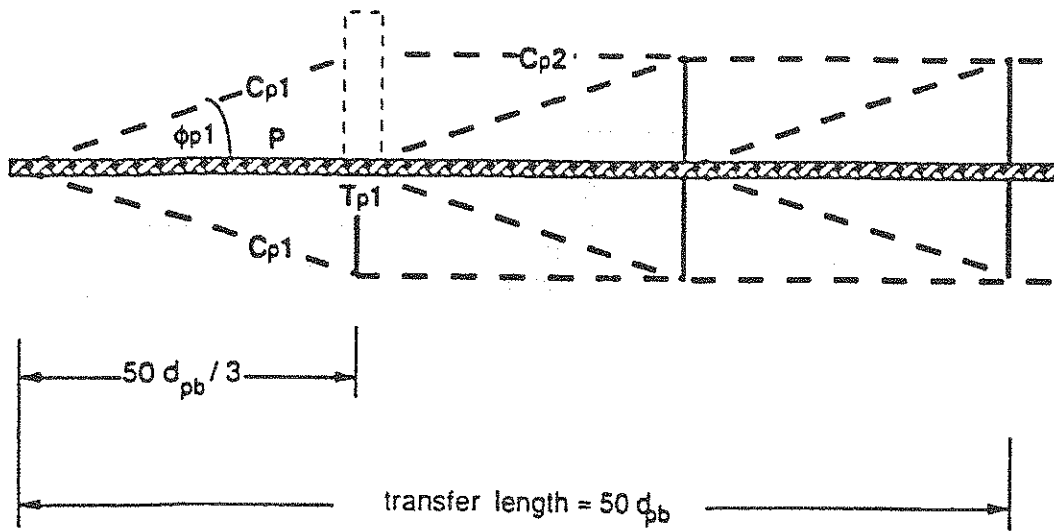
the compatibility effects so important at the service load state. A good example is the effect of tendon eccentricity. As shown in Fig. 2.30(c), the elastic stress distribution can result in tension on the top fiber. If the fully plastic strut- and- tie model shown in Fig. 2.30(d) is used, the free rotation of the joints possible in the assumed fully plastic members results in concentration of stresses in the lower chord only and no forces in the upper chord, verticals or diagonals. From knowledge of compatibility this is clearly inadmissible although equilibrium is satisfied.

If the end region of the eccentrically prestressed member is treated as a 'D' region as shown in Fig. 2.30(e), and if the boundary forces corresponding to the calculated elastic stresses at the boundary with the 'B' region are applied as indicated in Fig. 2.30, a very realistic force path can be used to construct the strut- and- tie model shown. T_1 is the tensile force while C_2 is the offsetting compression force. This 'D' region model clearly indicates that tensile reinforcement is required on the top fiber area and along the support face if concrete tensile stresses are not considered to adequately carry the tensile force. This tensile force, T_1 , is the force which must be applied to any strut- and- tie model used to represent the prestressing effect (see T_p in Fig. 2.30(b)). In Fig. 2.30(b), the chord forces shown are nominal forces. The load factors as well as the material reduction factors have to be taken into account in design. In post-tensioned members, if no bond is provided after prestressing, the prestressing steel cannot be considered as reinforcement. The tendon force is applied as an applied force or the tendon is considered as a constant force tie. Figure 2.31 shows the proposed strut-and-tie-models for a prestressed concrete member with curved or harped tendons.

$$C_{p1} = P / (2 \cos \phi_{p1})$$

$$C_{p2} = P / 2$$

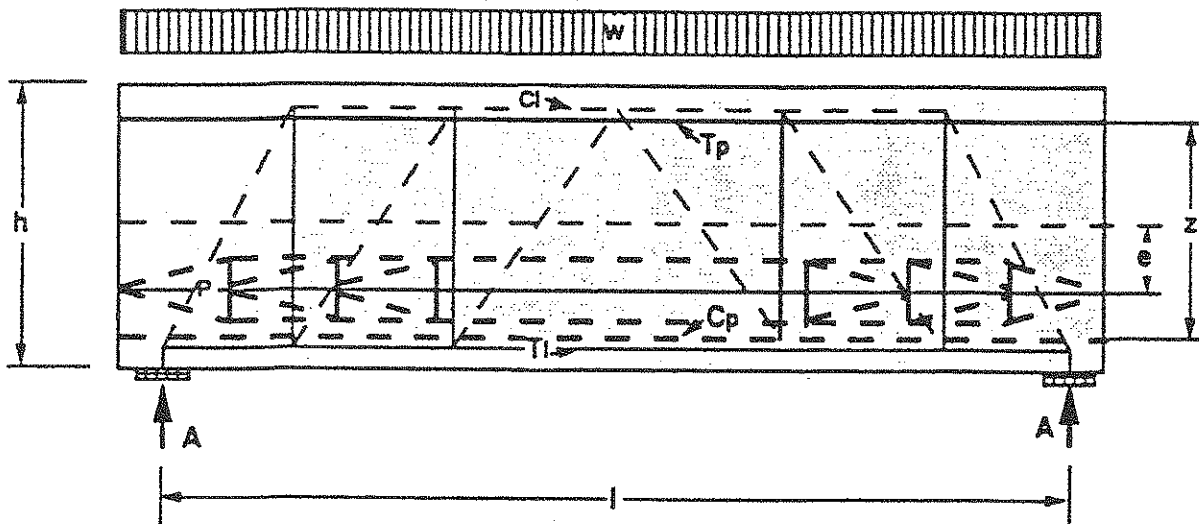
$$T_{p1} = (P \tan \phi_{p1}) / 2$$



Proposed compression strut diffusion angle:

$$\phi_{p1} = 12^\circ$$

(a) Pretensioning force transfer

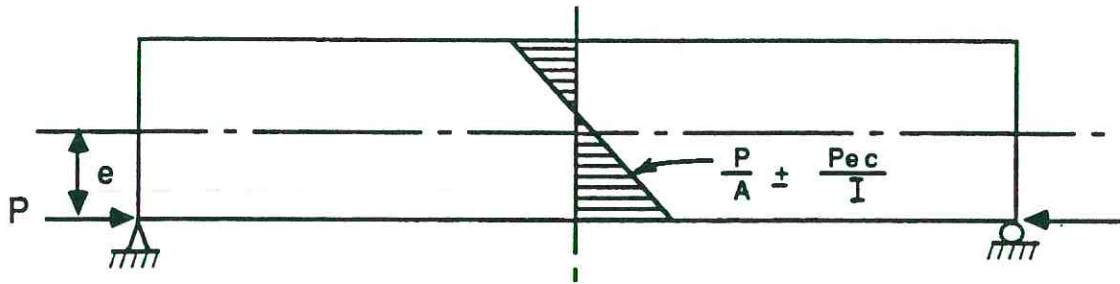


$$T_p = w_t b (-P/A_t + P e y_t / I_t)$$

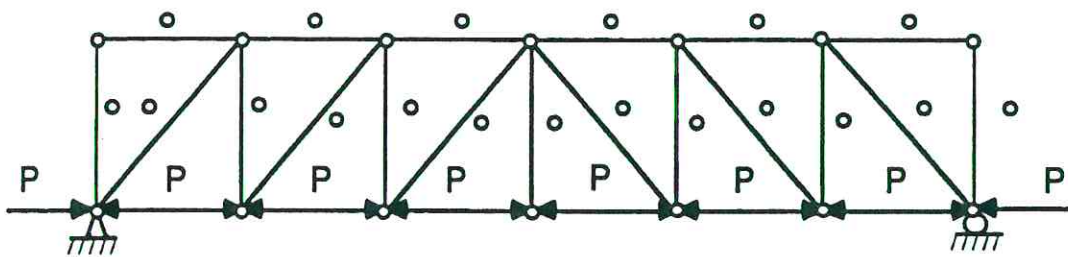
$$C_p = w_c b (-P/A_c - P e x_c / I_c)$$

(b) Overall Model

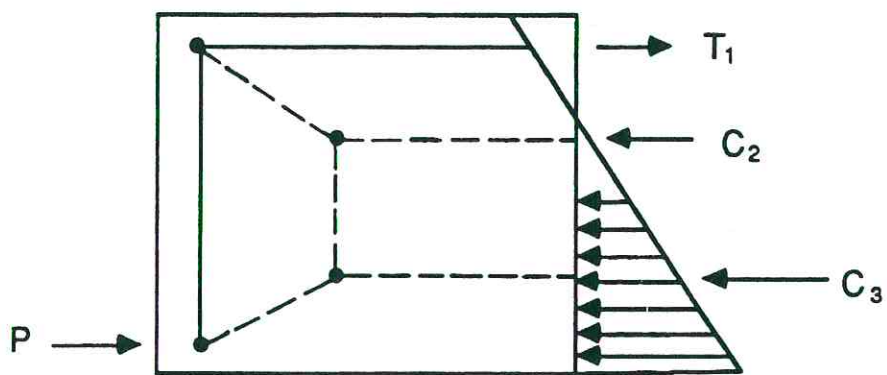
Figure 2.30: Strut-and-tie-models for prestressed concrete



(c) Eccentric Pretension Force



(d) Fully Plastic Strut-and-Tie Model



(e) Strut-and-Tie Model for the end "D" region

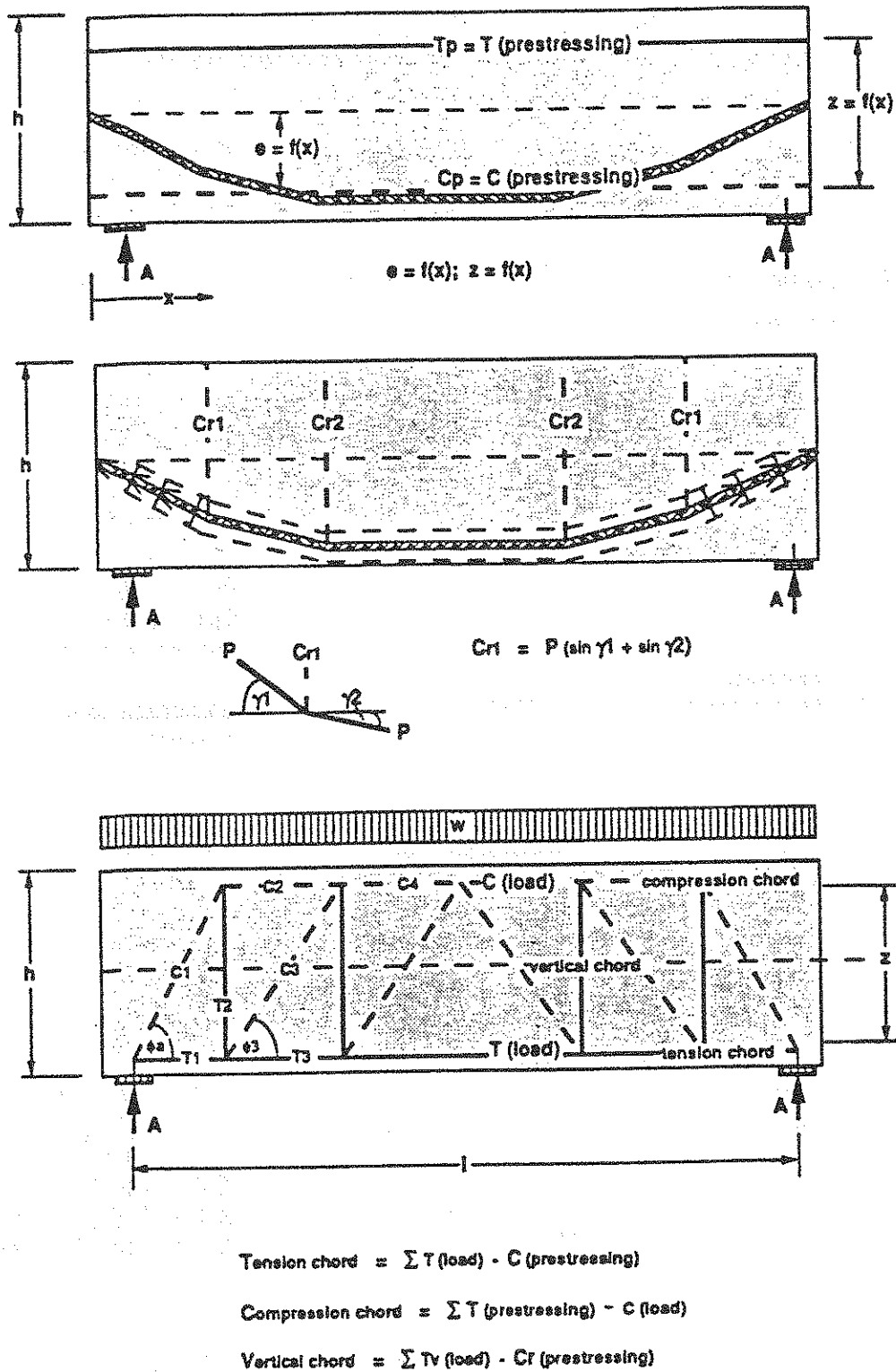


Figure 2.31: Strut-and-tie-model for prestressed concrete beam with curved tendon

Should it be desired to use strut- and- tie models in 'B' regions it can be done, if inefficiently. This section presents a summary of the design steps involved in such use of the strut- and- tie approach for prestressed concrete members. Table 2.16 show the analysis procedures for prestressed beams using the strut and tie model. The symbols are related to Fig. 2.30 and Fig. 2.31 and are defined as follows:

Table 2.16: Design steps for 'B' regions of prestressed beams using the strut-and-tie-model

step	load situation	selected model	strength limits
(1) Pretensioned	wires cut	$\alpha = 12^\circ$	$Cp1 = P / (2 \cos 12^\circ)$ $Ap1 = (7 d_p)^2 \pi / 4$ $Cp1 / Ap1 \leq v_c f'_c$ or service state limits
(1) Bonded or Unbonded Post-Tensioned	immediately after prestressing	$\phi = 12+3/(a/h)$	anchorage zone analysis (see 4.2.6)
(2) Pretensioned Bonded or Unbonded Post-Tensioned	Prestress + Dead Load	compression chord tension chord	$\sum [T(\text{prestr.}) - C(\text{load}) - T] \leq 0$ (tension) $\sum [T(\text{load}) - C(\text{prestr.})] \leq b w_c v_c f'_c$ or service state values
(3) Pretensioned Bonded or Unbonded Post-Tensioned	Prestress + Dead Load + Live Load	compression chord tension chord verticals	$\sum [T(\text{prestr.}) - C(\text{load}) - T] \leq b w_c v_c f'_c$ or service state values $\sum [T(\text{load}) - C(\text{prestr.}) - T] \leq b w_c 3 (f'_c)^{0.5}$ (tension) $\sum [Tv(\text{load}) - Cr(\text{prestr.})] \leq T$
(4) Pretensioned Bonded Post-Tensioned	ultimate	compression chord tension chord	$\sum C(\text{load}) \leq b w_c v_c f'_c$ $\sum T(\text{load}) \leq T + P$
(5) Unbonded Post-Tensioned	ultimate	compression chord tension chord	$\sum C(\text{load}) \leq b w_c v_c f'_c$ $\sum T(\text{load}) \leq T + P$

Load situations:

- I = prestress alone = $f_{se} = (f_{pi} - \text{losses})$
 II = dead load
 III = live load

$$v_e^* = 0.45 \text{ (ACI 318-89-chapter 18) [4] (service state)}$$

proposed strut-and-tie-model: $v_e = f(f'_c)$ (see Section 2.9)

- $T = T_p + T_s$
 $T_p = A_p f_{py} - P$
 $T_s = \text{regular reinforcement capacity}$
 $= A_s f_{sy}$
 $f_{py} = \text{yield strength of the prestressed steel}$
 $A_p = \text{area of the prestressed steel}$
 $f_{sy} = \text{yield strength of the regular reinforcement}$
 $A_s = \text{area of regular reinforcement}$
 $P = \text{prestressing force}$

For curved tendons the radial compression component "Cr" can be computed from the deviations between the tangents to the curve (Fig. 2.32). The section length should be chosen according to the spacing of the vertical tension members (stirrups or lumped stirrups).

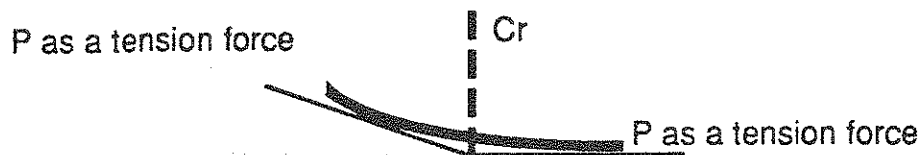


Figure 2.32: Approximation for radial compression component of curved tendon

$$C_r = w_b s_1$$

where

C_r = vertical compression component of the curved prestressing tendon

s_1 = spacing of the vertical chords from the chosen strut-and-tie-model

If the prestressed tendon is following a parabolic curve a uniform load over the length of the span can be computed (see Fig. 2.33):

$$w_b = 8 P h / (L)^2$$

P = prestressed force

h = sag of parabola

L = length of span

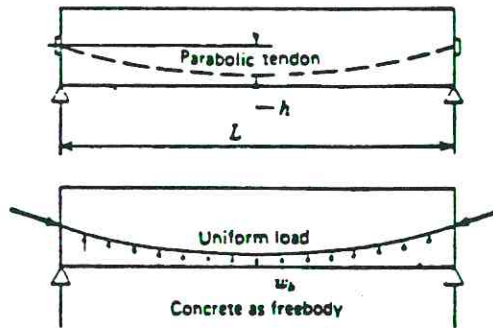


Fig. 2.33: Prestressed beam with parabolic tendon (from Ref. [92])

The width of the compression- and tension chord can be found according to Fig. 2.34. The half of the width is the distance from the center line of the chords to the outside fiber of the member.

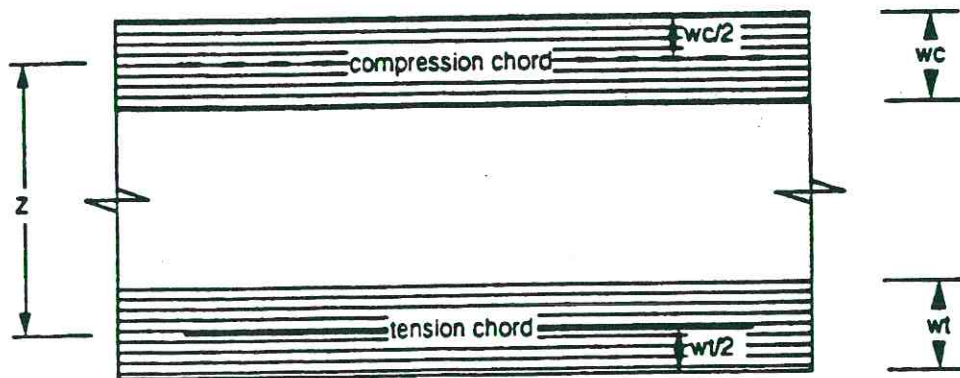


Fig. 2.34: Width of the compression - and tension chord

2.6 Node Background

The nodes of the strut- and- tie- model represent the locations of change of direction of internal forces, which in the structure occurs over a certain length and width in the node region. The intersecting strut- and- tie forces have to be linked together and balanced in equilibrium in the node region.

If one of the struts or ties represents a concentrated stress field (e.g. near a single load, a support or concentrated reinforcement) the deviation of forces tends to be locally concentrated and the node region is relatively small. These kind of nodes are called "singular nodes" and have to be dimensioned with special care. The special studies about CCT (Compression-Compression-Tension) - and CTT (Compression-Tension-Tension)- nodes given in Ref. [38, 39] and summarized in Report 1127-1 provide information upon which design recommendations are based.

Splices or joints of overlapping reinforcement are the special but frequent case of nodes occurring between two ties or reinforced struts for which specific rules based on comprehensive tests have to be used.

Where wide concrete stress fields join each other, the node region extends over a considerable length of struts and ties. Such "smeared nodes" need not be checked for safety, if the same D-region contains a singular node.

Numerous possibilities exist for detailing nodes. In all cases, the flow of forces can be visualized by strut- and- tie- models with singular nodes at the deformations of the bar. Bond is in fact a load transfer mechanism involving both compressive and tensile stresses.

Singular and smeared nodes may be grouped into subsets relating to the type of elements which they join. Four different kind of nodes can be worked out from a strut- and- tie- model (see Fig. 2.35).

- CCC: Compression- Compression- Compression
- CCT: Compression- Compression- Tension
- CTT: Compression- Tension- Tension
- TTT: Tension- Tension- Tension

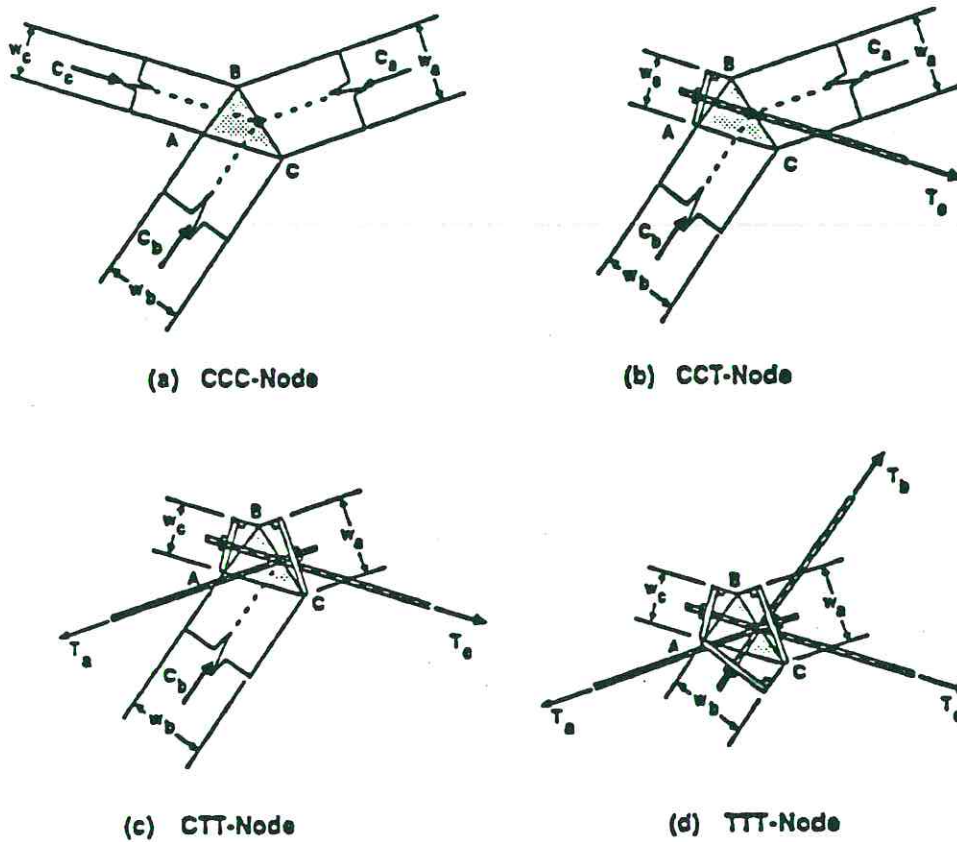


Figure 2.35: Types of nodes

Evaluation of the nodal regions includes checking the nodal boundary stresses and determining reinforcement development requirements for nodes which contain tension ties. Each of these steps requires the determination of the physical boundaries of the node. The dimensioning of nodes is largely determined by two constraints:

- All the lines of actions of struts and ties as well as any external forces must coincide
- The widths and relative angle of the struts and ties constrain the nodal geometry

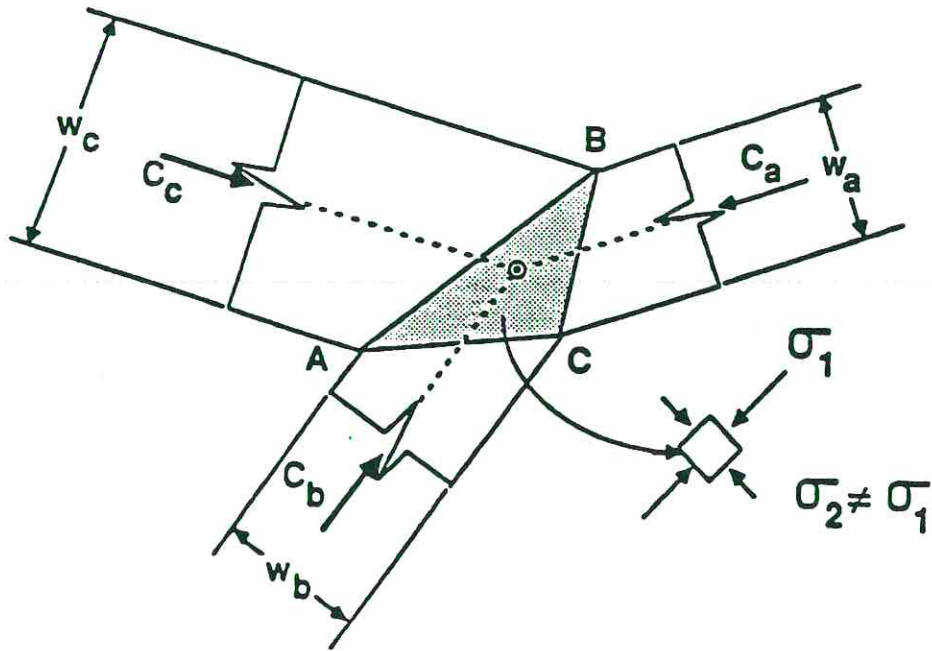
If the nodal geometry can be varied it should be chosen to minimize the stresses in the nodal region. This is accomplished by selecting a geometry in which the stresses along the border of the node do not exceed the limiting value of the effective concrete strength ($f_{cs} = v_c f_c$). In order to get a state of planar hydrostatic stress, the geometry should be selected so that the stresses on all the node faces are equal. Both principal stresses within the nodal region would then equal the stress at the boundary of the node [27, 28].

2.6.1 CCC - Nodes

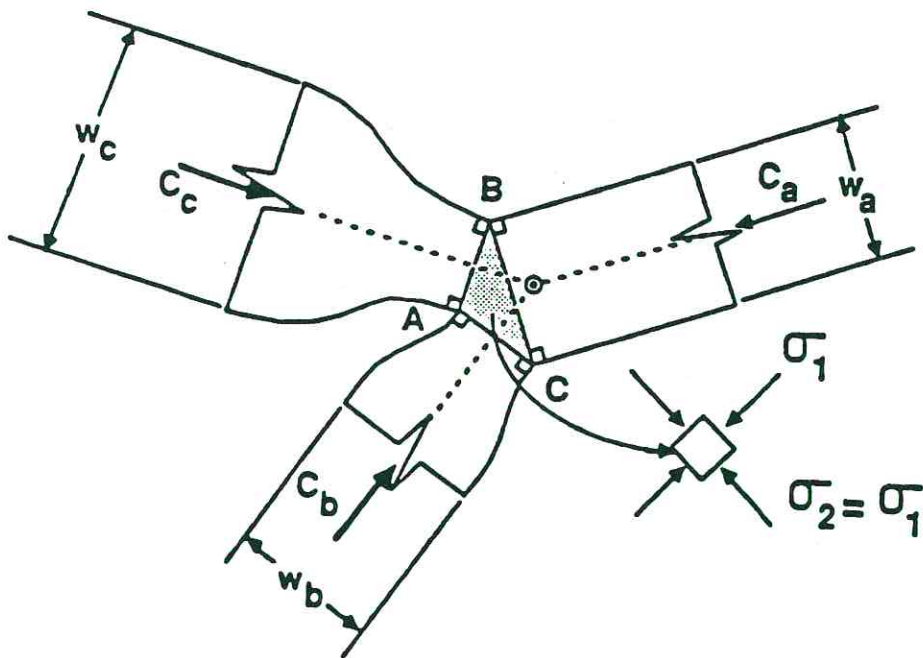
For a CCC-node under a hydrostatic stress state the strut forces are proportional to their width and the sides of the node are perpendicular to the axis of each of the struts. It should be recognized that the geometry of the model may not allow for equilization of the boundary stresses. Such a situation is shown in Fig. 2.35a. Following Schlaich and Schäfer [2], this stress state is tolerable if the maximum ratio of stresses between any two sides does not exceed 2.0. In order to get an hydrostatic state of stress, the geometry of the node can be changed as shown in Fig. 2.36b. The intersection of the strut centerlines actually lies outside the nodal region in this case. Bottle-shaped struts are often used where one of the nodal boundaries is fixed as in the case of a node adjacent to a bearing plate. A reduction of the width of the struts is required to produce a hydrostatic state of stress. In this case a more convenient approach proposed by Schlaich and Schäfer [2] can be used to check the concrete strength in the nodal zone (see Fig. 2.37):

$$\begin{aligned} a_0 &= a \cdot \tan \phi_{c2} \cdot \tan \phi_{c3} / (\tan \phi_{c2} + \tan \phi_{c3}) \\ \sigma_b &= C_1 / (a b) \\ \sigma_{c0} &= C_0 / (a_0 b) \end{aligned}$$

A hydrostatic stress in a CCC-node is only given if the compression struts are perpendicular to the node sides.

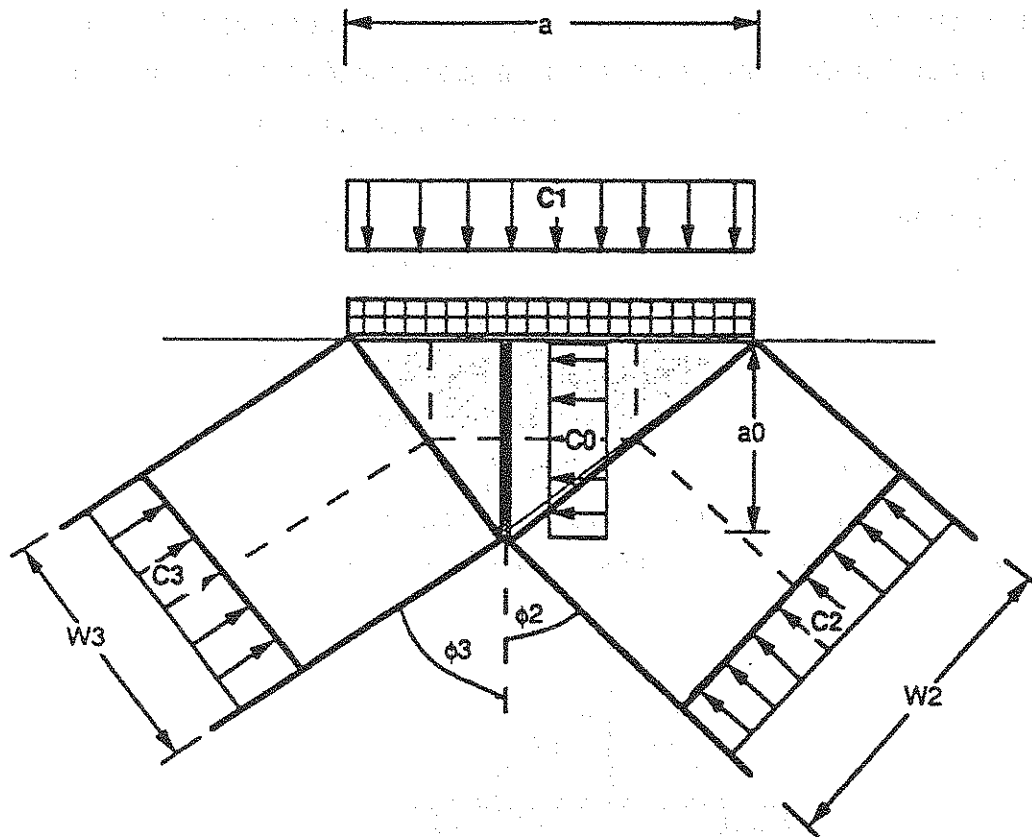


(a) CCC-node with unequal pressure (from Ref. [7])



(b) Struts created by hydrostatically dimensioned node (from Ref. [7])

Figure 2.36: CCC Nodes



$$\sigma_1 = \sigma_2 = \sigma_3 = \sigma_0 \text{ (hydrostatic stress)}$$

$$a_0 = \frac{a \cdot \tan \phi_2 \cdot \tan \phi_3}{\tan \phi_2 + \tan \phi_3}$$

$$\text{for } \phi_2 = \phi_3 = \phi$$

$$a_0 = a / 2 \tan \phi$$

Figure 2.37: Dimensions for hydrostatic stress check in CCC-node

For design purposes some general rule has to be adopted to check the stresses in a CCC-node. The stresses from the struts without bearing plates must be checked with dimensions relating to the bearing plates. It is very useful to subdivide the node under the bearing plate into two sub-nodes as shown in Fig. 2.38. A key assumption is the distance from the centerline of action of the force to the sub-nodes. The distance proposed is the quarter width of the bearing plate ($a/4$). By studying the strut- and- tie- model shown it can be seen that for CCC-nodes with only one bearing plate, the angle of inclination of the struts relative to the plate becomes an important factor. In order to conform with test results of post-tensioned anchorages, the CCC-nodes are best split into two parallel sub-nodes [42, 43] as shown in Fig. 2.38. The strut- and- tie- pattern depends on the bearing plate width, a , because for increasing width a decrease in the required tie force "T" must follow. The design concrete efficiency factor ν recommended in Section 2.8 is a lower bound solution and compared to test results gives a safe approach. The stresses under the bearing plate should recognize the degree of local confinement and be checked utilizing the proposed expressions of Roberts given in Section 2.4.

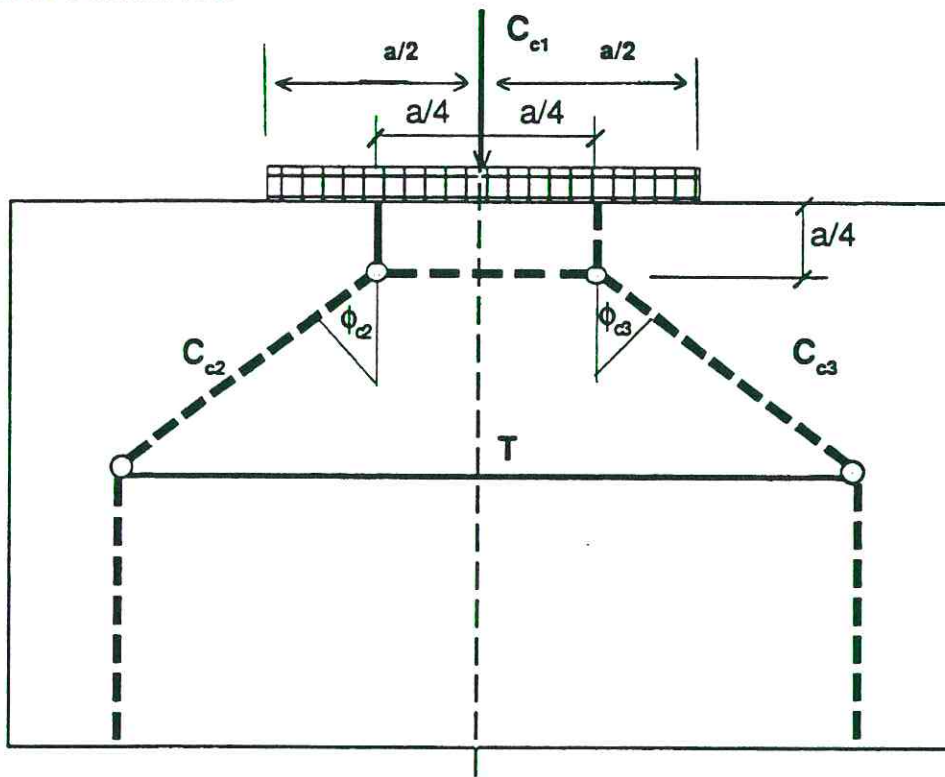


Figure 2.38: CCC-node

The two approaches to compute the stresses in a CCC - node are compared in Fig. 2.39. It can be seen that for the "hydrostatic" stress solution the width of the horizontal compression strut is dependent on the compression angle and on the width of the bearing plate. For the "quarter width of the bearing plate" solution the horizontal compression strut width is dependent only on the bearing plate width. The comparison is made for equal compression angles with the following equations:

- hydrostatic stress solution: $a_0 = a \tan \phi_2 \tan \phi_3 / (\tan \phi_2 + \tan \phi_3)$
- quarter width of the bearing plate solution: $a_0 = a / 2$

a = bearing plate width

a_0 = horizontal compression strut width

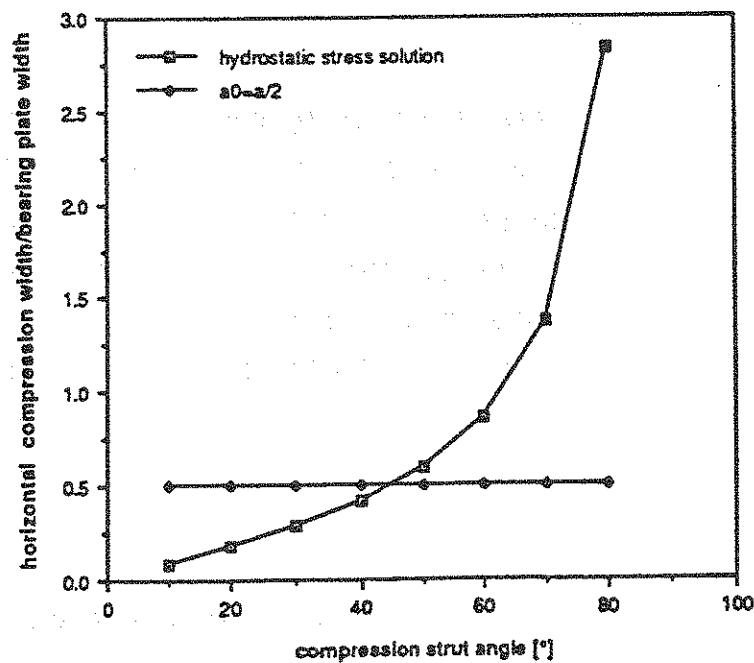


Fig. 2.39: Comparison of the horizontal compression strut width

2.6.2 CCT - Nodes

For the CCT-nodes, two different reinforcing details can occur. Theoretically, but rarely occurring in practice, the anchorage of reinforcement can be developed by anchoring the tie forces from behind with an anchor plate (Fig. 2.40). The usual and more practical case is anchorage by providing sufficient development length behind the node as shown in Fig. 2.41. When using an anchor plate, the determination of the node geometry is clear. Special care should be taken to provide adequate bending strength and stiffness in the anchor plate (plate bending results in higher bursting forces) and to provide a proper connection with the tie. A smooth surface for the tie where it crosses the node is theoretically better than a good bond quality because strain compatibility with the bonded bar will tend to crack the concrete. Bearing plate anchorage of tie forces usually means diversion of compression fields. The compression stresses of the stress fields concentrate on the steel plate's surface, if the tie is developed in this way. The curvature of a deviated compression field is largest at the origin immediately adjacent to the bearing plate.

In the more usual case of reinforcing bars directly anchored without plates, either straight bars, hooks or loop anchorages may be used. Loop anchorages with confining direct pressure as from a bearing or direct load point are preferred. Hooks shall preferably be placed to have confining pressure transverse to the hook plane. Sufficient anchorage lengths have to be provided within as well as behind the node, if necessary. Anchorage begins where the compression struts (see Fig. 2.41) meet the surface of the bar. The bars should extend to the other end of the node region in order to engage the outermost fiber of the deviated compression strut.

For the effective widths of the struts- and- ties different proposals can be found in the literature. The equivalent concrete area approach [23, 24, 56] (see Fig. 2.42) describes the width as follow:

$$w_3 = \omega h = \rho f_y h / (v_e f'_c)$$

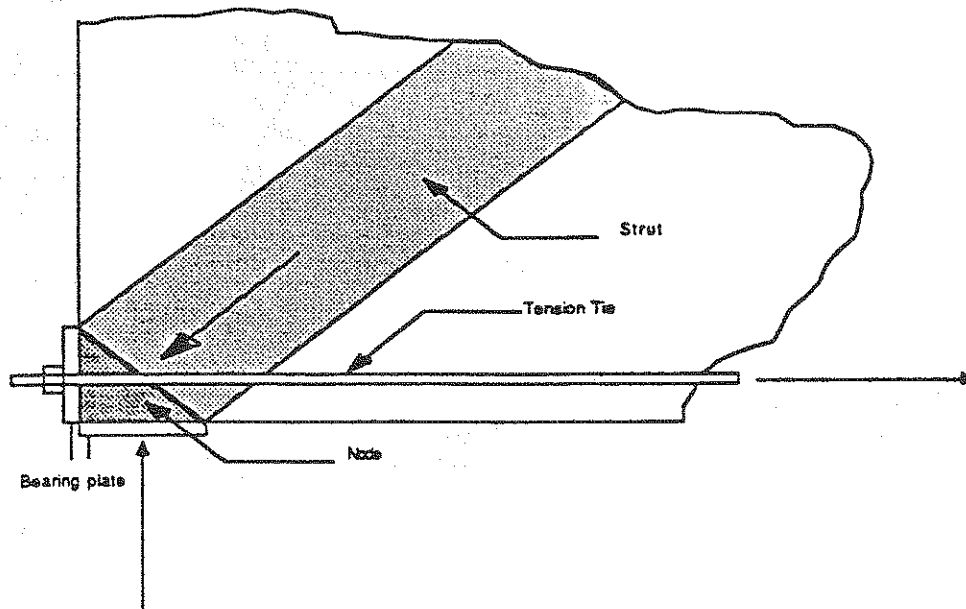
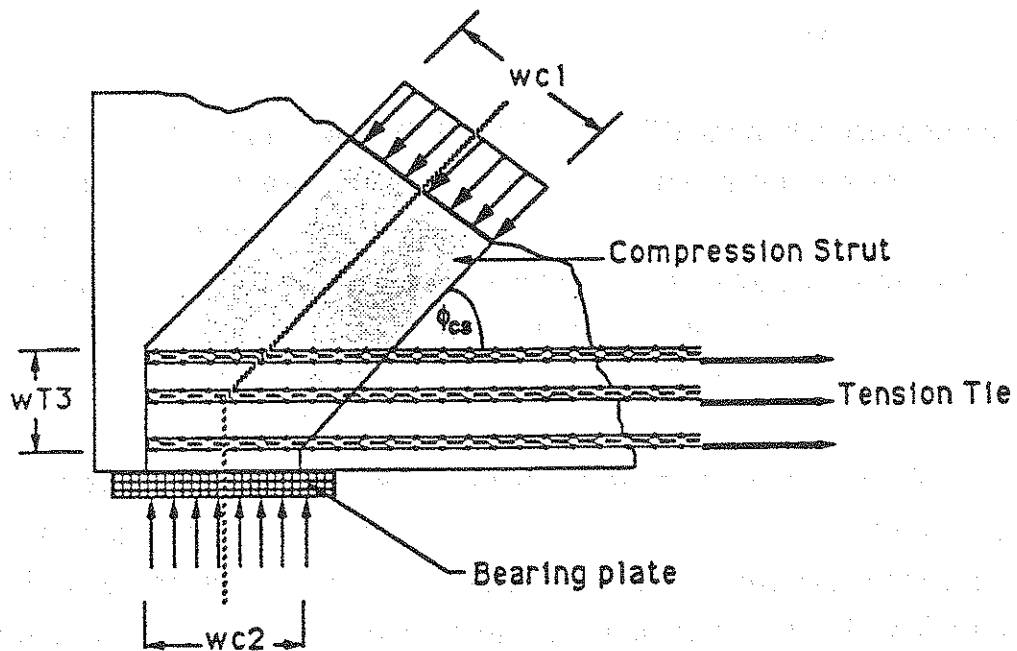


Figure 2.40: Anchorage detail for CCT-node:
Anchorage of reinforcement with anchor plate (from Ref. [7])



$$wc1 = wc2 \sin \phi_{cs} + wT3 \cos \phi_{cs}$$

Figure 2.41: Anchorage detail for CCT-node with directly anchored bars

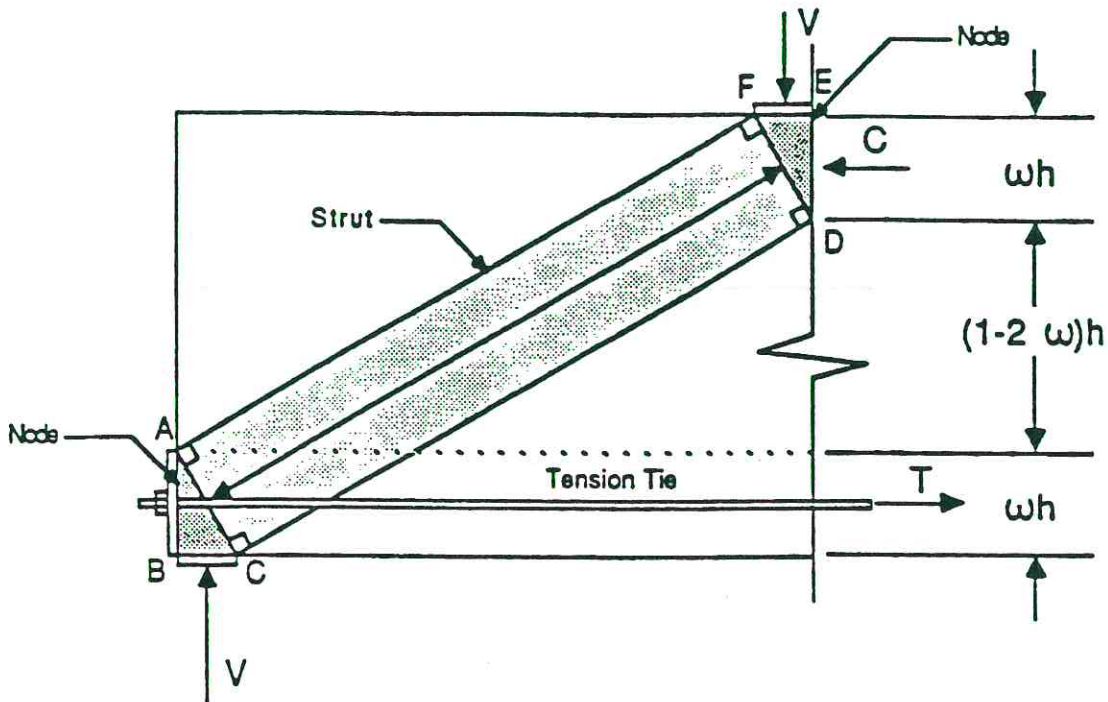


Figure 2.42: Equivalent concrete area approach to define the tie width (from Ref. [56])

Further proposals in the CEB-MC - Draft 1990 [64] suggest that dimensions of CCT-nodes are dependent on factors such as the relative magnitude of stress fields and the amount of tie reinforcement. For instance, where σ_2 is less than σ_1 and there are multiple layers of reinforcement, the width " w_3 " of the tensile tie may be as much as 20 % of the length (for slabs 20 % of the span length) or width of the entire D-region (see Fig. 2.43).

The fundamental aspects should allow the designer to determine the geometry of the CCT-node for varying reinforcement distribution and anchorage details (several layers, loops, hooks etc.). The experimental portion of the study by Bouadi [39, 131] provided information about the behavior and transfer of forces within the CCT-node as well as the ultimate strength. Geometric and reinforcing details for the test specimens are shown in Fig. 2.44. Test results with a concrete strength in the range from 2360 to 4680 psi showed crushing of the concrete struts only for the lower concrete strength specimen. In all the other

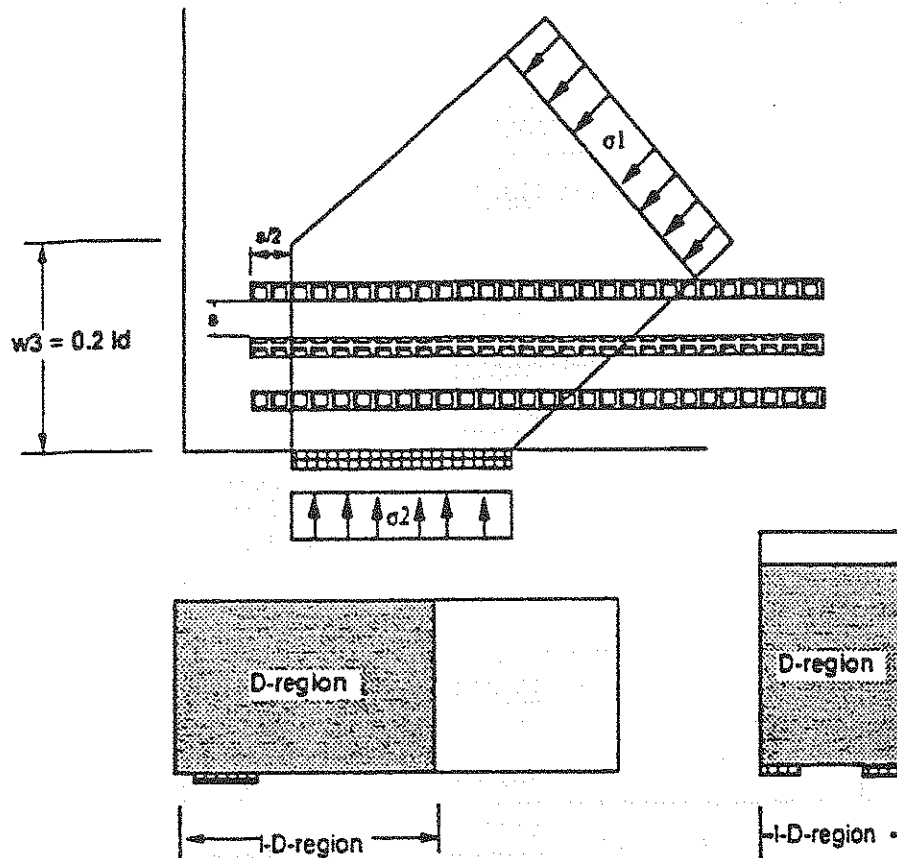
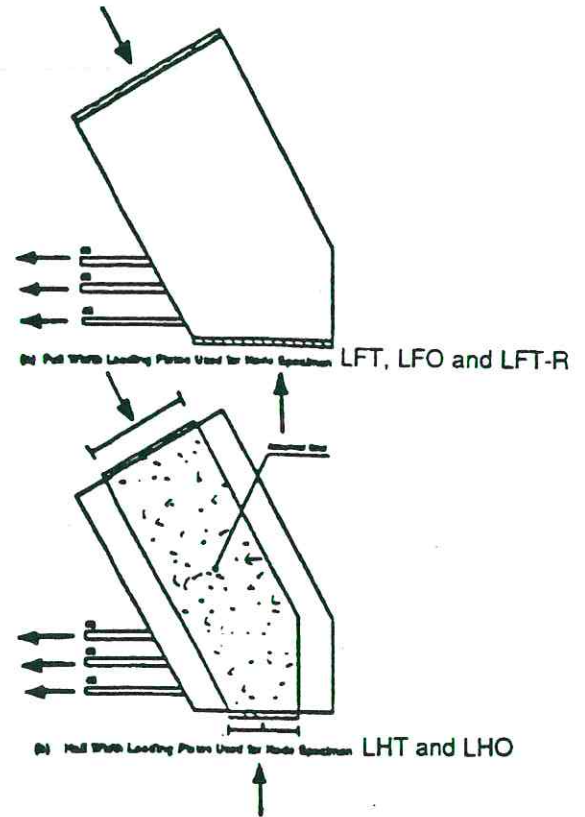


Figure 2.43: Proposed tie width by CEB-MC - Draft 1990 [64]

cases anchorage failure was obtained. The approach shown in Fig. 2.41, to define the geometry of CCT-nodes for anchored reinforcing bars anchored by development length behind the node, is based on the test results from Bouadi [39]. In his specimens, the compressive forces and the tensile force in the reinforcement bar were increased simultaneously. All specimens experienced post-yield failures including strut crushing, cover splitting, and gross slippage of reinforcement. In order to find the concrete strength efficiency factor for the CCT-node the specimens with concrete failure are compared in Fig. 2.45. The statistical data from the comparison in Fig. 2.45 are shown in Table 2.17. Included in the comparison are the different geometry of the nodes with different reinforcing details (for further information about the study see [39]). The limiting concrete strength in the strut used in the compression was based on an efficiency factor of $v_e = 0.8$.

Specimen	f_c (psi)	Beaming Plate	Tension Tie	
			Bars	Layout
LFT	2340	Full	3-#5, 8-#6	
LFO	2470	Full	3-#5, 6-#6	
LHT	2490	Half	3-#5, 8-#6	
LHO	2600	Half	3-#5, 8-#6	
LFT-R	2610	Full	3-#5, 6-#6	

Specimen	f_c (psi)	Beaming Plate	Bars	Layout
HFT	4860	Full	3-#5, 8-#6	
HFO-SS	5005	Full	6-#7	
HFO-HS	5015	Full	6-#7	
HFO-SL	5025	Full	6-#7	
HFO-HL	5025	Full	6 #7	



Specimen	f'_c - 28 day	failure load	loading plate ["]	failure mode
LFT	2360 psi	260 kips	14*12; 12*12	crushing of concrete
LFO	2360 psi	260 kips	14*12; 12*12	bond failure
LHT	2360 psi	240 kips	9*12; 6*12	crushing of concrete
LHO	2360 psi	240 kips	9*12; 6*12	crushing of concrete
LFT	2360 psi	345 kips	14*12; 12*12	crushing of concrete
HFT	4860 psi	538 kips	14*12; 12*12	splitting of the side
HFO-SS	4860 psi	450 kips	14*12; 12*12	splitting of the side
HFO-HS	4860 psi	415 kips	14*12; 12*12	splitting of the side
HFO-SL	4860 psi	470 kips	14*12; 12*12	splitting of the side
HFO-HL	4860 psi	433 kips	14*12; 12*12	splitting of the side

Figure 2.44: General information about the tested CCT-nodes (from Ref. [131])

A CCT-node can be analysed by checking the concrete strength after finding the geometry based on the approaches shown in Fig. 2.41. In order to optimize the CCT-node both stresses at the C_1 and C_2 faces should be the same (hydrostatic stress). The stress at the strut C_2 face depends on the strut width " w_{c1} " the tie width " w_{T3} " and the angle " ϕ_{cs} ". Fig. 2.46 shows the geometric inter-relation of these factors with various strut angles " ϕ_{cs} ". The relation may be used for dimensioning the width of the strut or to change the strut angle. The best way to design a CCT-node is to strive for hydrostatic stress ($\sigma_1 = \sigma_2 = \sigma_3 = 1.0$ where σ_i is the stress on node side i) which leads to an optimal efficiency. The following equation can be used to find the optimal solution (see Fig. 2.46):

$$\sigma_2 / \sigma_1 = (w_{c2} \sin^2 \phi_{cs} + w_{T3} (\sin 2\phi_{cs}) / 2) / w_{c2}$$

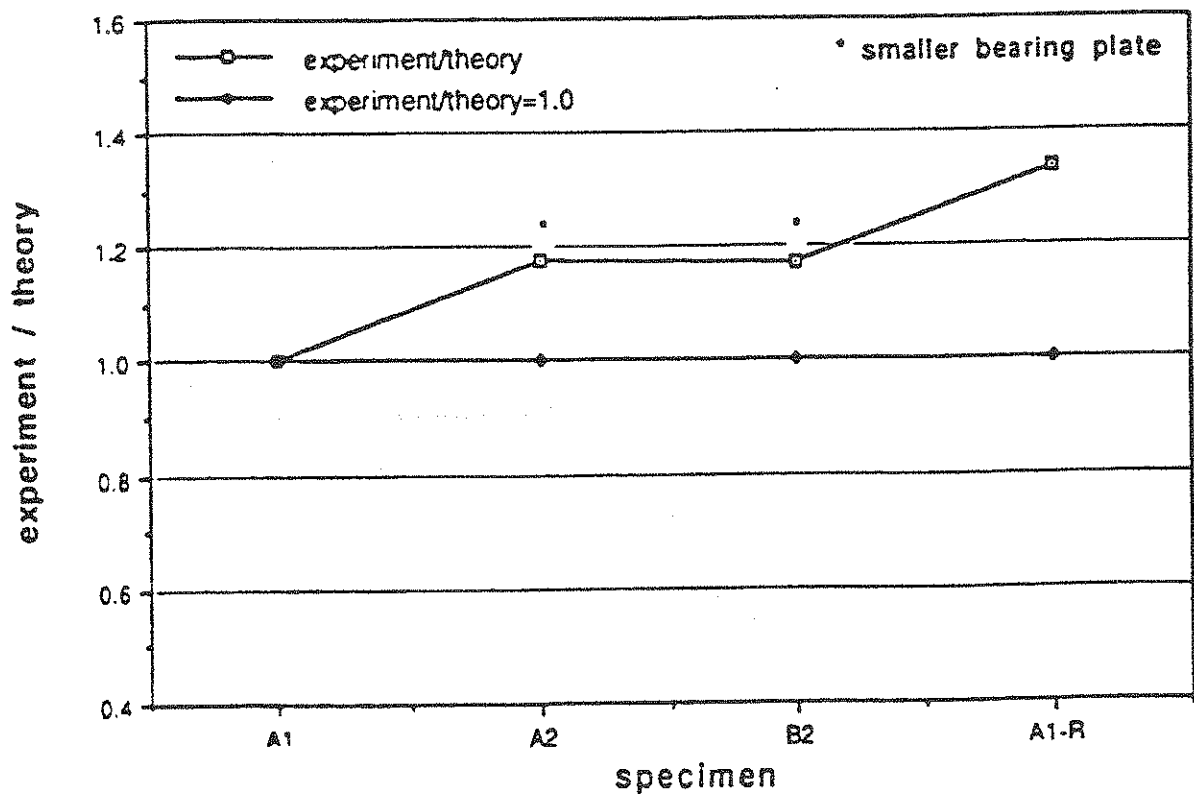


Figure 2.45: Comparison of test results with the concrete efficiency factor of $v_e = 0.8$

X ₁ : Column 1					
Mean:	Std. Dev.:	Std. Error:	Variance:	Coef. Var.:	Count
1.173	.138	.069	.019	11.773	4
Minimum:	Maximum:	Range:	Sum:	Sum of Sqr.:	# Missing:
1	1.338	.338	4.691	5.559	0

Table 2.17: Statistical data from Figure 2.45 (CCT-node)

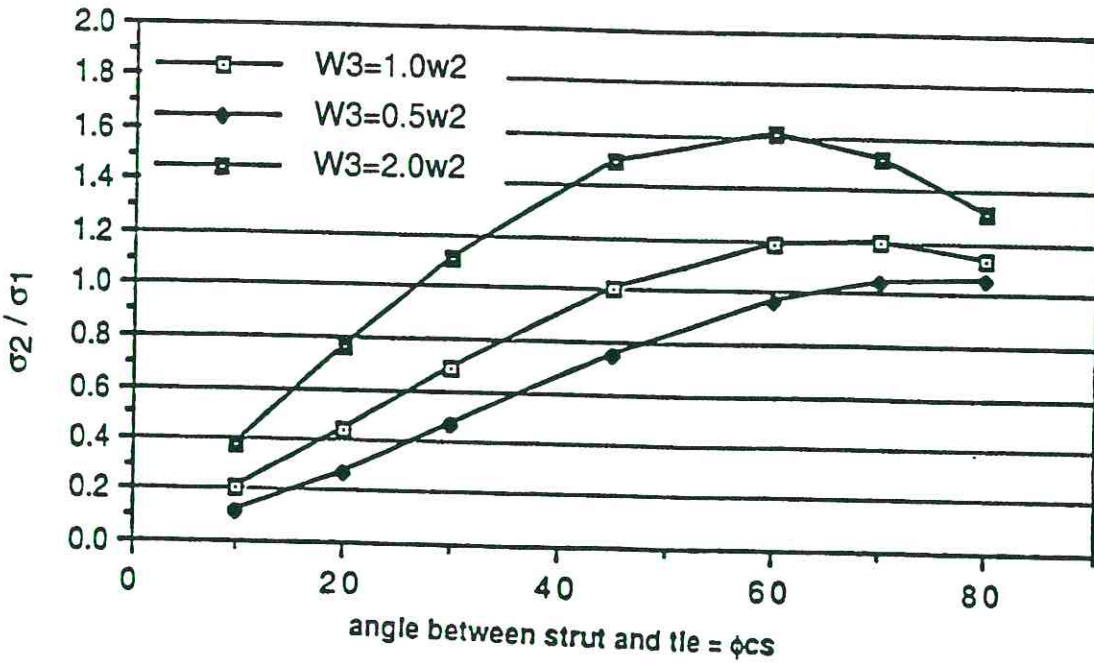


Figure 2.46: Dependency of the efficiency factor's for CCT - node

2.6.3 CTT - Node

The CTT-node is an intersection of a concrete compressive strut and two tensile ties. In steel trusses, as shown in Fig. 2.47, bolts, welds, and gusset plates are sized to safely transfer load between the members. In contrast, a CTT-node in a concrete member must rely on anchorage, bond, and other internal force transfer mechanisms to transfer strut and tie forces. Anchorage is achieved by providing proper development length or in special circumstances by attaching the reinforcement to bearing plates or other fixed components.

The following approaches are proposed in order to find the geometrical constraints for the CTT-node. The definition of the effective width plays an important factor in the dimensioning process. For the relatively rare case of a CTT-node with anchor plates, the widths of the plates are given as dependent constraints which tend to fix the width of the unknown compression strut. The more practical and generally occurring case is the CTT-node without a bearing plate. For this case the approach of Fig. 2.48 is proposed in order to define the effective strut width. As can be seen, it is similar to the approach used for the CCT-node.

The efficiency factor for the CTT-node was investigated in an experimental study by Anderson [38]. Table 2.18 shows several parameters of the test specimens. Two specimens, one with normal strength concrete (HHSR: $f'_c = 5780$ psi) and one with low strength concrete (LHSR), used reduced bearing plate area (4 in. instead of 10.6 in). Specimen LFAC: $f'_c = 3920$ psi was the only specimen in this study that was subjected to unequal forces in the tension ties. The purpose of the unequal force was to induce a different compression strut angle into the specimen. A 30 degree angle from the horizontal was chosen so the force in the longitudinal steel would be approximately 1.73 times the force in the transverse reinforcement.

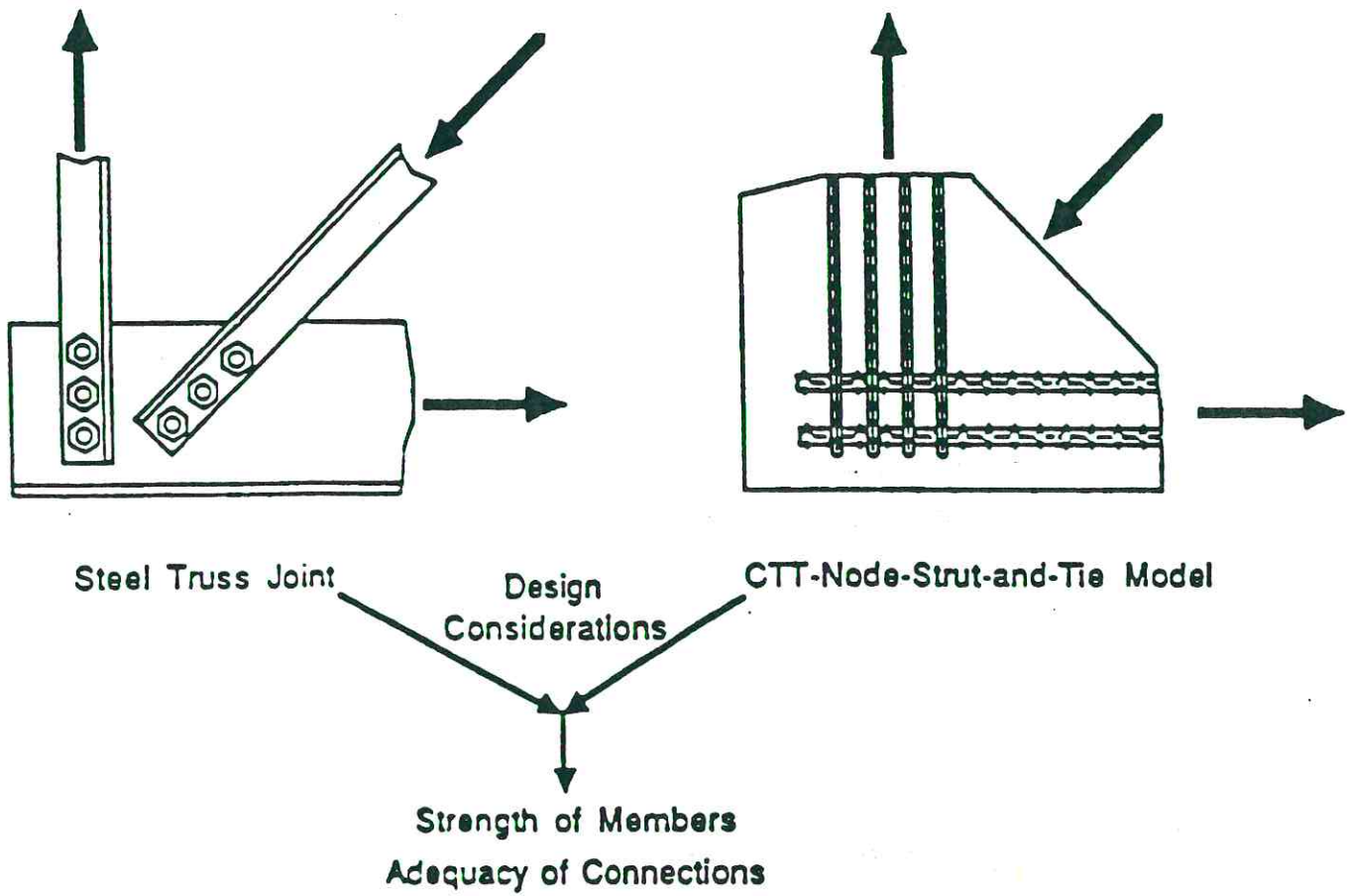
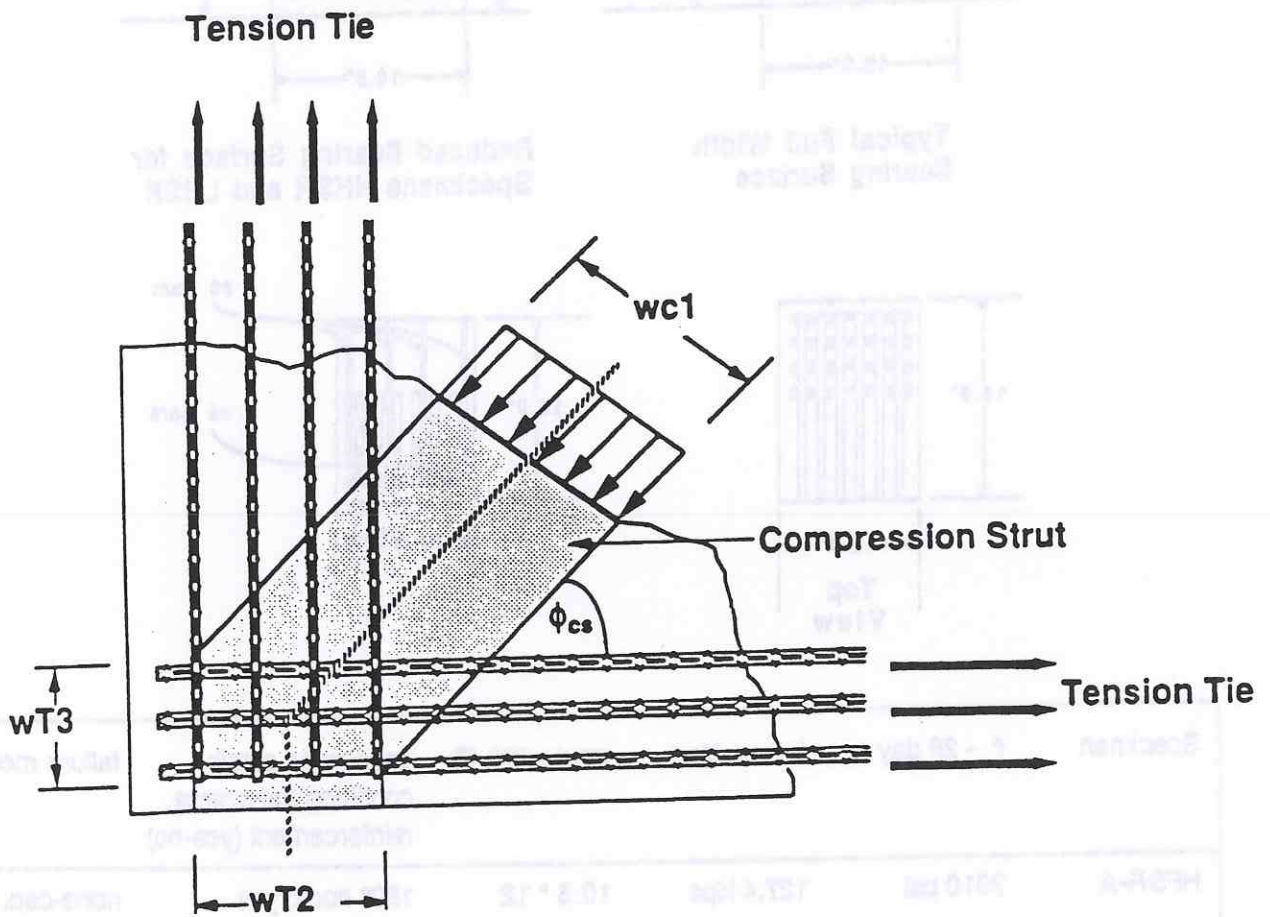
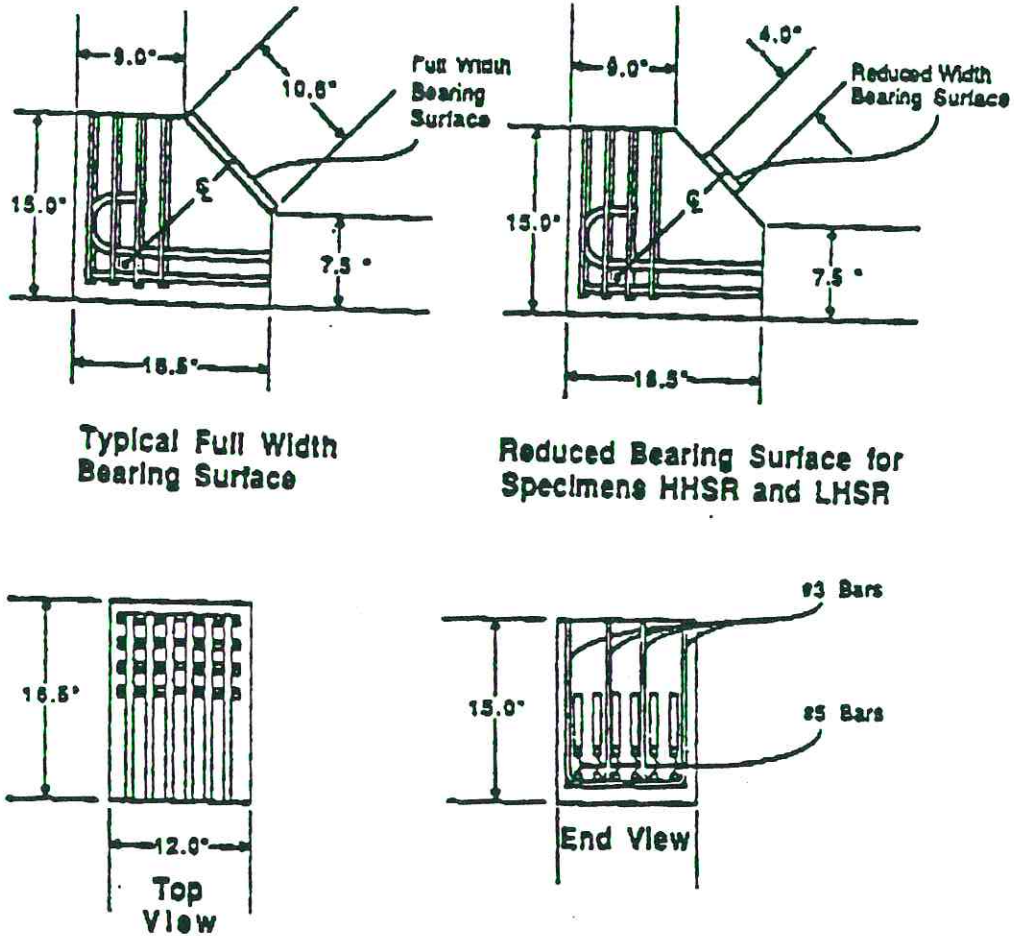


Figure 2.47: Comparison of design rationale used for nodal region of strut-and-tie-model and joint of steel truss (from Ref. [7])



$$wc1 = wt2 \sin \phi_{cs} + wt3 \cos \phi_{cs}$$

Figure 2.48: Geometrical approach to define the strut width for CTT-node



Specimen	f'_c - 28 day	failure load	strut width ["]	anchorage detail; confining transverse reinforcement (yes-no)	failure mode
HFSR-A	7010 psi	127.4 kips	10.6 * 12	180° hook; yes	none-cap. of setup
HFSR-B	5780 psi	137.5 kips	10.8 * 12	180° hook; yes	none-cap. of setup
HHSR	5780 psi	139 kips	4 * 12	180° hook; yes	none-cap. of setup
HFSB	5780 psi	138.1 kips	10.6 * 12	straight bar; yes	gross slip-trans.
HFNC	5780 psi	132.5 kips	10.6 * 12	180° hook; no	cover splitting
LFSR	3720 psi	117.4 kips	10.8 * 12	180° hook; yes	development-trans.
LHSR	3720 psi	130.2 kips	4 * 12	180° hook; yes	strut crushing
LFNC	3720 psi	117.8 kips	10.6 * 12	180° hook; no	cover splitting
LFAC	3920 psi	165.4 kips	10.6 * 12	180° hook; yes	development-long.

Table 2.18: General information about the tested CTT-nodes (from Ref. [33])

In the tests, general strut failures did not usually occur. The reinforcing anchorage detail was primarily responsible for limiting the ultimate load. However, for design purposes the actual efficiency factor for the concrete compressive strength is of interest. Only one specimen (LHSR: $f'_c = 3720$ psi) failed by concrete crushing. The bearing plate stress was 3836 psi. By using a concrete efficiency factor of 0.8 and by taking into account the smaller bearing plate width (4") compared to the compression strut width (6.37") the experiment / theory - ratio can be computed:

$$\begin{aligned}\sigma_c &= C / A_b = 184131 / (12 \cdot 4) = 3836 \text{ psi} \\ \sigma_c &= 3836 \text{ psi} \leq 0.8 \cdot 3720 (6.37/4)^{0.5} = 3754 \text{ psi}\end{aligned}$$

$$\text{experiment / theory - ratio} = 3836 / 3754 = 1.02$$

For this specimen with a concrete strength of 3720 psi a concrete efficiency factor of 0.8 could be safely used. The efficiency factors for CCT- and CTT-nodes must produce members in which the critical section will exhibit ductile behavior under extreme overload. This is done by ensuring that actual failure would occur only after the reinforcement yields. In order to guaranty ductile behavior, it is necessary to place a limit on the failure state stress levels in the concrete.

When designing a CTT-node the reinforcement in both ties should yield at the same time. In order to find the optimum strut angle for a given reinforcement pattern, the following approach can be used (see Fig. 2.49). It is a geometrical approach and is based on the compression strut width. Since the compression strut width "w1" is dependent on the tension tie widths "w2" and "w3" shown in Fig. 2.48, the optimal concrete efficiency for a CTT-node is given by the angle with the largest compression strut width "w1". The compression strut width can be computed:

$$w1 = w2 \sin \phi_{cs} + w3 \cos \phi_{cs}$$

Fig. 2.49 shows the compression strut width "w1" for various strut angle " ϕ_{cs} " and three different tension tie width ratios.

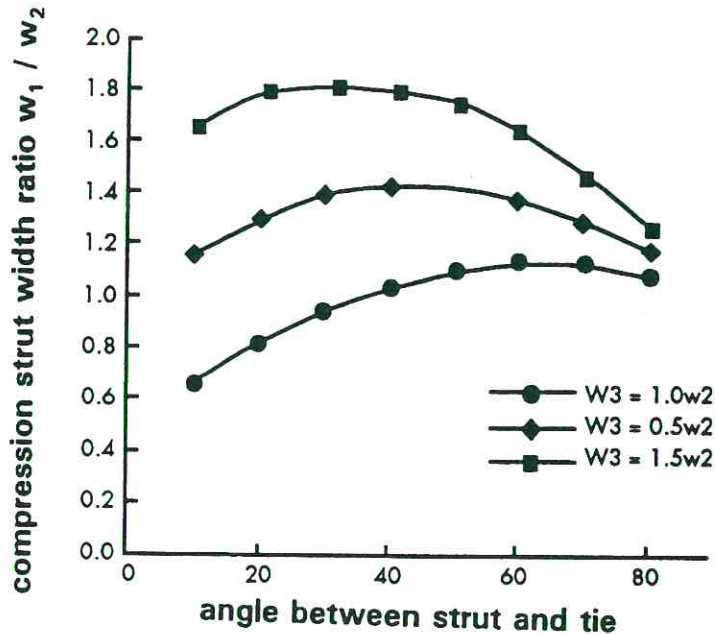


Figure 2.49: Dependency of the compression strut width for CTT-node

2.6.4 TTT-nodes

In those rare cases where the tensile strength is used as a tension tie, some global understanding about tensile strength has to be formulated.

Although it is difficult to develop design criteria for the case of concrete tensile ties, it would be even worse to maintain the formalistic view that the tensile strength of concrete cannot and therefore must not be utilized. Tracing the flow of forces in actual structures, to be gap free and consistent with strut- and- tie- models will sometimes show that equilibrium can only be satisfied if ties or tensile force can be accepted in places where, for practical reasons, reinforcement cannot be provided and the tensile strength of concrete is implicitly utilized (see Fig. 2.50).

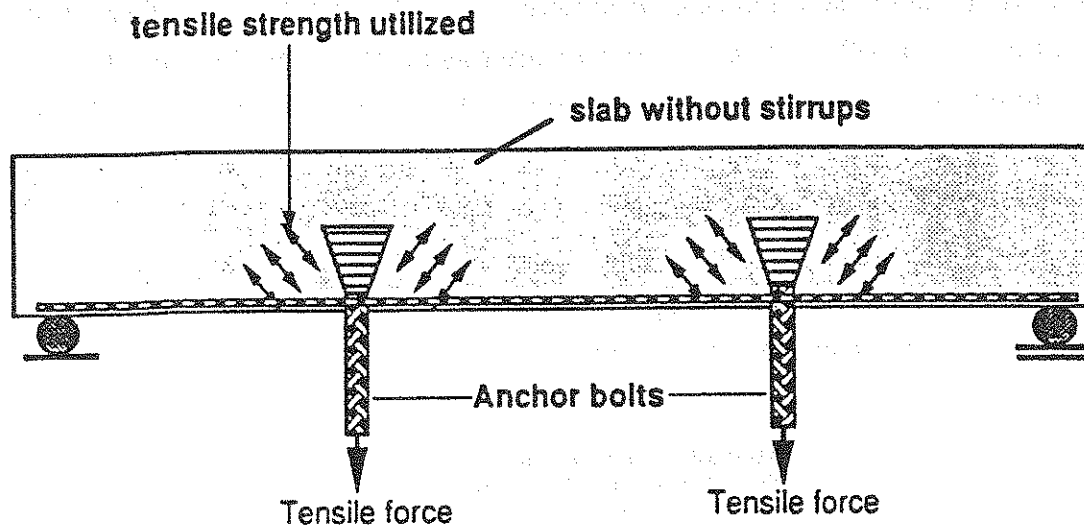


Figure: 2.50: Tensile strength of concrete implicitly utilized

The tensile strength of concrete is relatively low, about 5 to 15% of the compression strength. The tensile strength is more difficult to measure and the variance is greater than for compressive strength. For the biaxial- and triaxial range the tensile strength is assumed to be equal to the uniaxial tensile strength [24, 69]. While concrete tensile strength may play a part in the force transfer mechanism, it is generally more convenient to neglect its contribution. This is prudent for design purposes as the tensile strength of the concrete is very small relative to that of reinforcement. Also, the action of creep, shrinkage, external and internal thermal stresses and other load patterns may cause cracking which would inhibit the development of concrete ties. For most practical detailing problems, concrete tensile strength may be ignored. For those cases where the tensile strength is needed, a value of

$$f_{ct} = 3 (f'_c)^{0.5}$$

can be used.

If the tensile forces are transferred with reinforcing bars, the anchorage requirements became important. Anchorage is achieved by providing proper development length or in special circumstances by attaching the reinforcement to bearing plates or other fixed components. The key to determining anchorage requirements is selecting the point at which the reinforcement must be fully developed. When the ties at a node are to be fully developed, a conservative approach is to assume that the development length for each layer of tie reinforcement is assumed to begin at the intersection point of the different ties with the confined joint boundaries (see Fig. 2.51).

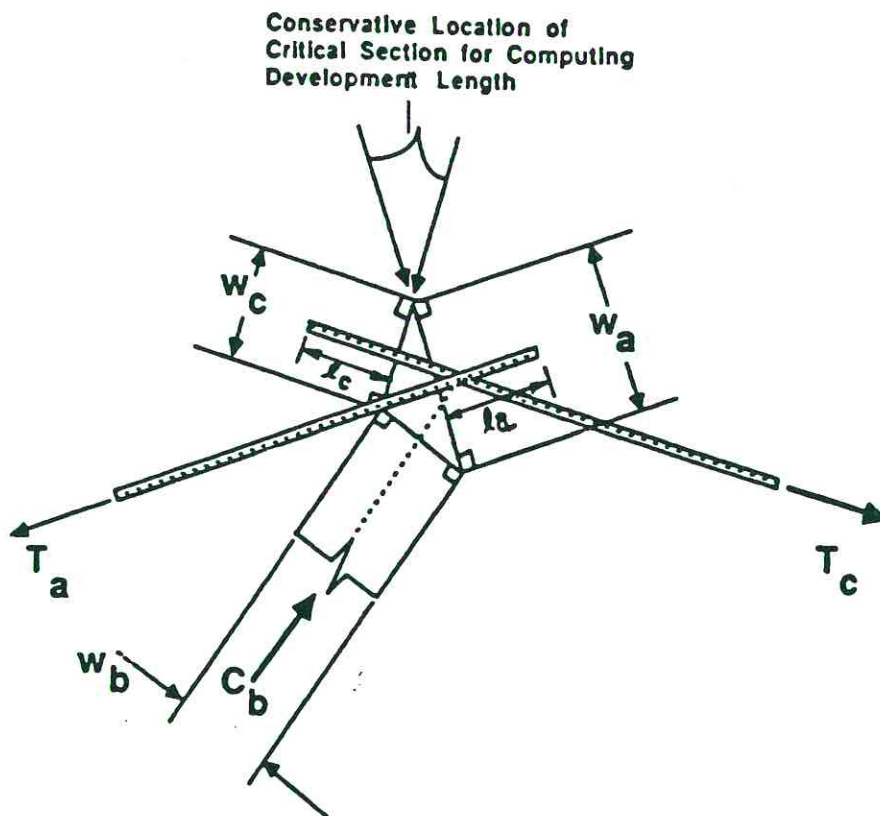


Figure 2.51: Conservative starting point for computing development length

Because the behavior of the tension controlled nodes (CTT- and TTT-node) is influenced by the tie anchorage details, it is appropriate to make a distinction between anchorage details that may be chosen. In Fig. 2.52, tie anchorages have been separated by type.

Positive anchorage details are those which do not rely appreciably upon bond stresses to resist the applied tensile force and include end plates and continuous reinforcing details. The positive anchorage detail must be designed so that the tie force is distributed over a sufficient area to prevent the node zone from being overstressed in compression. End plates and continuous reinforcement details are attractive from a design standpoint because they are fairly easy to evaluate.

Development anchorage details are those which are anchored with bent bars (hooks), bond strength or a combination of both. Development anchorage details are normally more economical, easier to fabricate and to place in the formwork. The disadvantage of the development anchorage details is the longer required anchorage length.

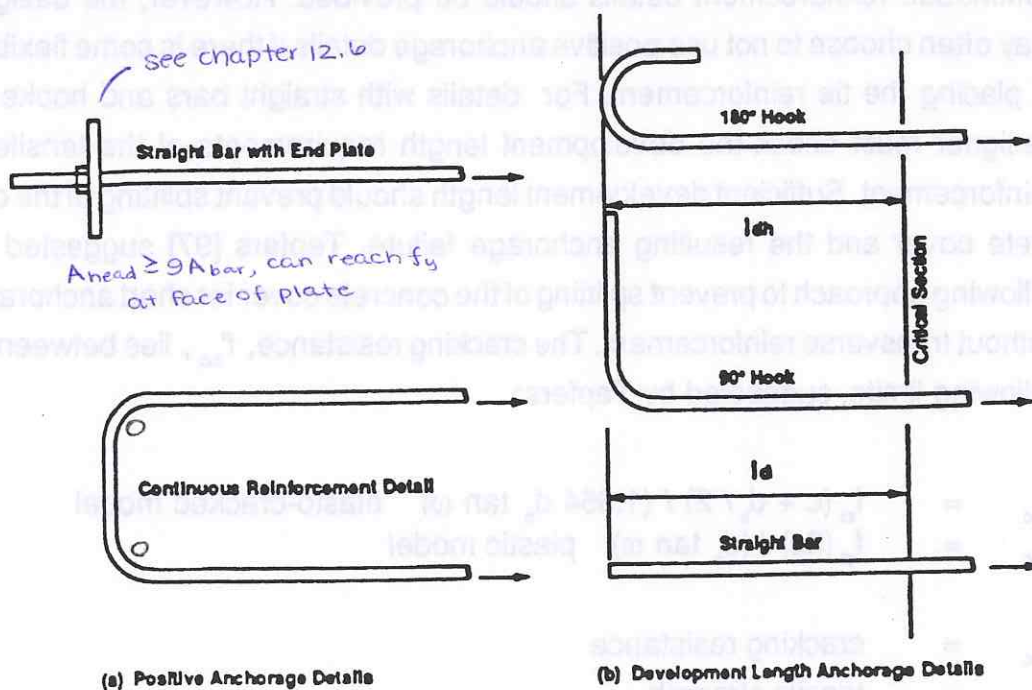


Figure 2.52: Positive and development length anchorage details

2.6.5 Anchorage Requirements in the nodal zone

All nodal zones are influenced by the tension tie anchorage details. If the applied tensile force is connected to bearing plates and does not rely appreciably upon bond stresses, then the tie actually provides a compression strut in terms of its action on the nodal zone.

Barton [7] and Anderson [38] call anchorages with end plates or continuous looped reinforcement "positive anchorage details." The positive anchorage must be designed so that the compression resulting from the tie force is distributed over a sufficient area to prevent the node from being overstressed. However, such positive anchorages are not necessarily required nor are they always desirable or practical construction alternatives for anchoring tensile ties. Except for small diameter reinforcement, positive anchorage details are more expensive and more difficult to construct than standard details such as straight bars or hooks. Where the transfer of strut- and tie- forces is felt to be so abrupt that sufficient bond anchorage forces cannot be developed, end plates or continuous reinforcement details should be provided. However, the designer may often choose to not use positive anchorage details if there is some flexibility in placing the tie reinforcement. For details with straight bars and hooks the designer must check the development length requirements of the tensile tie reinforcement. Sufficient development length should prevent splitting of the concrete cover and the resulting anchorage failure. Tepfers [97] suggested the following approach to prevent splitting of the concrete cover for short anchorages without transverse reinforcement. The cracking resistance, f'_{bc} , lies between the following limits, suggested by Tepfers:

$$f'_{bc} = f_{ct} (c + d_b / 2) / (1.664 d_b \tan \omega) \quad \text{elasto-cracked model}$$

$$f'_{bc} = f_{ct} (2c) / (d_b \tan \omega) \quad \text{plastic model}$$

$$f'_{bc} = \text{cracking resistance}$$

$$f'_{bc} = \text{tensile strength}$$

$$c = \text{concrete cover}$$

$$d_b = \text{diameter of reinforcing bar}$$

$$\omega = \text{average angle between the transverse cracks and the axis of the bar} \approx 45^\circ$$

Bar development length " l_d " is the necessary embedment to assure that a bar can be stressed to its yield point with some reserve to ensure member toughness under specific containment conditions. The necessary length is a function of a number of variables, mainly of the bond strength and confinement from both concrete cover and transverse reinforcement.. A great amount of research work has been done in the area of development length (Tepfers, R. [98], Jirsa, J; Lutz, L.; Gergely, P. [99], Orangun, C.; Jirsa, J.; Breen, J. [100]). The radial stress in the concrete surrounding a bar being developed can be regarded as a water pressure acting against a thick - walled cylinder having an inner diameter equal to the bar diameter and a thickness "c" (the smaller of the clear bottom cover c_b or half the clear spacing c_s to the next adjacent bar). Based on a comprehensive review of a broad range of test results, the following equation for the development length (l_d) in terms of the stress in the bar at the critical section (f_s), the bar diameter (d_b), concrete strength (f_c), cover (c) to diameter ratio, and transverse reinforcement amount (A_v), yield strength (f_y) and spacing (s) were proposed by Orangun, Jirsa and Breen [100].

$$l_d = d_b \left\{ \frac{f_s}{[4(f_c)^{0.5}] - 50} \right\} / \left\{ 1.2 + 3c/d_b + (A_v f_y) / (500 s d_b) \right\}$$

A modified form of this equation in terms of a series of modifiers is the basis for the recent changes in splice and development length design provisions in ACI 318-89 [101].

In CCT - and CTT - nodes the reinforcing bars are under lateral pressure from the compressive struts (see Fig. 2.53). When lateral pressure is applied the vertical component of the radial pressure tends to be balanced by the lateral pressure. The bond strength increases approximately in proportion to the square root of the lateral pressure. In addition, the distance between the bearing plate and the reinforcement bar, e , has an important effect as shown in the study by Lormanometee [102]. Different experimental studies were evaluated to develop a formulation for a possible reduction of the development length for a reinforcement bar under lateral pressure. Only tests in which failure occurred before the bars yielded were included. The lateral pressure acts similar to the action of transverse reinforcement. The overall strength of a splice with transverse reinforcement and lateral pressure can be expressed as follows:

$$U = U_c + U_v + U_p$$

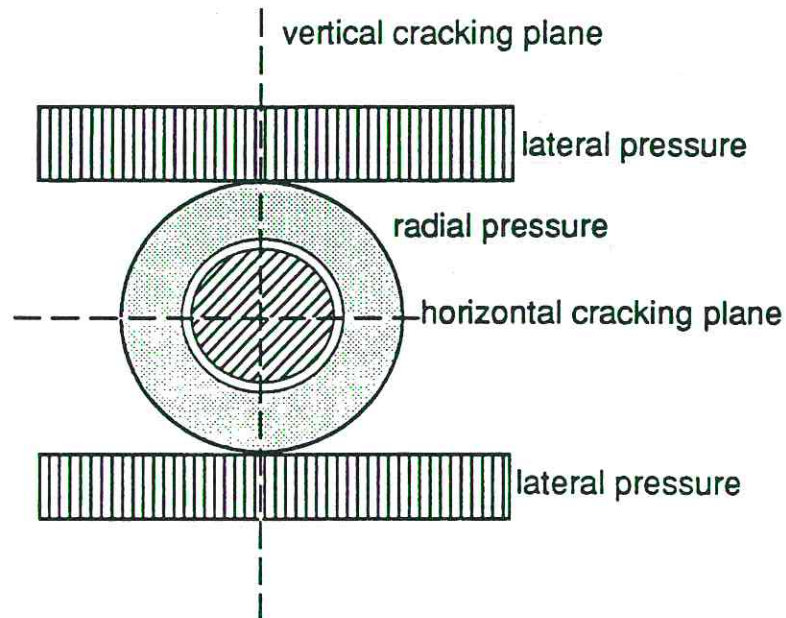


Figure 2.53: Lateral pressure on reinforcement bar

$$\begin{aligned}
 u &= (f'_c)^{0.5} (1.2 + 3c/d_b + 50d_b/l_s) \\
 u_r &= (f'_c)^{0.5} [A_r f_{yt} / (500s d_b)] \\
 u_{lp} &= (f'_c)^{0.5} [(f'_n)^{0.5} (200 - e^2) / 1000]
 \end{aligned}$$

The development length can then be computed:

$$l_d = \frac{d_b \{f_s / [4(f'_c)^{0.5}] - 50\}}{\{1.2 + 3c/d_b + (A_r f_{yt}) / (500s d_b) + [(f'_n)^{0.5} (200 - e^2) / 1000]\}}$$

$$\begin{aligned}
 (A_r f_{yt}) / (500s d_b) &\leq 3.0 \\
 [(f'_n)^{0.5} (200 - e^2) / 1000] &\leq 6.0 \text{ (see Fig. 2.54)}
 \end{aligned}$$

The comparison with test results from Lormanometee [102] and Schmidt-Thrö, Stöckl and Kupfer [103] are shown in Fig. 2.55 and the statistical data is shown in Table 2.18. The proposed relationship is conservative for all except one of the test results and is generally quite conservative. A multiplying factor of 1.25 is required to make the results consistent with the current ACI and AASHTO expressions which indirectly introduce a ϕ factor as $1/\phi = 1/0.8 = 1.25$.

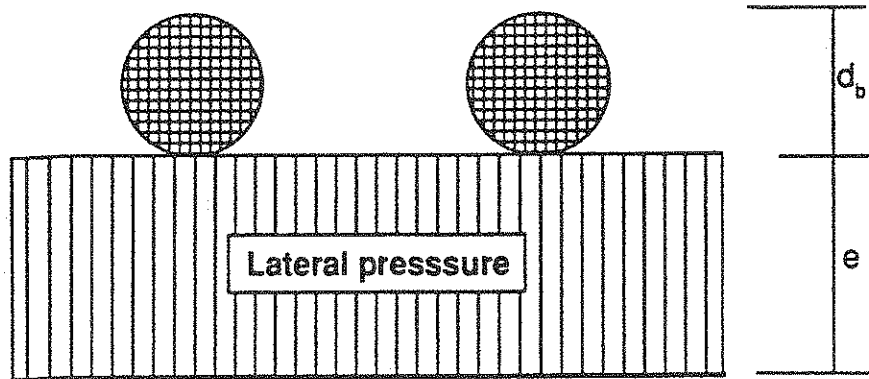


Figure 2.54: Lateral pressure and the distance "e" to the reinforcing bar

Development length anchorage details include straight and hooked bars. For these details the designer must check the development length requirements of the tension tie reinforcement. For CCT-nodes confining reinforcement had only a low effect ($\approx 2\%$). Similarly, for the CTT-node in which the transverse reinforcement anchorage hooks were turned nearly parallel to the longitudinal bars (but not closed), the ultimate load decreased by only a maximum of 4% in comparison with closed confined reinforcement.

By using hooks instead of long bars for the anchorage, the ultimate load decreased by 8% for CCT (specimen C2 and D2) and for CTT (specimen HFSR-A) nodes. Using a transverse U for the second tie in CTT-nodes provided lateral confinement, but prying action at the 90° bend can produce splitting cracks. In order to control splitting cracks of the end cover it is suggested that the longitudinal reinforcement be extended a short distance ($\approx s/2$ or 2 in.) past the transverse reinforcement.

Table 2.19: Statistical data from comparison in Figure 2.55

X ₁ : Column 1					
Mean:	Std. Dev.:	Std. Error:	Variance:	Coef. Var.:	Count:
3.275	.967	.19	.935	29.532	26
Minimum:	Maximum:	Range:	Sum:	Sum of Sqr.:	# Missing:
.91	5.17	4.26	85.14	302.18	0

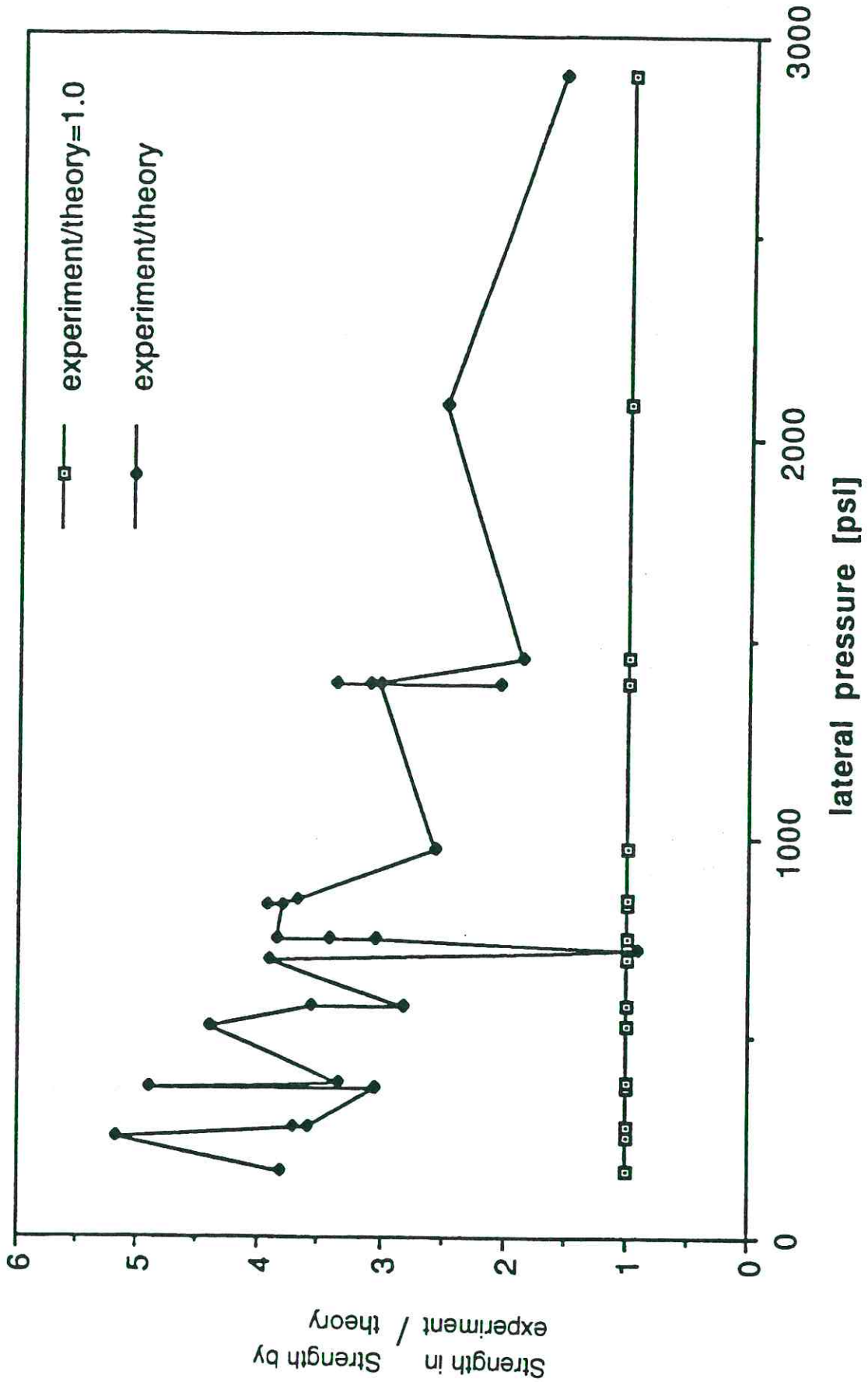


Figure 2.55: Comparison of a theoretical approach and test results for the development length of straight bars with confinement from bearing plates

2.7 Model optimization

Since strut- and- tie models are lower bound solutions for the actual load carrying capacity of a structure, any correctly formulated and correctly detailed strut- and- tie model should safely carry the design loads applied. In many cases different models can be developed for the same external load configuration. Doubts could arise as to whether the most efficient model has been chosen. In selecting the model, it is helpful to realize that loads try to use the path with the least forces and deformations. This simple criterion for optimizing a model may be formulated as follows:

$$\sum F_i l_i \epsilon_{mi} = \text{minimum}$$

F_i = force in strut or tie i

l_i = length of member i

ϵ_{mi} = mean strain of member i

This equation is derived from the principle of minimum strain energy for linear elastic behavior of the struts and ties after cracking. The contribution of the concrete struts can generally be omitted because the strains of the struts are usually much smaller than those of the steel ties. Since reinforcing ties are much more deformable than concrete struts, Schlaich et al [28] propose that the model with the least and shortest ties is the best.

As a more general approach for model development the following considerations are important constraints:

- ease of fabrication
- equilibrium
- ductility
- serviceability

In many cases, practicality and ease of fabrication will have the greatest influence upon the configuration of the design model. Models which result in details that are overly congested or difficult to fabricate should be avoided. The reinforcement

pattern for the D region should be compatible with the reinforcement scheme used in adjacent portions of the structure. In order to satisfy the requirements of the theory of plasticity, a model must be in equilibrium under the applied loads. However, if the selected strut and-tie-model is to fully develop, the load carrying capacity of the strut- and-tie- elements and the rotational capacity of the nodes must not be exceeded before the ties yield. Furthermore, acceptable serviceability at usual working load levels requires that crack widths be limited by provision of sufficient, closely spaced reinforcement in regions of high tension and hence cracking. Attention must be paid to elastic analysis predictions of high tension zones to ensure crack control reinforcement is appropriate. In addition to the accepted standards for flexural reinforcement distribution and both minimum and maximum bar spacings, minimum reinforcement to control shrinkage, creep and thermal stresses should be provided.

A more sophisticated optimization process would recognize that the fabrication and placement costs of the local confining reinforcement and additional anchorage at the nodes is substantially higher than the costs of longitudinal reinforcement. A more realistic approach would provide for different unit costs for the major classifications of reinforcement. The following approach can be used:

$$\sum l_l C_l + \sum l_t C_t + \sum f l_d C_N = \text{minimum}$$

l_l	=	length of the longitudinal reinforcement
l_t	=	length of the transversal reinforcement
l_d	=	development length
C_l	=	cost per unit length of the longitudinal reinforcement
C_t	=	cost per unit length of the transversal reinforcement
	≈	1.2 times the cost of C_l
C_N	=	cost per unit length of the node reinforcement
	≈	1.5 times the cost of C_l
f	=	CCC-node = 0.0
		CCT-node = 1.0
		CTT-node = 2.0
		TTT-node = 3.0 (reinforced TTT-node)

In order to prevent extreme strut angles (which may result in excessive cracking), the angles between compression struts and tension ties should be limited to between 25 and 65 degrees. In summary, some guidelines for model optimization have been proposed. The designer should taken into account practical considerations in combination with the proposed strut- and- tie- model principles in the development of a suitable model.

2.8 Concrete efficiency factors for design

2.8.1. Unconfined Nodes and Undisturbed Concrete Struts

The effective concrete strength in the various compression fields or struts is less than the concrete cylinder strength. General agreement between the theory developed for the strut- and- tie- models and test results is only obtained if a concrete efficiency factor is introduced to limit the concrete capacities in nodes and struts. When compared with a large number of test results (Fig. 2.23) the following functions gave acceptable results.

$$v_e = 0.5 + 15 / (f'_c)^{0.5}$$

$$v_e = 0.5 + 20 / (f'_c)^{0.5}$$

As a design simplification, a linear relationship falling between these two functions was chosen as shown in Fig. 2.56. The basic efficiency factor should be taken as 0.8 for concrete compressive strengths up to and including 4000 psi. For strengths above 4000 psi, the efficiency factor should be reduced continuously at a rate of 0.05 for each 2000 psi of strength in excess of 4000 psi, but the efficiency factor should not be taken less than 0.65.

$$f_{ce} = v_e f'_c$$

$$v_e = 0.8 \text{ for } f'_c \leq 4000 \text{ psi}$$

$$v_e = 0.9 - 0.25 f'_c / 10000 \text{ for } 4000 < f'_c < 10000 \text{ psi}$$

$$v_e = 0.65 \text{ for } f'_c \geq 10000 \text{ psi}$$

This basic efficiency factor can be used for checking compressive fields and short struts within unconfined or lightly confined nodes, as well as applications where the compressive struts act over undisturbed or uncrushed concrete as occurs in many wall type applications where no tensile cracking is expected.

2.8.2 Compression Diagonals

As shown in 2.4.1.1, the effective concrete strength in the compression diagonals must be reduced with an additional factor of 0.6. This is particularly important in thin web members and cores where fairly wide cracks must be crossed by the struts.

$$v_{ed} = 0.6 v_e$$

There are many reasons why the efficiency factor for compressive diagonals is less than the global efficiency factor for unconfined nodes and undisturbed compression fields. The web strength might depend somewhat on the stirrup spacing in the longitudinal direction and the resultant control of inclined web cracking. In addition the effective strength of the web may be reduced because of cracks developed in early loading stages and having directions other than that of the final cracks [21, 28, 62, 65, 66]. Finally, in beams and girders the compression zones are highly concentrated and the struts in the web concrete have a corresponding concentration of load which may lead to more local failure of the concrete at a stress level which as an average over the web is less than the effective compression strength in more uniform compression fields.

2.8.3. Confined Nodes

In certain applications such as post-tensioned anchorage zones, a very large amount of local confinement may be desirable to allow the safe development of very high compression stresses in a local zone node. In such cases the confined node effective compressive stress is designated as f_{e3} and may be determined as:

(a) For nodes confined with closely spaced spiral reinforcement :

$$f_{e3} = v_e f'_c (A/A_b)^{0.5} + 4.0 (A_{core} / A_b) f_{lat} (1 - s/d)^2 \leq 2.5 f'_c$$

The term " $(1 - s/d)^2$ " reflects the reduction in effectiveness of spiral associated with increasing spacing of the spiral wires.

(b) For nodes confined with orthogonal reinforcement such as closed square hoops and with longitudinal reinforcement to anchor the corners of the hoops:

$$f_{e3} = v_e f'_c (A/A_b)^{0.5} + 2.0 (A_{core} / A_b) f_{lat} (1 - s/d)^2 \leq 2.5 f'_c$$

(c) For nodes confined with orthogonal reinforcement such as closed square hoops but without longitudinal reinforcement anchoring the corners of the hoops:

$$f_{e3} = v_e f'_c (A/A_b)^{0.5} + 1.0 (A_{core} / A_b) f_{lat} (1 - s/d)^2 \leq 2.5 f'_c$$

In (a), (b), and (c) the following limits apply:

$$\begin{aligned} A/A_b &\leq 4 \\ 1 &\leq A_{core} / A_b \leq 3 \end{aligned}$$

In (a), (b), and (c), the symbols are defined as:

v_e	=	basic efficiency factor as defined in Section 2.8.1
f'_c	=	concrete compressive strength
A	=	area of confined concrete concentric with and geometrically similar to the bearing plate
A_b	=	effective area of the bearing plate
A_{core}	=	area of the confined strut
A_s	=	cross sectional area of the confining reinforcement
f_{lat}	=	$2 A_s f_s / (s d)$
f_y	=	yield strength of confining reinforcement
d	=	diameter of confined core
s	=	pitch or spacing of confining reinforcement
f_s	=	design stress in confining reinforcement
	=	f_y for $f'_c \leq 7000$ psi
	=	$C \mu 25 / (\pi d A_s) \leq f_y$ for $f'_c > 7000$ psi
μ	=	Poisson ratio ($\approx 1/6$ or 0.17 for f'_c up to 10000 psi)
C	=	compression loads

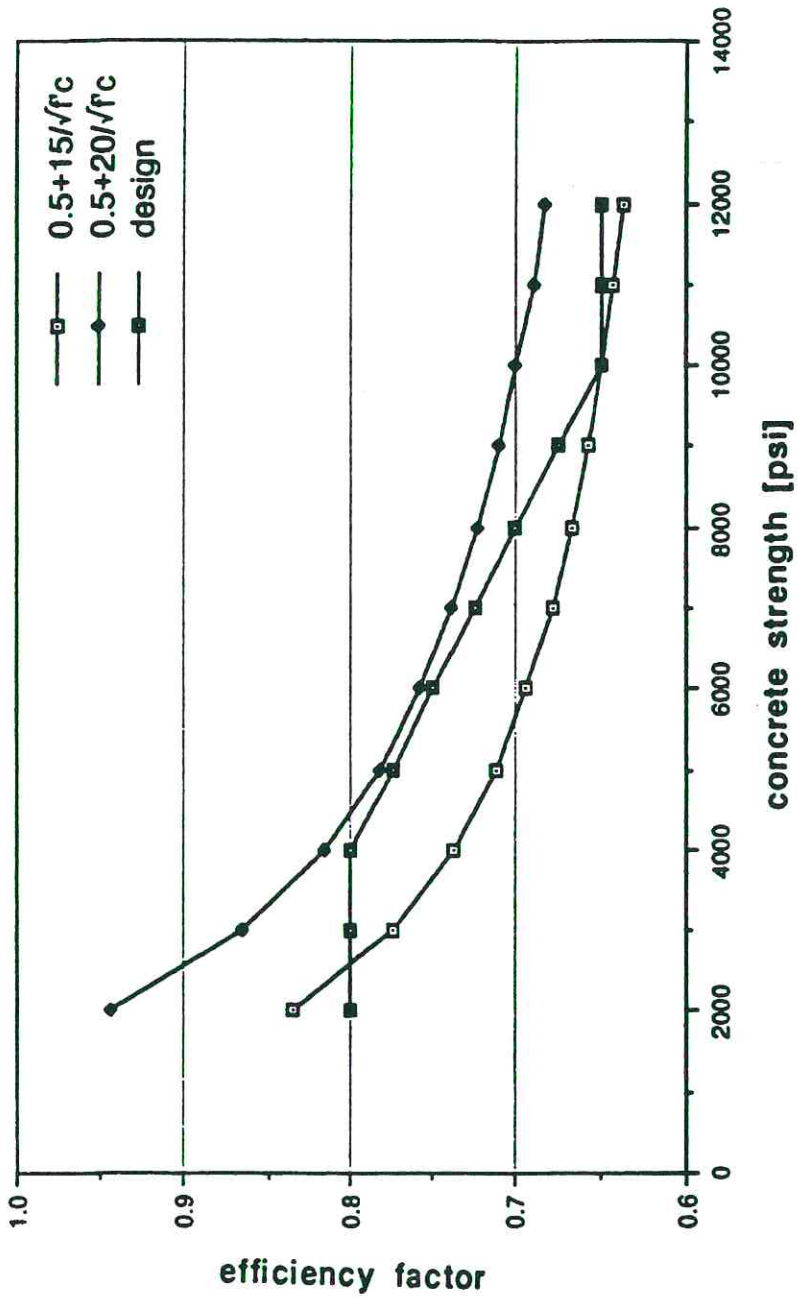


Figure 2.56: Design approach for concrete efficiency factor

2.9 Anchorage requirements for design

Generally the development lengths for straight bars and for hooks should be taken as recommended in ACI 318-89 considering such effect as concrete cover, bar spacing, and transverse confining reinforcement. Since the ACI 318-89 provisions neglect the often beneficial effect of local bearing pressures such as occur at regions where direct loads are applied or direct supports are provided, such local confinement can be considered if for design purposes the development length for straight bars is computed as:

$$l_d = \frac{1.25 d_b \{f_s / [4(f'_c)^{0.5}] - 50\}}{\{1.2 + 3c / d_b + (A_v f_{yt}) / (500 s d_b) + [(f_n)^{0.5} (200 - e^2) / 1000]\}}$$

$$(A_v f_{yt}) / (500 s d_b) \leq 3.0$$

$$0 \leq [(f_n)^{0.5} (200 - e^2) / 1000] \leq 6.0$$

The proposed formula take the lateral pressure into account whenever the distance between the closest bar surface and bearing plate, e , is 14 in. or less..

CHAPTER 3. PROCEDURES

3.1 General Analysis - Structural Analysis

Dimensioning is in principle an iterative process. Figure 3.1 shows the general procedure for designing and dimensioning concrete structures. For many conventional structures and even for large numbers of regions in unusual structures, the strain profiles will be linear and many of the regions will be B-regions. It will ordinarily be simpler and quicker to dimension the B-regions with conventional sectional analysis and design procedures as given in ACI[4] and AASHTO[3] standards. However, in D regions strut- and- tie models should be used. Steps for detailing using the strut- and- tie models are also indicated in Fig. 3.1 in an iterative loop.

From the flow of forces an appropriate strut- and- tie model is chosen and loaded with the applied forces and boundary forces. After computing the strut and tie forces the compression struts, tension ties and the nodal zones have to be dimensioned. There is a close relation between the detailing of the struts bearing on the node, of the ties anchored in the node, and the node itself, because the detail of the node chosen by the design engineer affects the flow of forces. This method implies that the structure is designed according to the lower bound theorem of plasticity. Since concrete permits only limited plastic deformations, the strut- and- tie- model has to be chosen in a way that the deformation limit is not exceeded at any point before the assumed state of stress is reached in the rest of the structure. This is especially important for the main members, which carry a significant portion of the load. According to Schlaich et al. [28] it is desirable that the struts and ties follow the elastic flow paths closely with a deviation of at most 15° from the elastic principal stress directions. The proposed design recommendations are applicable to either prestressed or conventionally reinforced concrete members. The general assumptions for the application of the strut- and - tie- model in the design procedure are:

- Yielding of the reinforcement is required prior to concrete - or anchorage failure
- the ties transfer only uniaxial forces and neglect dowel action, aggregate interlock, tensile strength across cracks etc.

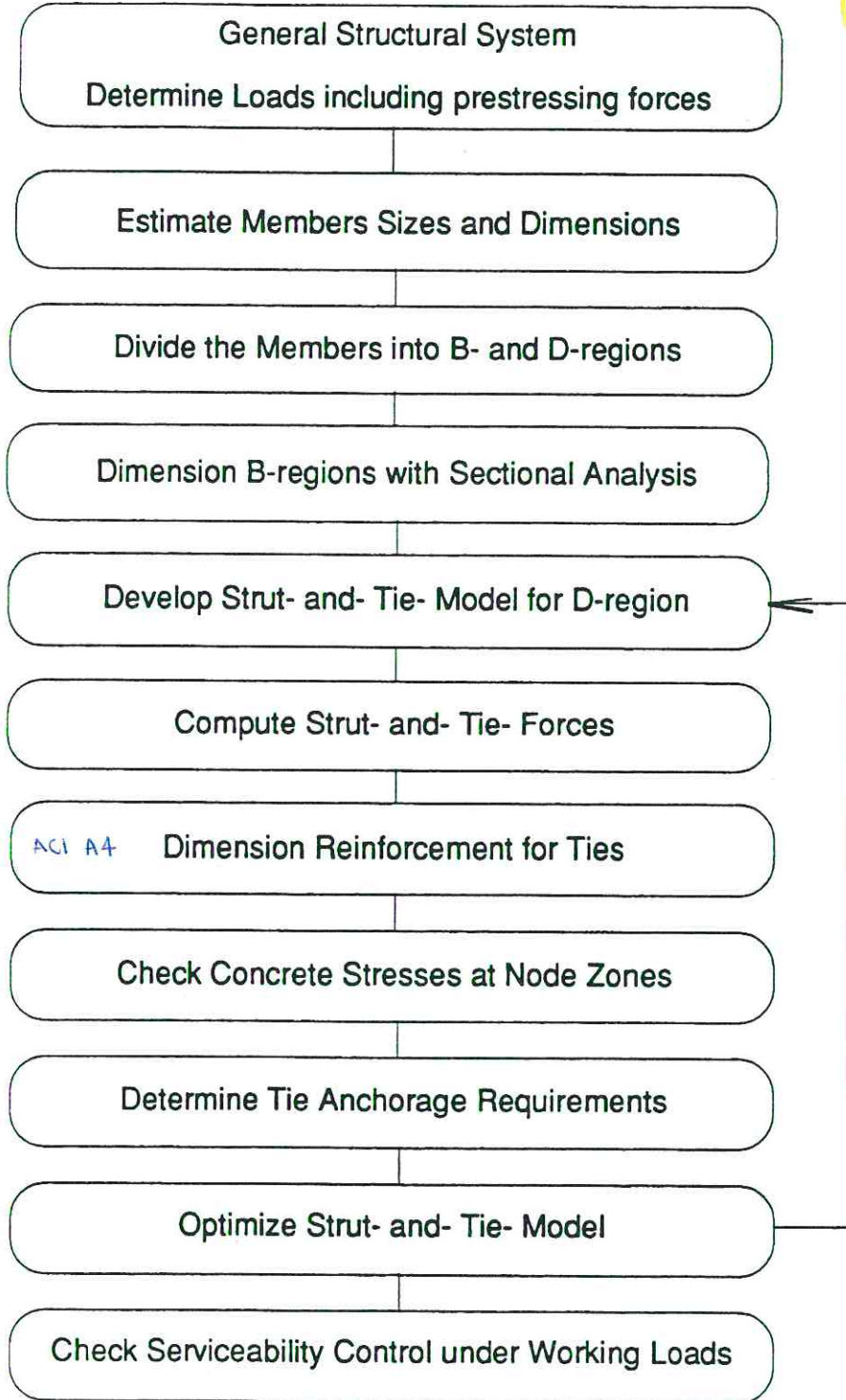


Figure 3.1: Design Procedure for Concrete Structures

For the D-region it is of considerable value to find out how much reinforcement is needed and where it should be placed. The most outstanding contribution of strut- and- tie modelling is the ease and rapidity of determining reinforcement requirements. Checking of nodes and struts is far more complex and involved. For the highly loaded members the strut- and- tie- model should follow the elastic load path rather closely. For low loaded D-regions a larger deviation than 15 degrees from the elastic principal stress directions is permissible (max 45°). Also the angle between struts and ties entering a singular node should not be too small in order to prevent skew cracks ($\geq 15^\circ$ and preferably 25°) and diagonal crushing of the concrete prior to yielding of the reinforcement.

3.2 Checking and Dimensioning Concrete Compression Struts

The struts in the model are resultants of the compression stress fields. The path of the compressive forces may be visualized as the flow of compressive stresses with varying sections perpendicular to the force path direction [104]. As the strut- and- tie- model is an idealization of the real structure, the struts are assumed as straight and concentrated at the nodes. The straight line of a compression strut can be refined for higher stressed struts and some possible tensile forces can be counted as shown in Fig. 3.2.

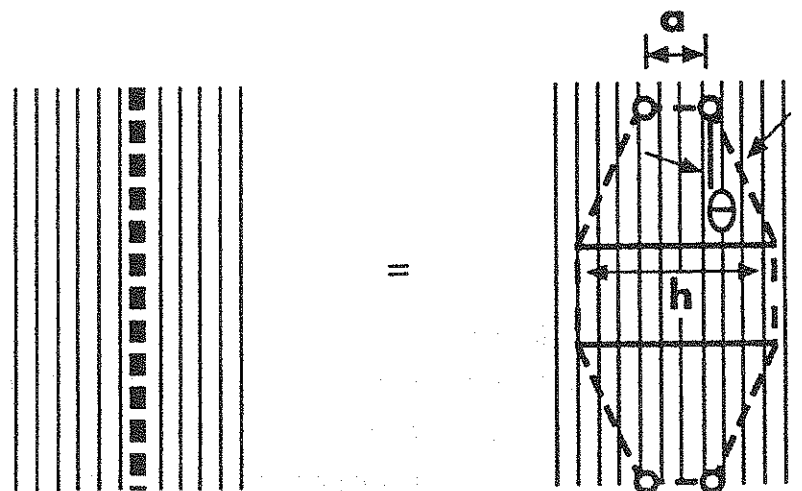


Figure 3.2: Compression fields and strut- and- tie- model

In order to be consistent with the factored load design methods of AASHTO and ACI, load factors must be incorporated into the force calculations and ϕ factors must be incorporated into the resistance calculations. For concrete compression struts ϕ factors as used in concrete column design seem most appropriate.

ϕ	=	concrete strength reduction factor
	=	0.75 members with spiral reinforcement conforming to Sec. 10.9.3 (ACI 318-89)
	=	0.7 for other reinforced members (ACI 318-89)
f'_c	=	concrete compressive strength based on standard 6-in. x 12-in. cylinders at 28 days age

For dimensioning purposes the following approaches are proposed:

a) Compression fields, like fan, bottle, prism (Fig. 2.6a, b, c):

σ	\leq	$\phi f_{ce} = \phi v_e f'_c$
v_e	=	concrete efficiency factor
v_e	=	0.8 for $f'_c \leq 4000$ psi
v_e	=	$0.9 - 0.25 f'_c / 10000$ for $4000 < f'_c < 10000$ psi
v_e	=	0.65 for $f'_c \geq 10000$ psi

b) Compression diagonal struts

$$\sigma \leq \phi 0.6 f_{ce} = \phi 0.6 v_e f'_c$$

c) Confined Compression fields (Fig. 2.6d)

σ	\leq	$\phi f'_{core}$
f'_{core}	=	$[(v_e f'_c (A/A_b)^{0.5} + \alpha (A_{core} / A_b) f_{lat} (1 - s/d)^2)] \leq 2.5 f'_c$
α	=	4.0 for spiral confinement
	=	2.0 for square closed hoop confinement anchored with longitudinal reinforcement
	=	1.0 for square closed hoop confinement without longitudinal reinforcement anchorage
f_{lat}	=	lateral pressure = $2 f_y A_s / (d s)$ for $f'_c \leq 7000$ psi
		= $2 f_s A_s / (d s)$ for $f'_c \geq 7000$ psi

$$f_s = C \mu 2 s / (\pi d A_s) \leq f_y$$

C = compression load
 μ = poisson ratio ($\approx 1/6$ or 0.17 up to 10,000 psi)
 A = area of confined concrete concentric with and geometrically similar to the bearing plate
 A_b = area of the bearing plate
 A_{core} = area of the confined strut
 $A/A_b \leq 4$
 $1 \leq A_{core} / A_b \leq 3$

In determining the spread or diffusion of concentrated forces it is necessary to assume or define a strut diffusion angle, the angle with respect to the strut axis at which the compression force spreads out from the edge of a bearing plate. For the strut diffusion angle for heavily loaded members or under bearing plates (anchorage zone) the following proposals are given. MacGregor [62] proposes a diffusion angle of 15 degrees. An elastic finite element analysis by Burdet [42] shows for various ratios of bearing plate width to compression field width from 0.1 to 0.9, diffusion angles vary between 27 to 22 degrees. The experimental study by Sanders [43] gave somewhat lower values. Figure 3.3 show the various approaches with the proposed equation (see Fig. 3.4)

$$\text{diffusion angle [deg]} = 12 + 3 / (a/h)^{0.5}$$

a = bearing plate width (see Fig. 3.2)
 h = compression field width (see Fig. 3.2)

In case of doubt, or if the detail being considered is especially critical, larger diffusion angles can be used. This will lead to larger values of the tension force in the ties. The location of the elastic resultant can be estimated with sufficient accuracy for design by using an apparent diffusion angle of $12 + 3 / (a/h)^{0.5}$. The solution with diffusion angle of 26.5° (slope: 1:2) proposed by Burdet [42] will lead to conservative answers when compared with the elastic finite element analysis for cases having ratios a/h larger or equal to 0.15. If no other information about the a/h ratio is available, the diffusion angle can be estimated for design by using an apparent diffusion angle of 21.8° (slope 2 : 5).

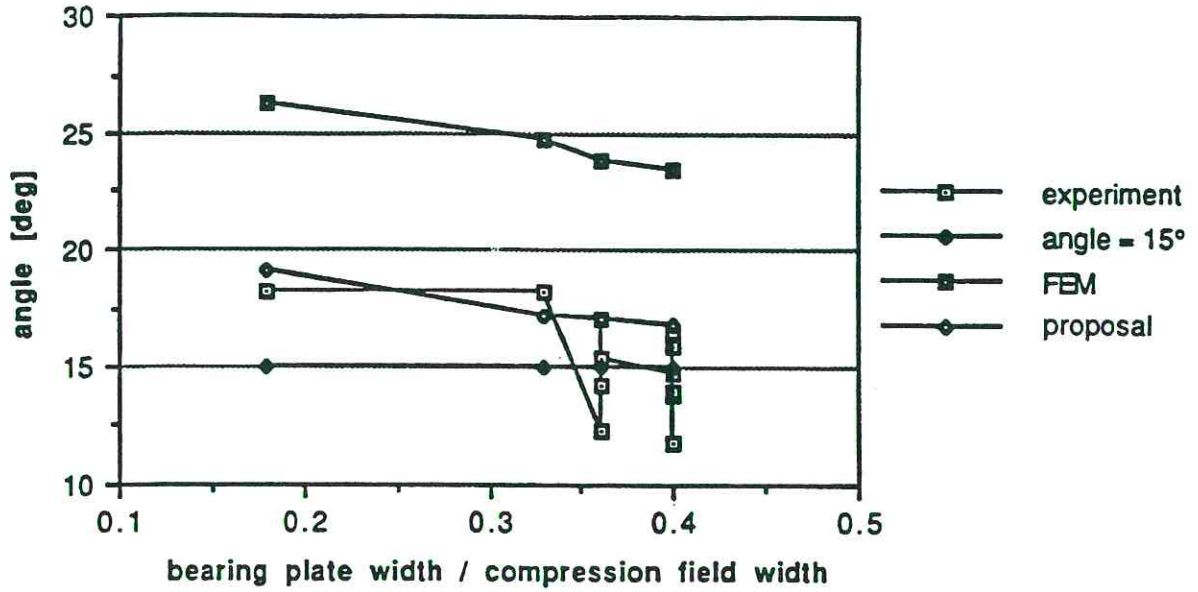


Figure 3.3: Comparison of various diffusion angle

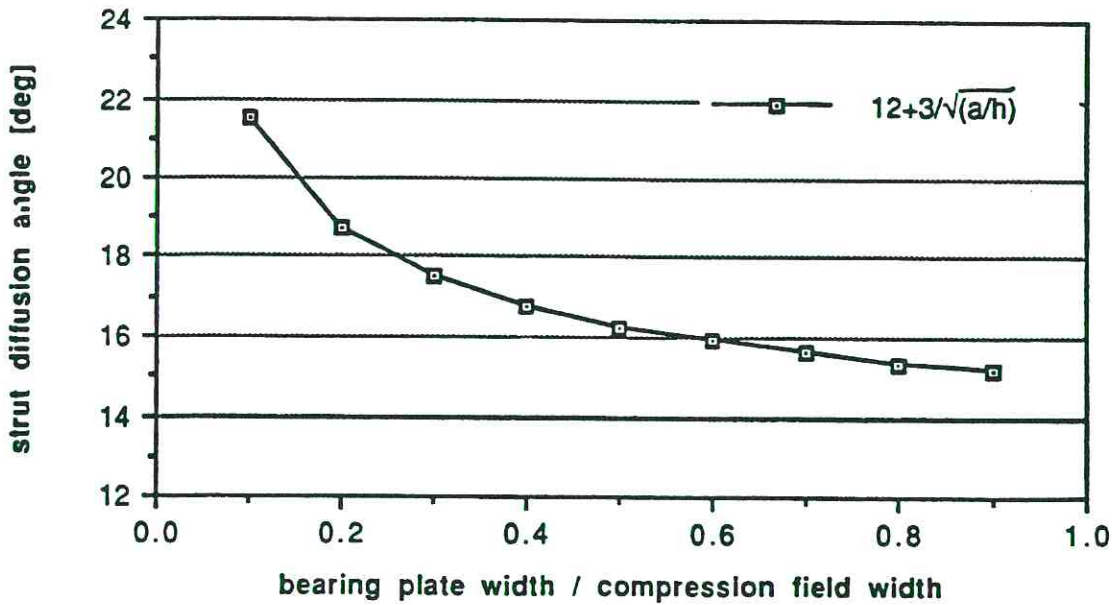


Figure 3.4: Proposed diffusion angle for design

3.3 Checking and Dimensioning Tensile Ties

The reinforced concrete ties are essentially linear or one-dimensional elements between two nodes. All of the tensile force has to be transferred by reinforcing ties. From the known tensile forces found by equilibrium at the node regions, the dimensions of the reinforcement can be computed. In order to select normal spaces and reinforcing bar diameters it is necessary to determine the effective width of the reinforcing tie (Fig. 3.5).

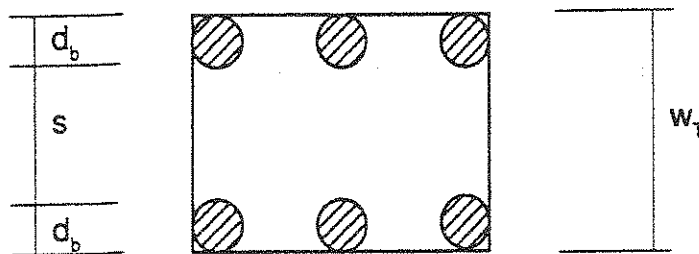


Figure 3.5: Width of the reinforcing tie

The dimensioning is a check against the yield strength of the reinforcing bars and prestressed tendons

$$T_u \leq \phi T_n$$

$$T_n \leq f_y A_s + \Delta f_{py} A_p$$

- f_y = yield strength of the reinforcing bar
- Δf_{py} = available part (non-prestressed portion) of the yield strength of the prestressed steel
- A_s = area of the reinforcing bar
- A_p = area of the prestressing tendons
- ϕ = 0.9 for steel tensile ties and 0.65 for concrete used in tension

Prestress forces are to be applied to the strut- and- tie model as external loads (external force pair) with friction forces in the transmission zone (Fig. 2.31) in the analysis and dimensioning. Only the available remainder of the yield strength above the effective prestress force can be used for carrying tensile forces from the strut and tie model (internal forces) (see Table 2.16).

After selecting the required spacing for the reinforcing bars and prestressing tendons the width of the tie is determined as the outside dimension of the reinforcement layers. The width is necessary for dimensioning the node regions. For those instances when it is desirable and permissible to count on the tensile strength of the concrete to carry equilibrium forces where no progressive failure seems possible, the following approach can be applied (width of the tension tie assumed as 1 in.)

$$\begin{aligned} T_n &\leq 3 \sqrt{f_c} h \\ h &= \text{depth of the tension tie} \end{aligned}$$

If the tensile stress field is crossed by a compression field, the reduced biaxial strength shown in Fig. 3.6 must be considered.

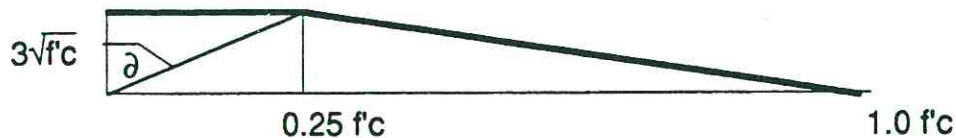


Figure 3.6: Assumption for the biaxial compressive-tensile strength

The maximum angle " ∂ " between the compression and the tensile field is

$$\text{arc tan } \partial = \sqrt{f_c} / 24$$

For the resulting tensile - compression forces a parallel bounding failure curve can be assumed.

3.4 Checking and Dimensioning Nodes: Determining Anchorage Requirements

D-regions usually contain either smeared or singular nodes. The singular nodes are more critical and need more attention. The following dimensioning and anchorage requirements must be applied to either smeared or singular nodes. The stress peaks in smeared nodes are less critical because a greater amount of surrounding concrete is normally available. For multiple, widespread reinforcement layers it is difficult to choose the node width (Fig. 3.7).

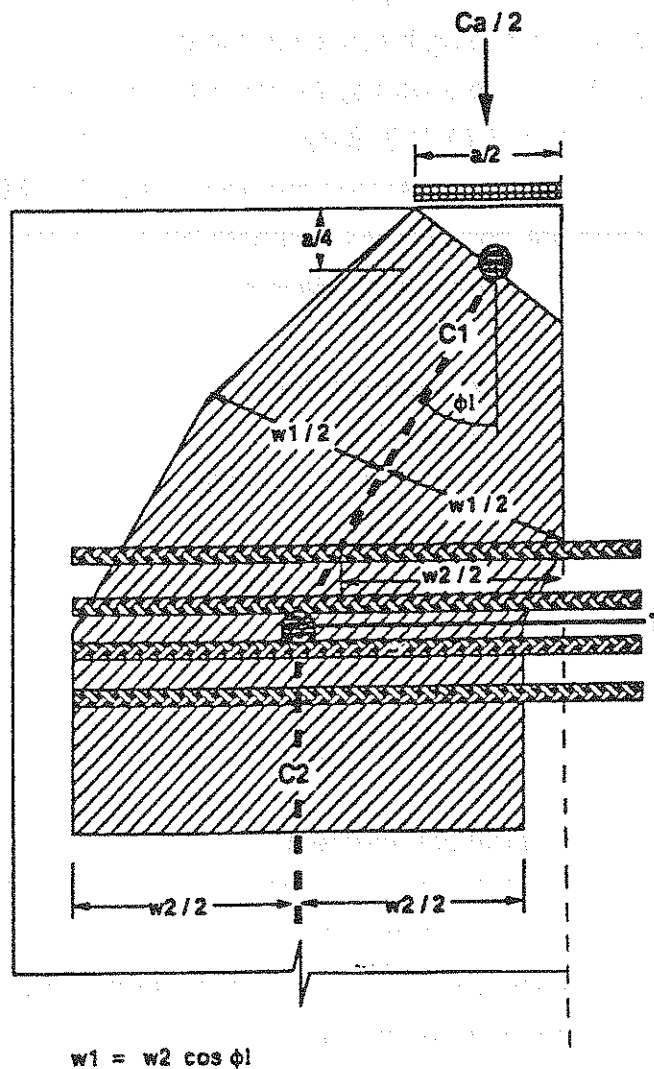


Figure 3.7: Strut width for smeared node

For the concrete efficiency factors and the anchorage requirements in smeared nodes the rules for singular nodes (CCC, CTT, CCT, TTT) should be applied.

3.4.1 Checking and Dimensioning CCC - nodes

The following factored load stress limits are proposed (see Section 2.8)

$$\begin{aligned} \sigma &\leq \phi f'_{ce} \\ f'_{ce} &= v_e f'_c \leq 2.5 f'_c \\ v_e &= \text{concrete efficiency factor} \\ \phi &= \text{concrete strength reduction factor} \\ &= 0.75 \text{ members with spiral reinforcement conforming to} \\ &\quad \text{Sec. 10.9.3 (ACI 318-89)} \\ &= 0.7 \text{ for other reinforced members (ACI 318-89)} \\ f'_c &= \text{concrete compressive strength based on standard 6-in. x} \\ &\quad \text{12-in. cylinders at 28 days age} \end{aligned}$$

a) Unconfined Nodes without bearing plates

$$\begin{aligned} v_e &= 0.8 \text{ for } f'_c \leq 4000 \text{ psi} \\ v_e &= 0.9 - 0.25 f'_c / 10000 \text{ for } 4000 < f'_c < 10000 \text{ psi} \\ v_e &= 0.65 \text{ for } f'_c \geq 10000 \text{ psi} \end{aligned}$$

b) Confined nodes

$$\begin{aligned} \sigma &\leq \phi f'_{cce} \\ f'_{cce} &= [(v_e f'_c (A/A_b)^{0.5} + \alpha (A_{core} / A_b) f_{lat} (1 - s/d)^2)] \leq 2.5 f'_c \\ \alpha &= 4.0 \text{ for spiral confinement} \\ &= 2.0 \text{ for square closed hoop confinement anchored with} \\ &\quad \text{longitudinal reinforcement} \\ &= 1.0 \text{ for square closed hoop confinement without longitudinal} \\ &\quad \text{reinforcement anchorage} \\ f_{lat} &= \text{lateral pressure} = 2 f_y A_s / (d s) \text{ for } f'_c \leq 7000 \text{ psi} \\ &\quad = 2 f_s A_s / (d s) \text{ for } f'_c > 7000 \text{ psi} \end{aligned}$$

c) Unconfined nodes with bearing plates

$$\begin{aligned}\sigma &\leq \phi f_{be} \\ f_{be} &= v_e f'_c (A/A_b)^{0.5} \leq 2.5 f'_c \\ A/A_b &\leq 4\end{aligned}$$

d) Triaxially confined nodes

The increase in strength due to three-dimensional states of compressive stresses may be taken into account if the simultaneously acting transverse compressive stresses are considered reliable. This may be particularly appropriate if supplementary transverse prestressing is applied.

When threedimensional compressive strength is appropriate

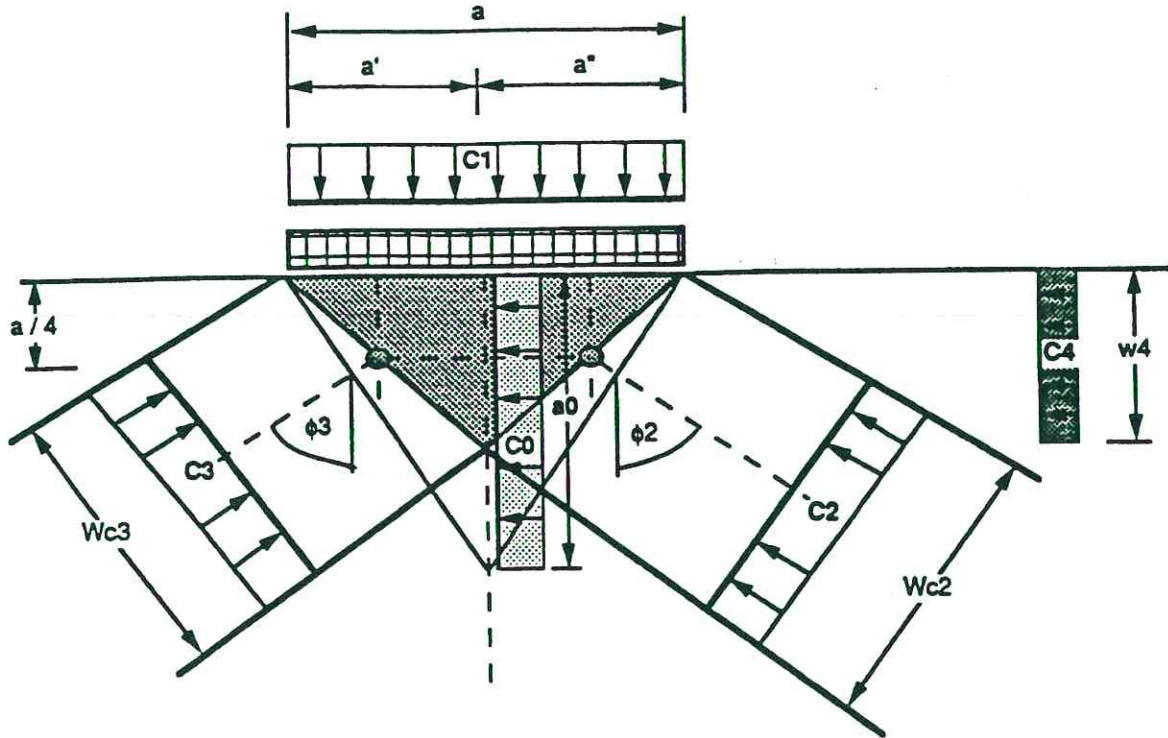
$$\begin{aligned}\sigma &\leq \phi f_{c3} \\ f_{c3} &\leq 2.5 f'_c\end{aligned}$$

The dimensioning for CCC-nodes based on the proposed strut width approaches given in Section 2.6.1 can be determined as shown in Fig. 3.8. For a more general application with borders of the compression strut assumed to be not parallel, the strut width "w3" at a certain distance "y" from the concrete surface can be computed by using the proposed geometrical approaches shown in Fig. 3.9.

In a CCT-node where the tension reinforcement is welded or bolted to the anchor plate, the stress configuration in the nodes is then similar to those in CCC-nodes. A smooth surface of the tie where it crosses the node is better than high bond from deformations because strain compatibility with the bonded bar will tend to crack the node's concrete. The proposed CCC-node strength can be applied for this kind of load transfer. In addition the anchor plate has to be checked for bending strength and the welding connection with the tie must also be checked.

3.4.2 Checking and Dimensioning CCT - nodes

For CCT-nodes the width of the strut can be found by considering geometrical constraints such as bearing plates and by assuming that the effective width of the tensile tie is governed by the dimensions from the inside to the outside reinforcement layer (wT). With a single layer of reinforcement wT is taken as the bar diameter as shown in Figs. 3.10 and 3.11. With multiple layers of reinforcement wT is taken as shown in Fig. 3.12.



$$C1 = C2 * \cos \phi2 + C3 * \cos \phi3$$

$$C1 = C1' + C1''$$

$$C1' / a' = C1'' / a''$$

$$C4 = C3 * \cos \phi3$$

$$C4 = C2 * \cos \phi2$$

$$a0 = \frac{a (\tan \phi2 * \tan \phi3)}{\tan \phi2 + \tan \phi3}$$

$$w4 = a / 2$$

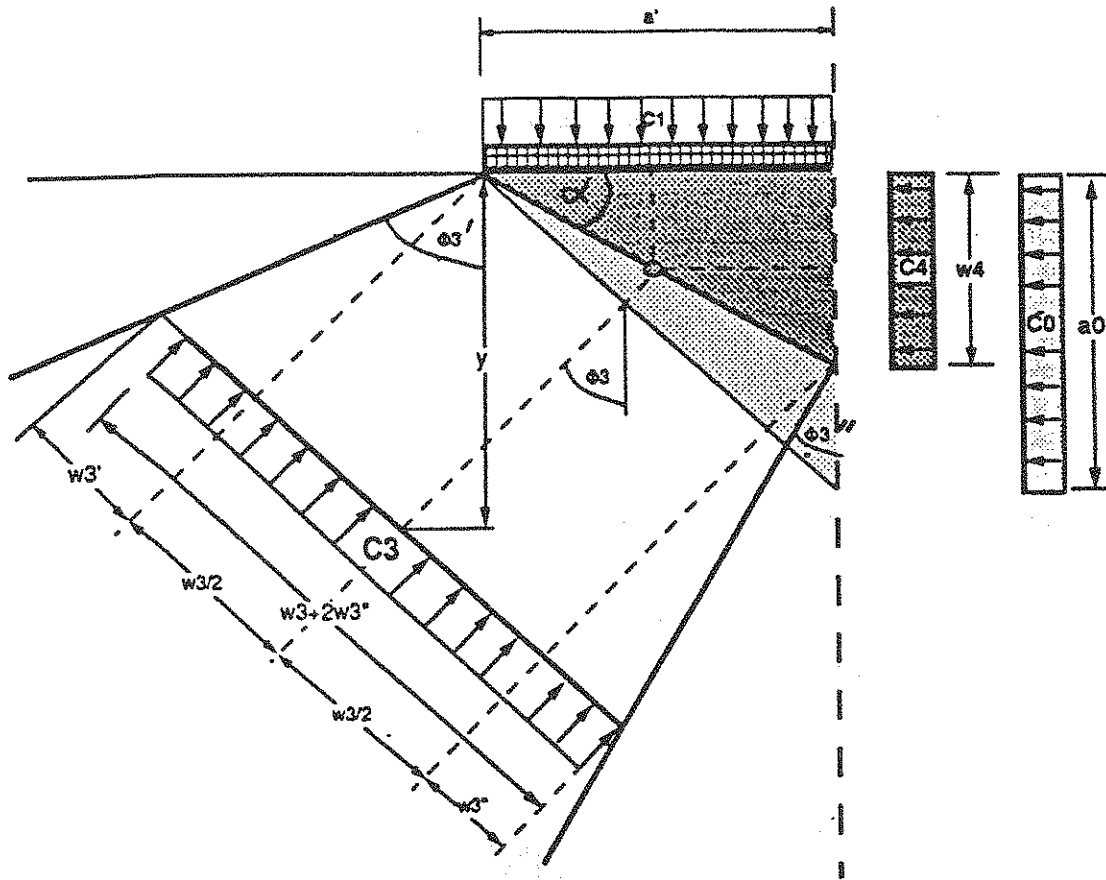
If $w4 \geq a0$ then hydrostatic stress

$$C0 \leq v * f_c * b * a0$$

$$wc2 = a'' \cos \phi2 + a / 2 \sin \phi2$$

$$wc3 = a' \cos \phi3 + a / 2 \sin \phi3$$

Figure 3.8: Geometrical relation for CCC-node for dimensioning process



$$w_4 = a / 2$$

$$\begin{aligned} w_{c3} &= w_3 + 2 w_3' && \text{for } w_3' \leq w_3'' \\ w_{c3} &= w_3 + 2 w_3'' && \text{for } w_3' \geq w_3'' \end{aligned}$$

$$w_3 = a / 2 \sin \Phi_3 + a' \cos \Phi_3$$

$$w_3' = \frac{\tan (\Phi_3' - \Phi_3)}{4 \cos \Phi_3} [4 y - a (\sin \Phi_3)^2 - a' \sin 2\Phi_3]$$

$$\alpha = \arctan [a / (2a')]$$

$$w_3'' = \frac{\tan (\Phi_3 - \Phi_3'')}{8 \cos \Phi_3} (8y - [\tan \Phi_3 - 2 \tan (\Phi_3 - \alpha)] * [a \sin 2\Phi_3 + 4 a (\cos \Phi_3)^2])$$

Figure 3.9: Geometrical relation for CCC-node with borders not parallel to the compression strut

$$W_{2c} = W_{1c} \sin \phi + W_T \cos \phi$$

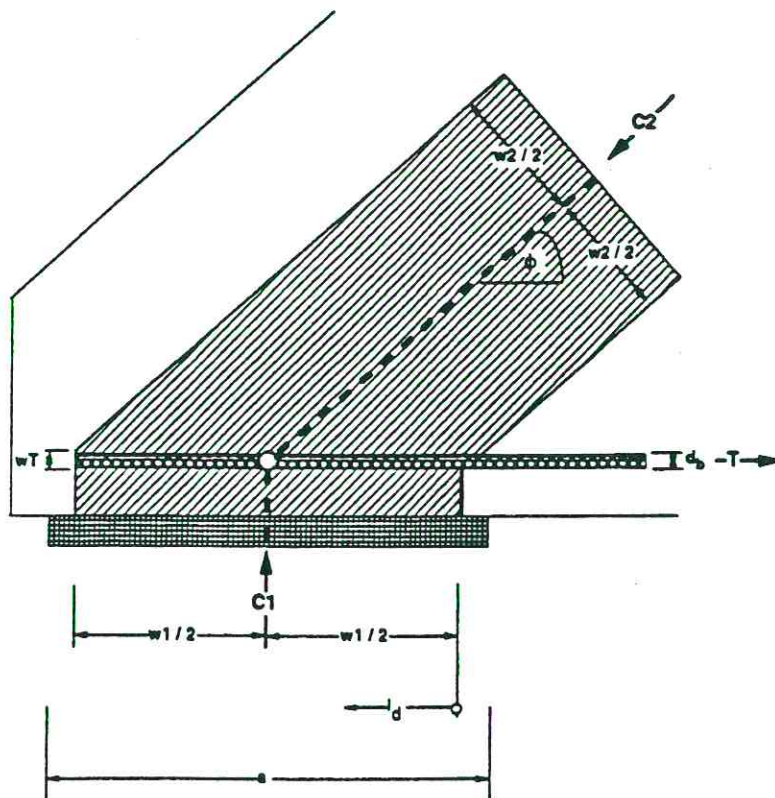
The concrete stresses should be checked:

$$\begin{aligned} \sigma_1 &\leq \phi f_{ce} (A/A_b)^{0.5} \leq 2.5 f_c \\ \sigma_2 &\leq \phi f_{ce} (A/A_b)^{0.5} \leq 2.5 f_c \\ A/A_b &\leq 4 \end{aligned}$$

$$\begin{aligned} f_{ce} &= v_e f_c \\ \phi &= 0.7 \end{aligned}$$

The efficiency factor for the concrete compression strength should be taken as:

$$\begin{aligned} v_e &= 0.8 \text{ for } f_c \leq 4000 \text{ psi} \\ v_e &= 0.9 - 0.25 f_c / 10000 \text{ for } 4000 < f_c < 10000 \text{ psi} \\ v_e &= 0.65 \text{ for } f_c \geq 10000 \text{ psi} \end{aligned}$$

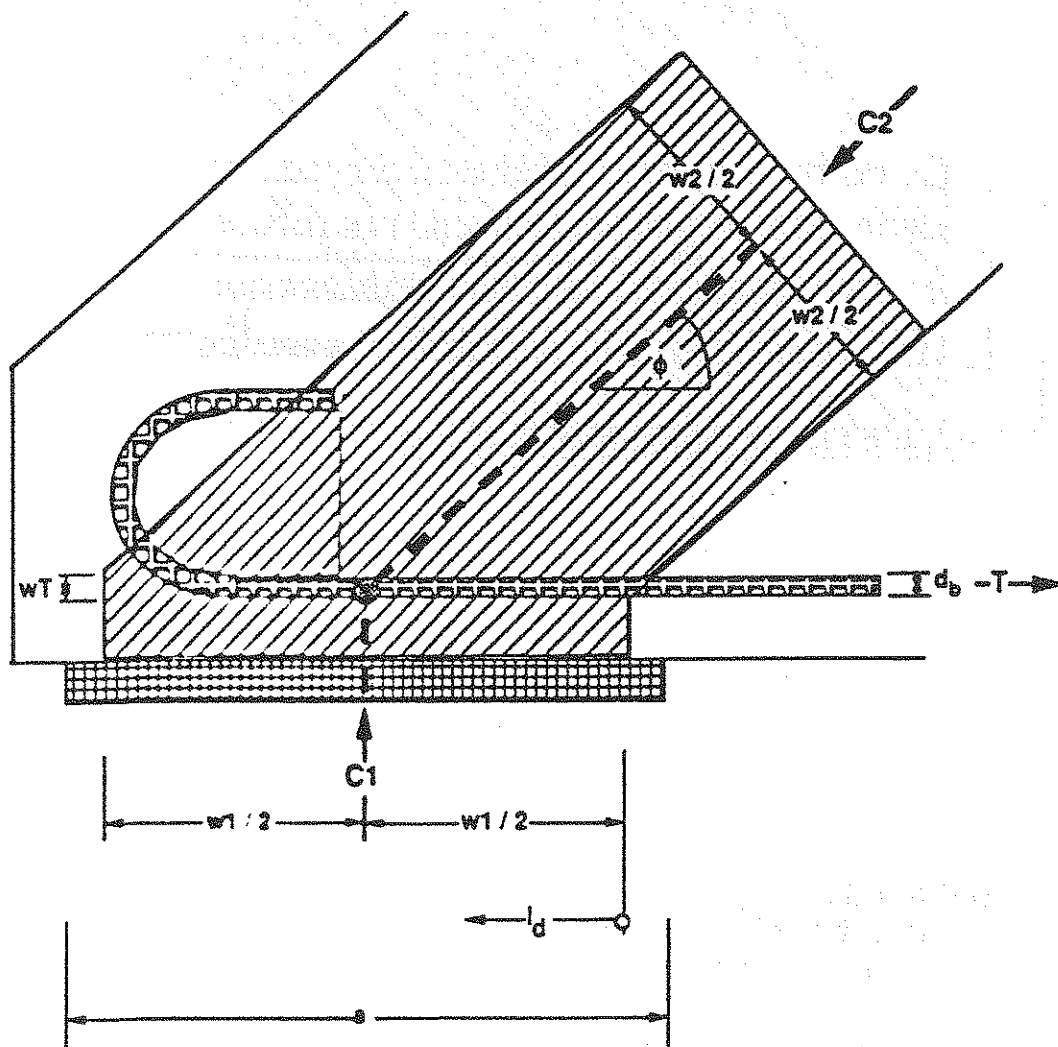


$$wT = d_b$$

$$w2 = w1 \sin \phi + wT \cos \phi$$

Figure 3.10: CCT-node with single straight reinforcement bar

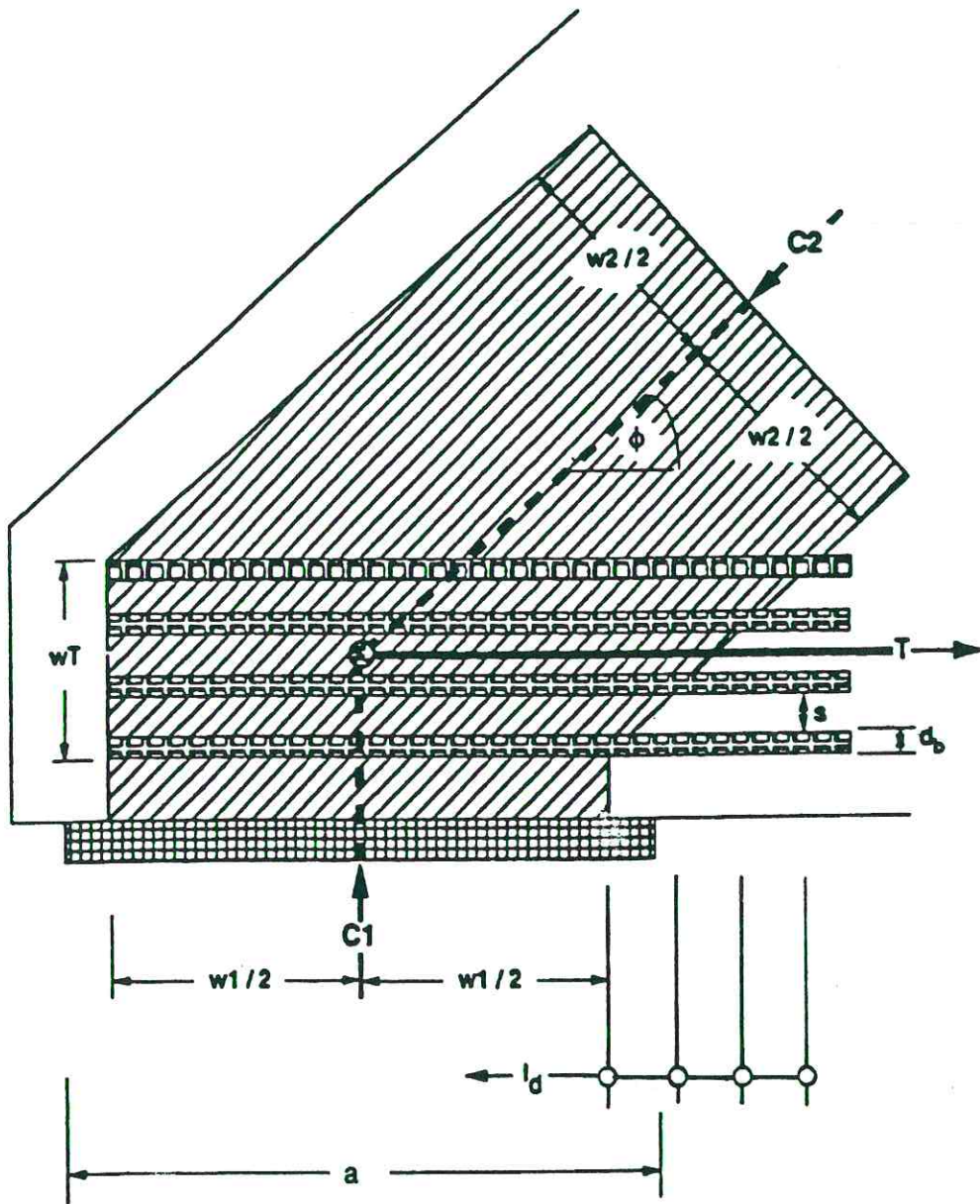
The nodal zone must also fulfill the requirement for minimum development length, concrete cover and bar spacing limits. Test results [39] show that vertically oriented hooks decrease the ultimate load of the CCT-nodes by 4 to 8% as compared to straight bars with full development lengths. This decrease is probably not significant given the other uncertainties in the design process. The advantage of hooks is that the required anchorage length can be minimized (Fig. 3.11). With multiple layers of reinforcement, the available l_d can be taken from the intersection of each bar layer with the nodal zones (Fig. 3.12).



$$wT = d_b$$

$$w_2 = w_1 \sin \phi + wT \cos \phi$$

Figure 3.11: CCT-node with hooked bar



$$w_T = n d_b + (n-1) s$$

n = number of reinforcing bar layers
 s = clear bar spacing

$$w_2 = w_1 \sin \phi + w_T \cos \phi$$

Figure 3.12: CCT-node with multiple reinforcement bar layers

3.4.3 Checking and Dimensioning CTT - nodes

The dimensioning process for the CTT- node is similar to the proposed approach for the CCT-node. The strut width can be computed from the geometrical boundaries or widths of the tension ties (see Figs. 3.13 and 3.14).

$$w_c = w_{1T} \sin \phi + w_{2T} \cos \phi$$

For CTT-nodes the concrete compression efficiency factor should be taken as:

$$\phi \leq \phi f'_{ce} (A/A_b)^{0.5} \leq 2.5 f'_c$$

$$A/A_b \leq 4$$

$$f'_{ce} = v_e f'_c$$

$$\phi = 0.7$$

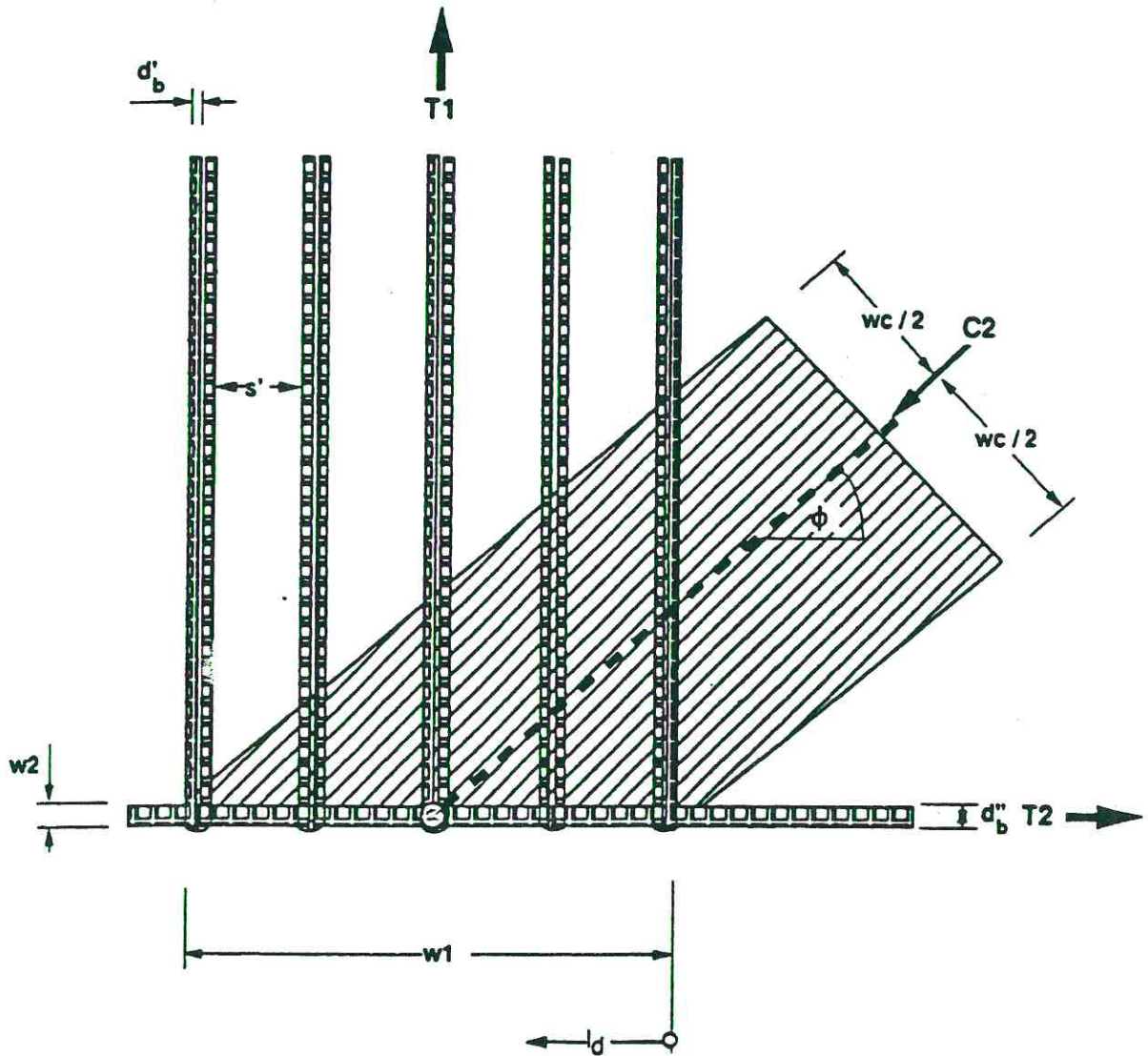
The efficiency factor for the concrete compression strength should be taken as:

$$v_e = 0.8 \text{ for } f'_c \leq 4000 \text{ psi}$$

$$v_e = 0.9 - 0.25 f'_c / 10000 \text{ for } 4000 < f'_c < 10000 \text{ psi}$$

$$v_e = 0.65 \text{ for } f'_c \geq 10000 \text{ psi}$$

Test results [38] shown that the outside layers of reinforcement close to a surface of the member are the most critical. Major cracks which initiate at the surface and generally follow the theoretical strut angle decrease the bond strength. Reinforcement should be provided across all planes of weakness to control cracking. Confining reinforcement normal to planes of hooks and bends is especially important [38]. Fig. 3.13 show singular tensile ties and Fig. 3.14 show multiple tensile ties for CTT - nodes.



$$w1 = n' d'_b + (n' - 1) s'$$

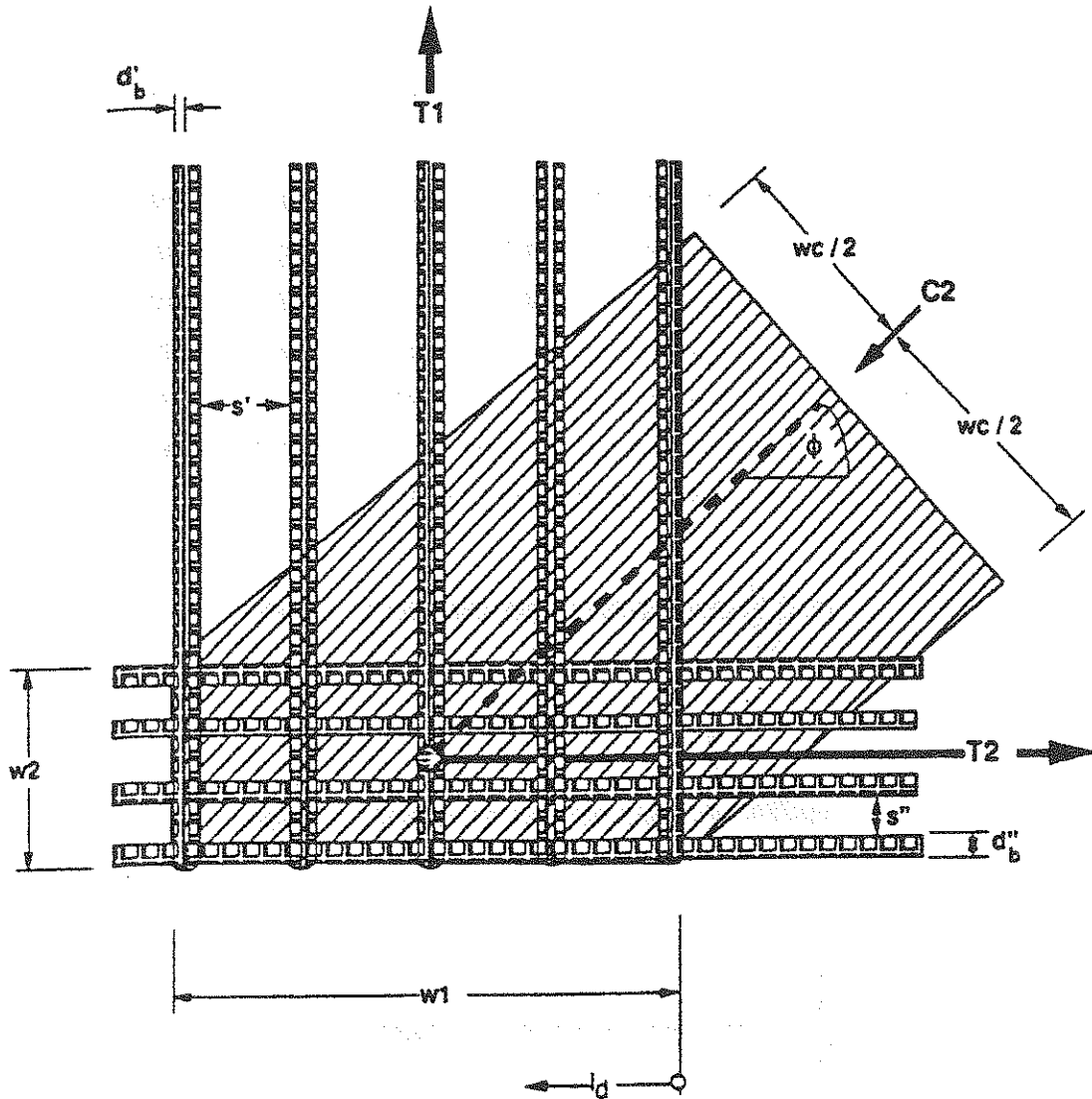
$$w2 = d''_b \text{ or conservatively: } w2 = 0$$

n' = number of reinforcing bar layers

s' = clear bar spacing

$$wc = w1 \sin \phi + w2 \cos \phi$$

Figure 3.13: CTT-node with single reinforcement bar layer



$$w_1 = n' d'_b + (n' - 1) s'$$

$$w_2 = n'' d''_b + (n'' - 1) s''$$

n = number of reinforcing bar layers

s = clear bar spacing

$$w_c = w_1 \sin \phi + w_2 \cos \phi$$

Figure 3.14: CTT-node with multiple reinforcement bar layers

3.4.4 Checking and Dimensioning TTT - nodes

For TTT-nodes the anchorage requirements have to be checked. It must be evident that satisfactory behavior and adequate strength can be attained only by the efficient interaction of concrete and steel. In details where the length available for end anchorage is very short, special devices, such as illustrated in Fig. 3.15, may be required to ensure the development of the reinforcing bar strength. For TTT-nodes the largest tensile tie should be anchored with looped - or hooked bars. This is illustrated in Fig. 3.16.

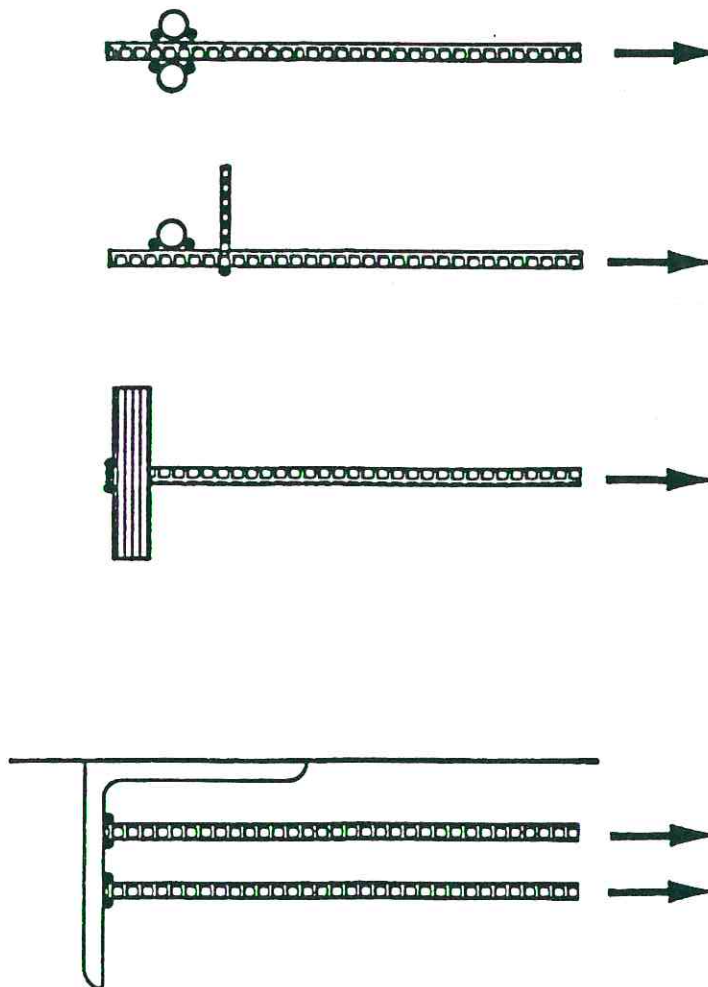


Figure 3.15: Special anchorage devices (from Ref. [105])

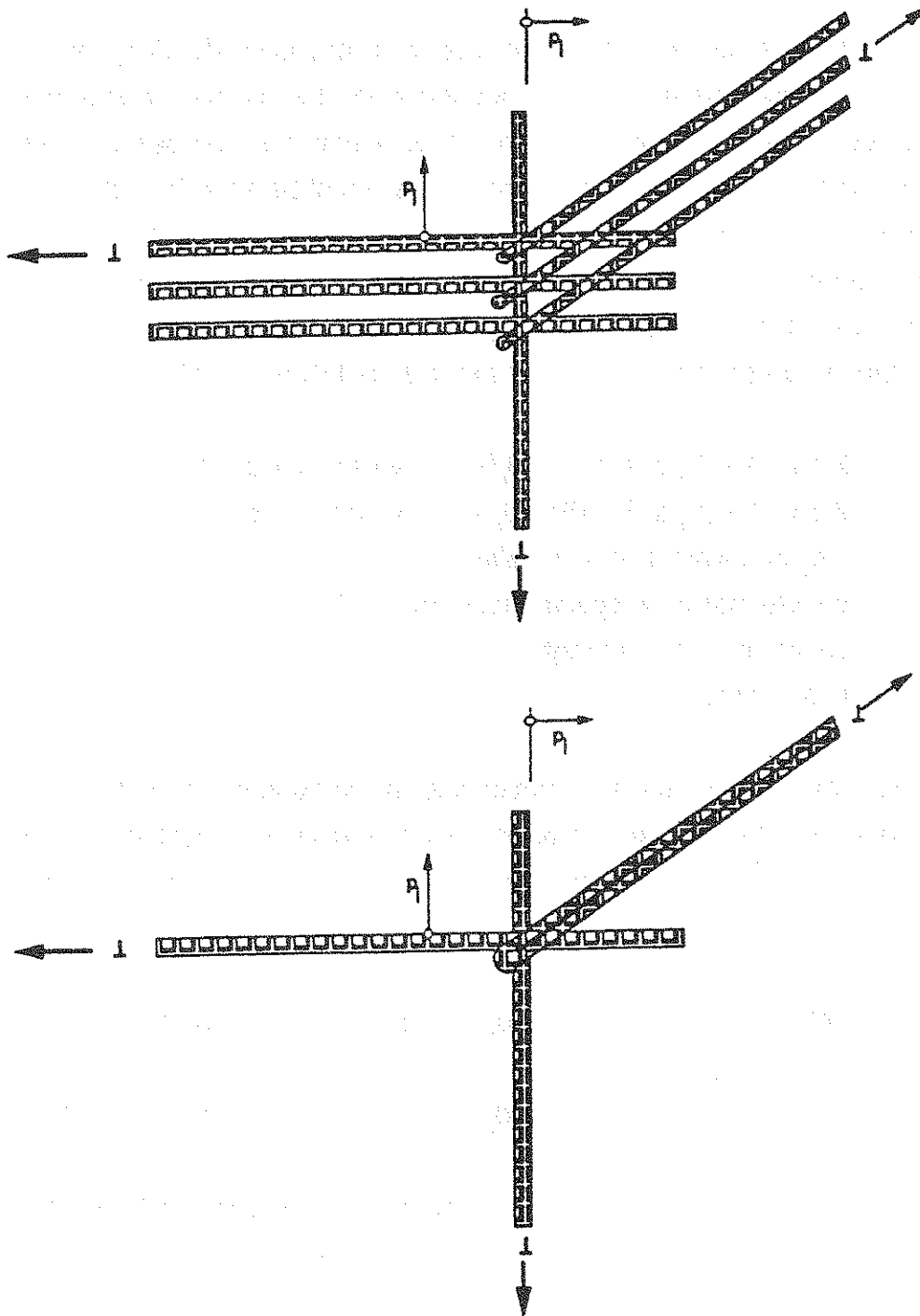


Figure 3.16: TTT - node with looped bar

3.4.5. Curved Tensile Ties

When tensile ties are curved some special considerations for detailing must be given. The out of axis deviation force induced when the tie tries to straighten under the applied tension must be anchored back into the member by closely spaced "tie back" stirrups. The stirrup spacing "s" must be so selected that the cover will not break away between two stirrups when the curved bar tends to straighten. Leonhardt [106] has suggested that by considering the approximate flexural stiffness of the curved bars and by limiting the tensile stress in the cover concrete, the stirrup spacing should not exceed the following values:

$$\begin{aligned}
 s &\leq 2 \Delta s / [1 - (f'_{ct} c R) / (420 d_b^2)] && \text{when } (s_1 + d_b) \geq 3 c \\
 s &\leq 2 \Delta s / [1 - (f'_{ct} s_1 R) / (840 d_b^2)] && \text{when } (s_1 + d_b) < 3 c \\
 \Delta s &= 3 d_b \text{ or } c \text{ whichever is smaller} \\
 s_1 &= \text{parallel bar clear spacing (see Fig. 3.17)} \\
 f'_{ct} &= \text{concrete tensile strength} \\
 R &= \text{radius of curvature}
 \end{aligned}$$

The equations are based on the assumption that the working stress in the curved bar does not exceed 34 ksi. The stirrups can be omitted when the radius of the bar is large enough so that the cover concrete will be sufficient to supply the radial tensile force.

$$\begin{aligned}
 R &\geq 240 d_b^2 / c && \text{when } (s_1 + d_b) \geq 3 c && \text{for } f'_c = 4000 \text{ psi} \\
 R &\geq 400 d_b^2 / s_1 && \text{when } (s_1 + d_b) < 3 c && \text{for } f'_c \geq 4000 \text{ psi}
 \end{aligned}$$

In order to prevent splitting in the plane of the bars, Leonhardt [106] proposes some minimum cover unless transverse reinforcement is provided (see Fig. 3.17).

$$c \geq 92 d_b^2 / R \quad \text{for } f'_c \geq 4000 \text{ psi}$$

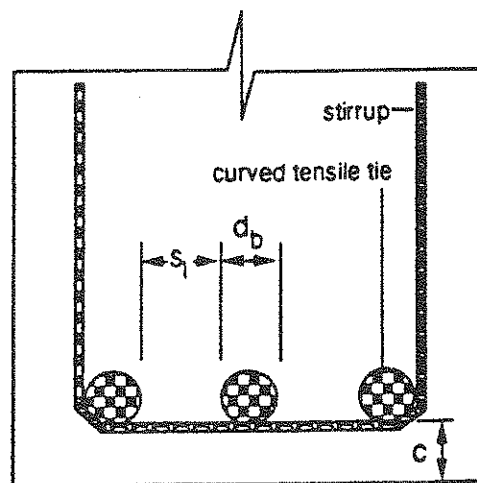
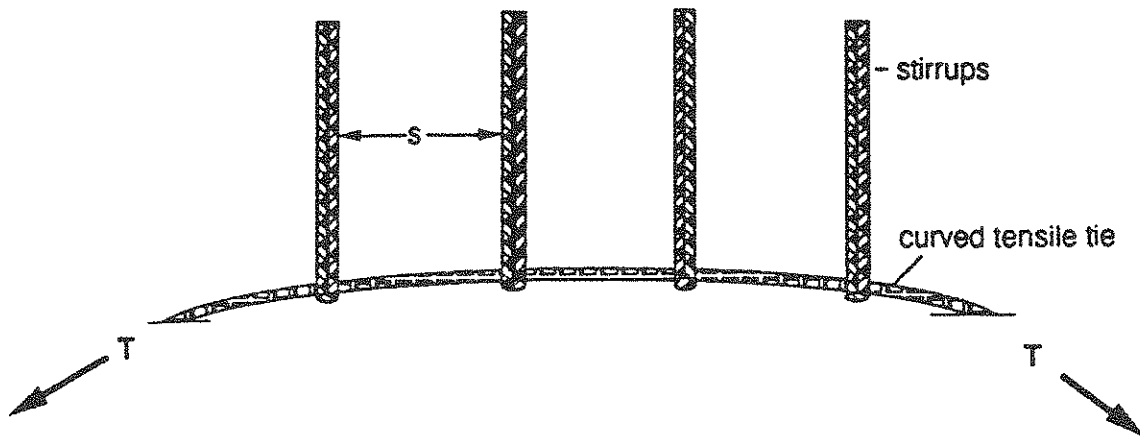


Figure 3.17: Dimensions for curved tensile ties (from Ref. [105])

CHAPTER 4. DESIGN AIDS

4.1 Detailing aids

Recent advances in the understanding of the behavior of concrete structures have resulted in more sophisticated methods of analysis. Computer oriented analysis and plotting techniques enable the elastic or inelastic analysis of highly indeterminate structures to be carried out speedily. However, an elaborate analysis becomes worthless if the computations are not translated into successful structures. The design process is a sequential and iterative decision-making process. The first step is to define the needs and priorities which a building or bridge has to fulfill. These may include functional requirements, aesthetic considerations, and economic aspects. Based on the constraints, needs and priorities, possible layouts of the architectural, structural and other systems are developed. Preliminary cost estimates are made and the final choice of the system to be used is based on how well the overall design satisfies the prioritized needs within the budget available. Once the overall layout and general structural concept have been selected, the structural system can be designed to ensure structural adequacy. Based on the selected design a structural analysis is carried out to determine the external and internal forces in the structure. When a structure or structural element becomes unfit for its intended use, it is said to have reached a limit state. The limit states for concrete structures can be divided into three basic groups.

- Ultimate limit states: These involve a structural collapse of part or all of the structure. Such a limit state should have a very low probability of occurrence since it may lead to loss of life and major economical losses. (100 year lifetime probability $\approx 10^{-5} \approx \beta = 4.2$)
- Serviceability limit states: These involve losses of the functional use of the structure but not collapse of any part of the structure. (100 year lifetime probability $\approx 10^{-3} \approx \beta = 3$)

- Special limit states: This class involves major but repairable damage to the structure due to abnormal conditions, such as long-term physical or chemical instability
(100 year lifetime probability $\approx 10^{-3} \approx \beta = 3$)

For normal concrete structures the determination of acceptable levels of safety against occurrence of each limit state are carried out by the building code or design specification authorities. They specify the load combinations and safety factors to be used in checking the limit states.

Since many repetitive computations are necessary to proportion concrete structures, handbooks containing tables or graphs of the more common quantities are available from several sources. The American Concrete Institute and the Prestressed Concrete Institute [107] publishes its Design Handbook in several volumes, the German Concrete Group publishes its yearly "Betonkalender" [108], the Concrete Reinforcing Steel Institute publishes the CRSI Handbook [109]. In recent years, specialized computer programs have been replacing design aids in many applications [110].

Detailing consists not only of the preparation of plans giving concrete dimensions, reinforcement placing drawings and reinforcing bar details, but incorporates the whole thought process through which the designer enables each part of the structure to perform safely under the various limit states. This chapter gives some background for typical application of the strut- and-tie model. It is intended to assist in establishing design parameters for some specific applications. These design guidelines should help a designer develop and dimension a strut- and- tie- model and apply the model to different situations. This chapter draws on the analytical and experimental results presented in the earlier sections. It uses these results to develop design procedures for concrete structures. Overall, it should lead to a better understanding of the force flow in D-regions and the designer should have substantially improved knowledge regarding the design process.

A foremost practitioner of strut- and- tie model detailing is Dr. Jorg Schlaich. He and his coworkers have developed a series of detailing aids [1,2] for comonly occurring situations. A number of these aids are given in Appendix A herein as further assistance to the designer interested in applying strut- and- tie models.

The general design approach ensures a reasonably ductile behavior by incorporating relationships to preclude premature anchorage or concrete failure and requiring that reinforcement yield substantially before final failure. One of the advantages of the strut- and- tie- model is that both prestressed and reinforced concrete structures can be treated with the same model. Experience indicates that the models are of most use in the 'D' regions of a structure.

The required checks for a concrete structure are:

- ultimate limit state: factored loads and reduced nominal resistances
- serviceability limit state: working loads and acceptable stress or deformation states
- durability: technological aspects and requirements

The proposed strut- and- tie- model is based on the plasticity analysis for cracked concrete and gives a lower bound for the ultimate limit state analysis as long as premature anchorage or concrete strut failures are precluded.

4.2 Types

The detailing process for D-regions begins with isolating the D-regions from the B-regions in a structure and development of a preliminary strut- and- tie model. In order to find the appropriate strut- and- tie- model the load path can be traced, general knowledge of appropriate models can be used, or in complex cases results of an elastic finite element analysis should be used.

All the design factors specified in this section are based on the 28-day design concrete compression strength. Concrete strengths up to about 12000 psi have been studied and included in the proposed parameters. However, the present design methods, such as those in the AASHTO - Specification [4]- and the ACI Building Code [2] were actually developed using concrete strengths varying mostly from 2500 to 6500 psi. For higher strength concrete the average ratio of proportional limit stress to ultimate strength under uniaxial loading ranges from 55 to 84 percent [58]. Tests at the University of Texas at Austin by Khana [111] indicate that for normal strength concrete the proportional limit under uniaxial load is generally between 40 and 43 percent of the ultimate strength .

The principal reinforcing steels available have nominal yield strength between 40 and 75 ksi, with 60 ksi being the most widely used. The ACI Code 318-89 [4] provides that the specified yield strength will be the stress corresponding to a strain of 0.35%. All standard bars are deformed round bars, designated by size from #3 to #18: this number corresponds roughly to the bar diameter in one-eighths of an inch.

The principal prestressing tendon materials are seven-wire strand, smooth wire, smooth bars and deformed bars . The yield strength varies between 120 and 270 ksi [55]. A minimum amount of reinforcement is necessary to ensure distributed cracking and should be placed to avoid infrequent wide cracks. In critical cross sectional areas, crack prediction formulas can be used to distribute reinforcement to avoid wide cracks.

4.3 Typical Examples of Detailing Aids

The design examples given in this section are typical D-region details. Figure 4.2 shows several different examples which will be developed in subsequent subsections. For clarity in presentation no nominal resistance reduction factors (ϕ) or load factors have been used in the following examples. For actual design purposes the nominal concrete strength " $v f'_c$ " must be further reduced with the appropriate " ϕ " or resistance reduction factor. The design loads must be increased with the appropriate load factors. Since these vary from code to code and with actual applications, they are not included herein in the interest of simplicity.

Nodes shown in Fig. 4.1 can occur in the different examples. Equilibrium must be established in the nodes. The forces depend on the choice of their position and are known from the boundary conditions of the B-regions. If nodes with more than 3 forces occur the principle remains the same.

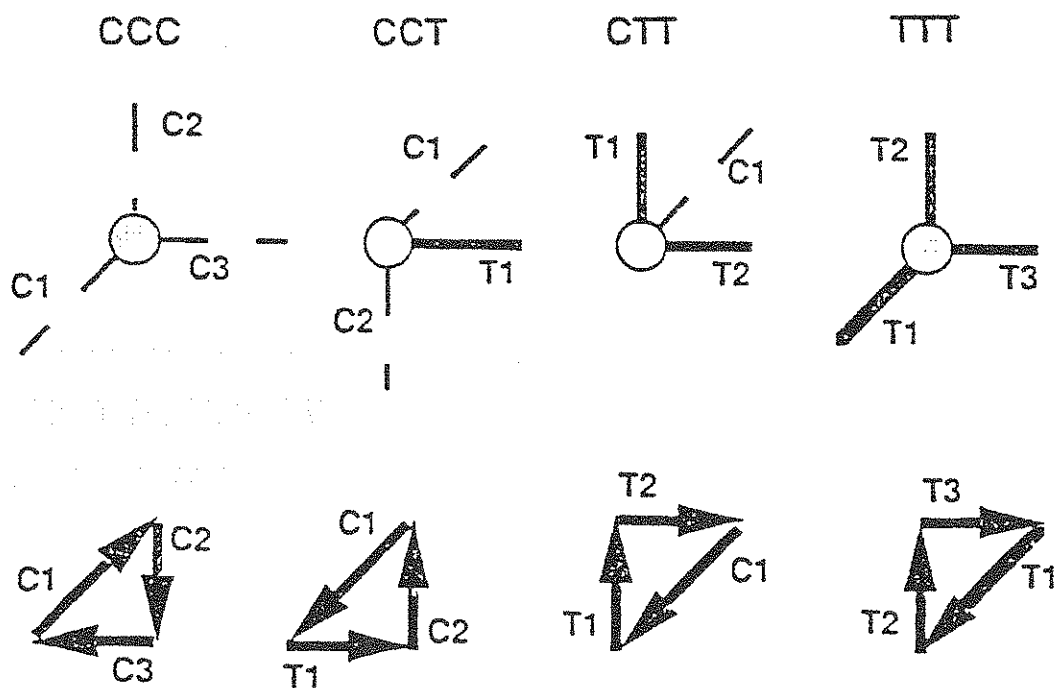


Figure 4.1: Types of nodes

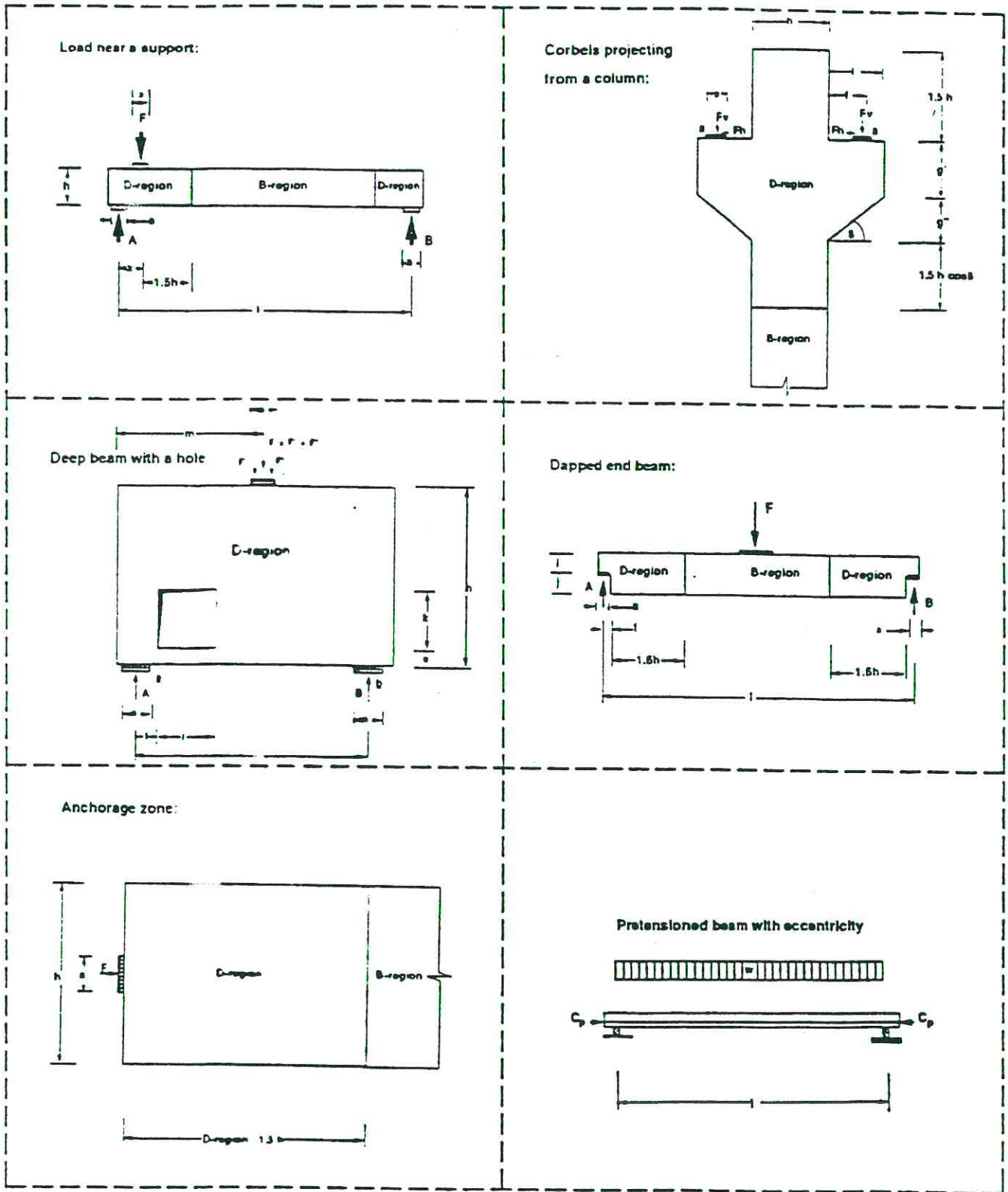


Figure 4.2: Examples to be presented in Detail

4.3.1 Load near a support

For a heavy point load located near a support as shown in Fig. 4.3 and Fig. 4.4, the proposed strut- and- tie- model is a logical approach to represent the flow of forces indicated by the elastic analysis results shown in Fig. 4.3. If the load is applied at a distance from the support smaller than the height of the specimen ($x \leq h$), then a compression field between the support and the load provides the primary internal force mechanism. This is also the reason why no traditional shear reinforcement is needed in the area between the point of the load application and the support. The strut- and- tie- model chosen reflects that the primary compression strut between the external forces is a bottle shaped compression field. The highly loaded bottle shaped compression field can be represented with the local strut- and- tie- models shown in Fig. 4.4. The local ties (T1) are dependent on the force diffusion angle " ϕ_1 " and the compression force. The T1-force in the tension ties can be provided for practical purposes by using equilibrium to proportion orthogonal vertical and horizontal ties. The detailed calculation in Example 4.1 shows that the tie forces in the bottle compression field can be of large magnitude and have to be taken into account.

The bearing plate forces "F" were divided into two individual forces with separate nodes. The magnitude of each force is determined from the overall analysis according to the proportion flowing to the left support and that flowing to the right support. In order to get uniform compression in the struts the bearing plate width has to be also subdivided into two dependent widths matching the compression forces F' and F'' . The example shows that the new strut- and- tie- angle based on the widths a' and a'' for this case does not have a significant influence on the strut- and- tie- forces. The difference is only about 1%. It could have a significant influence if the two compression struts "Ca" and "C4" had to carry similar forces and the bearing plate is much larger (see Section 4.3.5 anchorage zone). The inclined compression struts outside of the support region are assumed to be at an inclination of 45° as traditional in shear design ($\phi_7 = 45^\circ$). Thus the shear panel length becomes equal to the height Z in panels to the right of section cd in Fig. 4.4.

Example 4.1: Load near a support

Design a beam end for the member shown in Fig. 4.4 to transfer a vertical reaction load applied within a distance $x \leq d$ to a supporting column. The load to be transferred is 200 kips. Member dead load is neglected for clarity in this example. Use $f'_c = 5,000$ psi and $f_y = 60,000$ psi.

The computational steps are:

- Estimate member sizes and dimensions
- Divide member into B- and D-regions (see Fig. 4.4)
- Develop a strut- and- tie- model (see Fig. 4.4)
- Compute the external forces
- Compute the strut- and- tie- angle
- Compute the strut- and- tie- forces
- Dimension reinforcement for ties
- Determine anchorage requirements
- Check concrete stresses

To prevent large crack widths under working loads some arbitrary reinforcement spacing limits are applied in the final design layout in Fig. 4.7.

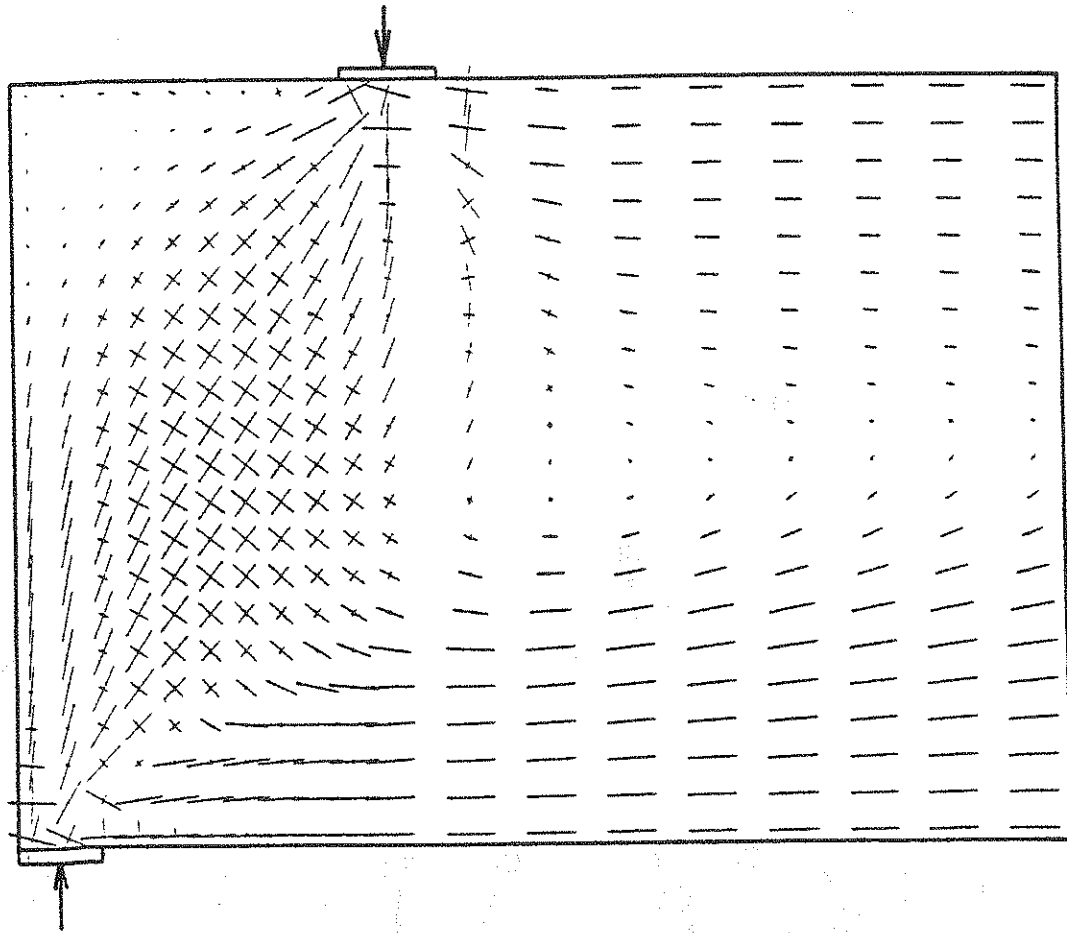


Figure 4.3: Elastic finite element analysis: principal stresses

Example: Load near support

174

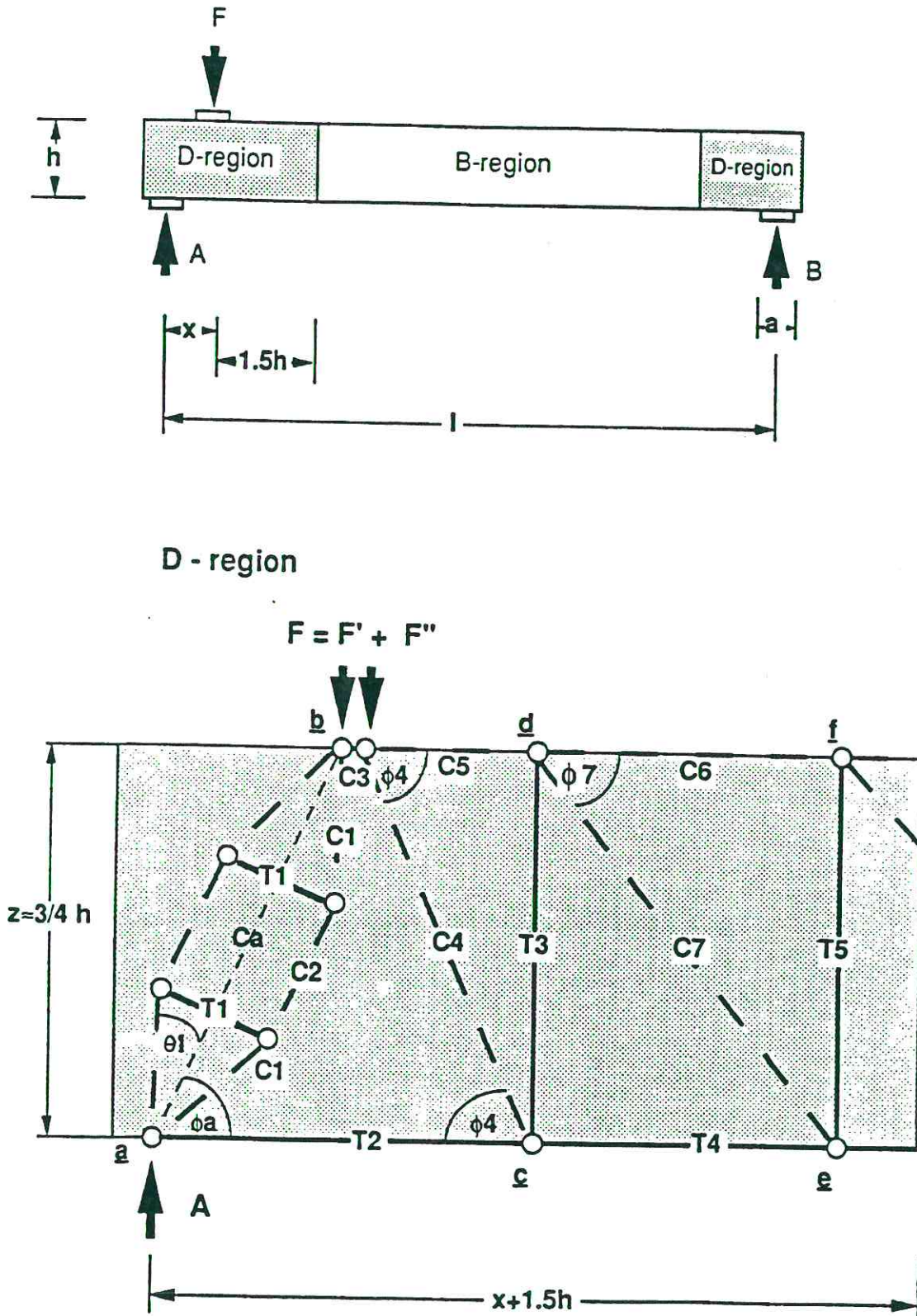


Figure 4.4: Strut and tie model for load near a support

Load and dimensions:

$$F = 200 \text{ kips}$$

$$l = 300 \text{ in.}$$

$$h = 40 \text{ in.}$$

$$x = 20 \text{ in.}$$

$$a = 10 \text{ in.}$$

$$b = 12 \text{ in.}$$

$$z = 0.9 d = 0.9 \cdot 0.85 \cdot h = 3/4 h = 30 \text{ in.}$$

$$\text{Minimum clear cover} = 1.5 \text{ in.}$$

External forces:

$$A = F (l-x) / l$$

$$A = 186.7 \text{ kips}$$

$$F' = A$$

$$B = F x / l$$

$$B = 13.3 \text{ kips}$$

$$F'' = B$$

Strut and tie angle:

$$\tan \phi_a = z / x = 0.75 h / x$$

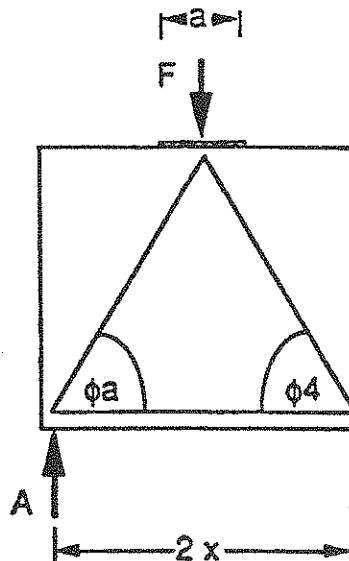
$$\tan \phi_a = 0.75 \cdot 40 / 20$$

$$\tan \phi_a = 1.5; \arctan 1.5 = 56.3^\circ \text{ (old } \partial a)$$

$$\phi_a = 56.3^\circ$$

$$a/h = 0.25$$

$$\theta_1 = 12 + 3 / \sqrt{(a/h)} = 18^\circ$$



Internal forces:

$$Ca = A / \sin \phi_a = 186.7 / \sin 56.31$$

$$Ca = 224.4 \text{ kips}$$

$$C1 = Ca / (2 \cos \theta_1) = 118.0 \text{ kips}$$

$$C2 = Ca / 2 = 112.2 \text{ kips}$$

$$T1 = (Ca/2) \tan \theta_1 = 36.5 \text{ kips}$$

$$F' = Ca \sin \phi_a = 186.7 \text{ kips}$$

$$F'' = F - F' = 13.3 \text{ kips}$$

$$a'' = F'' * a / F$$

$$a'' = 13.3 * 10 / 200 = 0.66 \text{ in.}$$

$$a' = a - a'' = 9.34 \text{ in.}$$

New strut and tie angle:

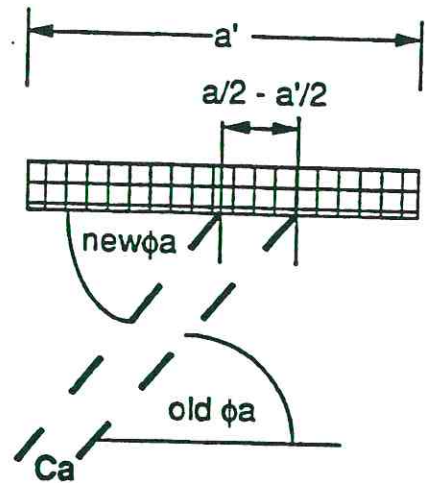
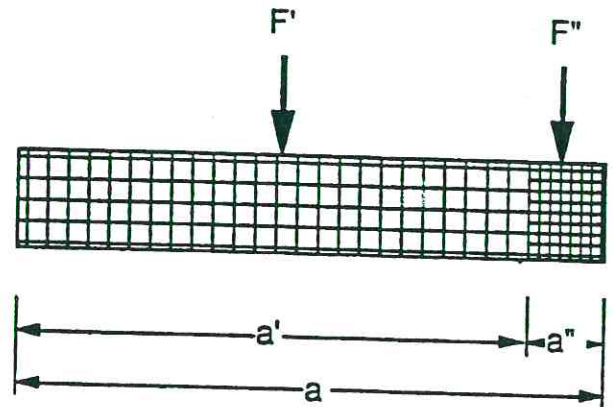
$$\phi_a = \arctan [z / (x - a/2 + a'/2)]$$

$$\phi_a = 56.75^\circ \text{ (new } \partial a)$$

$$\phi_4 = \arctan [z / (x - a/2 + a''/2)]$$

$$\phi_4 = 62.9^\circ$$

ϕ_7 is chosen to be 45°



New Internal forces:

$$C_a = A / \sin \phi_a = 223.2 \text{ kips}$$

$$C_1 = C_a / (2 \cos \theta_1) = 117.3 \text{ kips}$$

$$C_2 = C_a / 2 = 111.6 \text{ kips}$$

$$T_1 = C_a / 2 * \tan \theta_1 = 36.3 \text{ kips} \quad (\text{Negligible change})$$

$$F' = C_a \sin \phi_a = 186.7 \text{ kips}$$

$$F'' = F - F' = 13.3 \text{ kips} (= F'' \text{ (old)})$$

$$T_2 = A / \tan \phi_a = 122.4 \text{ kips}$$

$$C_3 = T_2 = C_a \cos \phi_a = 122.4 \text{ kips}$$

$$C_4 = F'' / \sin 62.9 = 14.9 \text{ kips}$$

$$C_5 = C_3 - C_4 \cos 62.9 = 115.6 \text{ kips}$$

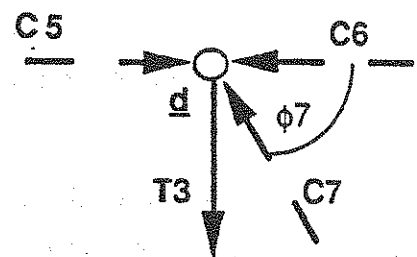
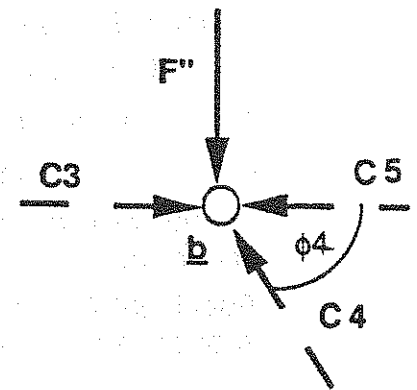
$$T_3 = C_4 \sin 62.9 = F'' = 13.3 \text{ kips}$$

$$T_5 = T_3$$

$$C_7 = T_3 / \sin \phi_7 = 18.8 \text{ kips}$$

$$C_6 = C_5 - C_7 \cos \phi_7 = 102.3 \text{ kips}$$

$$T_4 = C_5 = 115.6 \text{ kips}$$



Compute the reinforcement for the ties:

From Fig. 4.4, two T1 ties are required.

$$T1 = 36.3 \text{ kips}$$

$$T1h = T1 \sin \phi a = 30.4 \text{ kips}$$

$$A_{sh} = T1h / f_y = 0.51 \text{ in.}^2 \quad (\text{per each T1 tie}) \quad \text{Grade 60}$$

$$\text{total } A_{sh} = 1.02 \text{ in.}^2 < 6 - \#4 = 1.20 \text{ in.}^2$$

For the horizontal component T1h 3 pairs of #4 bars are spaced evenly on the sidefaces (see Fig. 4.7)

$$T1v = T1 \cos \phi a = 19.9 \text{ kips}$$

$$A_{sv} = T1v / f_y = 0.33 \text{ in.}^2 \quad (\text{per each T1 tie}) \quad \text{Grade 60}$$

$$\text{total } A_{sv} = 0.66 \text{ in.}^2 < 4 - \#4 = 0.80 \text{ in.}^2$$

For the vertical component T1v two No. 4 U stirrups were used in the heavy shear span.

Additional #4 U stirrups are placed under the load and just outside the support (see Fig. 4.7).

For the horizontal tensile tie T2 try No. 6 bars.

$$T2 = 122.4 \text{ kips}$$

$$A_{s2} = T2 / f_y = 2.04 \text{ in.}^2 < 5 - \#6 = 2.20 \text{ in.}^2$$

Use five No. 6 bars in the flexural tension zone (see Fig. 4.7).

$$T3 = T5 = 13.3 \text{ kips}$$

$$A_{s3} = A_{s5} = 13.3/60 = 0.22 \text{ in.}^2 \geq 2 - \#3 = 0.22 \text{ in.}^2$$

Use #3 U stirrups

Since $\phi 7$ is assumed at 45° , spacing of these stirrups can be $z = 30$ in. However, such wide spacing is unwise since major diagonal cracks could form between such widely spaced stirrups. Stirrup spacing should be restricted to $z/2$ or $30/2 = 15$ in. #3 is the smallest practical size. Use #3 U @ 15" (see Fig. 4.7).

For the continuing horizontal tensile tie T4 try the same No. 6 bars as for T2 (flexural reinforcement)

$$A_{s4} = 115.6/60 = 1.93 \text{ in.}^2 < 5 - \#6 = 2.20 \text{ in.}^2$$

Anchorage requirements:

The horizontal #4 bars and the vertical #4 stirrups provided to take the T1 tie forces should be well anchored by hooking the horizontal bars around the stirrups and hooking the vertical stirrups around the bottom and top bars. No special check would be required for a member of this size as such hooked stirrups could be easily developed.

The main flexural reinforcement (Tie T2) anchorage at the support needs careful examination. Using the provisions of ACI 318-89, for a clear cover over all reinforcement of 1.5 inches and with #4 stirrups, the effective cover below and outside the #6 bars is 2 inches. The clear spacing between the 3- #6 bars in the bottom layer is 2.88 inches. Thus the cover is greater than $2 d_b$ and the clear spacing is greater than $3 d_b$ satisfying ACI 318-89 Sec. 12.2.3.1 d. Hence, a multiplier of 1.0 is used with the basic development length.

$$l_d = 1.0 l_{db} = 0.04 A_{bt} / \sqrt{f_c} = 0.04(0.44) 60,000 / \sqrt{5,000} = 14.9 \text{ inches.}$$

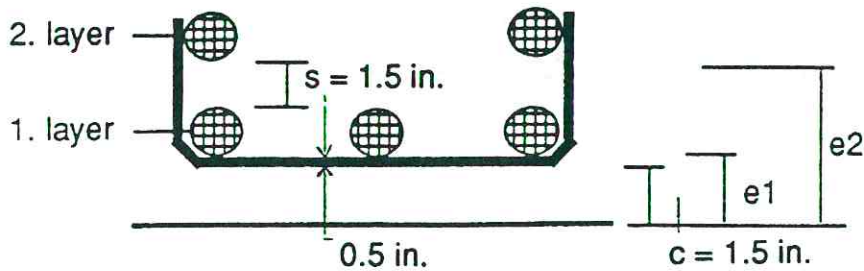
Should the #6 bars need to be hooked, the basic development length for the hooked bar from ACI 318-89 Sec. 12.5.2 is

$$l_{dh} = l_{hb} = 1200 d_b / \sqrt{f_c} = 1,200 (0.75) / \sqrt{5,000} = 12.73 \text{ inches.}$$

However, since the side cover over the hook is less than 2 1/2 inches, ACI 318-89 Sec. 12.5.4 would require that stirrup ties be spaced along the entire l_{dh} at a spacing of not more than $3 d_b$, or 2.25 inches. This would make placement of concrete very difficult and so hooked bars are not very desirable here.

In order to illustrate the effect of confinement due to the bearing plate and stirrups provided, the more complex development length equation will also be checked.

$$l_d = \frac{1.25 d_b \left\{ f_s / \left[4 (f_c')^{0.5} \right] - 50 \right\}}{\left\{ 1.2 + 3 c / d_b + (A_v f_{yt}) / (500 s d_b) + \left[(f_n)^{0.5} (200 - e^2) / 1000 \right] \right\}}$$



$$l_d = 8 \text{ in. for } a = 10 \text{ in.}$$

The initial estimate of the bearing plate size was based on a length $a = 10$ inches and a width equal to the beam width $b = 12$ inches. The bearing stress at reaction A is thus $f_n = A / ab = 187k / (10) (12) = 1.56$ ksi, well within the concrete bearing capacity. From the clear cover selected (1.5 inches minimum), the #4 stirrups chosen for the Tl_v ties, and the spacing between layers selected ($s = 1.5$ inches), the values of e_1 and e_2 can be calculated as 2.0 inches and 4.25 inches, respectively.

$$l_d = \frac{(1.25)(0.75) \left[\left(\frac{60,000}{4\sqrt{5,000}} \right) - 50 \right]}{\left[1.2 + \left(3 * 2.0 / 0.75 \right) + \left(\frac{2 * 0.20 * 60,000}{500 * 15 * 0.75} \right) + \left(\frac{\sqrt{1560} (200 - 2.0^2)}{1000} \right) \right]} = 7.2 \text{ in.}$$

Hence, if anchorage at the support becomes critical, the beneficial effect of confinement can be considered. This reduces the necessary development length for the lower layer of bars to 7.2 in. and for the upper layer to 7.4 in., say 7.5 in. for both.

If the main flexural reinforcement runs to within 1.5 in. (for cover) of the end of the beam as shown in Fig. 4.7 and Fig. 4.5, the length of bar available for meeting the requirements in node a is $15 - 1.5 + (0.75 / 2) (\cot 56.8) = 13.75$ in. for the lower layer and $15 - 1.5 + (0.75 / 2 + 2.25) (\cot 56.8) = 15.22$ in. for the upper layer. Thus the bars in the upper layer clearly exceed the 14.9 in. required for l_d according to ACI 318-89. The bars in the lower layer provide only 92% of the required l_d according to the ACI 318-89 provisions* but do provide 188% of the required l_d when the local confinement due to the bearing plate is considered. Hence these straight bars can be considered effectively anchored as detailed.

* (There is certainly *not* this degree of accuracy implicit in the computations.)

Concrete stresses at node zones:

concrete strength: $f'_c = 5$ ksi

efficiency factor: $v_e = 0.9 - 0.25 (5,000) / 10,000 = 0.775$

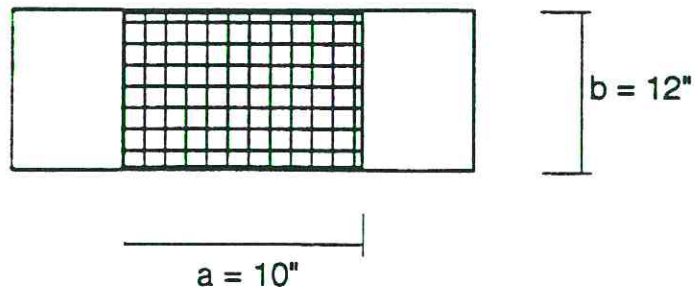
Normally the compressive stress in nodes need only be checked where concentrated forces are applied to the surface of the structural member; e.g. below bearing plates, anchor plates and over supports.

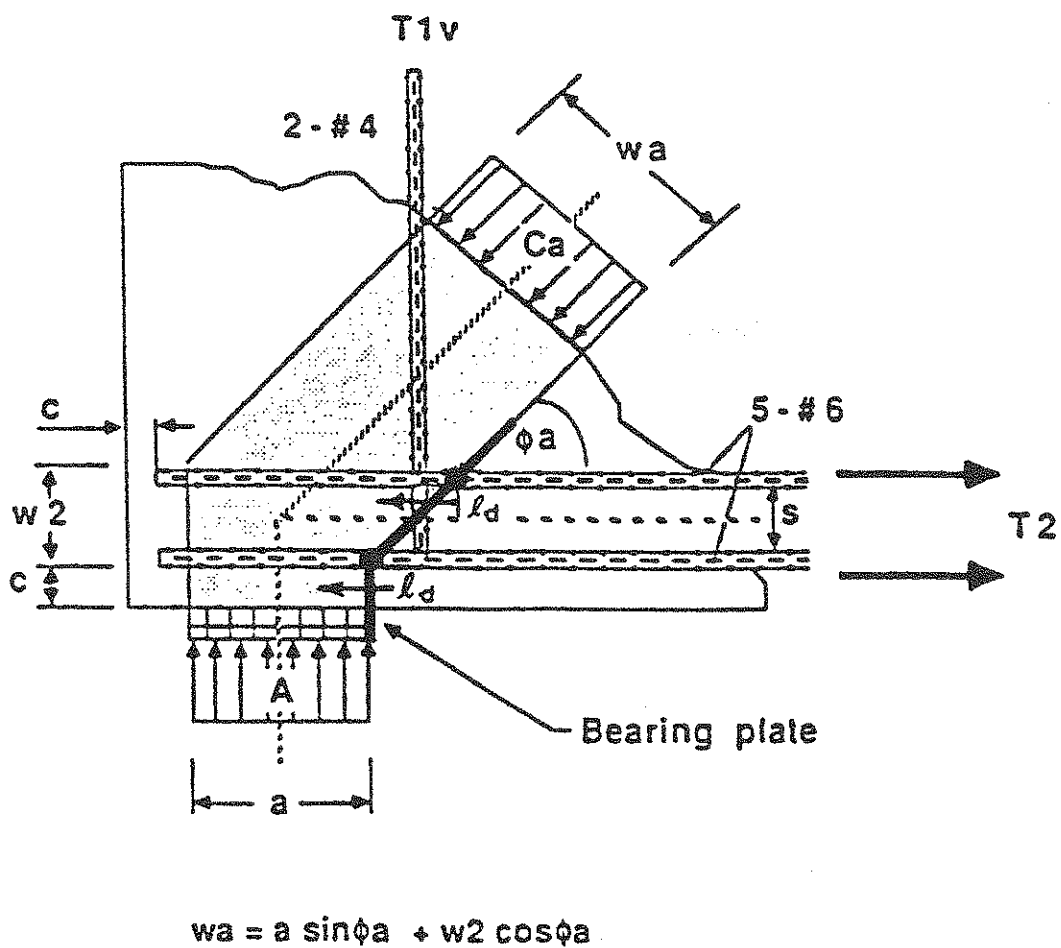
Node a (Fig. 4.4): CCT - node

See Fig. 4.5 for node geometry.

$$\begin{aligned} a &= 10 \text{ in} & b &= 12 \text{ in.} \\ \phi_a &= 56.8^\circ & C_a &= 224.4 \text{ k} \\ w_2 &= 2 d_c + s = 2 * 6/8 + 1.5 = 3.0 \text{ in.} \\ w_a &= a \sin \phi_a + w_2 \cos \phi_a = 10 \sin 56.8 + 3 \cos 56.8 = 10.0 \text{ in.} \quad (\text{See} \\ & & & \text{Fig. 4.5)} \end{aligned}$$

$$\begin{aligned} \sigma_{ca} &= C_a / (w_a * b) \leq v_e f'_c \\ \sigma_{ca} &= 224.4 / (10.0 * 12) = 1.87 \text{ ksi} \leq 0.775 * 5 = 3.88 \text{ ksi} \\ \sigma_a &= A / (a * b) \leq v_e f'_c [a_c b / (a b)]^{0.5} \\ \sigma_a &= 186.7 / (10 * 12) = 1.56 \text{ ksi} \leq 0.775 (10 / 10)^{0.5} * 5. \\ \sigma_a &= 1.56 \text{ ksi} \leq 3.88 \text{ ksi with full width bearing plate} \end{aligned}$$

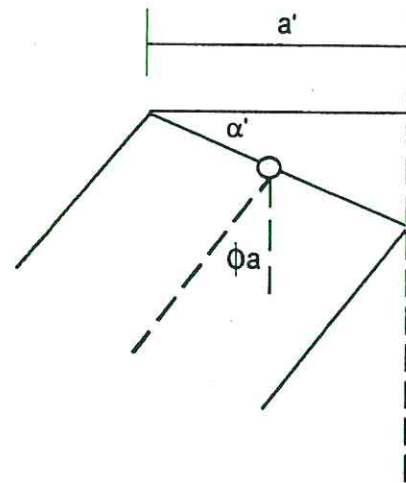


Figure 4.5: Node a - CCT - node

Node b Fig. 4.4): CCC node

See Fig. 4.6 for node geometry

a	=	10 in.
a'	=	9.34 in.
a''	=	0.66 in.
b	=	12 in.
ϕ_a	=	56.8°
ϕ_4	=	62.9°
Ca	=	223.2 k
F	=	200 k
$C3$	=	122.4 k
$C4$	=	14.9 k
$C5$	=	115.6 k



$$\sigma_1 = F / (a * b) \leq v_e f'_c$$

$$\sigma_1 = 200 / (10 * 12) = 1.67 \text{ ksi} \leq 0.775 * 5. = 3.88 \text{ ksi} \quad \text{OK}$$

$$\sigma_{cwa} = Ca / (wa * b) \leq v_e f'_c$$

$$\alpha' = \arctan [a / (2a')] = 28.16^\circ$$

$$wa = a \cos (\alpha' - \phi_a) / (2 \sin \alpha') = 9.3 \text{ in.}$$

or

$$wa = a' \cos \phi_a + a / 2 \sin \phi_a = 9.3 \text{ in.}$$

Note: wa was computed as 10.0 in. at the lower node — this is approximately correct)

$$\sigma_{cwa} = 223.2 / (9.3 * 12) = 2.0 \text{ ksi}$$

$$\leq 0.775 * 5. = 3.88 \text{ ksi} \quad \text{OK}$$

$$\begin{aligned}\sigma_{cw4} &= C4 / (w4 * b) \leq v_e f'_c \\ \alpha' &= \arctan [a / (2a'')] = 82.48^\circ \\ w4 &= a \cos (\alpha'' - \phi4) / (2 \sin \alpha'') = 4.75 \text{ in.} \\ \sigma_{cw4} &= 14.9 / (4.75 * 12) = 0.26 \text{ ksi} \leq 0.775 * 5. = 3.88 \text{ ksi} \quad \text{OK}\end{aligned}$$

$$\begin{aligned}\sigma_{c3} &= C3 / (w3 * b) \leq v_e f'_c \\ w3 &= a/2 = 5 \text{ in} \\ \sigma_{cw3} &= 122.4 / (5 * 12) = 2.04 \text{ ksi} \leq 0.775 * 5. = 3.88 \text{ ksi} \quad \text{OK}\end{aligned}$$

$$\begin{aligned}\sigma_{cw5} &= C5 / (w5 * b) \leq v_e f'_c \\ w5 &= a/2 = 5 \text{ in.} \\ \sigma_{cw5} &= 115.6 / (5 * 12) = 1.93 \text{ ksi} \leq 0.775 * 5. = 3.88 \text{ ksi} \quad \text{OK}\end{aligned}$$

The assumption that $w5 = a/2$ assumes a hydrostatic type node. Note that the computed uniform stress in C5 is only 1.93 ksi or only 45% of the $0.85 f'_c$ assumed at failure in compression zones under ACI or AASHTO [3,4]. This indicates that the initial assumption $z = 30$ in. was very conservative. The actual z at this load level is more like $40 - 2/3 (5.0) - 3.28 = 33.4$ in. Calculations could be revised on this basis but since everything has checked OK at the lesser assumed z , forces would be decreased. Therefore, this analysis is conservative.

Concrete stresses in compression diagonal struts:

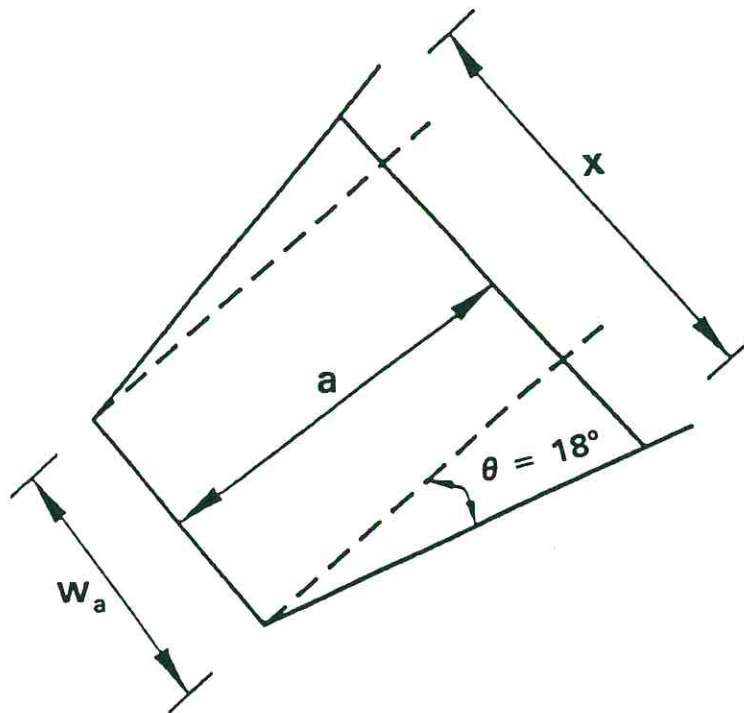
Since this application of load results in a heavy diagonal strut rather than a compression field, it might be useful to check the main strut system for the criteria $\sigma \leq 0.6 v_e f'_c = (0.6) (0.775) (5) = 2.33 \text{ ksi}$.

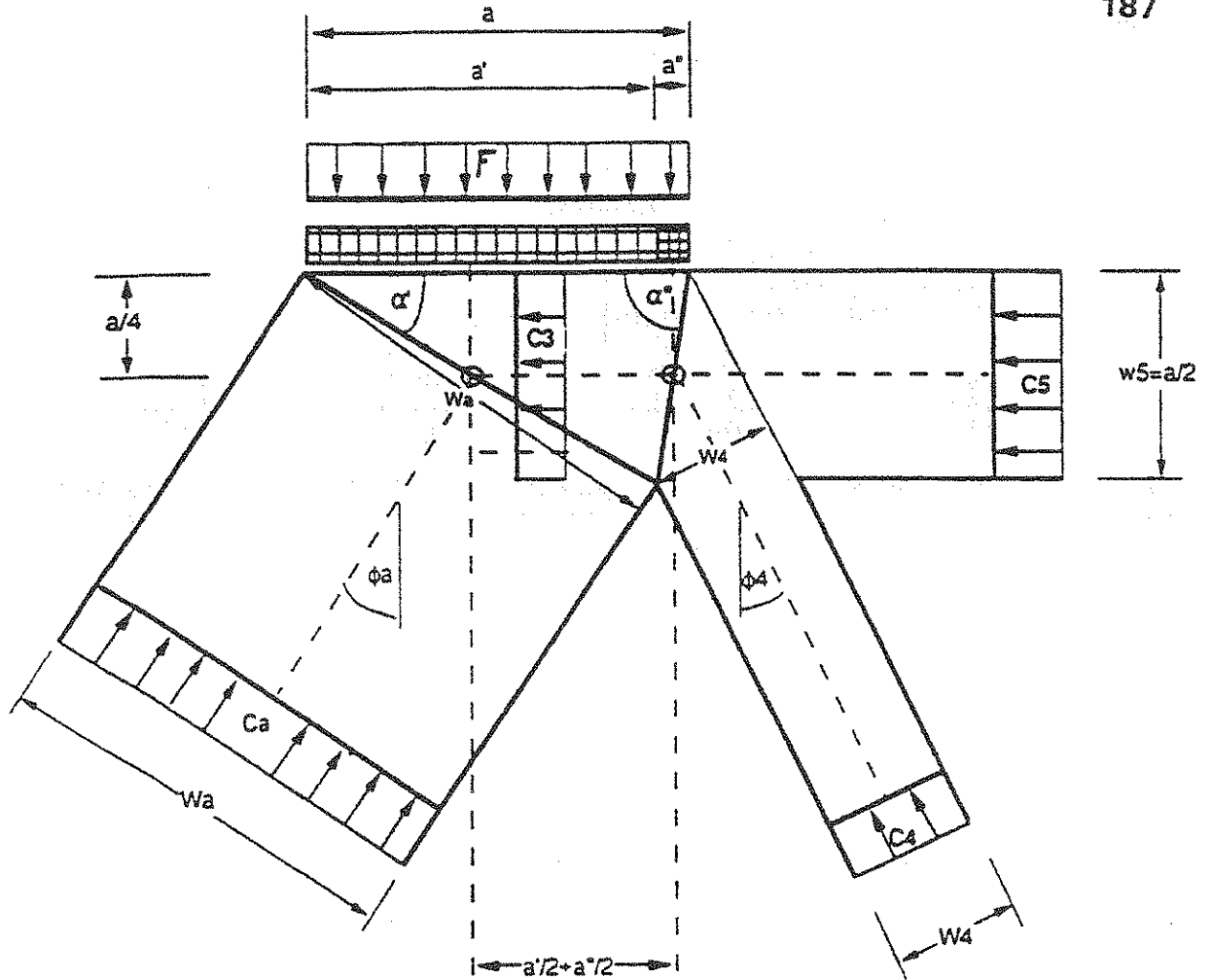
Since the nodes were checked for the concentrated C_a force, it is not likely that C1 or C2 will govern. However, to check the level of stress in the

struts take $C_2 = 112.2$ k distributed over a strut width x at a distance a from the center of the lower node. Since θ_1 was assumed at 18° , $x = w_a + 2 a \tan \theta = 10 + (2)(10) \tan 18 = 16.5$ in. $\sigma_2 = C_2 / b x = 112.2 / (12)(16.5) = 0.57$ ksi < 2.33 ksi (OK)

Details:

The complete layout of reinforcement is shown in Fig. 4.7. It is emphasized that many different arrangements could be used depending on the strut-and-tie model selected.





$$w_3 = w_5 = a/2$$

$$\alpha' = \arctan a / (2a')$$

$$\alpha'' = \arctan a / (2a'')$$

$$w_a = a \cos (\alpha' - \phi_a) / (2 \sin \alpha')$$

or

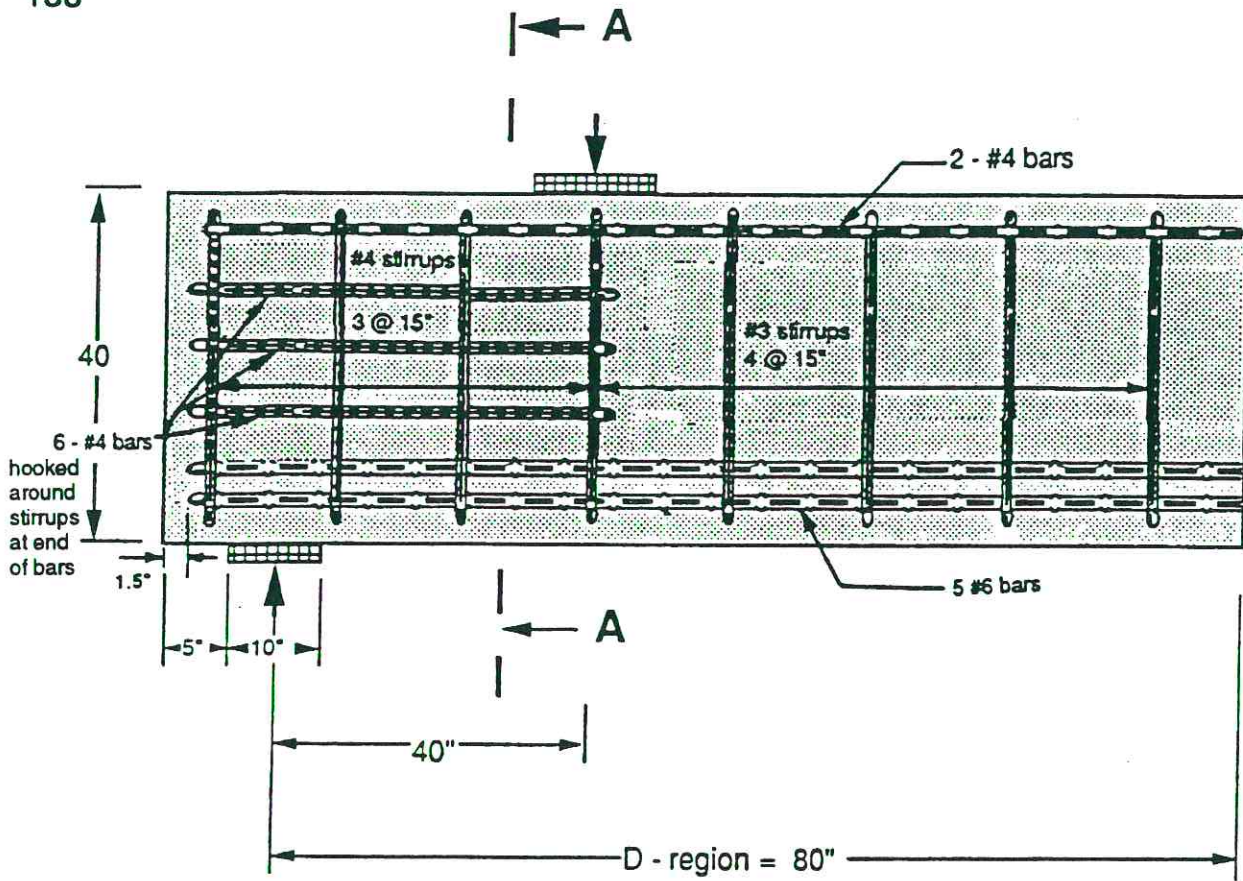
$$w_a = a' \cos \phi_a + a/2 \sin \phi_a$$

$$w_4 = a \cos (\alpha'' - \phi_4) / (2 \sin \alpha'')$$

or

$$w_4 = a'' \cos \phi_4 + a/2 \sin \phi_4$$

Figure 4.6: Node b: CCC - node



Section: A - A

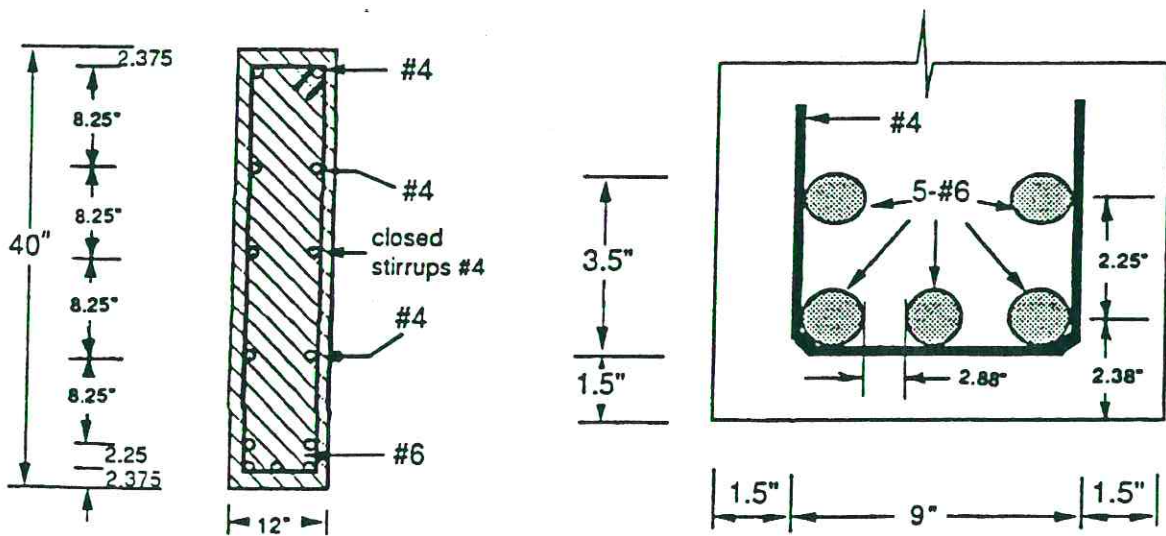


Figure 4.7: Reinforcement layout

4.3.2 Corbel projecting from a column

A corbel is a short member that cantilevers out from a column or wall to support a load (see Fig. 4.8). The corbel is generally built monolithically with the column or wall. The term corbel is generally restricted to cantilevers having shear span-to-depth ratios, $a/d \leq 1.0$ [62]. The design of corbels and brackets is based primarily on experimental results. The strut- and- tie- model allows one to visualize the flow of forces in the typical D - region. Hagberg [112] also proposed a truss analogy for design of concrete brackets. Experimental and nonlinear finite element analysis studies were done by Cook and Mitchell [113] for corbels with vertical and horizontal loads.

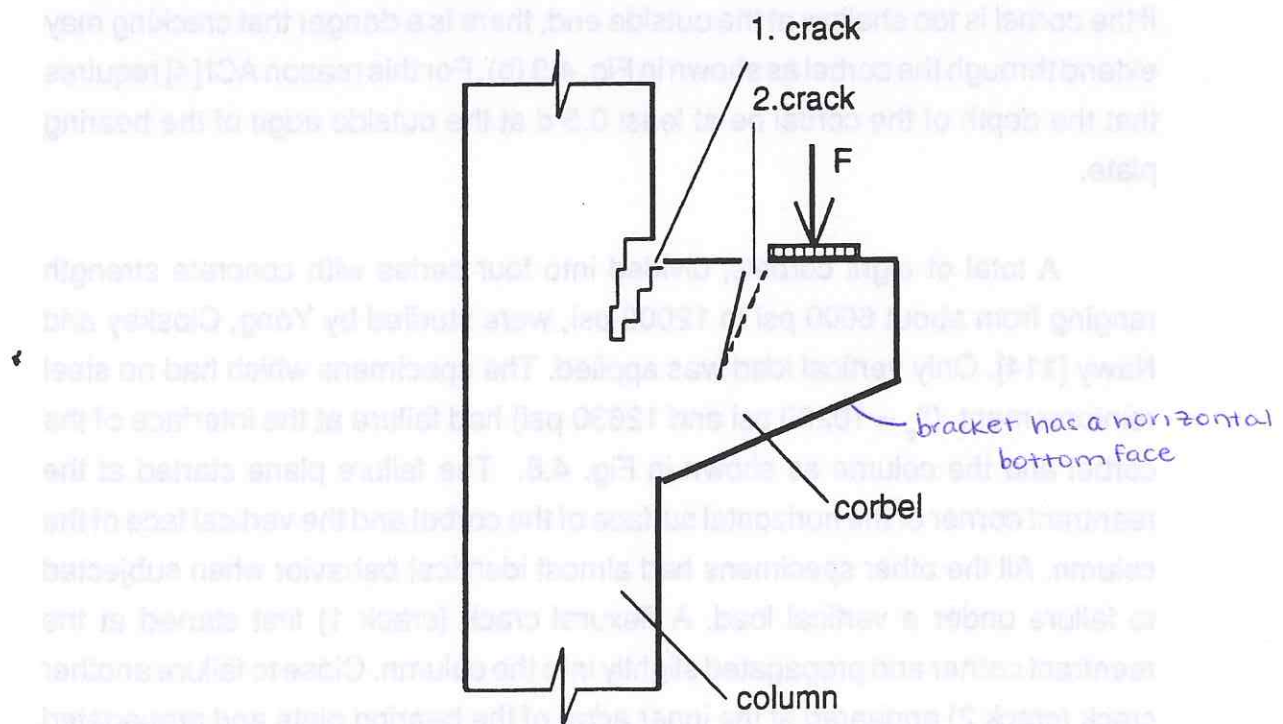


Figure 4. 8 : Typical cracking patterns of corbels

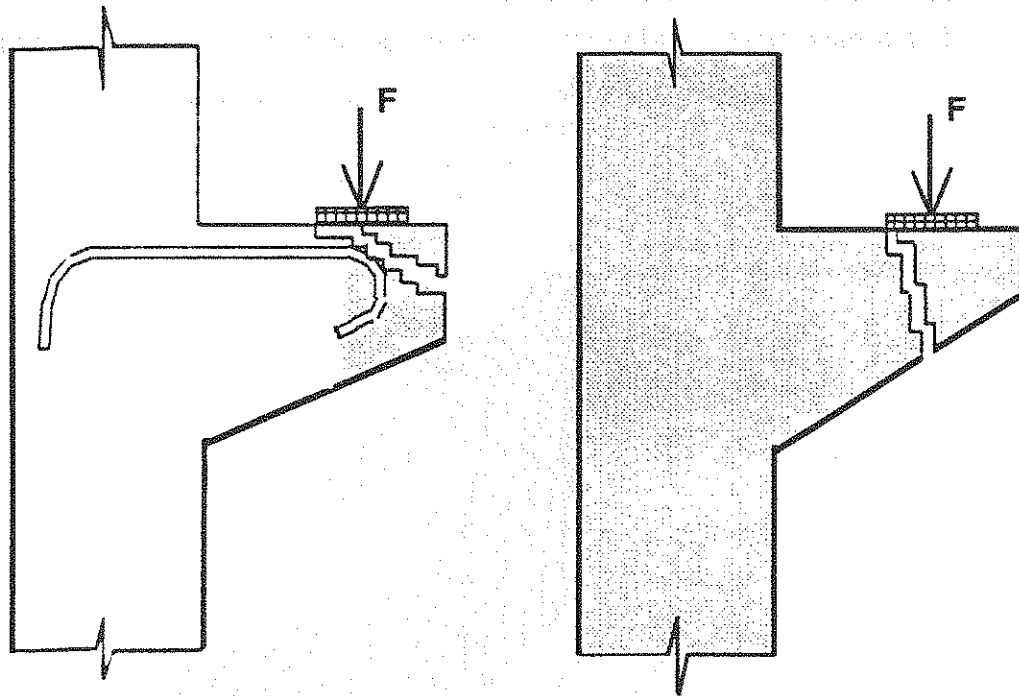
In tests, corbels display several typical modes of failure, the most common of which are:

- yielding of the tension tie
- failure of the end anchorages of the tension tie, either under the load point or in the column
- failure of the compression strut by crushing or shearing
- local zone failure under the bearing plate

When using a reinforcement tie hooked downward, as shown in Fig. 4.9(a), the concrete outside of the hook may split off. In order to avoid this problem closed ties extending past the loading plate may be used, or straight bars may be used but should be anchored at their ends by welding them to a cross bar or plate. If the corbel is too shallow at the outside end, there is a danger that cracking may extend through the corbel as shown in Fig. 4.9 (b). For this reason ACI [4] requires that the depth of the corbel be at least $0.5 d$ at the outside edge of the bearing plate.

A total of eight corbels, divided into four series with concrete strength ranging from about 6000 psi to 12000 psi, were studied by Yong, Closkey and Nawy [114]. Only vertical load was applied. The specimens which had no steel reinforcement ($f'_c = 10260$ psi and 12630 psi) had failure at the interface of the corbel and the column as shown in Fig. 4.8. The failure plane started at the reentrant corner of the horizontal surface of the corbel and the vertical face of the column. All the other specimens had almost identical behavior when subjected to failure under a vertical load. A flexural crack (crack 1) first started at the reentrant corner and propagated slightly into the column. Close to failure another crack (crack 2) appeared at the inner edge of the bearing plate and propagated at a faster rate than the initial crack towards the interface of the column and the sloping face of the corbel.

It is obvious that the horizontal reinforcement is a very important factor. Also some additional reinforcement has to be placed under the concentrated load. The compression strut develops additional tension as indicated earlier for bottle compression struts. The same type of force flow was found in the previous Example 4.1 "load near support".



a. failure crack outside of the hook

b. failure crack through the corbel

Figure 4.9: Possible failures of corbels

The distribution of principal stresses in a trapezoidal corbel and its supporting column, obtained by Franz and Niedenhoff [115] from photoelastic models, is presented in Fig. 4.10. The load received from a gantry girder is simulated. An evaluation by Park and Paulay [105] of that study reveals the existence of four conditions:

- The shape of the corbel has little effect on the state of the stresses. In a rectangular corbel, the outer corner opposite the load point is virtually stress free.
- The compression force along the sloping edge of the corbel is also approximately constant, indicating that a diagonal compression strut develops.
- The inclined tensile stresses arising from the change of direction of the compression force are very small.
- The tensile stresses along the top edge are almost constant between the load point and the column face.

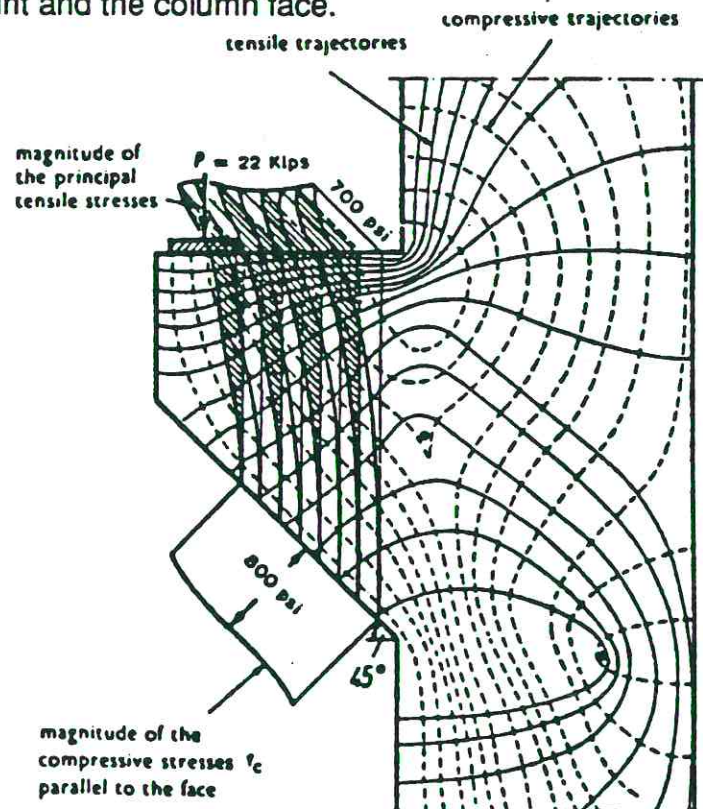


Figure 4.10: Stress trajectories in a homogeneous elastic corbel (from Ref. [115], Figure from Ref. [105])

In the traditional approach to the problem, one would have relied on the consideration of shear stresses. Indeed, corbels have often been reinforced with diagonals, as shown in Fig. 4.11, to take a substantial part of the shearing force. The investigations of Franz and Niedenhoff [115] have conclusively proved the inefficiency of this approach.

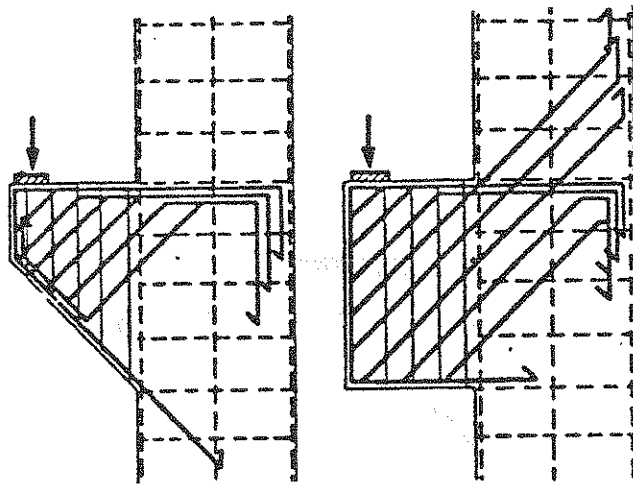


Figure 4.11: Diagonally reinforced corbels
(from Ref. [115], Figure from Ref. [105])

Park and Paulay [105] identified failure mechanisms as shown in Fig. 4.12 from the tests by Kriz and Rath [116].

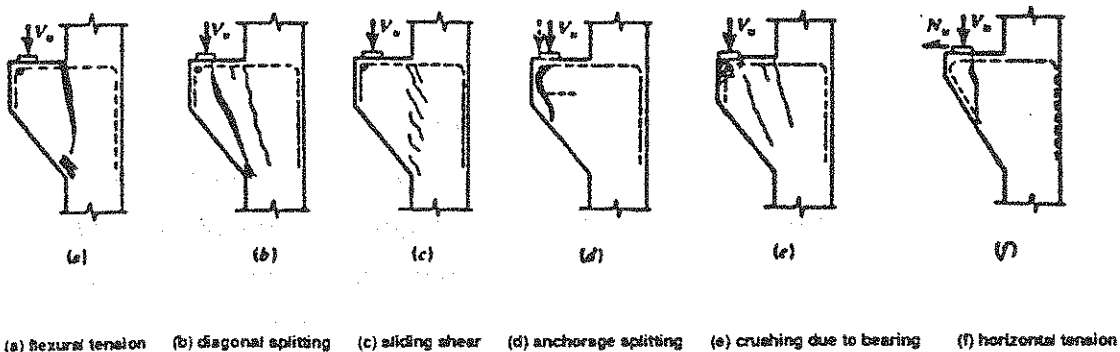


Figure 4.12: Failure mechanism in corbels: [From Ref. 105]

The strut-and-tie-model for a corbel shown in Fig. 4.13 is proposed and assumes that the concrete stress at the lower reentrant corner reaches the effective concrete strength [28]. A typical CCC -node is found in the lower corner and the tensile force in the upper chord can be computed without knowing the angle of inclination of the main compression strut. The flow of forces and typical CCC-node dimensions are shown in Fig. 4.14.

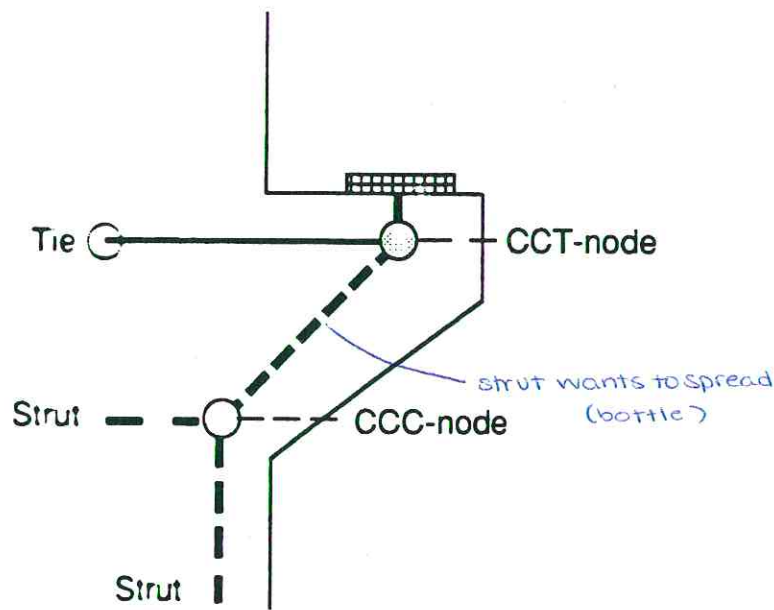


Figure 4. 13: Strut- and- tie- model for corbel .

Figure 4.15 shows eight test results from [117] with a concrete range from 5690 to 12630 psi, six test results from [118] with concrete strengths from 4200 to 5057 psi and one test from [113] with 5858 psi compared with the proposed strut-and- tie- model. The statistical analysis for the comparison is shown in Table 4.1. The proposed model is generally conservative and reasonably accurate.

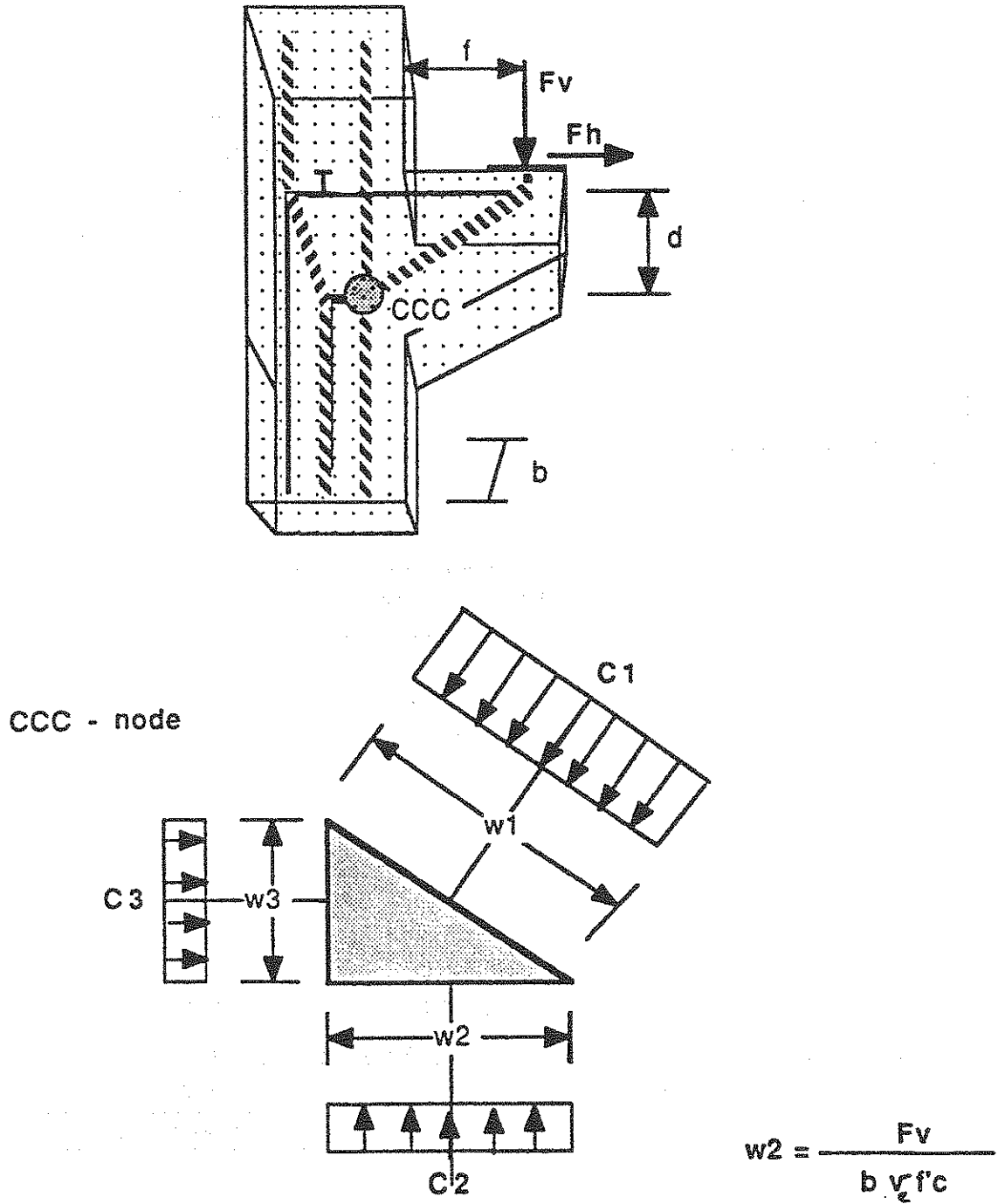


Figure 4.14: Corbel strut- and- tie model

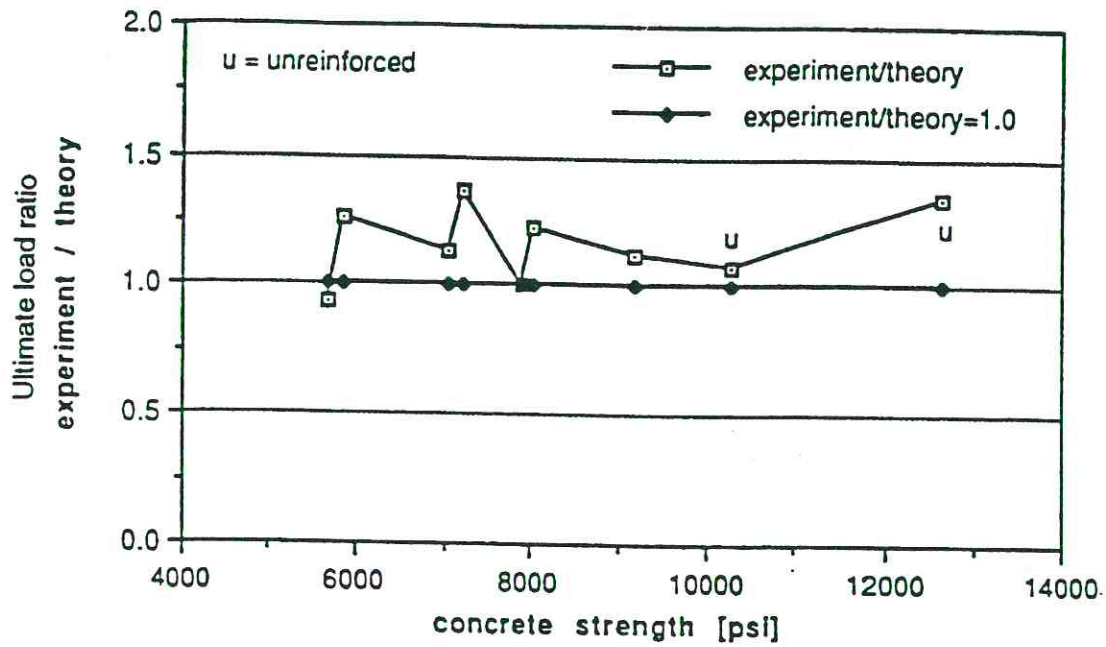


Figure 4. 15 : Strut- and- tie- model results compared with test results

X ₁ : Column 1					
Mean:	Std. Dev.:	Std. Error:	Variance:	Coef. Var.:	Count:
1.082	.155	.04	.024	14.311	15
Minimum:	Maximum:	Range:	Sum:	Sum Squared:	# Missing:
.93	1.442	.512	16.224	17.883	0

Table 4.1: Statistical analysis from Fig. 4.15 omitting unreinforced specimen

Example 4.2 : Corbel projecting from a column

Corbel projecting from a column

Design a pair of corbels to transfer vertical reactions of 200 kips and horizontal reactions of 40 kips to a supporting column. Use $f'_c = 8000$ psi and $f_y = 60,000$ psi. The computation steps are:

- Estimate member sizes and dimensions
- Divide member into B and D regions (see Fig. 4.16)
- Develop a strut- and- tie model (see Fig. 4.16)
- Compute external forces
- Compute the strut- and- tie angle
- Compute the strut- and- tie forces
- Dimension requirement for ties
- Determine anchorage requirements
- Check concrete stresses

Assume clear concrete cover over all reinforcement is 1.5 in.

Load and dimensions:

$F_v = 200$ kips
 $F_h = 40$ kips
 $h = 12$ in.
 $g' = 8$ in.
 $g'' = 6$ in.
 $b = 12$ in.
 $a = 5$ in.
 $f = 5.5$ in.
 $i = 9$ in.
 $d \approx 0.75 (g' + g'') = 10.5$ in.

Since tie reinforcement often has to be placed in multiple layers, cover and spacing requirements suggest that a conservative estimate be used for the effective depth, d . The basic strut- and- tie model shown in Fig. 4.16 is chosen for computing the strut and tie forces. The compression struts are again assumed as "bottle" struts. The location of node b is uncertain and depends somewhat on the location of C_4 . After C_4 is located the node b will be chosen on a 45° angle inward from the reentrant corner.

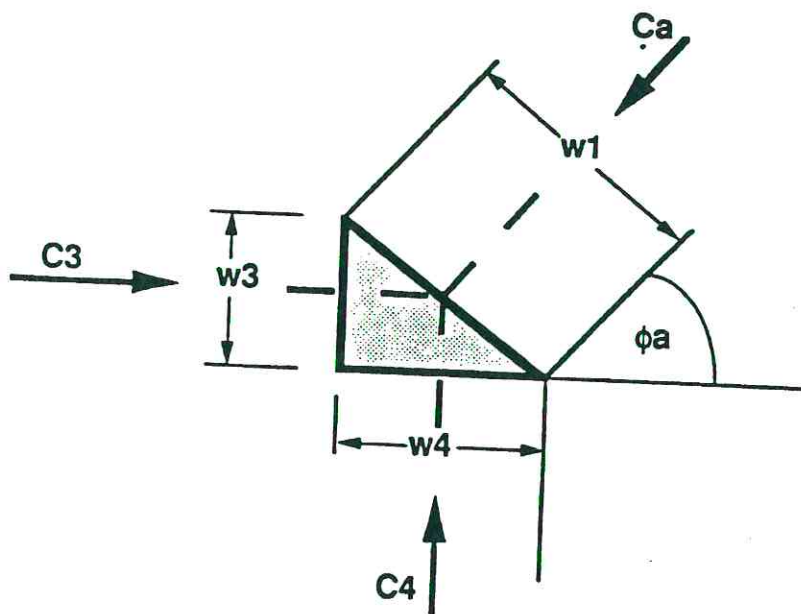
Strut and tie angle:

$$w_4 = C_4 / (b v_e f_c)$$

$$w_3 = w_4 / \tan \phi_a$$

$$\phi_a = \arctan (d - w_3/2) / (f + w_4/2)$$

w_3 , w_4 , ϕ_a are unknown but interrelated



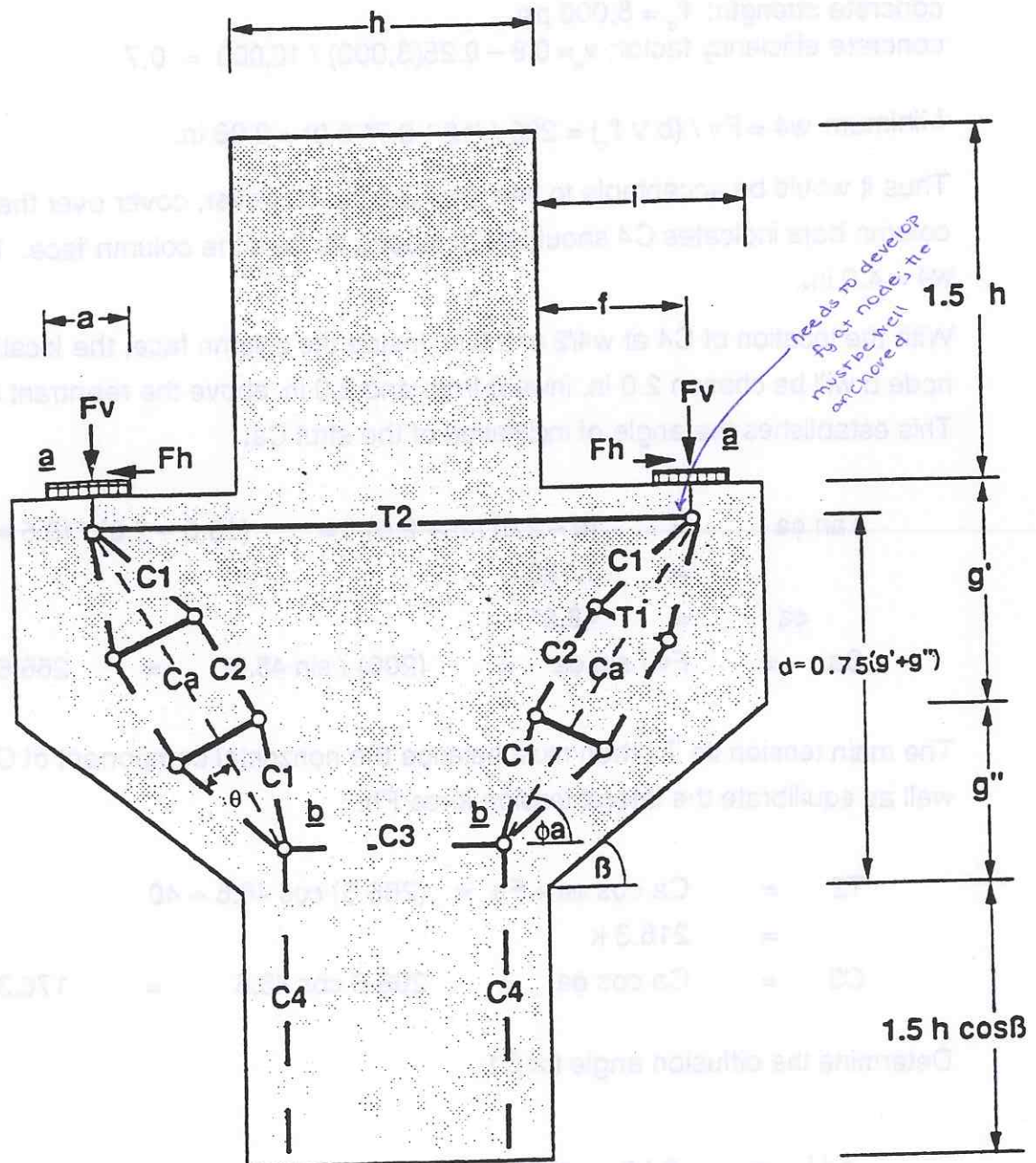


Figure 4.16: Strut-and-tie model for corbel projecting from a column

Internal forces:

$$C4 = Fv = 200 \text{ kips}$$

concrete strength: $f'_c = 8,000 \text{ psi}$

$$\text{concrete efficiency factor: } v_e = 0.9 - 0.25(8,000) / 10,000 = 0.7$$

$$\text{Minimum } w4 = Fv / (b v f'_c) = 200 / (12 * 0.7 * 8.0) = 2.98 \text{ in.}$$

Thus it would be acceptable to use $w4 = 3.0 \text{ in.}$ However, cover over the main column bars indicates C4 should be at least 2 in. from the column face. Use $w4 = 4.0 \text{ in.}$

With the location of C4 at $w4/2$ or 2.0 in. inside the column face, the location of node b will be chosen 2.0 in. inward from and 2.0 in. above the reentrant corner. This establishes the angle of inclination of the strut Ca:

$$\begin{aligned} \tan \phi_a &= (d - 2.0) / (f + 2.0) = (10.5 - 2.0) / (5.5 + 2.0) \\ &= 1.133 \\ \phi_a &= 48.6^\circ \\ C_a &= Fv / \sin \phi_a = (200) / \sin 48.6^\circ = 266.6 \end{aligned}$$

The main tension tie T2 then must balance the horizontal component of Ca as well as equilibrate the lateral tension force Fh.

$$\begin{aligned} T2 &= C_a \cos \phi_a + Fh = (266.6) \cos 48.6 + 40 \\ &= 216.3 \text{ k} \\ C3 &= C_a \cos \phi_a = 266.6 \cos 48.6 = 176.3 \text{ k} \end{aligned}$$

Determine the diffusion angle for C1:

$$\begin{aligned} a/i &= 5/9 = 0.55 \\ \theta &= 12 + 3 / \sqrt{0.55} = 16.0^\circ \\ T1 &= (C_a / 2) * \tan 16 = (266.6 / 2) (\tan 16) \\ T1 &= 38.2 \text{ kips} \end{aligned}$$

Reinforcement for Ties:

$$T1 = 38.2 \text{ kips}$$

$$T1h = T1 \sin \phi a = 28.7 \text{ kips}$$

$$A_{sh} = T1h / f_y = 0.5 \text{ in.}^2$$

Since there are 2 T1 forces to be provided for each corbel

$$\text{total } A_{sh} = 1.0 \text{ in.}^2 < 6 - \#4 \text{ (Grade 60)} = 1.20 \text{ in.}^2 \quad (\text{Use 3 closed ties})$$

$$T1v = T1 \cos \phi a = 25.3 \text{ kips}$$

$$A_{sv} = T1v / f_y = 0.42 \text{ in.}^2$$

$$\text{total } A_{sv} = 0.84 \text{ in.}^2 \approx 4 - \#4 \text{ (Grade 60)} = 0.80 \text{ in.}^2 \quad (\text{Use 1 closed tie and}$$

1 pair of bent bars which must be hooked over

and anchored by the topmost horizontal #7 closed tie)

$$T2 = 216.3 \text{ kips}$$

$$A_s = T2 / f_y = 3.60 \text{ in.}^2 = 6 - \#7 \text{ (Use 3 closed ties (Grade 60))} = 3.60 \text{ in.}^2$$

Concrete stresses at node zones:

Node a: CCT - node (Figures as in Example 4.1)

$$a = 5 \text{ in.}$$

$$\sigma_a = Fv / (a * b) \leq [a_c b / (a b)]^{0.5} v_e f'_c$$

$$\sigma_a = 200 / (5 * 12) = 3.3 \text{ ksi} \leq 0.7 * 8. * (1)^{0.5}$$

$$\sigma_a = 3.3 \text{ ksi} \leq 5.6 \text{ ksi} \quad \text{OK}$$

$$\sigma_{ca} = Ca / (wa * b) \leq v f'_c$$

$$wa = a \sin \phi a + w2 \cos \phi a = 5 * \sin 48.6 + 2.5 \cos 48.6 = 5.40$$

$$\sigma_{ca} = 266.6 / (5.40 * 12) = 4.11 \text{ ksi} \leq 0.7 * 8. = 5.6 \text{ ksi} \quad \text{OK}$$

Node b: CCC - node $w_4 = 4.0$ $w_3 = w_4 / \tan \phi_a = 3.52$
 $w_1 = \sqrt{4.0^2 + 3.52^2} = 5.32$

$$\begin{aligned} \sigma_{ca} &= C_a / w_1 b \leq 0.7 f'_c = 5.6 \text{ ksi} \\ &= 266.6 / (5.32) (12) = 4.18 \text{ ksi} < 5.6 \text{ ksi} && \text{OK} \\ \sigma_3 &= C_3 / w_3 b = 176.3 / (3.52) (12) = 4.17 \text{ ksi} < 5.6 \text{ ksi} && \text{OK} \\ \sigma_4 &= C_4 / w_4 b = 200 / (4.0) (12) = 4.17 \text{ ksi} < 5.6 \text{ ksi} && \text{OK} \end{aligned}$$

Anchorage requirements:

Three closed #7 ties were used for the main horizontal reinforcement. Because the tension tie in the strut- and- tie- model is assumed to be stressed to the yield strength in tension between the loading plate and the column, it must be anchored in the node zone a and outside the bearing plate for that tension. The closed ends of the ties should be sufficient positive anchorage. If straight bars were used they could be welded to an angle or bar at right angles to the tie (see Fig. 4.17), or be welded to a transverse reinforcing bar of the same diameter as the tie.

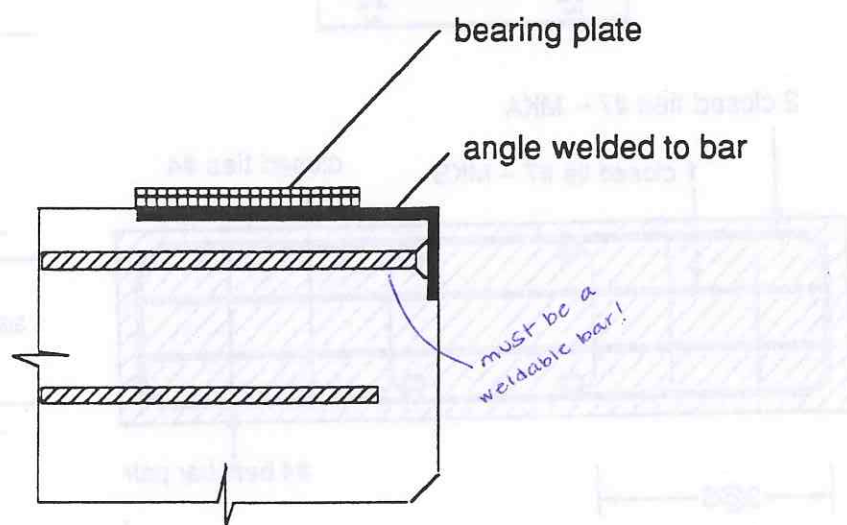
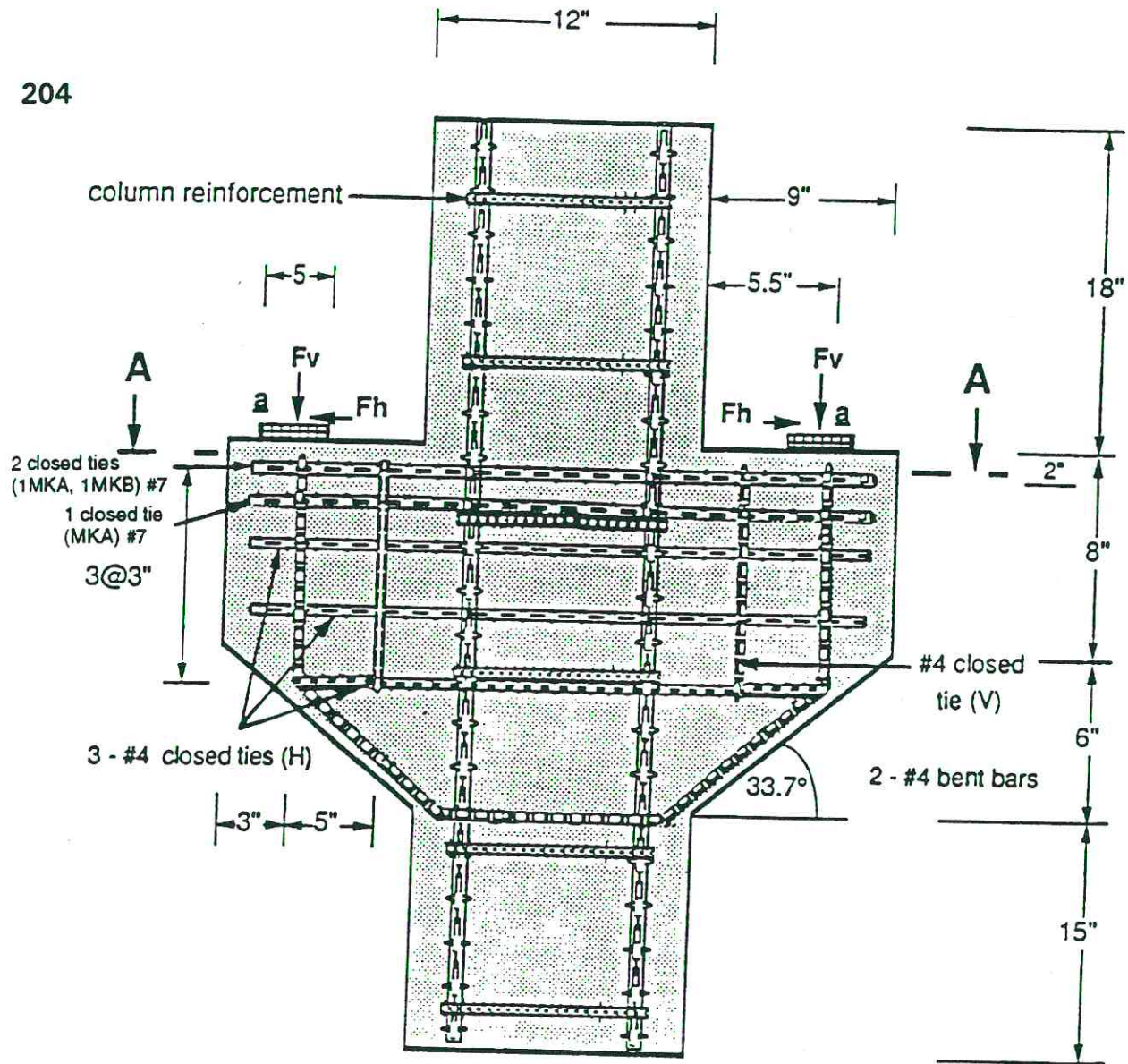


Figure 4. 17: Anchorage detail for corbel design (from Ref. [62])



Section: A - A

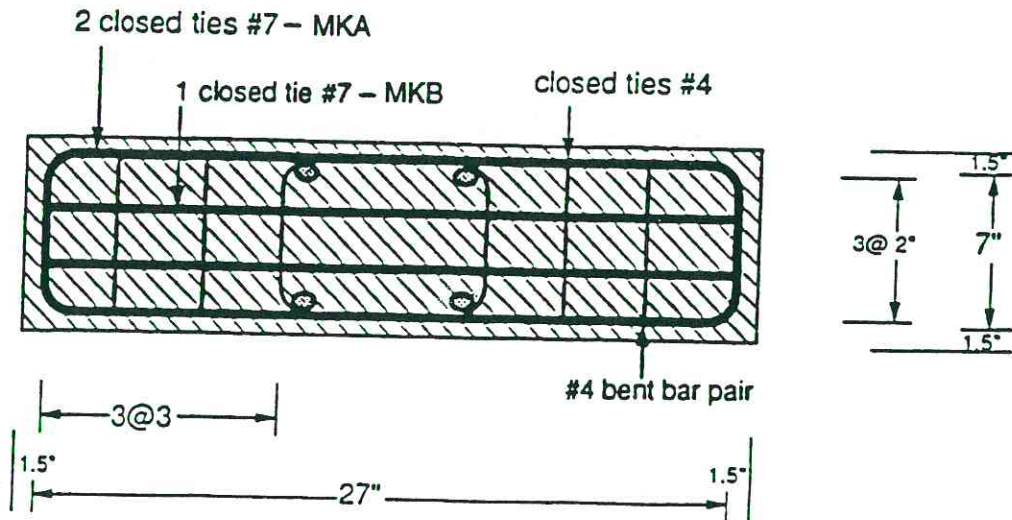


Figure 4.18: Reinforcement layout

4.3.3 Deep beam with a hole

A deep beam is a beam in which a significant amount of the load is carried to the supports by a compression thrust joining the load and the reaction rather than through flexural action. This occurs when a concentrated load acts closer than about $2d$ to the support, or for uniformly loaded beams when the span-to-depth ratio, " l/d ", is less than about 4 to 5. The ACI Code [4] specifies that deep beam action must be considered when designing for flexure if " l/d " is less than $5/2$ for continuous spans or $5/4$ for simple span (see also Ref. [105]).

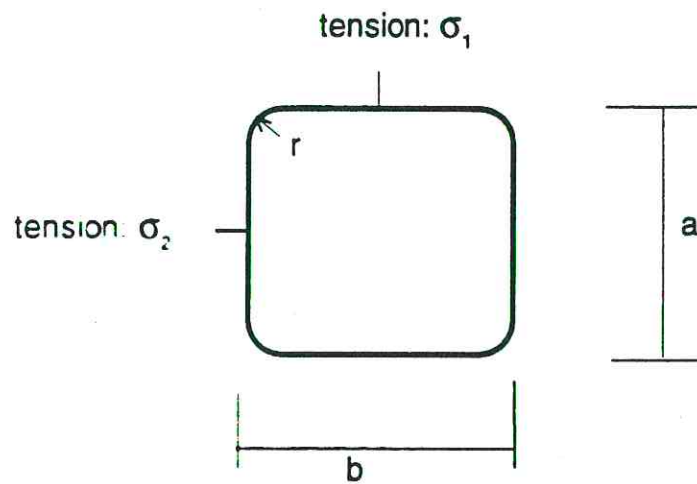
Cook and Mitchell [113] did some experimental verification and nonlinear finite element analysis of a uniform loaded T-beam with a hole in the web. The finite element analysis by Schlaich et al [28] and the experimental study by Cook and Mitchell [113] show that tensile forces are acting especially around the corner. This leads to the assumption that a diagonal tie has to be placed in the discontinuity zone in the tension region. The stress concentration factor for an infinite plate with a rectangular hole and subjected to biaxial stress is the highest such factor for all different forms of openings [119]. For a finite-width member with infinite thickness and a circular hole under biaxial tension the stress concentration factor is given by Ling [120] as:

$$\begin{aligned} K &= 12 / (7 - 5\nu) \\ \nu &= 0.16 \text{ for concrete} \\ K &= 1.93 \end{aligned}$$

For the corresponding case of a semi-infinite body, Tsuchida and Nakahara [121] developed stress concentration factors. The values with Poisson's ratio of 0.25 and r = radius of circular hole and m = distance from center of cavity to surface are:

$$\begin{aligned} r/m &= 0.5: & K &= 2.32 \\ r/m &= 0.8 & K &= 3.3 \end{aligned}$$

For rectangular openings the following mathematical results, with specific data obtained by computer, have been published: $\sigma_1 = \sigma_2$



$b=a;$	r/b	$=$	0.1	K	$=$	4.88
$b=a;$	r/b	$=$	0.3	K	$=$	2.76

Figure 4.19: Geometry for determining stress concentration factors

In addition, for $b/a = 1/2$, the stress concentration factor reaches the low value of 1.5 for the ellipse. In general it has been shown that the outside fiber at the hole has at least approximately 2 times higher stresses. If the radius of the rounding becomes smaller at the corners of rectangular openings, K increases rapidly.

Schlaich et al [28] proposed that, for this kind of problem, two separate strut-and-tie-models should be developed, each with a carrying capacity of 50%. One model should follow the elastic principal stress trajectories with a diagonal tension tie and the second model should have struts and ties parallel to the borders. From a practical standpoint it is very inconvenient to place diagonal reinforcement in many structures.

Test results from Shah [122] and Gaynor [123] for tests on reinforced concrete in-filled shear walls with openings gives some indication that first cracking appears near the openings. In order to prevent large cracking and for crack control under service load it seems reasonable to round off the corners (see Fig. 4.19: $r/b = 0.3$) and for geometrical discontinuities subjected to biaxial tension a quantity of diagonal reinforcement equal to about $1/8$ of the orthogonal reinforcement should be provided as an addition. In the general literature on design [62, 105, 113, 124] no detailed information about the required amount of diagonal reinforcement is given. As shown in Fig. 4.20, such diagonal reinforcement follows the principal tensile stress directions closely and should be very effective in controlling the reentrant corner crack width.

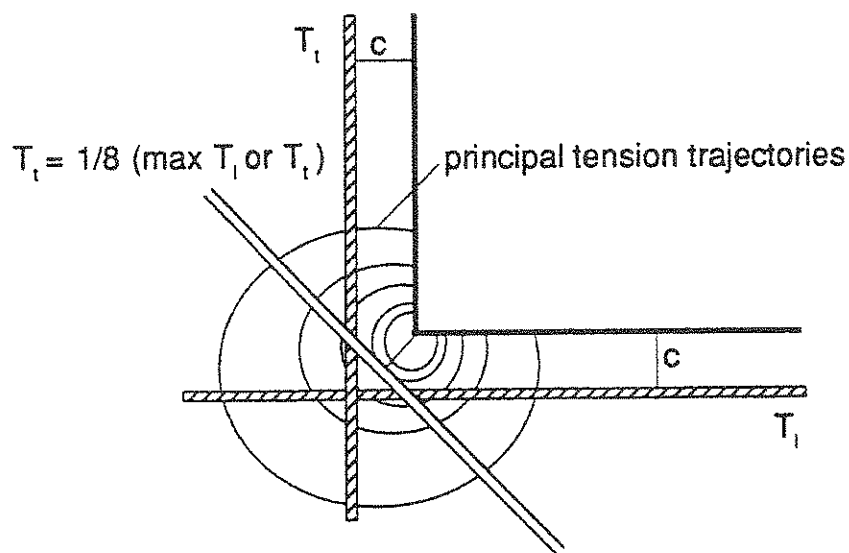


Figure 4.20: Principal tension trajectories and reinforcement for corner in tension

Example 4.3: Deep beam with a hole

Design a deep beam with an overall depth of 16'8" and an overall length of 27'6" to transfer a vertical load of 500 kips applied 14'7" from the left edge. The wall is supported on simple supports located 25'0" on centers (see Fig. 4.21(a)). The supports are 20" X 15" columns and the wall thickness is 15". There is a large hole 65 in. square located in the lower left corner. The hole has 30 in. of concrete below it and its left edge is 30 in. from the center of the left support. Concrete strength is 7000 psi and Grade 60 reinforcement is used.

Load and dimensions:

F	=	500 kips
l	=	300 in.
f	=	30 in.
j	=	65 in.
h	=	200 in.
e	=	30 in.
k	=	65 in.
m	=	160 in.
a	=	20 in.
b	=	15 in.

External forces

B	=	267 kips
A	=	233 kips

In developing a strut- and- tie model for this type of unusual structure, it is very useful to consider the elastic stress pattern indicated by a finite element analysis. A general pattern for a similar type of problem with the load located considerably more to the right has been provided by Schlaich et al [28] and is shown in Fig. 4.21(b). Based on the pattern of elastic stresses shown, it can be seen that significant tension acts in the diagonal direction at the upper right corner of the opening and lesser tension acts on the diagonal at the lower left corner of the opening. The thrust to the left of the opening is skewed slightly to the right, inclining towards the opening's upper left corner. Schlaich et al [28] have suggested two possible strut- and- tie models for the left side of the structure as shown in Fig. 4.21(c) and (d). They suggest the left reaction be considered as split on a 50–50 basis between these patterns. One minor problem with these suggested models is that there is no tie required beneath the opening. Inclining the thrust towards the upper corner of the opening in the section to the left of the opening would result in a tie requirement beneath the opening. The part of the wall to the right of the applied load is basically a straightforward case with the thrust being transferred by a bottle-shaped strut to the reaction at B and the lateral component of the strut force tied back by a lower tie. For this particular example, variations of the models suggested by Schlaich et al were adopted. For the portion of the wall to the left of the centerline of the applied load, it is assumed that the load carrying capacity will be shared equally (50–50) by the Strut- and- Tie Models shown in Fig. 4.21(e) and Fig. 4.21(f). The geometry of the models and the resulting strut compressions and tie tensions are shown on each figure. Note that in Fig. 4.21(f) C8 was assumed as a compression strut but in the solution (performed using a microcomputer program for a 2D truss based on SAP) was found to have a very low level of tension. Similarly T11 was assumed as a tension tie but analysis indicates a small amount of compression. While the two models to the left could be combined, it is easier to proportion reinforcement using the two separate models. The much simpler section to the right of the load is shown in Fig. 4.21(g) with the right reaction, 267 k, and an equal part of the load applied to a bottle strut and major tension tie.

Strut and tie angle

$$z \approx 7/8 h = 175 \text{ in.}$$

$$\tan \phi_b = 175/135 = 1.296$$

$$\phi_b = 52.35^\circ$$

$$a/h = 10/200 = 0.025$$

$$\theta_1 = 12 + 3/\sqrt{(a/h)} \leq 25^\circ$$

$$\theta_1 = 12 + 3/\sqrt{(0.025)} = 25.4^\circ \leq 25^\circ \quad \text{Use } 25^\circ$$

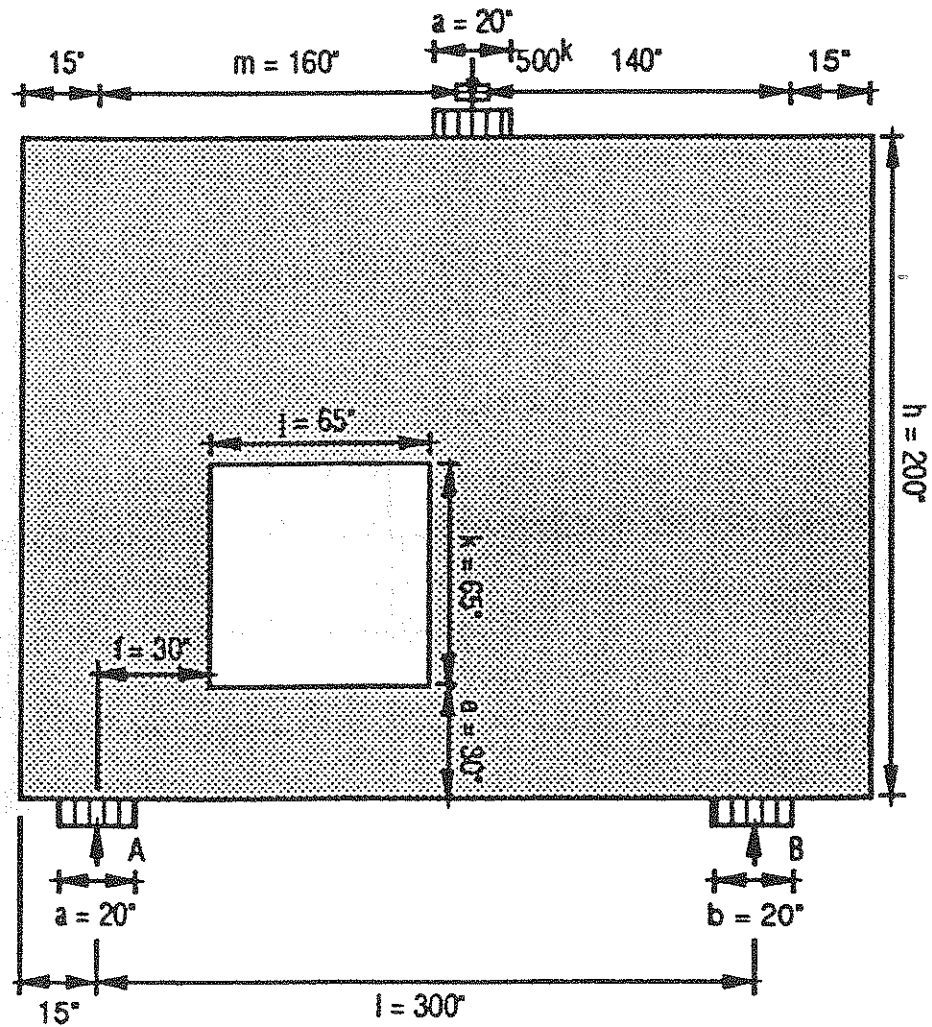
Internal forces

$$C_b = B/\sin \phi_b = 267 / \sin 52.35^\circ = 337.2 \text{ kips}$$

$$C_{14} = C_b/(2 \cos \theta_1) = 186 \text{ kips}$$

$$T_{14} = (C_b/2) \tan \theta_1 = 78.6 \text{ kips}$$

$$T_{13} = C_b \cos \phi_b = 206 \text{ kips}$$



(a) Example 4.3 Dimensions

Figure 4.21: Strut- and tie models for deep beam with a hole

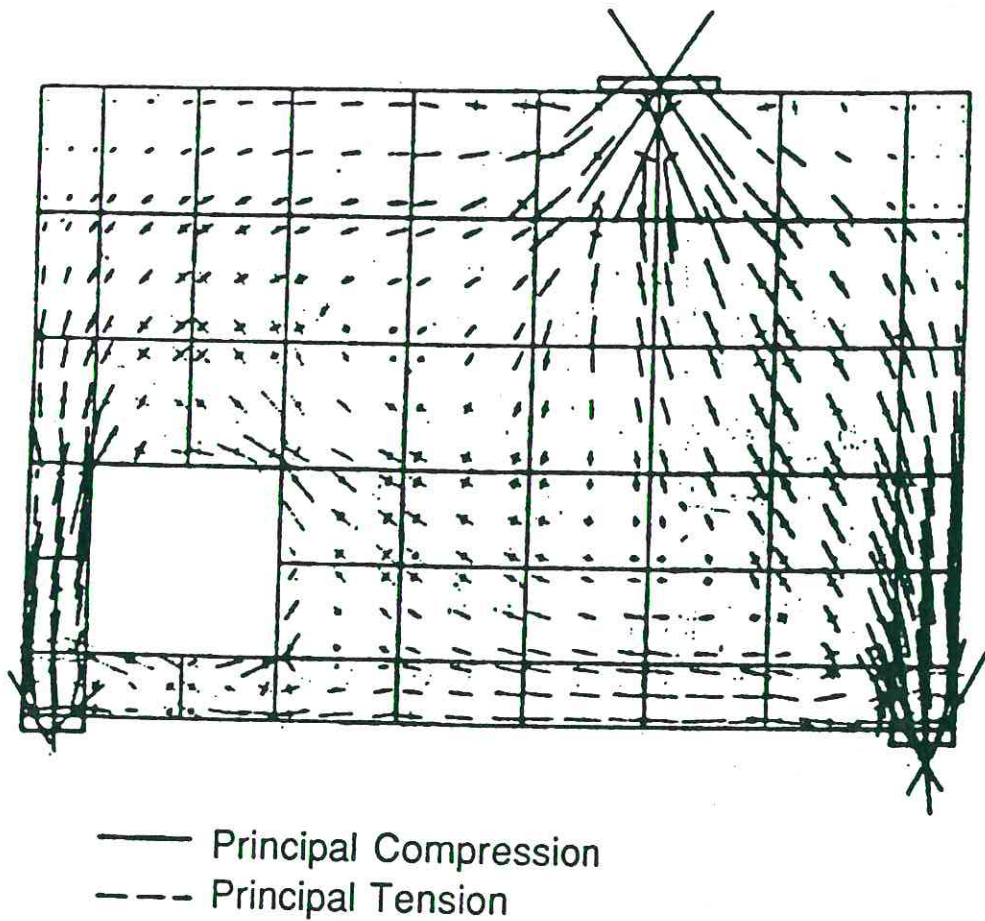


Fig. 4.21(b) Finite element analysis contours for similar structure with load placed farther to right (From Ref [28])

Figure 4.21: Strut- and- tie models for deep beam with a hole

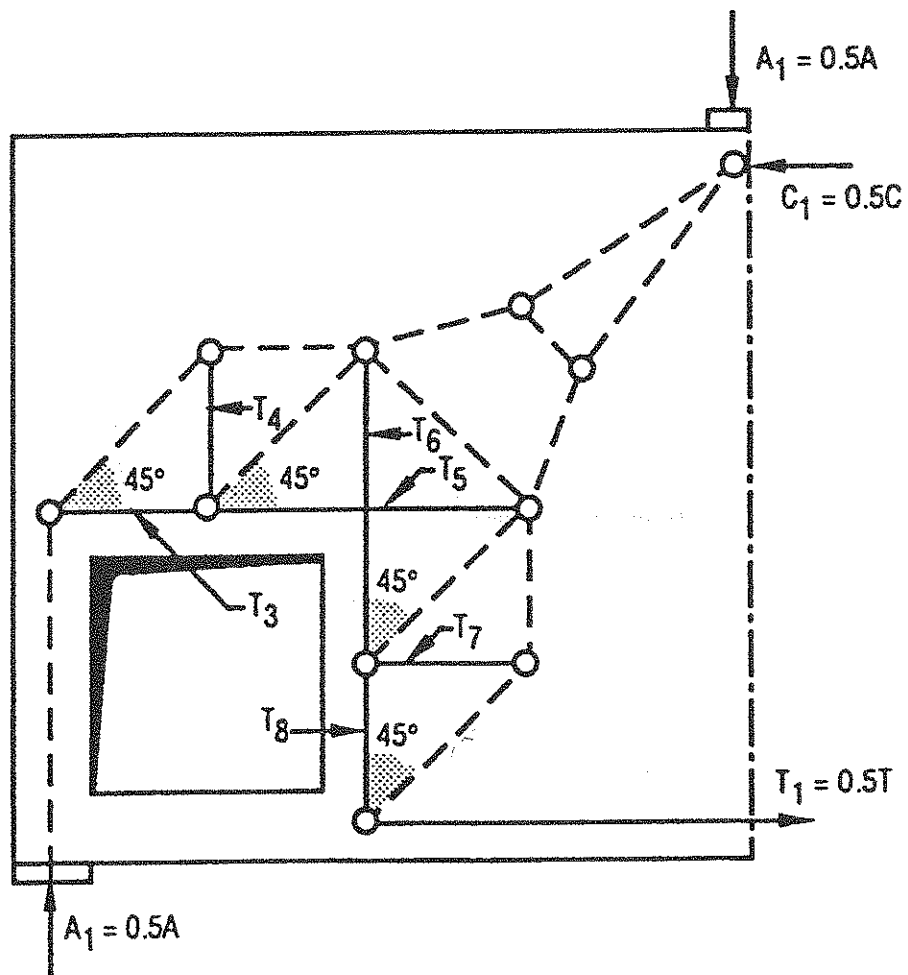


Fig. 4.21(c) Model 1, left side (From Ref [28])

Figure 4.21: Strut- and- tie models for deep beam with a hole

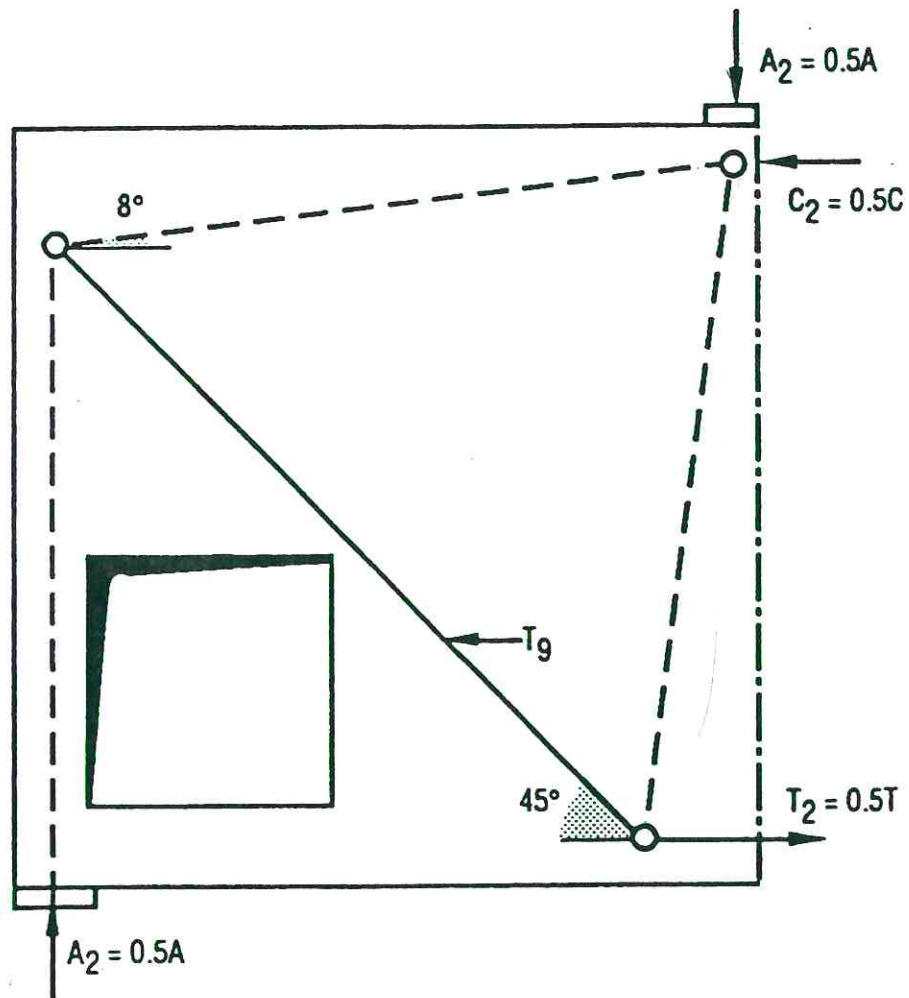


Fig. 4.21(d) Model 2, left side (From Ref [28])

Figure 4.21: Strut- and- tie models for deep beam with a hole

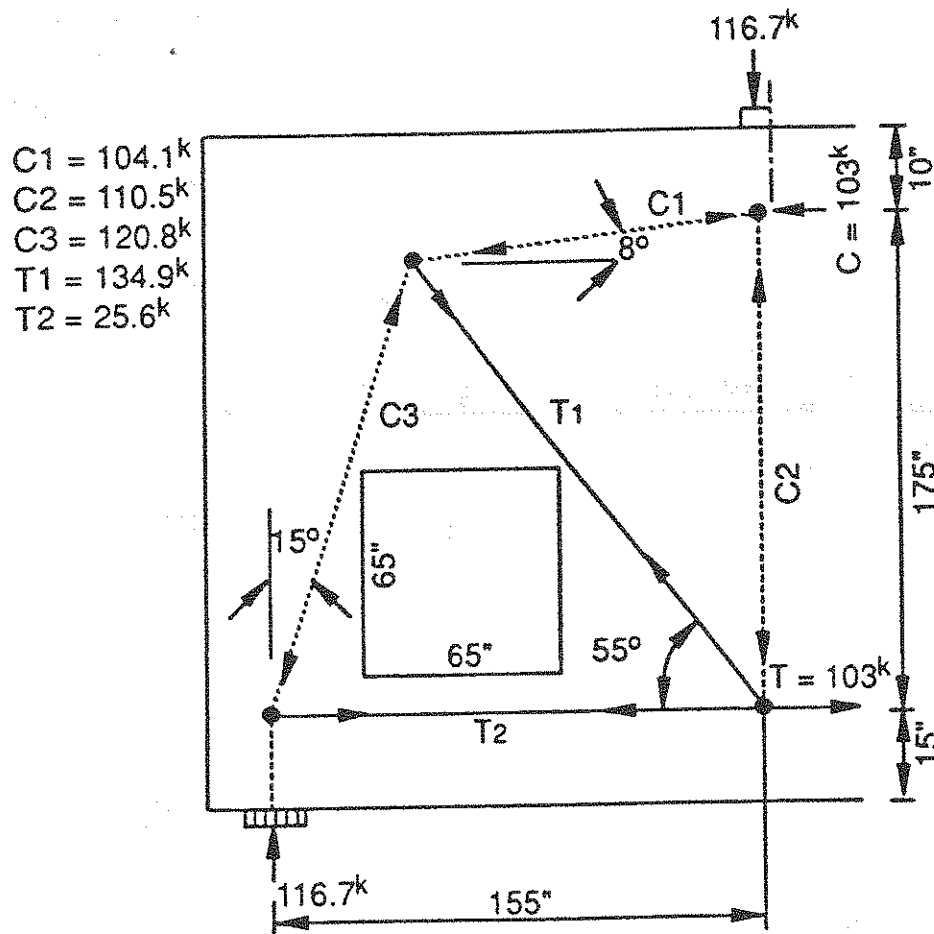


Fig. 4.21(e) Model 1 — 50% of load (left)

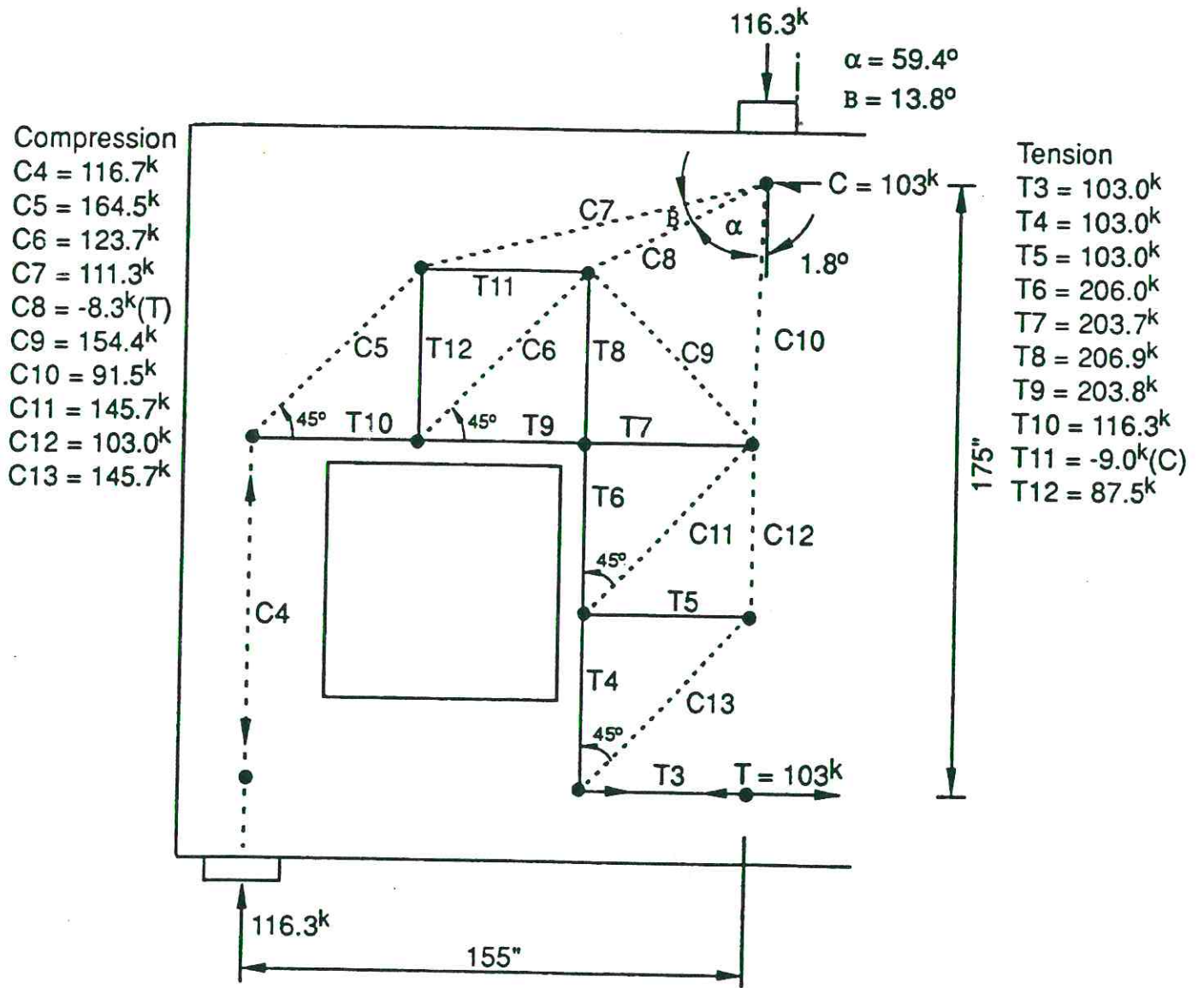


Fig. 4.21(f) Model 2 — 50% of load (left)

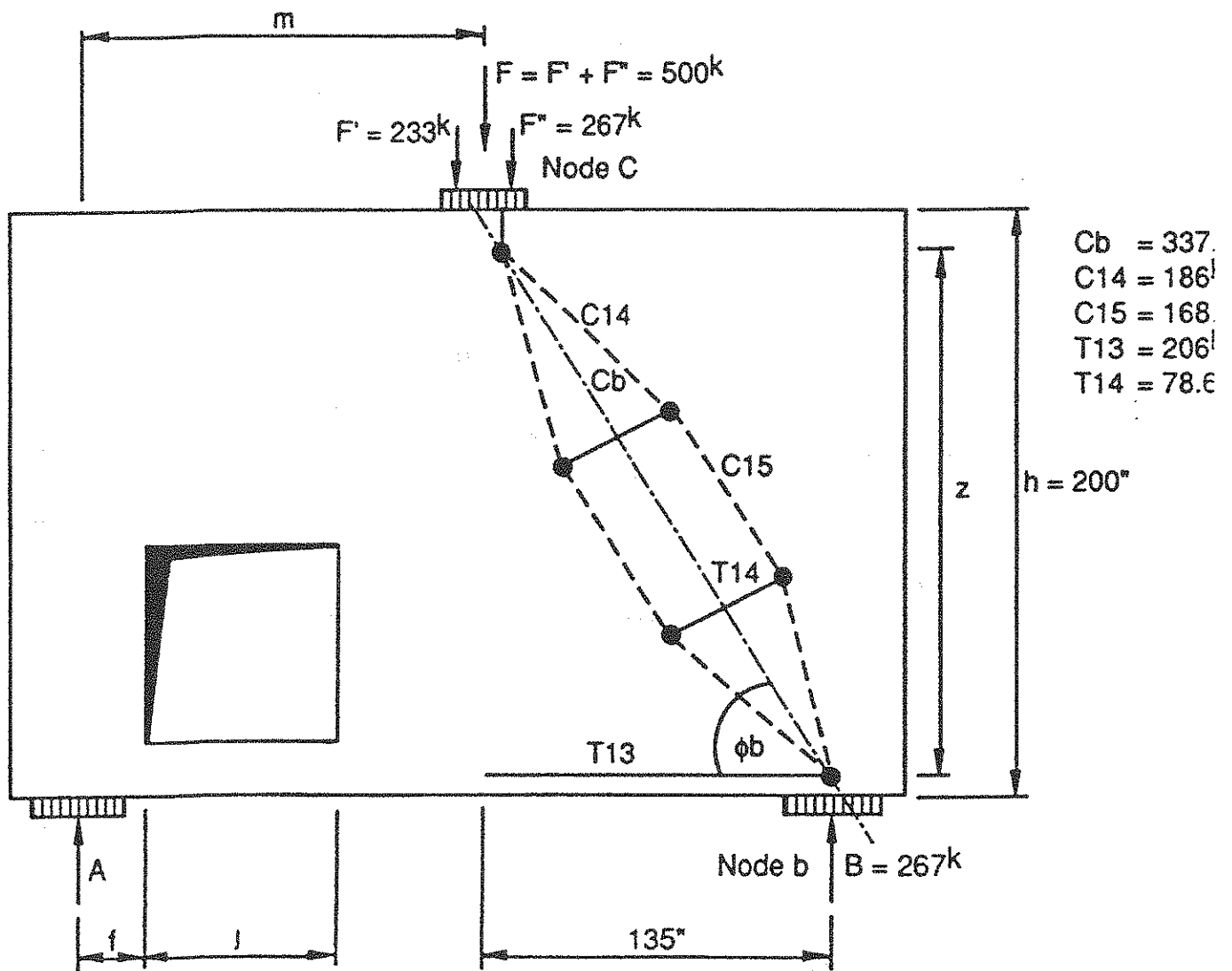


Fig 4.21(g) Model 3 — 100% of load (right)

Figure 4.21: Strut- and- tie models for deep beam with a hole

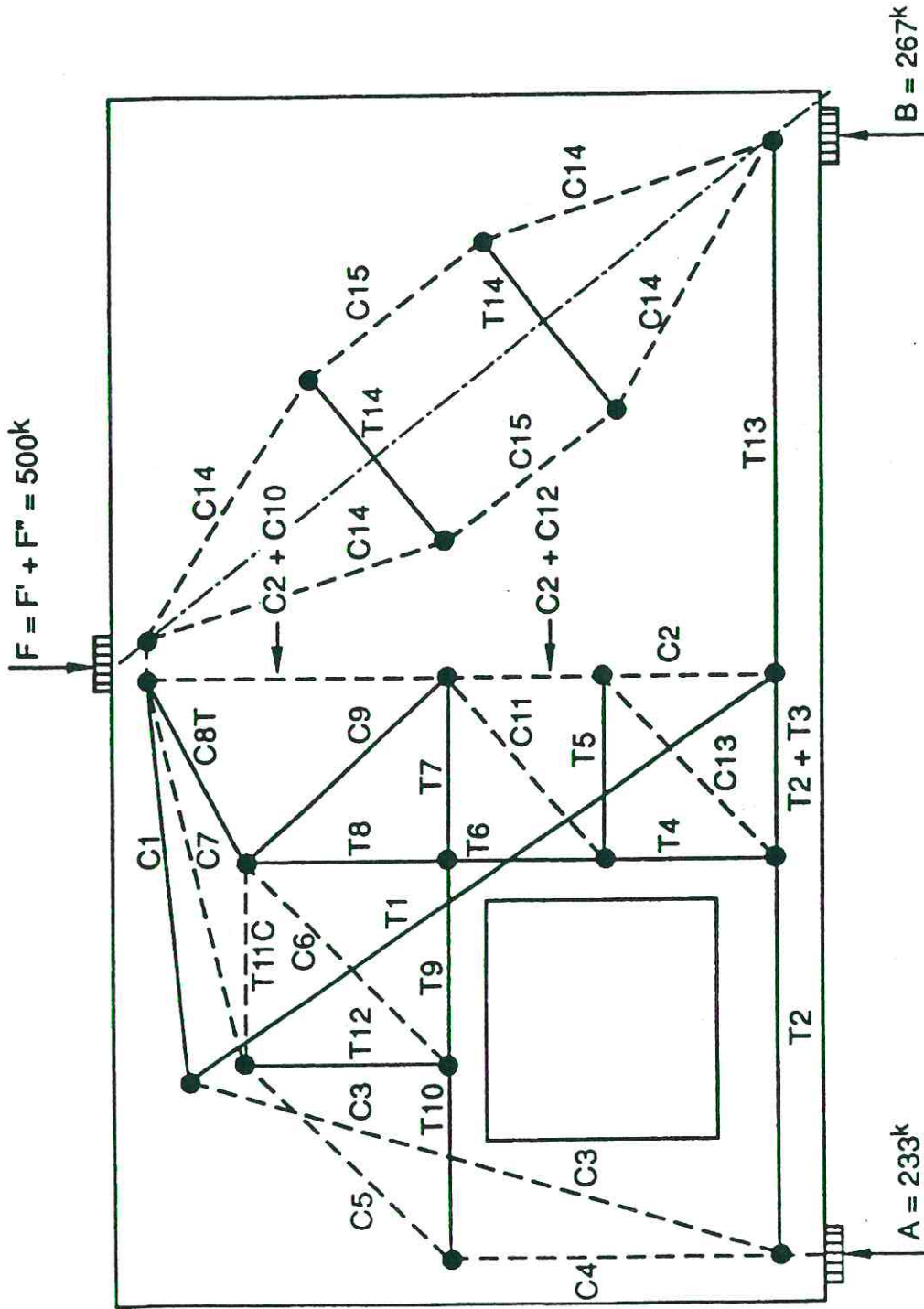


Fig. 4.21(h) Combined strut-and-tie models

Figure 4.21: Strut-and-tie models for deep beam with a hole

Reinforcement for ties: (All Grade 60)

$$\begin{aligned}
 T_{13} &= 206 \text{ kips} & A_s &= 206/60 = 3.38 \text{ in.}^2 \\
 &\text{Use } 6 - \#7 & &= 3.60 \text{ in.}^2 \text{ in lower right section (See Fig. 4.22)} \\
 T_{14} &= 78.6 \text{ kips} \times 2 = 157.2 \text{ k} \\
 T_{14v} &= T_{14} \cos \phi_b = 157.2 \cos 52.4^\circ = 96 \text{ k} \\
 A_{sv} &= 96/60 = 1.60 \text{ in.}^2 \\
 T_{14H} &= T_{14} \sin \phi_b = 157.2 \sin 52.4^\circ = 125 \text{ k} \\
 A_{sh} &= 125/60 = 2.08 \text{ in.}^2
 \end{aligned}$$

The vertical reinforcement, 1.60 in.^2 , needs to be spaced over a width of approximately 11 ft. or approximately 0.15 in.^2 per foot.

The horizontal reinforcement, 2.08 in.^2 , needs to be spaced over a height of approximately 14 ft. or approximately 0.15 in.^2 per foot.

Both of these values are quite low. The ACI Building Code Sec. 14.3 prescribes 0.0012 for minimum vertical wall reinforcement percentage and 0.0020 for minimum horizontal wall reinforcement percentage based largely on shrinkage and temperature considerations. Using the average would indicate minimum reinforcement

$$A_s = 0.0016 (12) (15) = 0.29 \text{ in.}^2/\text{ft.}$$

If this reinforcement is placed in 2 curtains, it would require $0.15 \text{ in.}^2 / \text{ft.}$ in each curtain. This would be nicely furnished by #4 at 16 in. spacing.

Use – 2 curtains at #4 spaced horizontally and vertically at 16 in. (See Fig. 4.22).

Anchorage requirements:

- #7 bars for T13 ties at node b (Fig. 4.22) (CCT node)

The 6 – #7 bars required can be efficiently placed in 2 layers of 3 bars each with a clear cover of 2 in., a clear spacing greater than 2 in. and the vertical #4 bars bent below the #7 bars. This results in 2-1/2 in. of concrete below the bars. From Fig. 3.12 and the dimensions shown in Fig. 4.21(a), assuming 2 in. clear cover over the tails of the #7 bars, $w_1 = 20$ in. and the length available to satisfy l_{db} requirements is $w_1 + 5 - 2 = 23$ in. From ACI 318-89 Ch. 12, $l_{db} = 0.04 A_b f_y / \sqrt{f'_c} = (0.04) (0.60) (60,000) / \sqrt{7000} = 17.2$ in. In a 15 in. thick wall with clear cover of 2 in., two #4 bar vertical curtains, and three #7 bars in a layer, the cover is 2-1/2 in. and the clear spacing is 3.7 in. which is greater than $3d_b$. Therefore, a factor of 1.0 is used.

$$l_d = 17.2 \text{ in.} < 23 \text{ in. available} \quad \text{OK}$$

No hooks required. Anchorage for the other end of these bars at nodes (a) and (c) (Fig. 4.22) will be checked as part of the left portion.

- #4 bars for T14 ties

The required l_d for these bars is short. $l_{db} = (0.04) (0.20) (60000) / \sqrt{7000} = 5.7$ in. Since cover is $4 d_b$ and spacing is $32 d_b$ in one direction and $20 d_b$ in the other, $l_d = 1.0 l_{db} = 5.7$ in. $> (.03) (0.5) (60000) / \sqrt{7000} = 10.8$ in. which governs here. Clearly there is no problem along the top or right edge of the wall. As a good detailing practice to provide confinement for the main tension tie, the vertical #4 bars should be U type hairpins and enclose the #7 bars in the main tension tie (see Fig. 4.22).

Check Node (b) (See Fig. 4.21(g)) – CCT Node

From Figs. 3.12 and 4.21(g), $w_1 = 20$ in., $db = 0.88$, $n = 2$, $s = 2$ in.,
and $\phi = 52.4^\circ$

$$w_T = 2(0.88) + (1)(2) = 3.76 \text{ in.}$$

$$w_2 = (20) \sin 52.4 + 3.76 \cos 52.4 = 18.1 \text{ in.}$$

$$\sigma_{cb} = C_b / (w_2 * b) < v_e f_c$$

$$\sigma_{cb} = 337.2 / (18.1 * 15) = 1.24 \text{ ksi} < 0.725(7) = 5.075 \text{ ksi} \quad \text{OK}$$

$$\sigma_1 = B / (a * b) < v_e f_c [a_c b / ab]^{0.5}$$

$$= 267 / (20 * 15) = 0.89 \text{ ksi} < 0.725(7) = 5.075 \text{ ksi} \quad \text{OK}$$

Check right part of Node (c) (See Fig. 4.21(g)) – CCC Node

From Figs. 3.9 and 4.21(g), $\phi_3 = 37.6^\circ$, $\phi_3' = 62.6^\circ$, $\phi_3'' = 12.6^\circ$,

$$a = 20 \text{ in.}, a' = (267/250)(10) = 10.68 \text{ in.}$$

Checking for $w_4 = a/2 = 10$ in.

$$C_4 = C_b * \cos \phi_3 = 337.2 \cos 37.6 = 267 \text{ k}$$

$$\sigma_4 = c_4 / (w_4 * b) \leq v_e f_c$$

$$= 267 / (10 * 15) = 1.78 \text{ ksi} < 0.725(7) = 5.08 \text{ ksi} \quad \text{OK}$$

Check strut cb at $y = a = 20$ in.

$$\sigma_3 = C_b / [(w_3' + w_3 + w_3'') * (b)] < 0.6 v_e f_c$$

$$= 267 / (22.02 * 15) = 0.80 \text{ ksi} < (0.6)(0.725)(7) = 3.05 \text{ ksi}$$

OK

Left Portion of Wall (Fig. 4.21h)**Reinforcement for Ties (All Grade 60)**

The two strut-and-tie models, which were proportioned to share the load on the left part of the structure equally, are superimposed and combined on Fig. 4.21h to expedite choice of reinforcement. Several of the members in each model are concurrent or nearly so (i.e., T2 +T3, C2 +C12, etc.). In these cases the required forces can be added and a single tie proportioned to take the total load. The following tie reinforcement is required:

Tension Tie	Force, K	As req'd, si	As provided, si
T1	135	2.25	4 - #7 = 2.40
T2	26	0.44	2 - #7 = 1.20*
T2 + T3	129	2.15	4 - #7 = 2.40
T4	103	1.72	6 - #7 = 3.60
T5	103	1.72	6 - #5 = 1.86
T6	206	3.44	6 - #7 = 3.60
T7	204	3.40	6 - #7 = 3.60
T8	207	3.45	6 - #7 = 3.60
T9	204	3.40	6 - #7 = 3.60
T10	117	1.95	4 - #7 = 2.40
T11C	9C	0	
T12	88	1.47	6 - #5 = 1.86

* Two other #7 bars required for T2 & T3 are carried to support A to avoid bar cutoff in tensile zone complications.

In satisfying these requirements, bars may be provided which simultaneously cover several cases. For instance T4, T6 and T8 are best satisfied by a single set of vertical bars. The maximum of these forces requires 3.45 si which can be nicely satisfied by 6 - #7 = 3.60 si. Similarly, the 6 #7 bars chosen for T13 are more than adequate for T2 +T3. Four are required to be bent up for T1 and two of them can continue to support A satisfying T2 amply. They are supplemented by 2 #7 in the T2 - T3 zone which must be lap spliced to the T13 bars.

The horizontal tie above the opening (T7 - T9 - T10) is nicely satisfied by 6 #7 with two of them bent down across the corner of the opening to cater to any tensile stress raisers at the reentrant corner. Lastly, the tensile ties T5 and T12 require smaller #5 bars well distributed over the tie zones. Again to counteract very local tensile stresses similar to those shown in Fig. 4.20 at the lower corners of the opening, inclined #4 bars are placed on the diagonal at each of these corners. All bars are arranged as far as possible in two curtains of reinforcement with a minimum of 2 in. of cover. Final bar patterns are shown in Fig. 4.22. Note that while no tension reinforcement is required in the C3-C4 strut areas to the left of the opening, minimum reinforcement for columns (reduced to 1/2% to reflect that the section is much larger than required for the compression load) is provided to control time dependent deformations and for general ductility. $A_s = (0.005)(30)(15) = 2.25 \text{ si.}$ Use 4 - #7.

Anchorage Requirements

When checking the right side of the wall it was determined that for #7 bars, $l_d = 17.2 \text{ in.}$ At support A at least 23 in. $> l_d$ is available. The smeared nodes at the right ends of the T5 and T7 ties require only normal l_d embedment past the node, as does the upper ends of the T12 and T8 ties. In the more critical cases at the left end of the T10 and T5 ties and at the bottom of the T4 tie, positive anchorages are provided by looping the ends of the bars. The orthogonal curtains of #4 bars provided for the T14 ties require no further check as they have ample length to satisfy l_d requirements.

Check Node (a) (See Fig. 4.21h) CCT Node.

From Figs. 3.12 and 4.21h, $WT = 20.88$ in., $W1 = 20$ in., and $\phi_b = 75^\circ$
(Conservative Assumption) $w1 = 20 \sin\theta + 20.88 \cos\theta = 24.7$

$$\sigma_{ca} = (C3+C4) / w1 b = (120.8 + 116.7) / (24.2)(15) = 0.64 \text{ ksi} \ll (.725)(7).$$

Check Node (d) [Intersection of T1, T2, C2, T13] CTT Node. Detailing continuous bars has satisfied T requirements. C2 has a force of 110k and must be basically equilibrated by the bends of the 4 #7 bars in the T1 tie. For this 55° bend, a standard inside bar diameter of $6 d_b$ would result in a bend contact area of approximately $(7) (0.88) \pi/4 = 4.84$ in. for each layer. An extremely conservative estimate of node pressures would be:

$$\sigma_{cd} = c2 / w1b = (110) / (4.84)(15) = 1.52 \text{ ksi} < (7.25)(7) = 5.08 \text{ ksi}$$

Note that all node cases are far from critical.

Bars shown as
2 x — indicate
one set in each
face curtain.

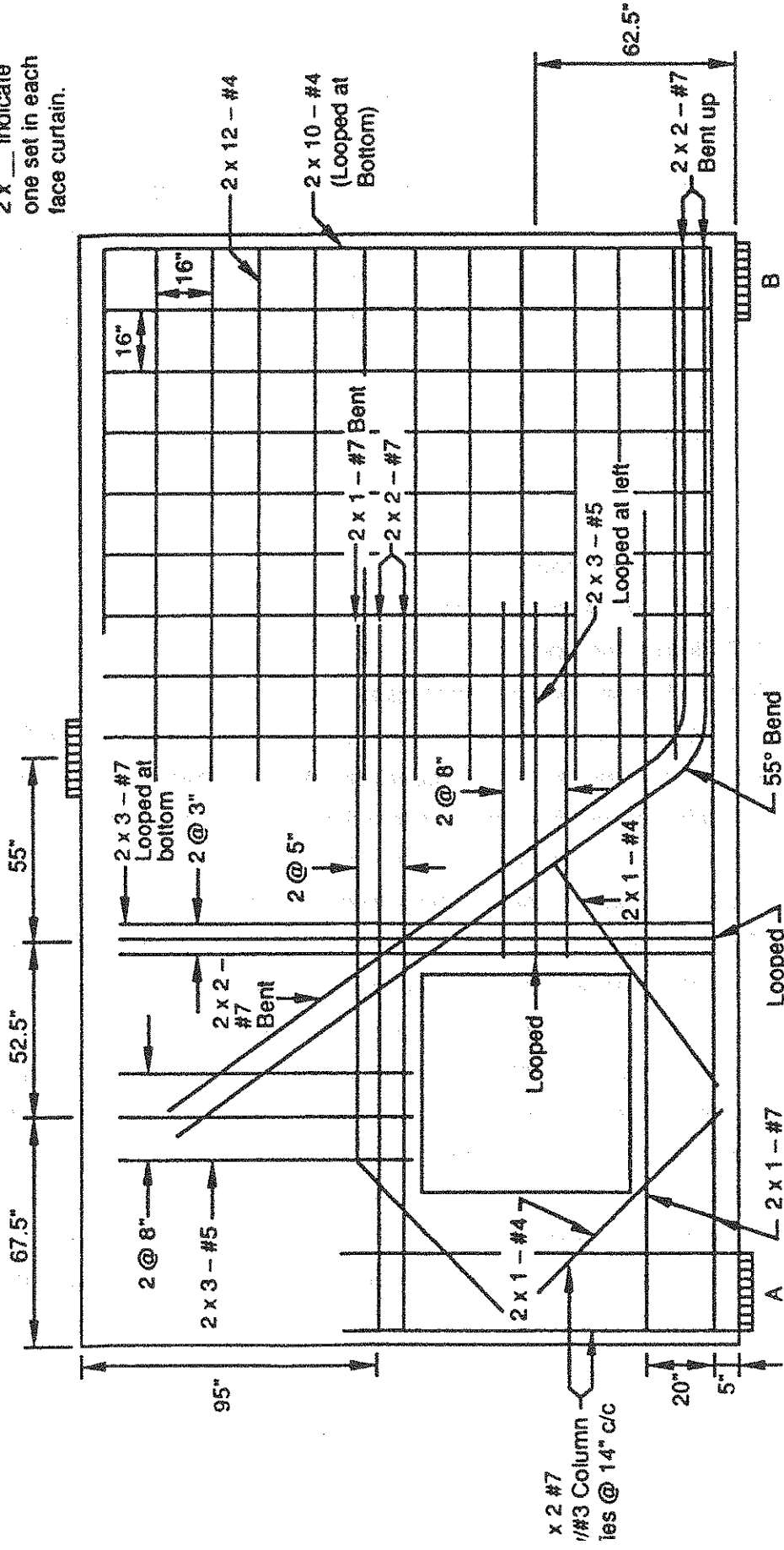


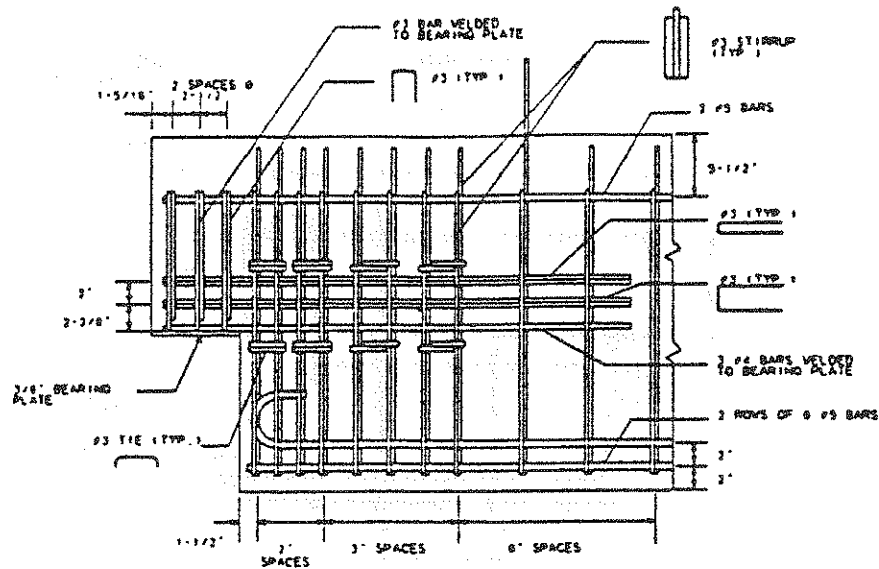
Figure 4.22: Reinforcement layout for deep beam with a hole

4.3.4 Dapped end beam

Dapped beams have applications in both building and bridge structures. Flexural reinforcement may be prestressed. A typical application for dapped end beams is as drop-in spans for semi continuous beams. The load distribution may vary significantly. The aspect ratio of the dapped end may differ depending upon the specific application. Barton [7] did some experimental verification on dapped beams designed with different models. A total of four details were tested using two beams. Each detail was designed for an ultimate load capacity of 100 kips and a concrete compression strength of 5000 psi. The different design models were:

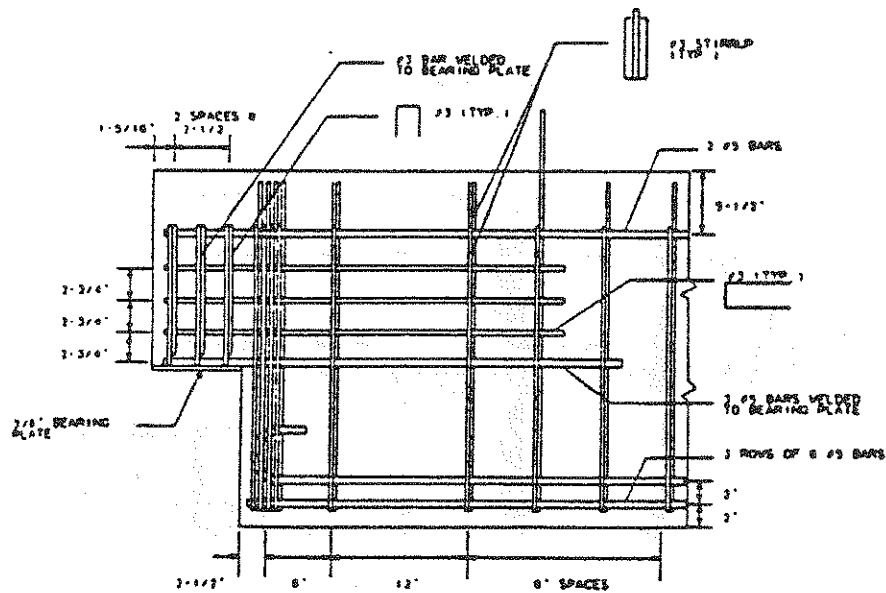
- strut- and- tie- model
- modified strut and tie model
- PCI design method
- Menon/Furlong design procedure

The reinforcement layouts for the different models are shown in Fig. 4.23 to Fig. 4.26. All four specimens cracked at the reentrant corner at load levels ranging from 20 to 33% of ultimate load. Maximum crack widths at an approximate service load of about 60 percent of ultimate were in the range of 0.009 to 0.012 in. The control of the diagonal crack at the reentrant corner is of primary concern for serviceability. Based on the performance of the PCI - detail (grouped vertical tie reinforcement) and the modified strut- and- tie- model (about 37% more horizontal and 50% less vertical reinforcement), it appears most efficient to place the location of the vertical and horizontal tie reinforcement as close as possible to the interface between the dap and the full section. In addition, the vertical tie reinforcement should be placed in a closely spaced group. Also the corner should be rounded in order to decrease the stress concentration. Studies by Cook and Mitchell [113] using both rectangular and inclined corners in dapped end beams indicate that the inclination helps to prevent cracks at the reentrant corner. The two most common strut- and- tie- models for dapped end beams are shown in Fig. 4.27 and Fig. 4.28. The selection of a particular model is a compromise between ease of fabrication and fidelity to the elastic principal stress



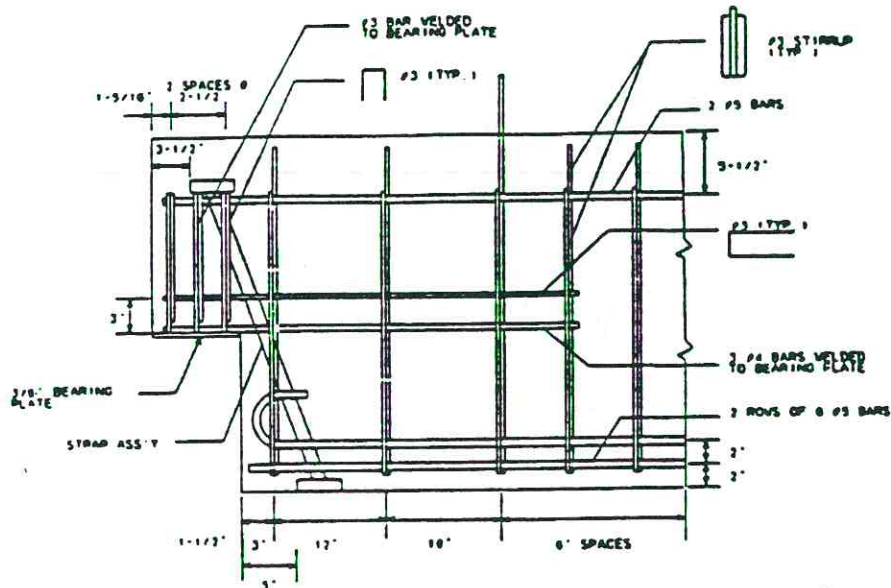
First cracking load: 19% of predicted failure load
 Ultimate load: 147 % of predicted failure load - anchorage failure of the stirrups and concrete compression failure

Figure 4.23: Reinforcement layout for strut- and- tie- model ST1 (from Ref. [7])



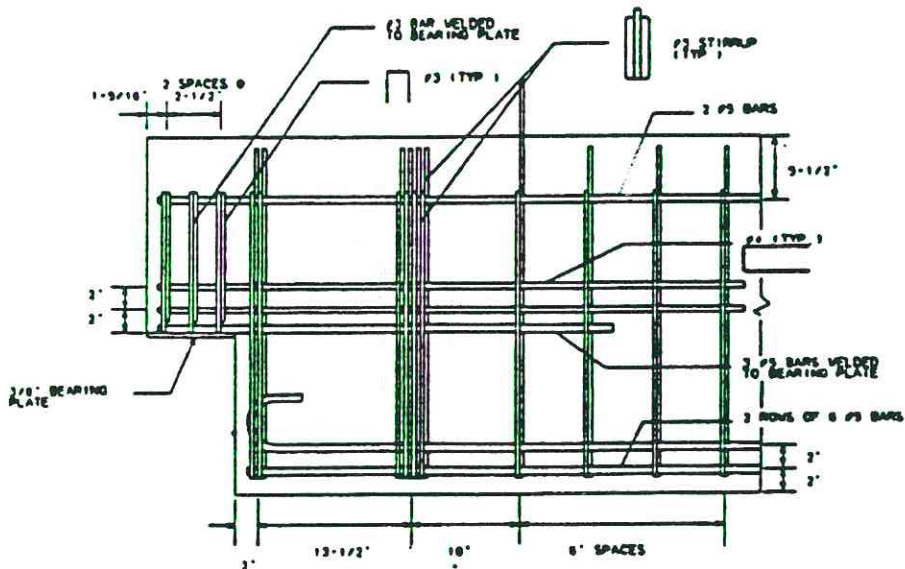
First cracking load: 28% of predicted failure load
 Ultimate load: 152% of predicted failure load - concrete compression failure

Figure 4.24: Reinforcement layout for PCI detail (from Ref. [7])



First cracking load: 22% of predicted failure load
 Ultimate load: 121% of predicted failure load - concrete compression failure

Figure 4.25: Reinforcement layout for Menon/Furlong - detail (from Ref. [7])



First cracking load: 29% of predicted failure load
 Ultimate load: 127% of predicted failure load concrete compression failure

Figure 4.26: Reinforcement layout for modified strut-and-tie model ST2 (from Ref. [7])

directions. The orthogonal model results in a reinforcement pattern which is easy to place and is well suited to the overall reinforcement pattern of the beam. However, the model forces the loadpath to deviate substantially from the elastic stress directions. This is also the reason that Schlaich et al [2] propose to place diagonal reinforcement as shown in Fig. 4.28 (should carry less than 70% of the overall capacity). The diagonal reinforcement is more difficult to place and anchor properly but follows the elastic principal stress directions closely.

The quantity of horizontal reinforcement anchored at the bearing plate in Fig. 4.27 is determined based on the angle of the inclined compression strut. Obviously, selecting a steep angle reduces the required amount of horizontal reinforcement. Based on force measurements by Barton [7], the compression strut angle ranged between 45 and 55 degrees and tended to increase as load was increased close to the ultimate load.

Anchorage of horizontal reinforcement within the dapped end may be provided by welding a portion of the reinforcement to the bearing plate at the bottom and by the use of continuous hoops. Of interest also is the anchorage of the other end of the horizontal reinforcement. Test results by Barton [7] indicate reinforcement outside of the second vertical tie developed significant force only for load levels greater than the design load. In both specimens ST1 and ST2, the measured force in the second set of vertical ties, corresponding to T4 in Fig. 4.27, were very low at the design ultimate stage. This was probably due to substantial tension carried by the concrete and the effects of other contributions such as aggregate interlock and dowel action. However, by the actual ultimate load on both specimens, the measured second vertical tie force in both specimens had achieved the level predicted by the models. Since the STM is a lower bound plastic model, this fulfills all assumptions. Different strut- and- tie- models were compared with test results from [7] to evaluate a design approach. The recommended strut- and- tie- model is shown in Fig. 4.29 and Fig. 4.30 and the statistical data comparing the test results with the computed ultimate loads using strut- and- tie models is given in Table 4.2 and in Fig. 4.31. In Report 1127-1 [131] it was noted that the strut angles in the test specimens ranged between 45° and 55° and tended to increase as load increased. Hence, an angle of 55° is used in the recommended model.

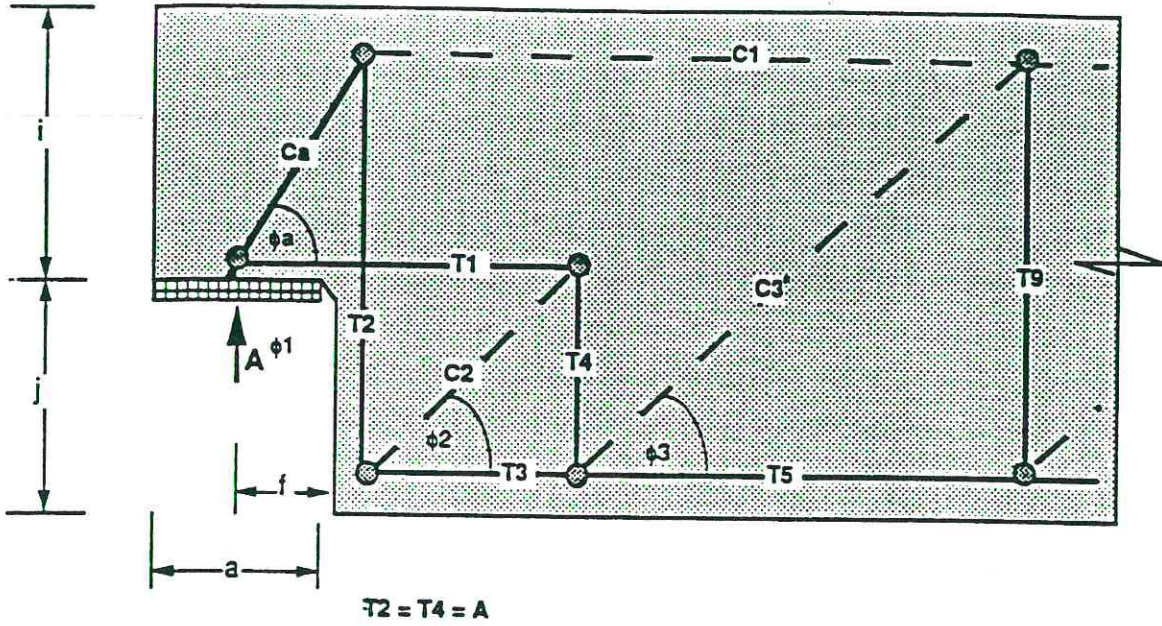


Figure 4.27: Orthogonal strut- and- tie- model (from Ref.[2])

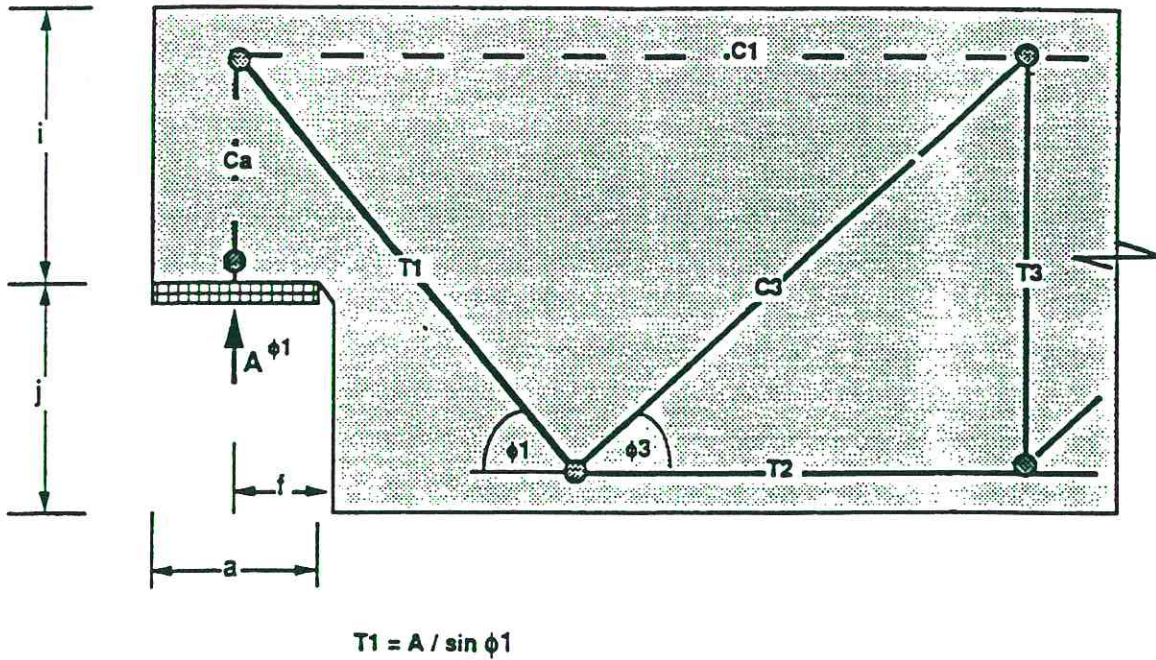
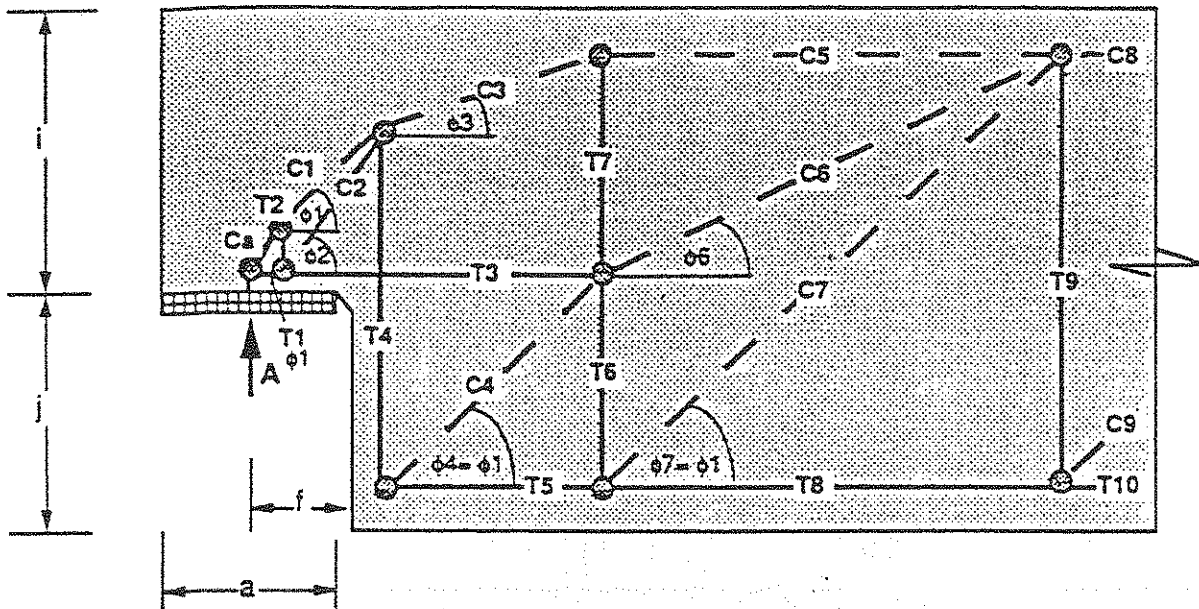


Figure 4.28: Diagonal strut- and- tie- model (from Ref.[28])

Dapped end beam: Strut- and- tie- forces



Strut- and- tie- forces:

$$C_a = A / \sin \phi_a$$

$$C_1 = C_a \cos \phi_a / \cos \phi_1$$

$$C_2 = T_2 / \sin \phi_2$$

$$C_3 = (C_1 \cos \phi_1 + C_2 \cos \phi_2) / \cos \phi_3$$

$$C_4 = T_4 / \sin \phi_4$$

$$C_5 = C_3 \cos \phi_3$$

$$C_6 = (C_4 \cos \phi_4 - T_3) / \cos \phi_6$$

$$C_7 = T_6 / \sin \phi_7$$

$$C_8 = C_5 + C_6 \cos \phi_6 + C_7 \cos \phi_7$$

$$T_1 = A / \tan \phi_a$$

$$T_2 = C_a \sin \phi_a - C_1 \sin \phi_1$$

$$T_3 = T_1 + C_2 \cos \phi_2$$

$$T_4 = C_1 \sin \phi_1 + C_2 \sin \phi_2 - C_3 \sin \phi_3$$

$$T_5 = T_4 / \tan \phi_4$$

$$T_6 = T_7 + C_4 \sin \phi_4 - C_6 \sin \phi_6$$

$$T_7 = C_3 \sin \phi_3$$

$$T_8 = T_5 + C_7 \cos \phi_7$$

$$\text{Control : } C_8 = T_8$$

Figure 4.29: Proposed strut- and- tie- model for dapped end beam

Dapped end beam: Strut- and- tie- angle

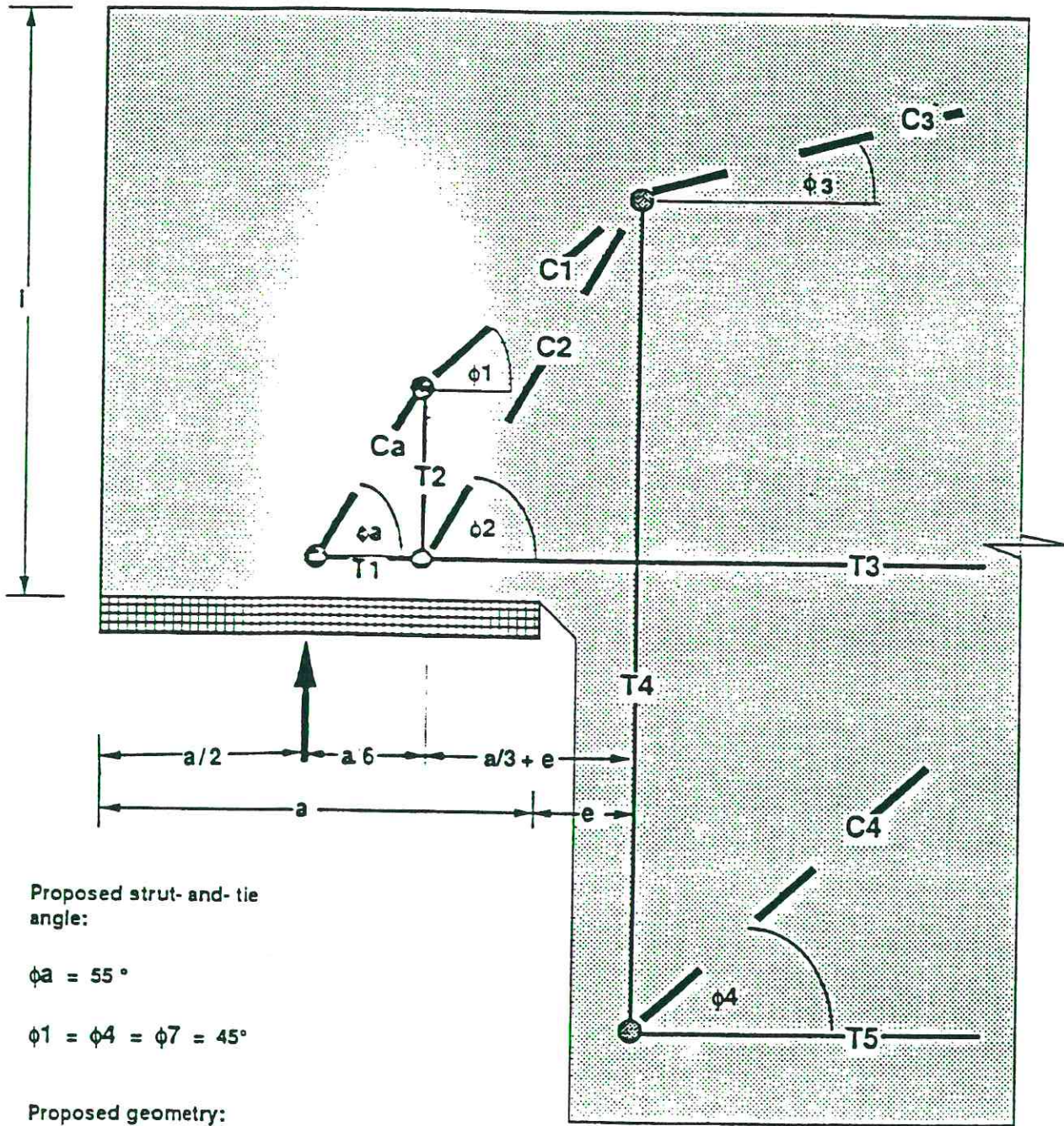


Figure 4.30: Proposed strut- and- tie- angle for dapped end beam

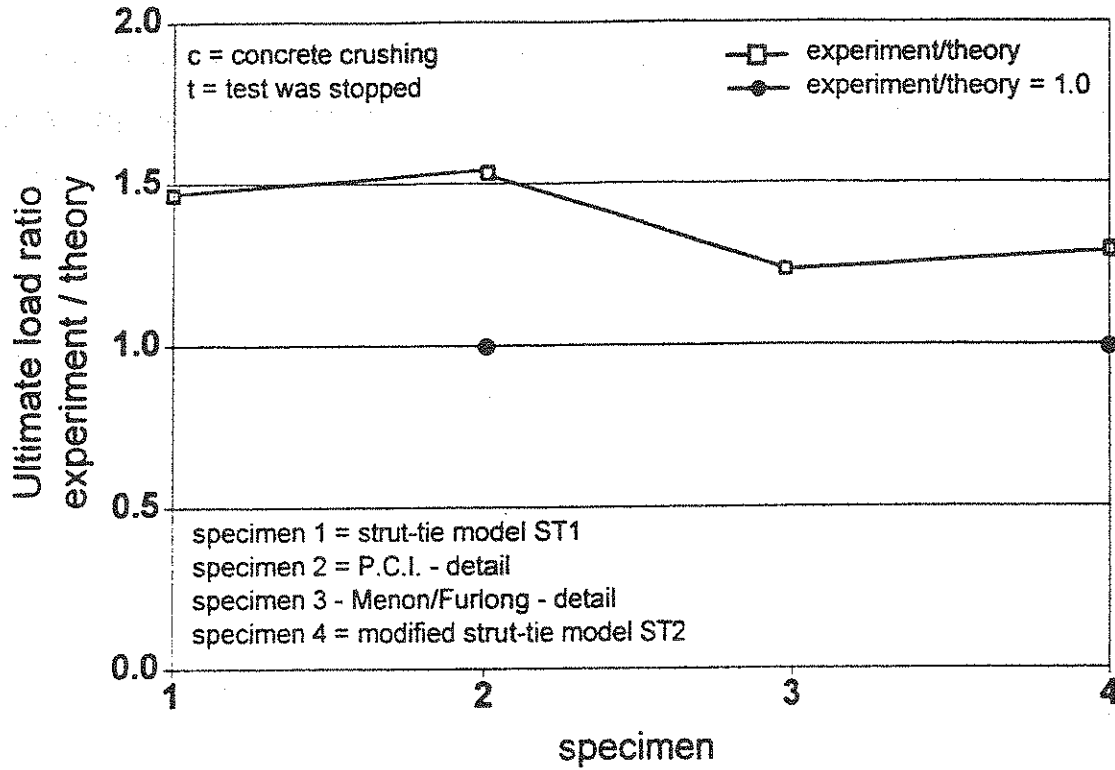


Figure 4.31: Comparison with the proposed strut-and-tie model using test results from Barton [7].

Table 4.2: Statistical data from Fig. 4.31

X ₁ : Column 1					
Mean:	Std. Dev.:	Std. Error:	Variance:	Coef. Var.:	Count:
1.37	.13	.37	---	0.09	4
Minimum:	Maximum:	Range:	Sum:	Sum Squared:	# Missing:
1.21	1.52	.31	5.47	7.55	0

Example 4.4: Dapped end beam

Design the end region of the dapped end beam shown in Figure 4.32 to carry a concentrated midspan load of 300 kips. Dead load of the span may be neglected in this example. Dap details are shown in Figure 4.32. Use $f'_c = 6000$ psi and Grade 60 reinforcement with a minimum cover of 2 in.

Load and dimensions:

(See Fig. 4.29 and Fig. 4.30 for symbol definitions)

F	=	300 kips
l	=	200 in.
h	=	30 in.
f	=	5 in.
j	=	14 in.
i	=	16 in.
a	=	10 in.
b	=	15 in.
e	=	5 in.

The beam may be divided into D regions near the ends and a central B region (a D region may be used under the load but is not checked here). The B regions will be more efficiently handled by ordinary section design procedures.

External forces:

$$A = B = 150 \text{ kips}$$

Strut and tie angle:

Where the D region meets the B region, estimate the effective lever arm z as:

$$z = 3/4 h = 22.5 \text{ in.}$$

From Fig. 4.30:

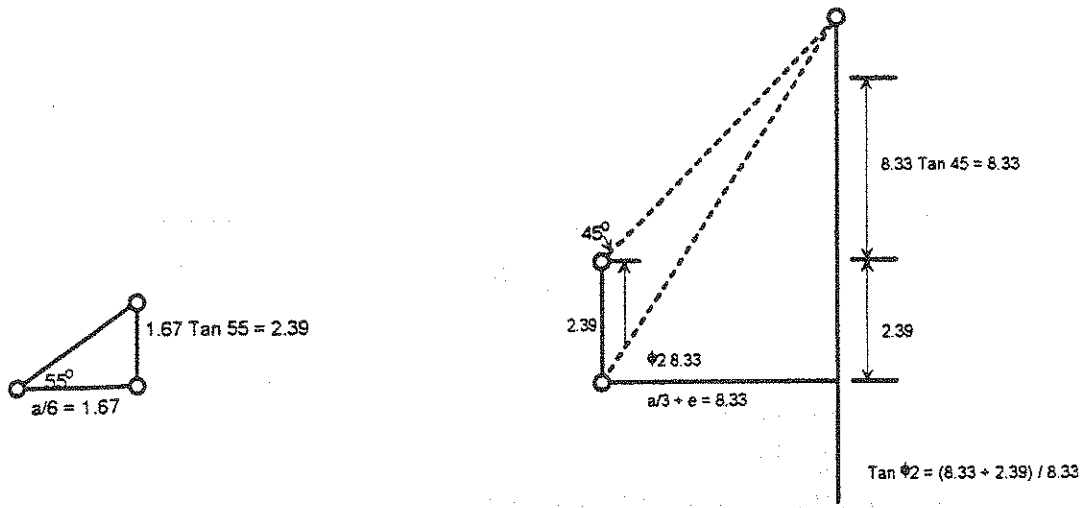
$$\phi a = 55^\circ$$

$\phi_2 = 45^\circ$
 $\phi_4 = 45^\circ$. From the geometry of Figure 4.30, one can compute
 $\phi_2 = \text{Arctan} \left[\left(2.39 + 8.33 \right) / 8.33 \right] = 52.1^\circ$
 $\phi_3 = \text{Arctan} \left(11.75 - 10.72 \right) / 11.75 = 5.0^\circ$

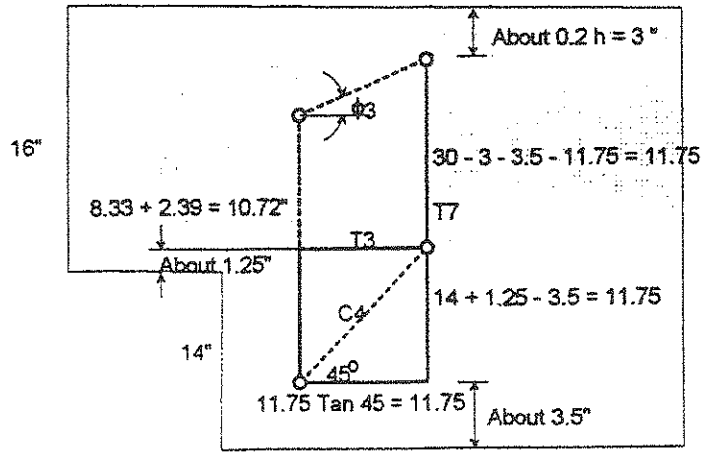
Internal forces:

$C_a = 150 / \sin 55^\circ = 183.1 \text{ kips}$
 $C_1 = C_a \cos \phi_a / \cos \phi_1$
 $C_1 = 148.5 \text{ kips}$

To find ϕ_2

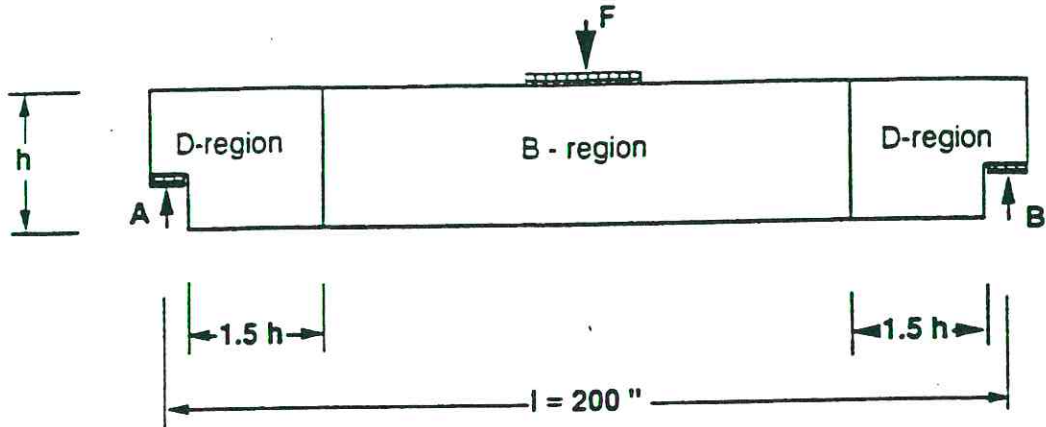


To find ϕ_3



Example: Dapped end beam:

236



D - region

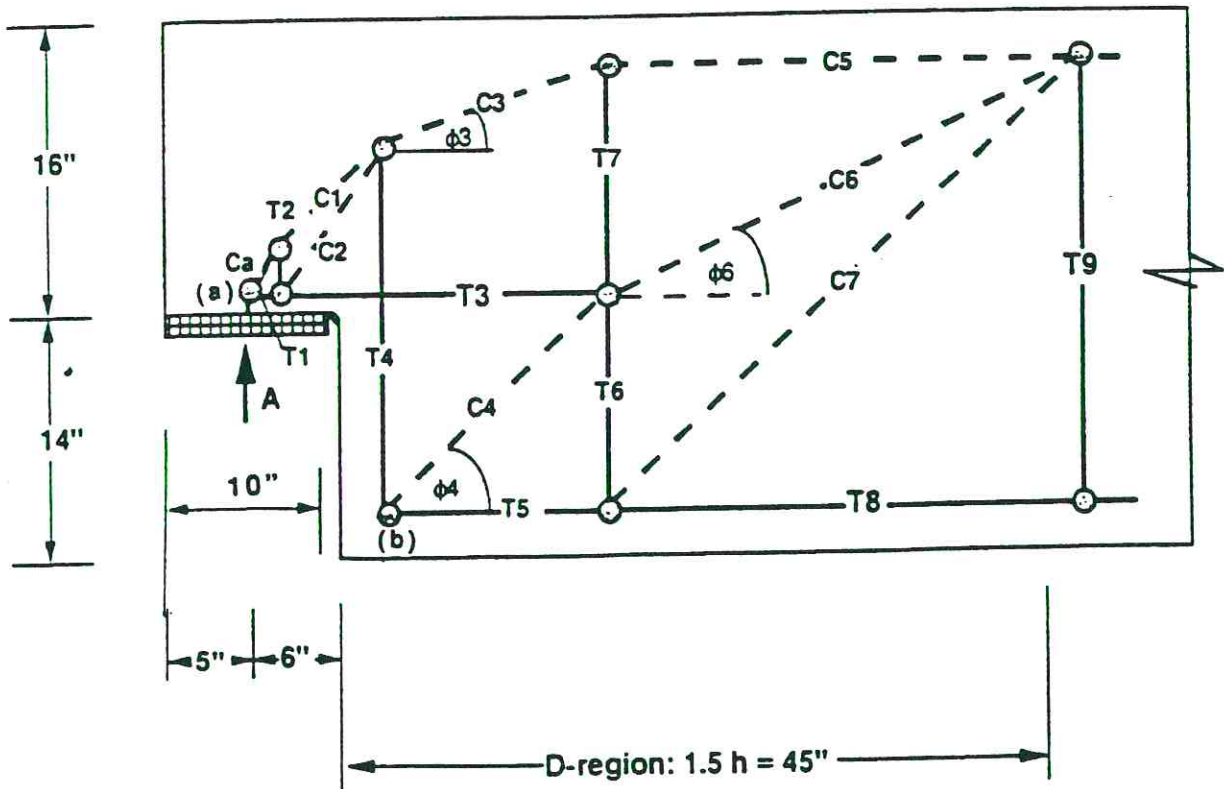


Figure 4.32: Strut- and- tie- model for example: dapped end beam

$$T1 = A / \tan \phi_a$$

$$T1 = 105 \text{ kips}$$

$$T2 = C_a \sin \phi_a - C1 \sin \phi1$$

$$T2 = 45 \text{ kips}$$

$$C2 = T2 / \sin \phi2$$

$$C2 = 57.0 \text{ kips}$$

$$C3 = (C1 \cos \phi1 + C2 \cos \phi2) / \cos \phi3$$

$$C3 = 140.5 \text{ kips}$$

$$T3 = T1 + C2 \cos \phi2$$

$$T3 = 140.0 \text{ kips}$$

$$T4 = C1 \sin \phi1 + C2 \sin \phi2 - C3 \sin \phi3$$

$$T4 = 137.7 \text{ kips}$$

To find $\phi6$

$$C4 = T4 / \sin \phi4$$

$$C4 = 194.8 \text{ kips}$$

$$C5 = C3 \cos \phi3$$

$$C5 = 140.0 \text{ kips}$$

$$T5 = T4 / \tan \phi4$$

$$T5 = 137.7 \text{ kips}$$

$$T7 = C3 \sin \phi3$$

$$T7 = 12.2 \text{ kips}$$

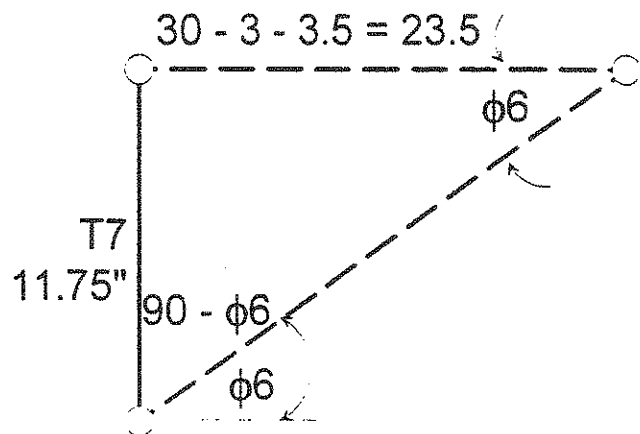
$$\phi6 = \arctan (11.75 / 23.5) = 26.6^\circ$$

$$C6 = (C4 \cos \phi4 - T3) / \cos \phi6$$

$$C6 = -2.5 \text{ kips}$$

$$T6 = T7 + C4 \sin \phi4 - C6 \sin \phi6$$

$$T6 = 151.1 \text{ kips}$$



$$\begin{aligned} C7 &= T6 / \sin \phi7 \\ C7 &= 213.6 \text{ kips} \end{aligned}$$

$$\begin{aligned} T8 &= T5 + C7 \cos \phi7 \\ T8 &= 288.7 \text{ kips} \end{aligned}$$

$$C8 = C5 + C6 \cos \phi6 + C7 \cos \phi7 = 288.8 \text{ kips (o.k.)}$$

Check $C8 = T8$ by method of sections

$$T8 = C8 = 150(1.67 + 8.33 + 11.75 + 23.5) / 23.5 = 289.5 \text{ kips}$$

Check OK

$$T9 = C6 \sin \phi6 + C7 \sin \phi7 = 149.9 \text{ kips}$$

$$\text{From method of sections } T9 = A = 150$$

Check OK

In practice, once geometry is defined a simple truss program on a computer could be used for these calculations.

Reinforcement for tensile ties:

All bars Grade 60

$$\begin{aligned} T1 &= 105 \text{ kips} \\ A_s &= 1.75 \text{ in}^2 \leq 6 - \#5 = 1.86 \text{ in}^2 \end{aligned}$$

$$\begin{aligned} T2 &= 45 \text{ kips} \\ A_s &= 0.75 \text{ in}^2 \leq 4 - \#4 = 0.80 \text{ in}^2 \end{aligned}$$

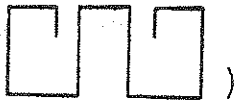
$$\begin{aligned} T3 &= 140.0 \text{ kips} \\ A_s &= 2.33 \text{ in}^2 \leq 8 - \#5 = 2.48 \text{ in}^2 \end{aligned}$$

$$\begin{aligned} T4 &= 137.7 \text{ kips} \\ A_s &= 2.30 \text{ in}^2 \leq 12 - \#4 = 2.40 \text{ in}^2 \end{aligned}$$

$$\begin{aligned} T5 &= 137.7 \text{ kips} \\ A_s &= 2.30 \text{ in}^2 \leq 4 - \#7 = 2.40 \text{ in}^2 \end{aligned}$$

T6	=	151.1 kips		
As	=	2.52 in ²	≤	14 - #4 = 2.80 in. ²
T7	=	12.2 kips		
As	=	0.20 in ²	≤	1 - #4 = 0.20 in. ²
T8	=	288.7 kips		
As	=	4.81 in ²	≤	8 - #5 + 4 - #7 = 4.88 in. ²
T9	=	150 kips		
As	=	2.50 in ²	≤	14 - #4 = 2.80 in. ²

A possible bar arrangement is presented in Fig. 4.33. Note that the T6 bars are run full height and provide substantial excess for the T7 bars. Note also that the #4 bars required for T6 and T9 are provided as Groups of closed 3 - W stirrups and 1 - U stirrup. The U stirrups provide a desirable transverse tie completely across the bottom flange. Where W stirrups are provided a short U is desirable on the bottom flange. (A W stirrup is a four-legged stirrup



Anchorage requirements:

The very congested conditions in the dap make it difficult to effectively anchor all the reinforcement. The 8 #5 bars provided for the T1 and T3 reinforcement should have positive anchorage by closed loops at the support. In addition, the lower layer should be welded to the bearing plate, if possible. The minimum development length for a Grade 60 #5 bar under ACI 318-89 provisions would be 14.5 in. There simply is not room available in the small dap to rely on development length, unless one relies on the confinement present, since the T1 force must be fully developed above the bearing plate which is only 10 in. long.

Similarly, the #7 bars provided for the T5 force need to be developed within the CTT node at the bottom corner of the full depth section. This is also a very congested corner. Under ACI 318-89, a standard #7 hook would have a basic development length of 13.5 in. However, the 2" clear cover over the #4 stirrups provides 2-1/2 in. side cover so that a multiplier of 0.7 may be used reducing the length to 9.5 in. However, the highly grouped T4 reinforcement greatly reduces the width w_1 of the node (see Fig. 3.14). It is highly desirable to space stirrups at no more than $3d_b = 2.64$ in. throughout the hook development length to allow use of an additional 0.8 factor reducing l_{d_n} to 7.6 in. This can be easily done by using the 3 stirrups required for the T4 tie at 1-1/2 in. on centers and then introducing 2 extra confining stirrups at 2-1/2-in. spacing. One of these can be counted towards the T6 tie force so only one additional stirrup is required.

Development of the other bars is routine.

Concrete stresses at node zones:

Concrete strength: $f'_c = 6000$ psi

Concrete efficiency factor: $\nu = 0.75$

The only critical appearing nodes are at (a) and (b) as shown in Fig. 4.32. The other nodes have substantially more area for node development.

Check node (a): CCT - node

See Fig. 3.12 for typical geometry based on proposed bar arrangement of Fig. 4.33

In this case because of the special strut-and-tie arrangement caused by the angle change ϕ , shown in Fig. 4.30, it would be unconservative to use the full bearing plate width, a , for w_1 , as shown in Fig. 3.12. Instead a width $a/2 + a/6 = 2/3 a$ will be used for w_1 since that should be fully effective in developing the T_1 force shown in Fig. 4.30.

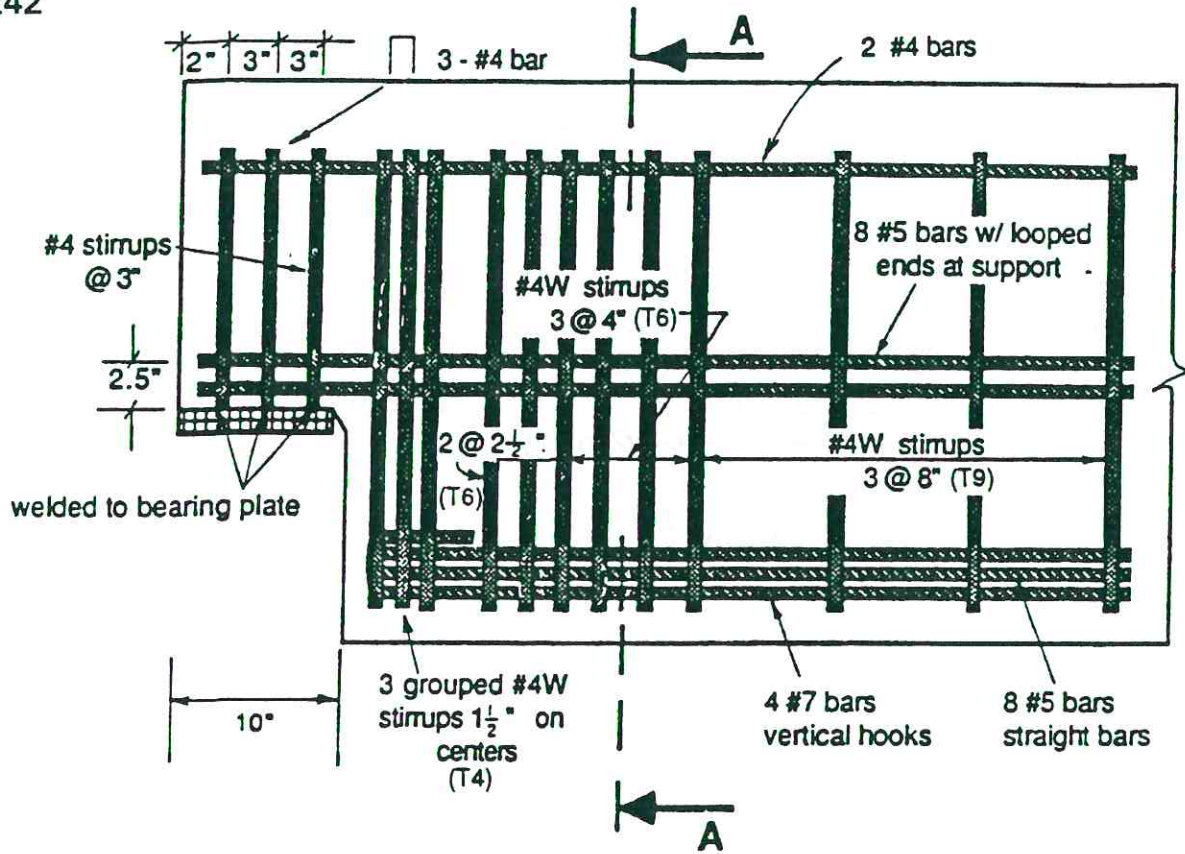
$$\begin{aligned} w_1 &= 2/3 (10) = 6.7 \text{ in.} \\ w_T &= 2(0.625) + (2 - 1) (1.25) = 2.50 \text{ in.} \\ w_a &= w_1 \sin 55^\circ + w_T \cos 55^\circ = 6.92 \text{ in.} \\ &\text{(} w_a \text{ is the same as } w_2 \text{ in Fig. 3.12)} \end{aligned}$$

$$\begin{aligned} \sigma_{ca} &= C_a / (w_a * b) \leq v_e f'_c \\ \sigma_{ca} &= 183.1 / (6.92 * 15) = 1.76 \text{ ksi} \leq 0.75 * 6. = 4.5 \text{ ksi} \quad \text{OK} \end{aligned}$$

Check node (b) CTT - node See Fig. 3.14 for typical geometry based on proposed bar arrangement of Fig. 4.33

$$\begin{aligned} w_1 (T_4) &= 3.5 \text{ in. (grouped \#4 stirrups } 3(0.5) + 2(1.0)) \\ w_2 (T_5) &= 1(0.88) + 2(0.62) + 2(1.12) = 4.36 \text{ in.} \\ w_c &= w_1 \sin 45^\circ + w_2 \cos 45^\circ = 5.55 \text{ in.} \end{aligned}$$

$$\begin{aligned} \sigma_{c4} &= C_4 / (w_c * b) \leq v_e f'_c \\ \sigma_{c4} &= 194.8 / (5.55 * 15) = 2.34 \text{ ksi} \leq 0.75 * 6. = 4.5 \text{ ksi} \quad \text{OK} \end{aligned}$$



Section: A-A

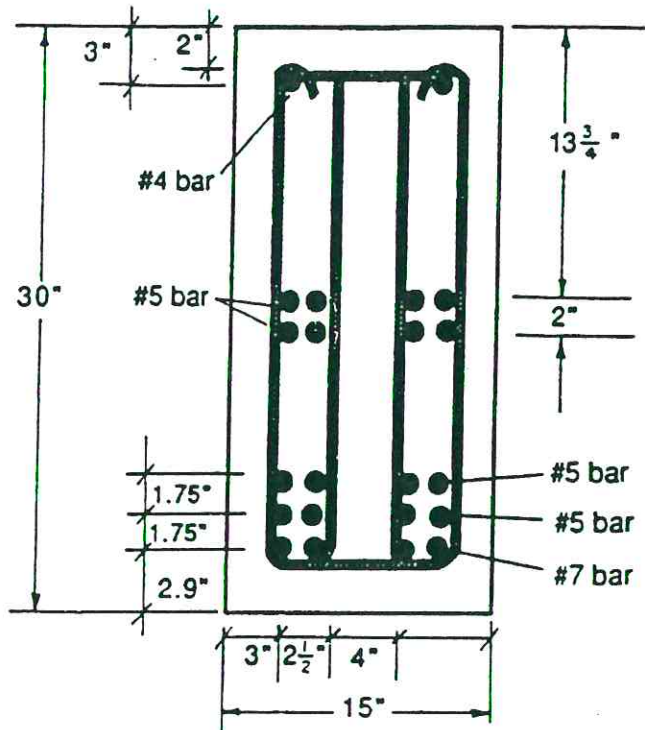


Figure 4.33: Reinforcement layout for dapped end beam

4.3.5 Anchorage Zone:

In post-tensioning concrete, the tensile force of the tendon is introduced into the concrete by means of end anchorage devices. Normally, the size of the anchorages is limited by the structural member size. This results in very large, highly concentrated forces which have to be introduced into the concrete. Anchorage devices transfer the posttensioning forces from the tendon wires, strands or bars to the concrete. Anchorage devices are in the form of steel plates or castings. The forces applied to the anchorage device will typically be very large. As a consequence, the concrete in the anchorage zone is subjected to high tensile (bursting, spalling and bending) and compressive (bearing) stresses. Confining reinforcement is used to increase the uniaxial compressive strength of the concrete to a three-dimensional state of strength around the anchorage device. The anchorage zone can be divided into the local zone immediately surrounding the anchorage device where the force is transferred from the device to the concrete, and the general zone where the highly concentrated force spreads out or diffuses into a linear stress gradient across the entire cross-section. The local zone is strongly influenced by the specific characteristics of the proprietary anchorage system. The state of stress in the local zone is highly complex and nonlinear, with a three-dimensional state of stresses. The general zone is the part of the anchorage zone that is more distant from the anchorage device and generally extends for a distance about equal to 1.0 to 1.5 times the depth of the section. In this zone the distribution of stresses induced by the posttensioning force becomes more uniform. According to Roberts [89] the extent of the local zone is defined as the greatest of the following:

- the maximum width of the local zone
- the depth of the confining reinforcing, but no greater than 1.5 times the width of the local zone

In order to consider a bearing plate as rigid, Roberts [89] indicates the thickness "t" must be:

$$t \geq (3 f_b n^2 / (0.75 f_y))^{0.5}$$

n = 1/2 of the diagonal or diameter of the plate minus the radius of the wedge plate

$$f_b = 0.85 F / A$$

A = gross area of plate

F = introduced compression force

If the plate cannot be considered rigid, it may be used but the effective bearing area shall be calculated as the area within a perimeter projected from the perimeter of the wedge plate through the bearing plate at a 45 degree angle. The behavior of the anchorage zone is controlled by the concrete strength and by the reinforcement. The layout of the reinforcement and the tensile capacity have a significant influence on the ultimate capacity and on its behavior at service state. Different failure modes can occur, either in the local or in the general zone. Failure in the local zone occurs in the immediate vicinity of the anchorage device. The surface of rupture is often in the shape of a pyramid or cone, delimited by crushed concrete. The failure is caused by an insufficient bearing strength of the concrete, by lack of confining reinforcement or by combination of both. The failure in the general zone is caused by the incapability of the transverse reinforcement to resist the bursting forces at the time of cracking or during subsequent loading, or by excessive compressive stresses in the concrete. A bending failure can be induced in the anchorage zone by the eccentricity of the post-tensioning force with respect to the overall cross section. This failure is caused by insufficient tensile capacity of the bending reinforcement.

Burdet [42] indicates that single anchor configurations can be loaded concentrically or eccentrically as shown in Fig. 4.34. The geometry of the tendon can be parallel to the axis of the anchorage zone or inclined, and also curved. Other external forces like transverse post-tensioning or transverse external forces can act on the anchorage zone.

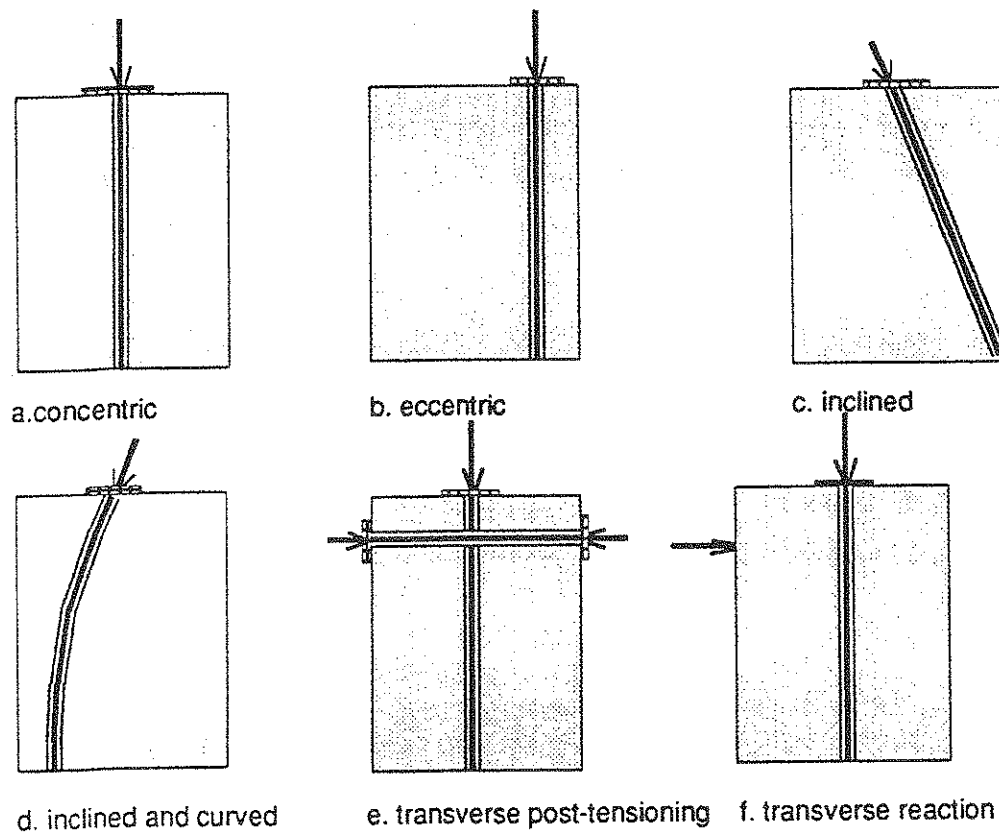


Figure 4.34: Possible configuration for single anchor (from Ref. [42])

Many different authors have studied the behavior of anchorage zones. Closed form elasticity solutions were presented by Guyon [125]. Among many others Magnel [126], Lenschow and Sozen [127], Schleeh [128], Stone and Breen [41], Burdet [42], Roberts [89], Sanders [43], Leonhardt [129] have presented theoretical and experimental solutions for local and general anchorage zones. However, the distinction between local zone and general zone was not clearly made until the recent work of Roberts [89], Sanders [43], and Burdet [42].

The different studies generally concentrated on the spalling forces and bursting forces. The spalling forces are the tensile stresses acting in areas of the concrete close to the end surface on either side of the anchorage device. These stresses are essentially induced by the condition of compatibility of displacements. Guyon recommended as a design value 4% of the applied load as the corresponding reinforcement in the form of a fine mesh, located as close to the face of the concrete as possible. Burdet [42] shows this to be conservative. Since such compatibility induced forces cannot be determined from an equilibrium based strut- and- tie model, the Guyon value is recommended for loaded-end face crack control.

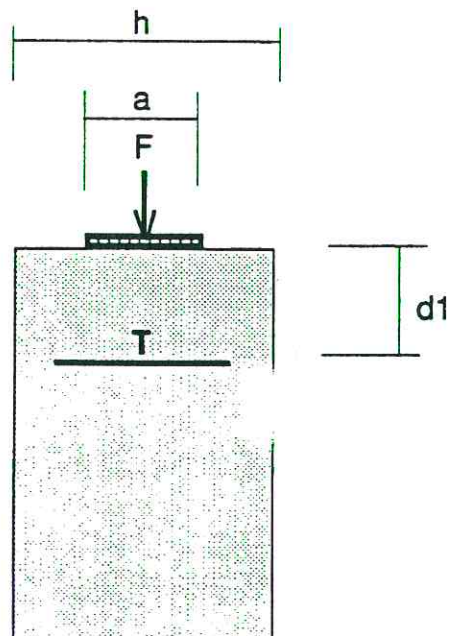


Figure 4.35: Concentric single anchor: geometry

The bursting stresses are the tensile stresses acting transversely to the axis of the tendon at a certain distance ahead of the anchorage. Bursting stresses are caused by the transverse spreading of the concentrated post-tensioning forces over the entire cross section. Figure 4.35 shows the geometry and nomenclature for the simplest case, that of a concentric single anchor. Figure 4.36 shows some comparison of Burdet's finite element analysis [42] and Guyon's analysis. For design purposes Guyon [125] and Leonhardt [129] presented the following equation to compute the total bursting force:

$$\begin{aligned}
 T &= \gamma F (1 - a/d) \\
 \gamma &= 0.25 \text{ (Guyon)} \\
 &= 0.30 \text{ (Leonhardt)}
 \end{aligned}$$

Many specifications have used similar equations. Good agreement with the finite load analysis can be seen from Fig. 4.36.

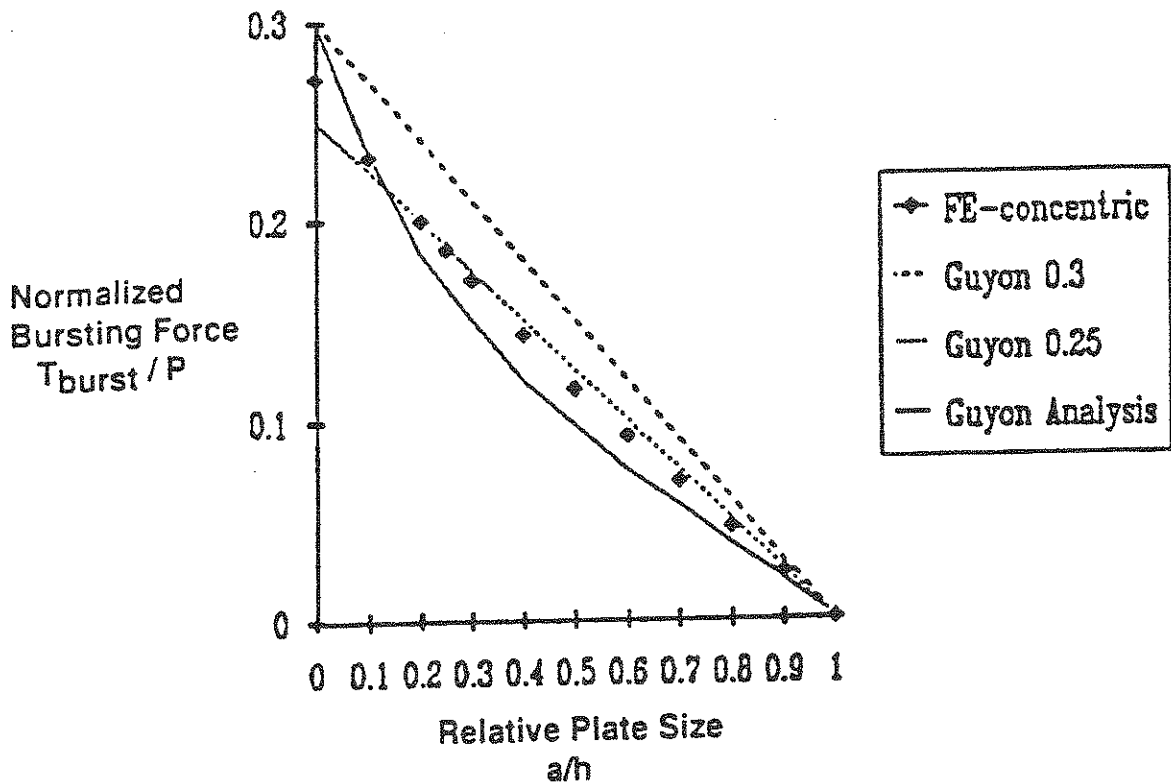


Figure 4.36: Comparison of finite element analysis with results from Guyon (from Ref. [42])

Two different strut- and- tie- models are shown for the concentric single anchor zone case in Fig. 4.37. Since the equations of equilibrium express the overall equilibrium of the structure, both logically must give the same answer. The thrust line model of Fig. 4.37(b) gives about 20 percent lower strain energy at ultimate load level [42] than the simple strut- and- tie- model shown in Fig. 4.37(a). This indicates more efficiency but is more related to the length of the transverse ties. Since in actual detailing, the ties would be extended towards the outer edges in both cases, this efficiency would not be practically developed and either can be used.

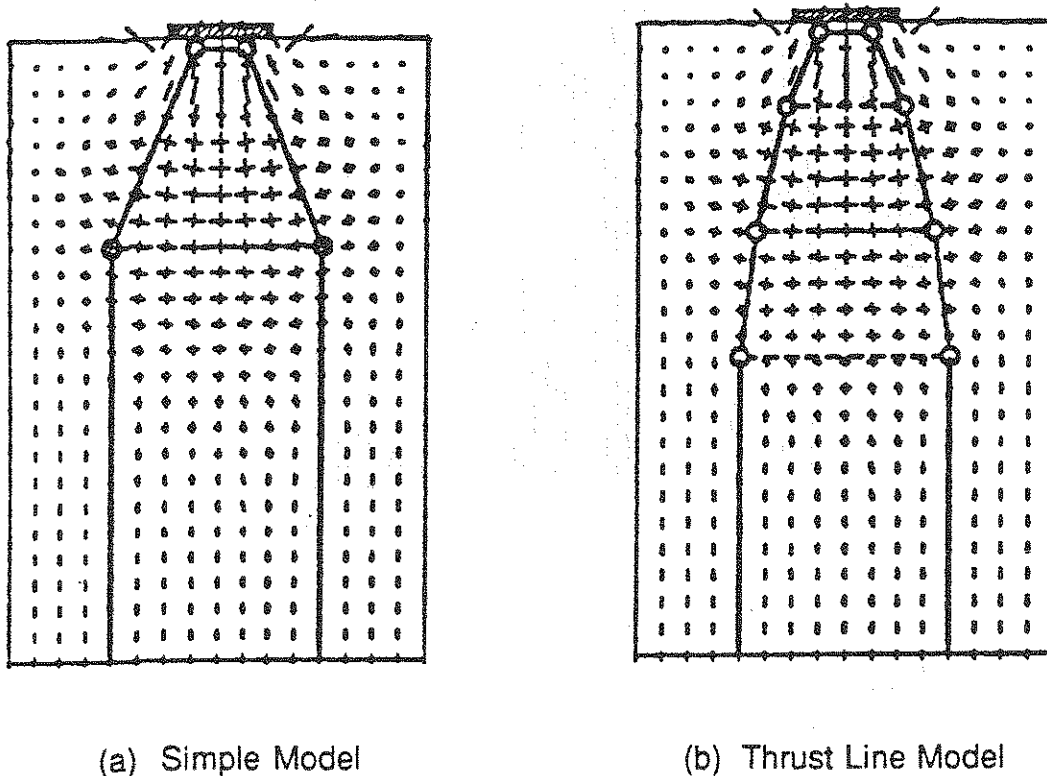

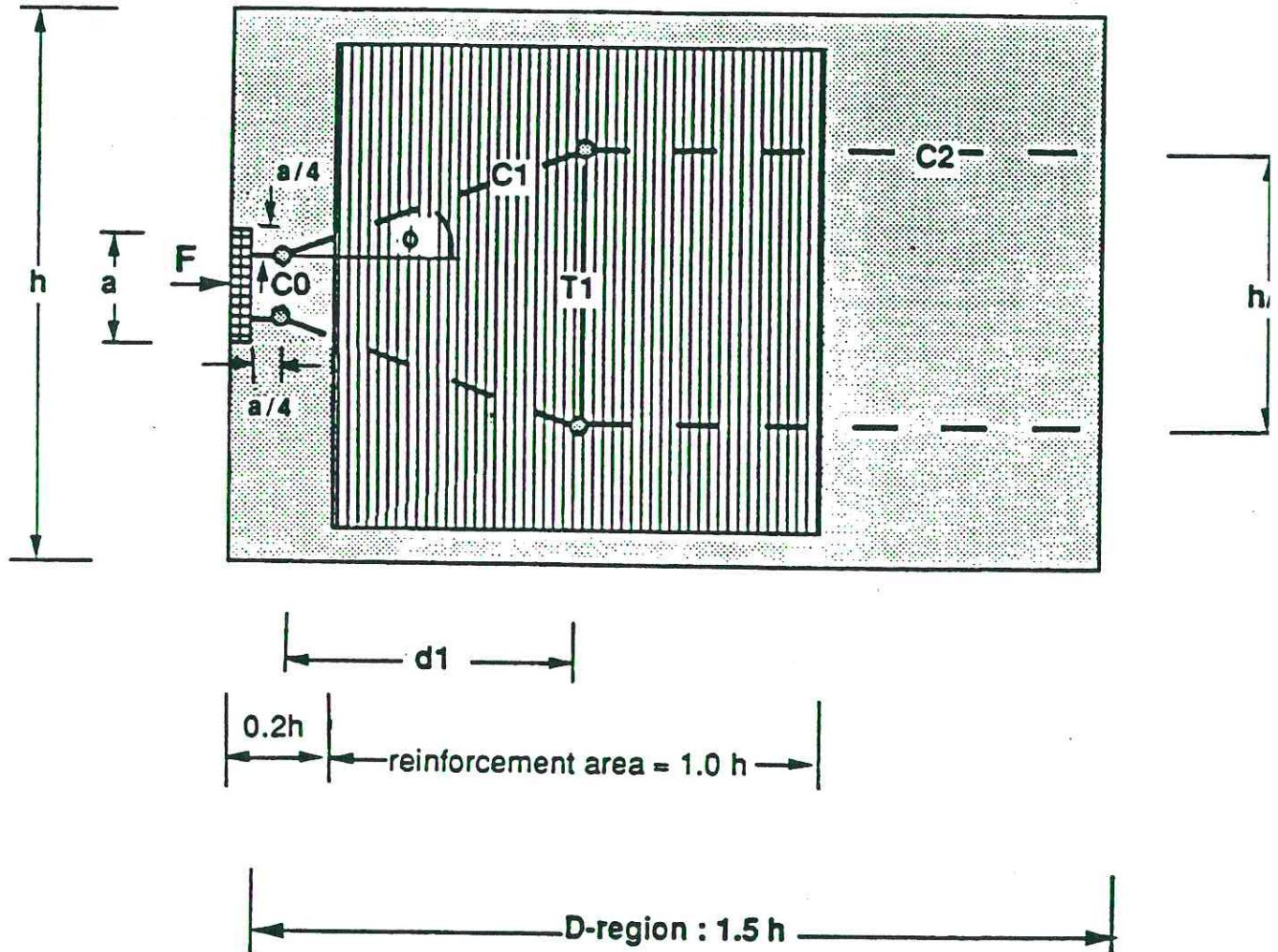


Figure 4.37: Comparison of two different strut- and- tie- models with principal stress vectors (from Ref. [42])

For design purposes the simple model of Fig. 4.37(a) can be used to determine the required reinforcement as shown in Fig. 4.38. The expressions for the angle of spreading of the compression force and the location of the centroid of the reinforcement shown in Fig. 4.38 are based on the results of Burdet [42]. The reinforcement should not be placed too close to the anchor. The thrust line model of Fig. 4.37(b) forces the designer to spread the reinforcement out more over the entire length of the D-region. When using the simple strut- and- tie model the reinforcement should be spread in a zone from $0.2 h$ to $1.2h$ [42]. Some additional transverse reinforcement should be placed normal to these stirrups to resist the spreading of the forces in the principal plane normal to this figure in the third dimension (see example:  # 3 bar).



Proposed strut angle and depth of the tension ties:

$$\phi_1 = 12 + 3 / \sqrt{(a/h)}$$

$$d_1 = h / (4 \tan \alpha) \quad \text{measured from centerline of bearing face of plate with } \alpha = 23.6$$

$$d_1 = (h - a) \text{ or } 4 \tan \phi_1$$

Figure 4.38: Proposed strut- and- tie- model for anchorage zone

Example 4.5: Anchorage zone

Design the reinforcement required in the post-tensioning anchorage zone shown in Fig. 4.39 to carry a maximum applied post-tensioning force of 500 kips applied to the centroidal axis of a beam with an overall height of 36 in. and a width of 12 in. The bearing plate is sufficiently rigid. It has a height of 8 in. and a width of 8 in. Assume concrete strength at time of stressing will be 6000 psi. Check both local zone for proper confinement and general zone for both transverse bursting reinforcement and spalling reinforcement. Both bars and spiral can be assumed as Grade 60.

Load and dimensions:

F	=	500 kips
h	=	36 in.
b	=	12 in.
a	=	8 in.
d	=	8 in. (diameter of spiral)
s	=	1.5 in. (pitch of spiral)

Spalling Force:

$$\text{Estimate } S = 0.04 F = 0.04 (500) = 20 \text{ kips}$$

$$\text{Required } A_s = 20/60 = 0.33 \text{ si}$$

$$\text{Use } 2 \text{ \#4 bars} = 0.40 \text{ si}$$

These spalling forces are resisted by the #4 stirrups and #3 ties next to the face as shown in Fig. 4.40.

General Zone: See Fig. 4.39.

Strut- and- tie- model:

$$\begin{aligned} \phi_1 &= 12 + 3/(a/h)^{0.5} \\ \phi_1 &= 18.4^\circ \\ d_1 &= (h - a) / (4 \tan \phi_1) \\ &= 21.0 \text{ in.} \end{aligned}$$

Internal forces:

$$\begin{aligned}
 C1 &= F / (2 \cos \phi_1) = 250 / \cos 18.4^\circ \\
 C1 &= 263.5 \text{ kips} \\
 C0 &= F / 2 \tan \phi_1 = 250 \tan 18.4 \\
 C0 &= 83.2 \text{ kips} \\
 C2 &= F/2 \\
 C2 &= 250 \text{ kips} \\
 \\
 T1 &= C1 \sin \phi_1 = \\
 T1 &= 83.2 \text{ kips}
 \end{aligned}$$

Reinforcement for tensile ties: (Grade 60)

$$\begin{aligned}
 T1 &= 83.2 \text{ kips} \\
 A_s &= 83.2 / 60 = 1.39 \text{ in}^2 \leq 8 - \#4 = 1.60 \text{ in}^2
 \end{aligned}$$

These bars must be distributed over a zone from 0.2 h (7.2 in.) to 1.2 h (43.2 in.) from the loaded face select #4 closed stirrups. One additional stirrup is located as close to front face as cover requirements allow to provide required spalling reinforcement. The 4 - #4 stirrups which satisfy the required 8 - #4 bars for T1 are then spaced at 8". This results in locations 10.5 in., 18.5 in., 26.5 in., and 34.5 in. as measured from the front face. One additional stirrup is provided at 42.5 in.

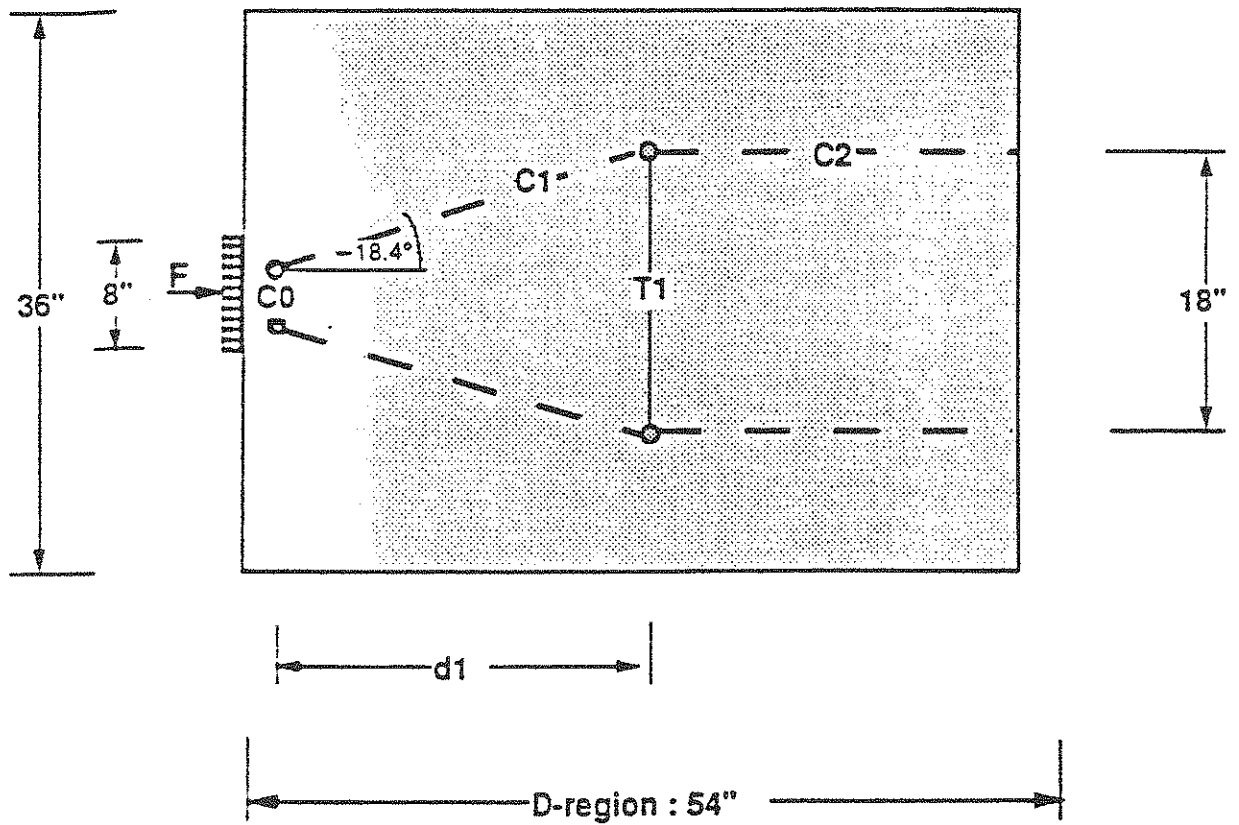
Out of plane:

A similar check must be made in the other principal plane. However, since the bearing plate width in that direction $a_2 = 8$ in. and $h_2 = b = 12$ in., there is appreciably less tensile bursting force. From Fig. 4.36, with $a_2/h_2 = 8/12 = 0.67$, the bursting force $T = 0.25 F (1 - a/h)$ seems quite accurate.

$$\begin{aligned}
 T &= (0.25) (500) (1 - 0.67) = 41.2 \text{ kips} \\
 A_s &= 41.2/60 = 0.69 \text{ in}^2
 \end{aligned}$$

This bursting force can be handled by a series of #3 ties ($A_s = 0.11 \text{ in}^2$). Six of these ties spaced in a region from $0.2 h_2 = 2.4$ in. to $1.2 h_2 = 14.4$ in. should control such transverse splitting. These #3 ties are shown on Fig. 4.40. They are also assisted by the spiral in this region.

Example: Anchorage zone



$$\phi_1 = 12 \cdot 3 / \sqrt{8 \cdot 36} = 18.4^\circ$$

$$d1 = 21 \text{ in.}$$

Figure 4.39: Strut- and- tie- model for example: anchorage zone

Anchorage requirements:

The #4 bars required for the T1 ties are adequately developed by bending them around #4 longitudinal bars placed in the corners.

Concrete stresses at node zones:

concrete strength: 6000 psi

efficiency factor: $v = 0.9 - 0.25(6000) / 10000 = 0.75$

The critical node in anchorages is usually at the anchor plate. The geometry is indicated in Fig. 3.8.

Check: CCC-node

Horizontal compressive stress in CCC-node

Since $w_4 > a_0$, hydrostatic stress

$$w_4 = a/2$$

$$w_4 = a/2 = 4 \text{ in.}$$

$$b = 12 \text{ in.}$$

$$\sigma_{c0} = C_0 / (w_4 * b) \leq v_e f'_c$$

$$\sigma_{ca} = 83.2 / (4 * 12) = 1.73 \text{ ksi} \leq 0.75 * 6. = 4.5 \text{ ksi} \quad \text{OK}$$

Vertical bearing plate stress with

spiral confining reinforcement

(See Sec. 3.4.1b for limits)

$$\sigma_{ca} = F / (a * b) \leq v_e f'_c (A / A_b)^{0.5} + 4 (A_{con} / A_b) f_{con}$$

$$f_{con} = [2 A_s f_y / (d s)] (1 - s/d)^2$$

$$d = 8 \text{ in.}$$

$$s = 1.5 \text{ in.}$$

$$A_s = (3/8)^2 \pi / 4 = 0.11 \text{ in.}^2 \quad (\text{Assumes a \#3 spiral})$$

$$f_{con} = 2 * 0.11 * 60,000 (1 - 1.5/8)^2 / (8 * 1.5)$$

$$f_{con} = 726 \text{ psi} = 0.726 \text{ ksi}$$

$$\begin{aligned}\sigma_{ca} &= 500 / (8 * 12) = 5.21 \text{ ksi} \leq 0.75 * 6 * (12/8)^{0.5} + 4 * [\pi 8^2 / (4 * 8^2)] * 0.726 \\ \sigma_{ca} &= 5.21 \text{ ksi} \leq 5.51 + 2.28 = 7.79 \text{ ksi} \quad \text{OK}\end{aligned}$$

In detailing of the spiral, a reasonable length is to extend the spiral to a distance from the bearing plate equal to $1.5a = 12$ in. Specific criteria for performance evaluation of anchorage devices with confining reinforcement is given by Roberts [89].

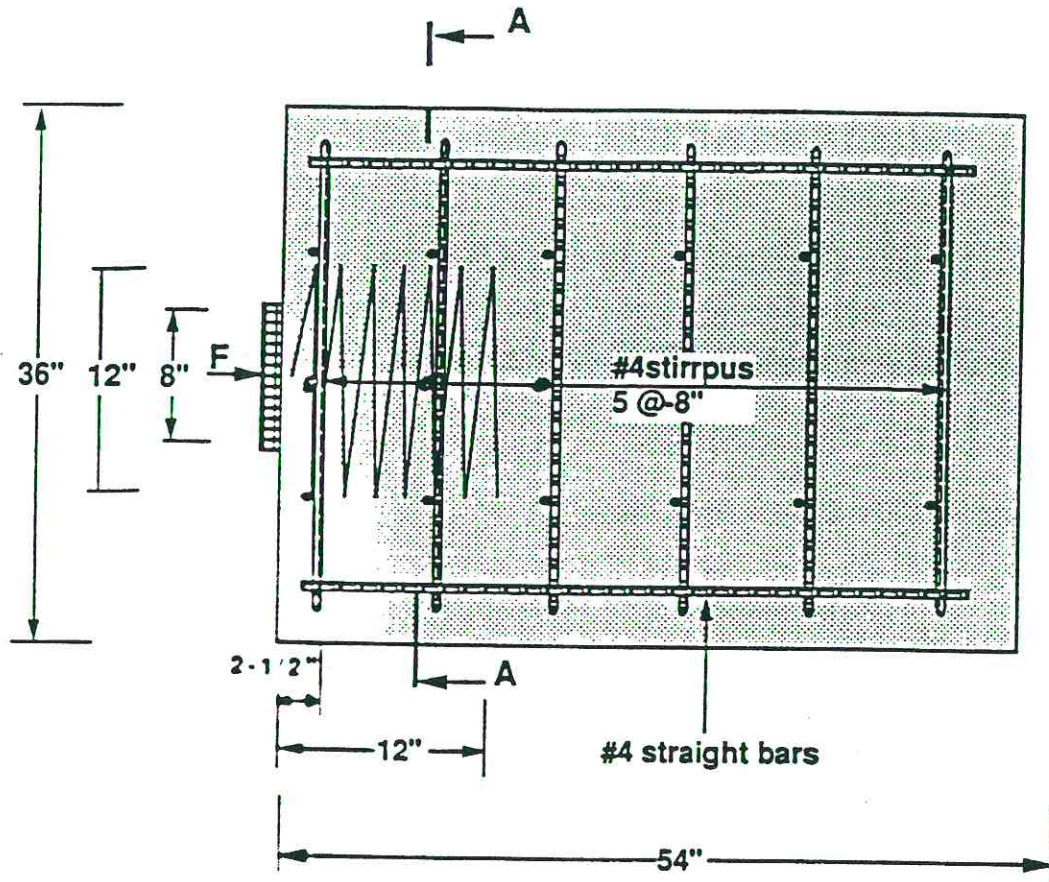
Compressive Strut Stresses:

In highly stressed anchorage zones, the stress level in the compressive struts can be quite high. This is one of the most likely applications in detailing of structural concrete where compression may occur. As the strut leaves the node, the force is diffusing and the strut widens as shown in Fig. 3.9. Burdet [42] suggests that the diffusion of the strut is helpful and that the strut should be checked at a level (y in Fig. 3.8) corresponding to the effective plate width, a . For this example $\phi_3 = 18.4^\circ$, the angle of spreading can be assumed as a 1:2 slope or diffusion angle of 26.5° .

From the geometry of Fig. 3.9, when $w_4 = a/2 = 4$ in., the strut width at a depth $y = a = 8$ in. can be found since $a' = a/2 = 4$ in. Since $w_3' > w_3''$, $w_3 + 2w_3'' = 16.47 + (2)1.26 = 18.99$ in.

$$\begin{aligned}\sigma_1 &= C_1 / w_1 b = 263.5 / 18.99 (12) = 1.16 \text{ ksi} < \\ &0.6 v_e f'_c = (0.6) (0.75) (6) = 2.70 \text{ ksi} \quad \text{OK}\end{aligned}$$

Note that at this depth, $y = a$, the strut stress is essentially the same as the stress at the end of the general zone $\sigma = 500 / (36) (12) = 1.16$ ksi.



Section: A - A

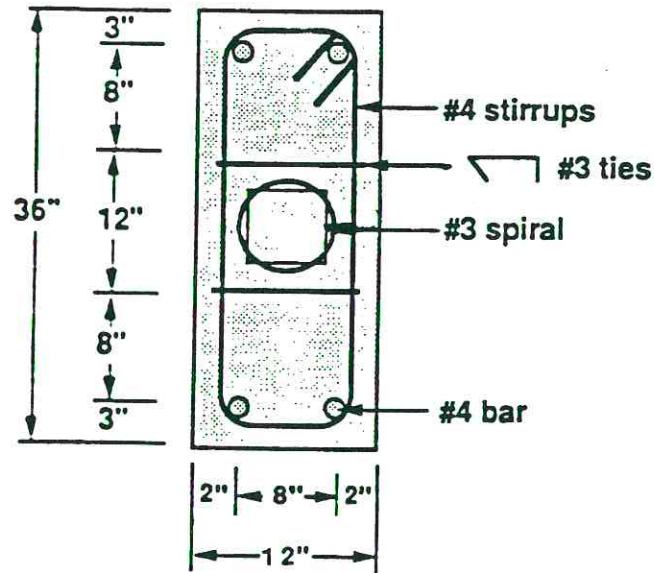


Figure 4.40: Reinforcement layout for anchorage zone

As a last example and in order to illustrate the application of strut- and- tie models in both 'D' and 'B' regions, a prestressed concrete beam will be analyzed using the strut- and- tie model as shown in Section 2.5.1. Use of the strut- and- tie model in B regions may be more cumbersome than ordinary sectional analysis. By prestressing, forces are artificially created with the help of hydraulic jacks. These forces act as loads on the prestressing steel and as loads on the concrete. The designer chooses the tendon profile, the type and the magnitude of the prestressing forces in such a manner that these artificial loads change the internal force path created by the actual loads. Proper prestressing ordinarily can prevent the formation of tension cracks under working loads. Also, the deflection under working loads can be greatly reduced, because prestress usually puts camber into a member under dead loading. A simple span beam is prestressed by introducing a negative moment to offset the expected actual positive moment and at the same time introducing a longitudinal compression to offset the tensile stresses from bending moment. Continuous beams are prestressed in a similar fashion but for best results require an effective eccentricity above middepth in negative moment zones. In ordinary computations, when continuous beams are prestressed, secondary moments are introduced because the reactions prevent full movement under the action of the prestress. One of the major advantages of strut- and- tie models is that the prestress is introduced as forces acting on the structure and their effect is directly considered for the actual boundary conditions.

Example 4.6: Pretensioned beam

The pretensioned beam with end eccentricity from Ref. [55] is investigated here with the strut- and- tie- model for a concrete strength $f'_c = 5000$ psi, $n = 7$, wire tension $f_{pi} = 135$ ksi* and a creep and shrinkage loss of 35 ksi. The concrete strength when tendons are released is assumed to be $f'_c = 4000$ psi. Dimensions are shown in Fig 4.41. In this example, the actual strands are initially lumped together as if one supersized strand for simplicity. In actuality the 1.5 in.² would have to be provided by 10 - 1/2-in.-diameter strands distributed on 2-in. centers which would result in a slightly higher centroid. In checking the chord stresses

*This assumed initial prestressing steel stress is about the lowest value which might be used effectively in prestressing. This leaves an equal reserve ($f_{pu} - f_{pi} = 270 - 135 = 135$) available for overloads before ultimate.

in the lower chord, this larger area corresponding to distributed strands will be used. Further assume $M_d = 65$ K-ft. and $M_1 = 80$ K-ft.

For the uncracked section, the steel is transformed as $(n-1) A_s$:

$$A_{\text{tot}} = 10 * 20 + 1.5 (7-1) = 209 \text{ in.}^2$$

y' from middepth of the concrete cross section

$$y' = -9 * 7 / 209 = -0.3 \text{ in. (below)}$$

$$I_{\text{tot}} = 10 * 20^3 / 12 + 200 * 0.3^2 + 9 * 6.7^2 = 7087 \text{ in.}^4$$

After cutting the tendons the compression and tension chord forces the strut-and-tie model shown in Fig. 4.42(b) can be computed:

$$P_i = (1.5) (135) = 202 \text{ kips}$$

$$\Sigma C_{p1} = P_i / (2 \cos 12^\circ)$$

$$= 202 / (2 \cos 12^\circ) = 103.3 \text{ kips}$$

In order to check the compressive stresses resulting from the application of this concentrated force by the distributed strands, it is assumed that the centroid of the strands is 3 in. from the bottom and that they are fully distributed over the width. Thus $AP1 = (2) (3) (10) = 60 \text{ in.}^2$

$$\text{For } f'_c = 5000, \sqrt{e} = 0.9 - 0.25 (5000/10000) = 0.775$$

$$\text{For } f'_c = 4000, \sqrt{e} = 0.8. \text{ For simplicity USE } \sqrt{e} = 0.75 \text{ throughout this example}$$

$$V_e f'_c = 0.75 * 4000 = 3000 \text{ psi}$$

$$\Sigma C_{p1} / A_{p1} = 103.3 / 60 = 1.72 \text{ ksi} \leq 0.75 * 4000 = 3.0 \text{ ksi} \quad \text{OK}$$

Of substantial concern is the need for lateral and vertical reinforcement throughout the transfer length to resist the tension forces T_{p1} shown in Figure 4.42(a).

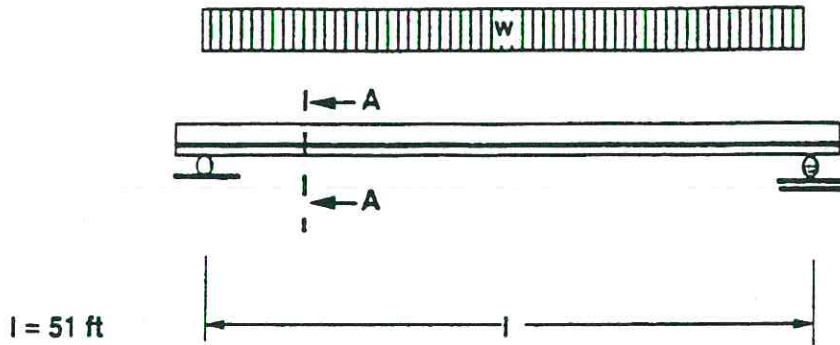
$$\Sigma T_{p1} = \Sigma P1 / 2 \tan \phi_{P1} = 202 / 2 (2.5 / 8) = 31.6 \text{ kips}$$

$$A_s = 31.6 / 60 = 0.53 \text{ si. Use 5 \#3 = 0.55 si.}$$

Note that these tension forces exist laterally as well as vertically so that only 1 leg on the bottom of each stirrup runs transversely to resist the lateral component. Thus A_s for each stirrup is 0.11 si. This reinforcement must be distributed within the transfer lengths of $50 d_b = 25$ in. as shown in Fig. 4.43

If the 'D' region at the end is isolated as shown in Fig. 4.42(c) and the combined stresses due to the prestress and its eccentricity are computed from $P/A + Pec / I$, the values given in Fig. 4.42(c) are found. Applying these stresses as forces $T1 = C2$ and $C3 = P1$ at their respective centroids as indicated, it is very easy to construct the force path and strut- and- tie model shown. This clearly illustrates that if tensile strength of concrete is not to be relied on, an area of steel $A_s = 26/60 = 0.43 \text{ si}$ should be provided in the end regions close to the top of the beam. Two #4 bars are provided as shown in Fig. 4.43. They also are useful for positioning and anchoring the stirrups. This 'D' region also indicates the need for a similar area of vertical reinforcement at the support. The closely spaced #3 stirrups provided over the support to work locally to resist strand splitting forces also work nicely over the full depth to provide this resistance. The advantage of strut- and- tie modelling in the 'D' regions is clear from these types of calculations.

Example: Pretensioned beam with eccentricity

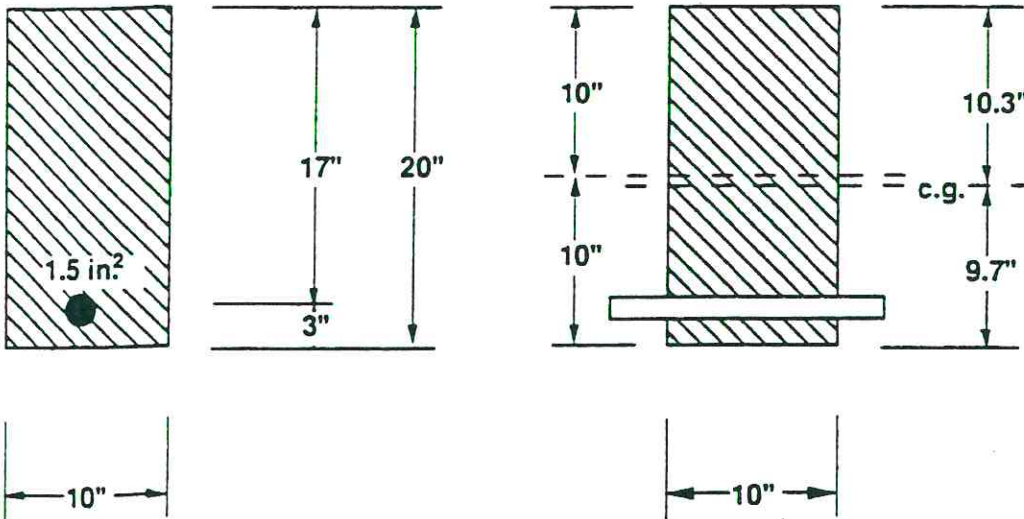


$$w_{dl+ll} = 0.446 \text{ k / ft}$$

$$M_{dl} = 65 \text{ k-ft} = 780 \text{ k-in.}$$

$$M_{ll} = 80 \text{ k-ft} = 960 \text{ k-in.}$$

Section: A - A



$$A_{tot} = A_c + (n-1) A_p$$

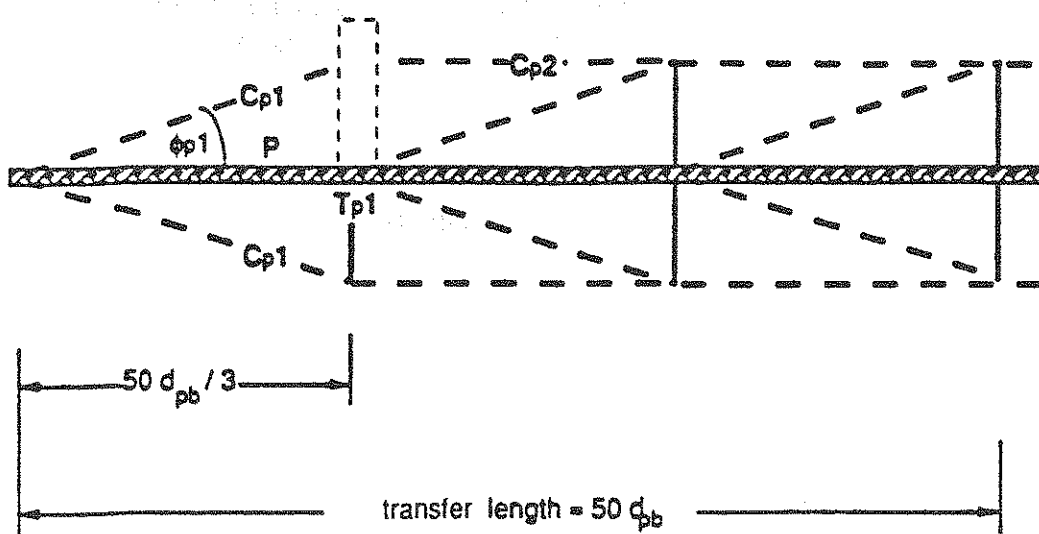
$$I_{tot} = b h^2 / 12 + A_c y_c^2 + (n-1) A_p e^2$$

Figure 4.41: Pretensioned beam: geometry (from Ref. [55])

$$C_{p1} = P / (2 \cos \phi_{p1})$$

$$C_{p2} = P / 2$$

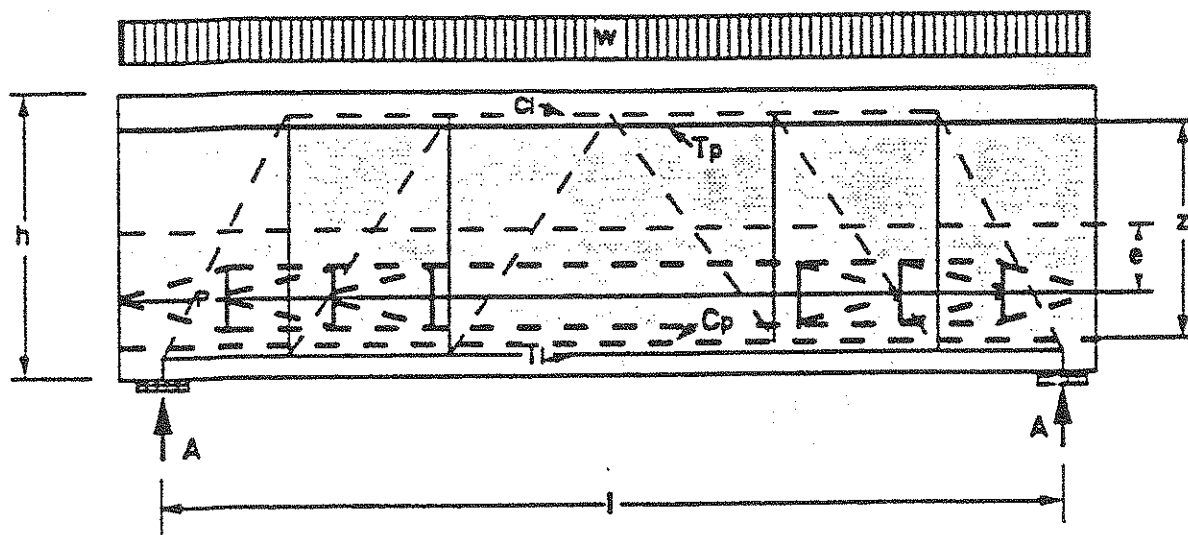
$$T_{p1} = (P \tan \phi_{p1}) / 2$$



Proposed compression strut diffusion angle:

$$\phi_{p1} = 12^\circ$$

(a) Transfer Length Forces



$$T_p = w_t b (-P/A_t + P e y_t / I_t)$$

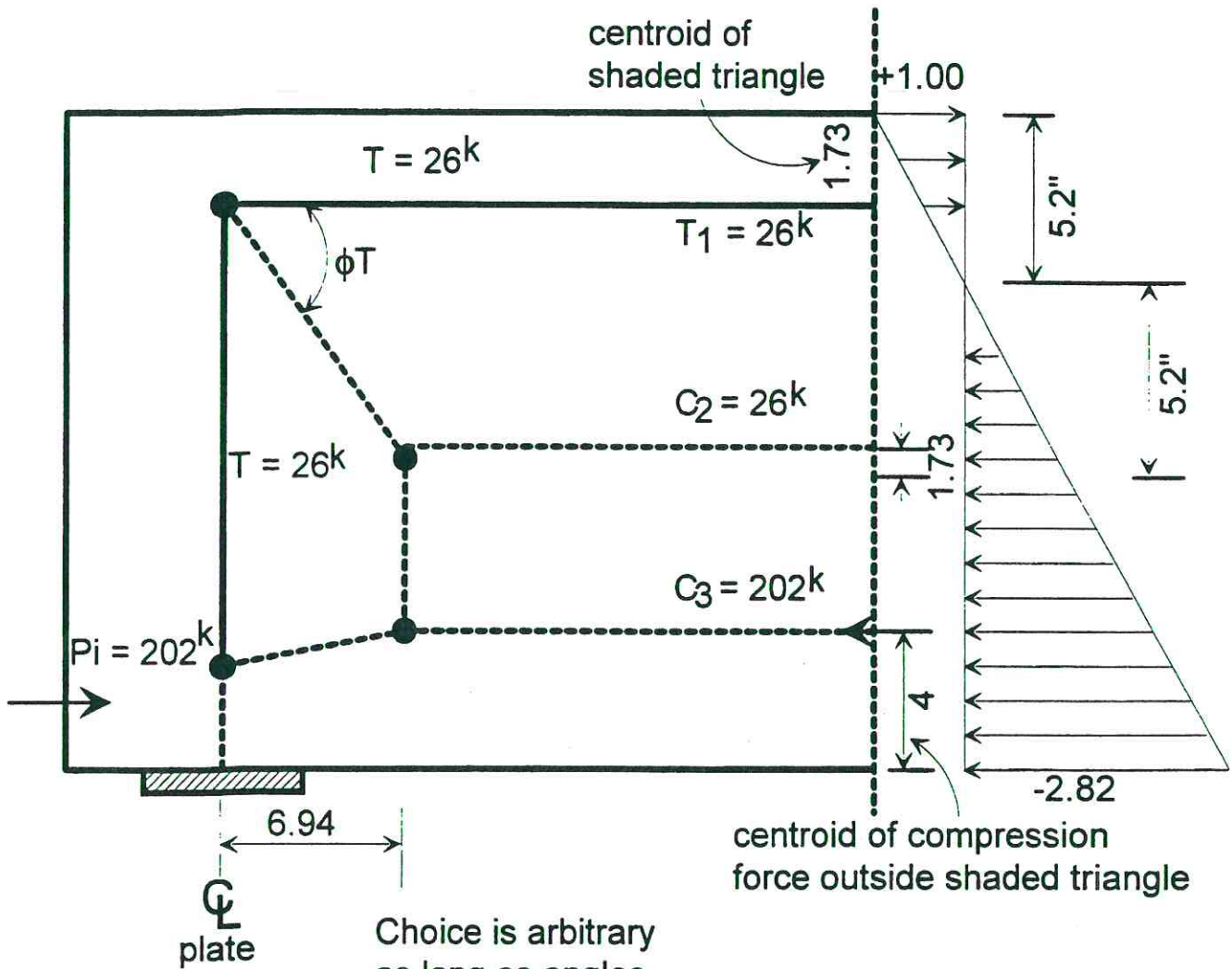
$$C_p = w_c b (-P/A_c - P e y_c / I_c)$$

(b) Model with tendon eccentricity effects

Figure 4.42: Strut- and- tie model for prestressed concrete

$$T_1 = \frac{1}{2} (1.0) (5.2) (10) = 26$$

$$C_2 = \text{is taken equal to } T_1$$



Choice is arbitrary as long as angles do not get to small. In this case, chosen so $\phi T = 45^\circ$

(c) "D" Region at end

Figure 4.42: Continued

Top chord: tension from prestressing forces after cutting the wires

It can be seen from Fig. 4.42(a) that the prestress force is applied to the lower chord gradually over the transfer length, $50 d_b = 25$ in. It is assumed that this can be approximated as three equal forces, P_i , each located about 8 in. apart. However, when compared to the length of the beam, the critical zone for tension on the top chord can be effectively checked with full prestress and no dead load moment. This is slightly severe but practical. The prestressing loads are applied to the overall beam as any other load would be. This load case illustrates one problem with strut- and- tie modelling. As previously shown in Fig. 2.30(d), if a simple truss model is used assuming free articulation at all joints, the application of a horizontal force concentric with the centroid of the lower chord to a simply supported, articulated, simple truss does not produce top chord forces. However, in a normal mechanics analysis, it is assumed that plane sections remain plane so that the conditions of deformation compatibility are introduced. These are not part of an equilibrium or plastic analysis. Thus in the highly elastic prestressed beam at service load conditions, these compatibility considerations are necessary and some beam analysis concepts must be introduced.

$$T_p = w_t b (-P / A_{tot} + P * e * y_t / I_{tot})$$

The effective top chord depth, w_t , is estimated as having a centroid about as far from the outer fiber as the centroid of the strands, 3 in. Since the beam has uniform width and since the final stress distribution is assumed uniform, $w_t = 6$ in. and the distance from the section centroid to the centroid of this chord is $10.3 - 3 = 7.3$ in. (One can see that lumping of all top chord fibers into a single chord reduces the accuracy of outer fiber stress calculations done in the traditional $P/A + Mc/I$ manner.)

$$T_p = 6 * 10 (- 202 / 209 + 202 * 6.7 * 10.3 / 7087) = 60.0 \text{ kips}$$

Bottom chord: compression from prestressing forces after cutting the wires

$$C_p = w_c b (-P / A_{tot} - P * e * y_c / I_{tot})$$

$$C_p = 6 * 10 (-202 / 209 - 202 * 6.7 * 9.7 / 7087) = 169.1 \text{ kips}$$

Check end section where dead load moment is zero under effect of prestress forces:

Top chord:

$$T_p = 60 \text{ kips} \leq 6 \sqrt{f'_c} A_t = [6 \sqrt{4000} (6) (10)] / 1000 = 22.7 \text{ kips N.G.}$$

At this section the tensile stresses on the top exceed permissible.

The strands should be draped, blanketed, or the cross-section changed.

The same result would be found in a conventional analysis.

Lower chord: $C_p = 169.1 \text{ kips} \leq 0.75 f'_c A_b = (.75) (4) (6) (10) = 180 \text{ kips OK}$

From dead load:

$$C_{dl} = T_{dl} = M_{dl} / z$$

$$z = 14.3 \text{ (from Ref. [55], or as a first approximation: } z = 3/4 h)$$

$$C_{dl} = T_{dl} = 780/14.3 = 54.55 \text{ kips}$$

Check centerline section under effect of dead load combined with prestress forces:

Top chord:

$$T (\text{prestr.}) - C (\text{load}) < 3 \sqrt{f'_c} A_t (\text{tension})$$

$$60 - 54.55 - 0 = 5.55 \text{ kips (tension } \leq 3 \sqrt{4000} (6) (10) / 1000 \text{ (tension))}$$

$$= 11.38 \text{ kips OK}$$

Bottom chord:

$$T (\text{load}) - C (\text{prestr.}) \leq -b w_t \sqrt{e} f'_c$$

$$54.55 - 169.1 = 114.55 \text{ (compression)}$$

$$\leq -6 * 10 * 0.75 * 4 = -180 \text{ kips (compression) OK}$$

*Use of $\sqrt{e} f'_c$ which is an ultimate term may be inconsistent with service load tensile stress checks. Note compression is OK with $0.6 f'_c$ as well.

From dead and live load:

$$\begin{aligned} C_{dl+ll} &= T_{dl+ll} = M_{dl+ll} / z \\ z &= 14.3 \text{ (from Ref. [55], or as a first approximation: } z = 3/4 h) \\ C_{dl+ll} &= T_{dl+ll} = 1740 / 14.3 = 121.7 \text{ kips} \end{aligned}$$

prestress drops (owing to losses) to $202 - (35 * 1.5) = 149.5$ kips

Check centerline section under effect of dead load, live load, and prestress after losses:

top chord:

$$T(\text{prestr.}) - C(\text{load}) \leq -b w_c v f'_c$$

$$60 * 149.5 / 202 - 121.7 = -77.6 \text{ (compression)}$$

$$\leq -10 * 6 * 0.75 * 5 = -225 \text{ kips (compression)}$$

OK

tension chord:

$$C(\text{prestr.}) - T(\text{load}) \leq b w_t 3 (f'_c)^{0.5}$$

$$w_t = 6 \text{ in.} \leq 2 \text{ in. (For a conservative check, the distance } w_t \text{ is here limited to the strand spacing from the outer fiber)}$$

$$169.1 * 149.5 / 202 - 121.7 = 3.45 \text{ (tension)}$$

$$\leq 10 * 2 * 3 * (5000)^{0.5} = 4.24 \text{ kips}$$

(tension) OK

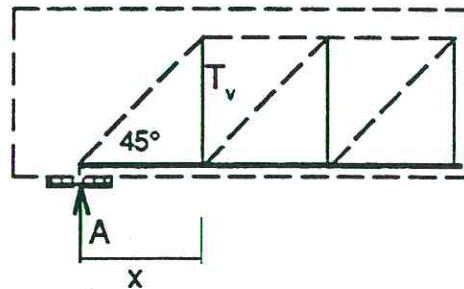


vertical chord:

$$T_v = A - w * x$$

$$T_v = 11.37 - 0.446 * 14.3 / 12$$

$$T_v = 10.84 \text{ kips}$$



In this case the tendon is straight so $C_r = 0$

$$T_v(\text{load}) - C_r \leq T$$

$$10.84 - 0 < \#3 \text{ U stirrup} = 2 * 0.11 * 60 = 13.2 \text{ kips}$$

Bennet, Abdul-Ahad and Neville [130] recommend that in reinforced and prestressed concrete beams in which a large shear is caused by loads varying or moving in position, the stirrup spacing should not exceed $0.75 h$, where h is the effective depth of the beam.

Use #3 U stirrups at 15 in. spacing as shown in Fig. 4.43.

Obviously the numbers and reinforcement would change if load factors and resistance factors were applied. However, the principles would be the same. It can be seen that the allowable stress checks using strut-and-tie models are more cumbersome than conventional sectional analysis procedures.

In order to illustrate the check for ultimate conditions, assume ACI Building Code load factors and $\phi = 1.0$. Then $M_U = 1.4(780) + (1.7)(860) = 2724$ in.k. $C_U = T_U = M_U / z = 2724 / 14.3 = 190.5$ kips. This load condition is truly plastic so the basic strut- and- tie model applies. Checking at the centerline with an effective prestress of 149.5 kips:

<u>Top Chord</u>	Σ	C (load)	<	$b w_c v_e f'_c$		
		190.5	<	(10) (6) (.75) (5)		
				= 225		OK
<u>Bottom Chord</u>	Σ	T (load)	<	T + P	=	$(A_p f_{py} - P_e) + P^*$
		190.5	<	(1.5) (250)	=	375 kips
						OK

$A_p f_{py} - P = A_c (f_{pv} - f_c)$ is the reserve capacity in the tendons after prestressing. This is the tension that can be developed in the tendons above that developed during prestressing.

Concrete stresses at support node: CCT - node

This check will be performed with the unfactored conditions as an illustration.

Again, in reality, proper load factors and ϕ factors would be required. For definitions refer to Fig. 3.12. In this case there would be 3 layers of 1/2" strands, each 2 in. on centers. Thus $wT = 3(0.5) + (2)(1.5) = 4.5$ in. The inclined compression struts were assumed at an angle $\phi = 45^\circ$. $C1 = A = (51)(0.446)(1/2) = 11.37$ kips. Thus $C2 = C1/\sin 45 = 11.37/\sin 45 = 16.08$ kips.

$$a = 8 \text{ in.}$$

$$wT = 4.5 \text{ in.}$$

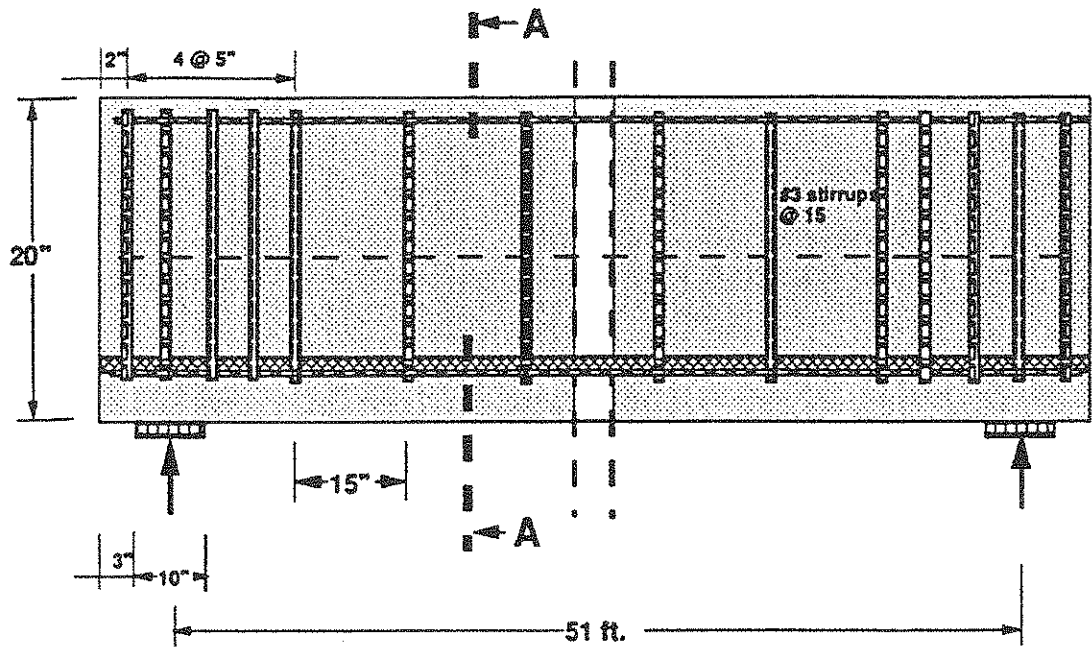
$$w2 = a \sin \phi + wT \cos \phi = 8 \sin 45 + 4.5 \cos 45 = 8.83 \text{ in.}$$

$$\sigma_{c2} = C2 / (w2 * b) \leq v_e f'_c$$

$$\sigma_{c2} = 16.08 / (8.83 * 10) = 0.18 \text{ ksi} \leq 0.75 * 5. = 3.75 \text{ ksi} \quad \text{OK}$$

$$\sigma_a = A / (a * b) \leq v_e f'_c [a_c b / (a b)]^{0.5}$$

$$\sigma_a = 11.37 / (8 * 10) = 0.14 \text{ ksi} \leq 0.75 (10 / 8)^{0.5} * 5. = 4.19 \text{ ksi} \quad \text{OK}$$



Section: A - A

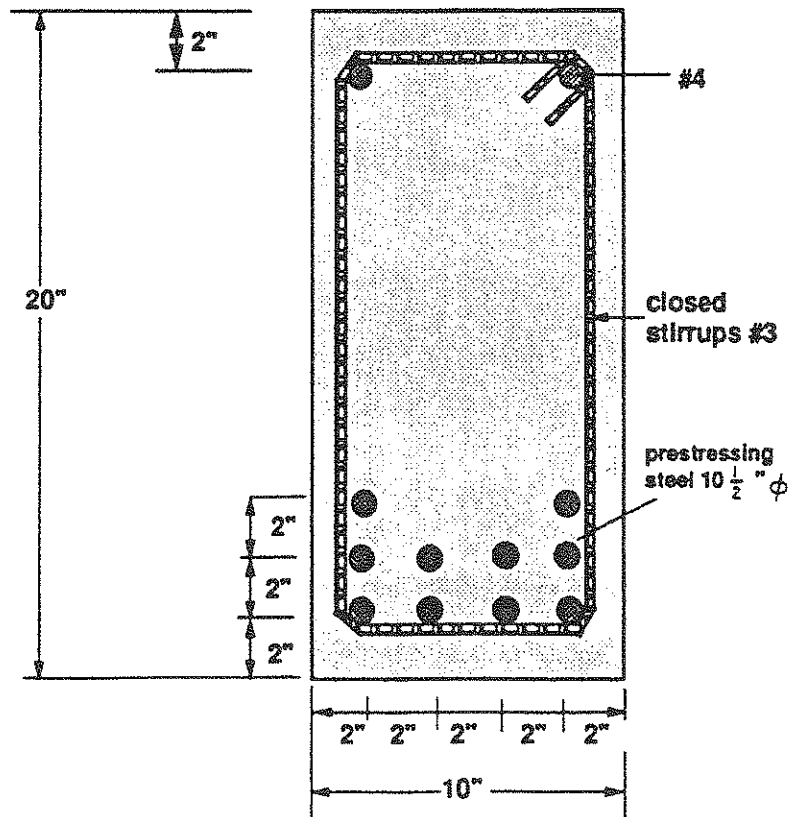


Figure 4.43: Reinforcement layout for pretensioned beam

CHAPTER 5. CONCLUSIONS AND RECOMMENDATIONS

In this report a methodology was suggested and an evaluation made of the strut- and- tie- models for detailing structural concrete. Comparison with experimental results from details as well as from single node zones were reported. The strut- and- tie- model represents a useful tool for detailing concrete structures. It emphasizes the internal force flow and provides some in-depth understanding of the behavior of geometrical and statical discontinuities. It is principally of value in dimensioning and detailing these 'D' or discontinuity regions. While it can be used in the more regular 'B' or Bernoulli regions where linear strain profiles are encountered, it is not as advantageous as ordinary structural concrete design procedure in those regions. After discussing the general principles, components and modeling techniques as well as dimensioning of the struts, ties and nodes in chapters 2 and 3, illustrative design examples were presented in chapter 4. Several typical strut- and- tie patterns are furnished in Appendix A.

For the majority of concrete structures it would be unreasonable and inefficient to model the entire structure with a strut- and- tie- model. It is advantageous to subdivide the given structure into B-regions and D-regions. After computing the elastic stress resultants or ordinary cracked reinforced concrete forces for the B-regions, the equivalent forces should be applied to the D-regions. Load paths can be sketched based on experience, design aids, experimental results or a finite element analysis. The strut- and- ties can be rearranged with consideration of practicality of the reinforcement layout. The proposed design recommendations are applicable to either prestressed or non-prestressed reinforced members.

The general assumptions for the application of the strut- and- tie- model in the design procedure are:

- yielding of the reinforcement is required prior to concrete or anchorage failure
- the ties transfer only uniaxial forces and neglect dowel action, aggregate interlock, and tensile strength across cracks.

Dimensioning is an iterative process. The compression struts can be checked by using the proposed approaches for concrete strength < 12500 psi. Detailed rules for the strut limits are given in Section 3.2. Detailed rules for geometry limits and admissible stresses for unconfined and confined nodes are given in Section 3.4.

In this report, the design procedures based on the strut- and- tie- model and the proposed detailing approaches are illustrated with a series of design examples. In addition, several strut- and- tie- models (from Ref. [2, 28]) which may be useful to the designer when detailing 'D' regions in concrete structures are included in Appendix A.

Study of the design examples indicates that use of the strut- and- tie model is an extremely efficient way of detailing reinforcement in 'D' regions. The calculations are relatively simple and straightforward and give the designer substantial insight. In contrast, the checks of struts and nodes are laborious and somewhat subjective. It was noted that in many applications these strut and node stresses were not close to controlling design. Hopefully, further application and familiarity with the method will give designers a "feel" for when detailed strut and node calculations are required and when they can be assumed as not governing.

6. References

1. Schlaich, J.; Weischede, D.: A practical Method for the Design and Detailing of Structural Concrete (in german). Bulletin d'Information no. 150. Comite Euro- International du Beton, Paris, 1982 163 pp.
2. Schlaich, J.; Schäfer, K.: Konstruieren im Stahlbetonbau (Design for Concrete Structures). In: Betonkalender, Berlin 1989, pp. 563-715
3. AASHTO: American Association of State Highway and Transportation Officials. Standard Specifications for Highway Bridges. 13th. edition, Washington, D.C., 1983
4. ACI 318-89: Building Code Requirements for Reinforced Concrete, Detroit, 1989
5. Ritter, W.: Die Bauweise Hennebique (The Hennebique System). In: Schweizerische Bauzeitung, Bd. XXXIII, No. 7, Zürich, 1899
6. Mörsch, E.: Der Eisenbetonbau, seine Theorie und Anwendung (Reinforced Concrete, Theory and Application), Stuttgart, 1902
7. Barton, D.: Design of Dapped Beams using the Strut- and - Tie- Model. Master's Thesis, The University of Texas at Austin, 1988
8. Withey, M.: Tests of Plain and Reinforced Concrete, Series of 1906 and 1907. Bulletin of the University of Wisconsin, Engineering Series, Vol. 4, No.2, 1907 - 1908
9. Talbot, A.: Tests of Reinforced Concrete Beams: Resistance to Web Stresses, Series of 1907 and 1908. Bulletin 29, University of Illinois Engineering Experiment Station, 1909
10. Henley, H.: Report of the Committee on Laws and Ordinances. National Association of Cement Users. Vol. 4, 1908, pp. 233 - 239
11. Richart, F.: An Investigation of Web Stresses in Reinforced Concrete Beams. Bulletin 166, University of Illinois, Urbana, 1927

12. Hognestad, E.: What do we know about Diagonal Tension and Web Reinforcement in Concrete? Circular Series 64, University of Illinois, Engineering Experiment Station, 1952
13. Kupfer, H.: Erweiterung der Mörsch'en Fachwerkanalogie mit Hilfe der Formänderungsarbeit (Expansion of Mörsch's Truss Analogy by Application of the Principle of Minimum Strain Energy) CEB-Bulletin 40, Paris, 1964
14. Lampert, P.; Thürlimann, B.: Ultimate Strength and Design of Reinforced Concrete Beams in Torsion and Bending. IABSE, No. 31-I, Zürich, 1971, pp. 107-131
15. Leonhardt, F.: Reducing the Shear Reinforcement in Reinforced Concrete Beams and Slabs. In: Magazine of Concrete Research, Vol. 17, No.53, 1965, p. 187
16. Rüschi, H.: Über die Grenzen der Anwendbarkeit der Fachwerkanalogie bei der Berechnung der Schubfestigkeit von Stahlbetonbalken (On the Limitations of Applicability of the Truss Analogy for the Shear Design of Reinforced Concrete Beams), Festschrift F. Campus'amici et alumni, Université de Liège, 1964
17. Lampert, P.: Postcracking Stiffness of Reinforced Concrete Beams in Torsion and Bending, ACI, Detroit, SP-35-12, 1973
18. Grob, J.: Ultimate Strength of Beams with thin walled open cross-sections. Bericht 56, Institut für Baustatik und Konstruktion-ETH, Zürich, 1970
19. Lüchinger, P.: Bruchwiderstand von Kastenträgern aus Stahlbeton unter Torsion, Biegung und Querkraft (Ultimate Strength of Box-Girders in Reinforced Concrete under Torsion, Bending and Shear). Institut für Baustatik und Konstruktion-ETH Zürich, Bericht Nr. 69, 1977
20. Müller, P.: Plastische Berechnung von Stahlbetonscheiben und -balken (Plastic Analysis of Walls under Bending and Shear). Institut für Baustatik und Konstruktion-ETH Zürich, Bericht Nr. 83, 1978

21. Nielsen, M.; Braestrup, N.; Jensen, B.; Bach, F. : Concrete Plasticity: Beam Shear-Shear in Joints -Punching Shear. Specialpublikation - Dansk Selskab for Bygningsstatik, Lyngby, 1978, 129 pp.
22. Mitchell, D.; Collins, M.: Diagonal Compression Field Theory - A rational Model for Structural Concrete in pure Torsion. ACI-Journal, Vol. 7, No. 8, 1974, pp. 396-408
23. Ramirez, J.; Breen, J.: Proposed Design Procedures for Shear and Torsion in Reinforced and Prestressed Concrete. Research Report 248-4F, Center for Transportation Research-The University of Texas at Austin, 1983, 254 pp.
24. Daschner, F.; Kupfer, H.: Versuche zur Schubkraftübertragung in Rissen von Normal- und Leichtbeton (Shear transfer across cracks in concrete). In: Bauingenieur 57, Berlin 1982, pp. 57-60
25. Dei, Poli, S.; Gambarova, P.; Karakoc, C.: Discussion on the papers "Shear Transfer across cracks in R.C. due to Aggregate Interlock and to Dowel Action (MRC, No. 126) and "Shear Transfer in R. C." (MCR, No. 130) by Millard, S. and Johnson R., Magazine of Concrete Research, Vol. 38, No. 134, 1986, pp. 47-51
26. MacGregor, J.; Gergely, P.: Suggested Revisions to ACI Building Code Clauses Dealing with Shear in Beams. ACI-Journal, Vol. 74, No. 10, 1977, pp. 493-500
27. Marti, P.: Truss Models in Detailing. In: Concrete International, V. 7, No.12,1985, pp. 66-73
28. Schlaich, J.; Schäfer, K.; Jennewein, M.: Toward a Consistent Design of Structural Concrete. PCI-Journal, Special Report, Vol. 32, No. 3, 1987, pp. 74-150
29. CSA: Design of Concrete Structures for Buildings. CAN3-A23.3-M84, Canadian Standards Association, Rexdale, 1984, 281 pp.
30. Cook, W.; Mitchell, D.: Studies of Disturbed Regions near Discontinuities in Reinforced Concrete Members. ACI-Structural Journal, 1988, pp. 206-216

31. Design and Construction Specifications for Segmental Bridges. Draft No.3 Post-tensioning Insitute, Phoenix, 1987
32. Kordina, K.; Hegger, J.; Teutsch, M.: Shear Strength of Prestressed Concrete Beams with Unbonded Tendons. ACI-Structural Journal, Vol. 86, No. 2, Mar-April 1989, pp. 143-149
33. Hartmann, D.; Breen, J.; Kreger, M.: Shear Capacity of High Strength Prestressed Concrete Girders. Research Report 381-2. Center for Transportation Research-The University of Texas at Austin, 1988, 244 pp.
34. Powers, T.: Shear Behavior of Prestressed Beams in Negative Bending. Master's Thesis, The University of Texas at Austin, 1989
35. Schaefer, T.: Verification of a Refined Truss Model for Shear Design in Reinforced and Prestressed Concrete Members. Master's Thesis, The University of Texas at Austin, 1981
36. Castrodale, R.W.: A Comparison of Design for Shear in Prestressed Concrete Bridge Girders. Master's Thesis, The University of Texas at Austin, 1982
37. Kotsovos, M.: Reader Comments: Toward a Consistent Design of Structural Concrete. PCI-Journal, 1988, pp. 171- 177
38. Anderson, R.: Behavior of CTT-Nodes in Reinforced Concrete Strut- and-Tie- Models. Master's Thesis, The University of Texas at Austin, 1988
39. Bouadi, A.: Behavior of CCT-Nodes in Structural Concrete for the Strut- and- Tie- Model. Master's Thesis, The University of Texas at Austin, 1989
40. Noguchi, H.; Watanabe, K.: Shear Resistance Mechanisms of Beam-Column Joints under Reversed Cyclic Loading. In: IABSE Colloquium, Delft, 1987, pp. 511-522
41. Stone, W.; Breen J.: Design of Post-Tensioned Girder Anchorage Zones. PCI Journal, Vol. 29, No. 1, 1984, pp. 64-109, and No. 2, 1984, pp. 28-61
42. Burdet, O.: Analysis and Design of Anchorage Zones for Post-tensioned Concrete Bridges. Ph. D. Dissertation, The University of Texas at Austin, May 1990

43. Sanders, D.: Design and Behavior of Post-tensioned Concrete Anchor age Zones. Ph. D. Dissertation, The University of Texas at Austin, August 1990
44. Schlaich, M.: Computerunterstützte Bemessung von Stahlbetonscheiben mit Fachwerkmodellen. Dissertation, ETH-Zürich, 1989
45. Yankelevsky, D.: Bond Action between Concrete and a Deformed Bar - A New Model. ACI-Journal, No. 82-13, 1985, pp. 154-161
46. Rode, U.: Framework Model for the Simulation of Fracture Behavior of Concrete. In: IABSE Colloquium, Delft, 1987, pp. 221-227
47. Hrennikoff, A.: Solution of Problems of Elasticity by the Framework Method. Journal of appl. Mech. 8, 1941
48. Soroushian, P.; Obaseki, K.; Rojas, M.; Sim, J.: Analysis of Dowel Bars acting against Reinforced Concrete Core. ACI- Journal No. 83-59, 1986, pp. 642-649
49. Vintzeleou, E.; Tassios, T.: Mathematical Models for Dowel Action under Monotonic and Cyclic Conditions. Magazine of Concrete Research, Vol. 38, No. 134, 1986, pp. 13-22 45.
50. Bazant, Z.; Gambarova, P.: Crack Shear in Concrete: Crack Band Microplane Model. Journal of Structural Engineering, ASCE, Vol. 110, No. 9, 1984, pp. 2015-2035
51. Divakar, M.; Fafitis, A, Shah, S.: Constitutive Modeling of Rough Interfaces in Sliding Shear. Trans. of the 2nd Int. Conf. on Constitutive Laws for Engineering Materials: Theory and Applications, Tucson, 1987, pp. 1027-1034
52. Walraven, J.: Fundamental Analysis of Aggregate Interlock. Journal of the Structural Division, ASCE, Vol. 107, No. 11, 1981, pp. 2245-2270
53. Gambarova, P.: Modelling of Interface Problems in Reinforced Concrete. In: IABSE Colloquium, Delft, 1987, pp. 1-16
54. Richart, F.; Brandtzaeg, A.; Brown, R.: A Study of the Failure of Concrete under combined Compressive Stresses. Bulletin No. 185, University of Illinois, Urbana, 1928, pp. 7-103

55. Ferguson, M.; Breen, J.; Jirsa, J.: Reinforced Concrete Fundamentals. John Wiley & Sons, 5th Edition, 1987
56. Thürlimann, B.; Marti, P.; Pralong, J.; Ritz, P.; Zimmerli, B.: Anwendung der Plastizitätstheorie auf Stahlbeton (Plasticity in Concrete Structures). Vorlesung, ETH- Zürich, 1983
57. Drake, K.: High -Strength Concrete in Seattle."High Strength Concrete, SP-87, ACI, Detroit, 1985, pp. 21-34
58. ACI Committee 363. State-of-the-Art Report on High Strength Concrete. ACI Journal, Vol. 81, No.4, 1984,
59. Carrasquillo, R.L.; Slate, F.O.; Nilson,A.H.: Microcracking and Behavior of High Strength subjected to Short-term Loading. ACI-Journal, Vol. 78, No.3, 1981, pp. 179 -186
60. Thürlimann, B.: Lecture Notes from Structural Seminar. The University of Texas at Austin (see: Ramirez [23])
61. Collins, M.; Mitchell, D.: Design of Disturbed Regions. Chapter 9. Prestressed Concrete Basics, Canadian Prestressed Concrete Institute, 1987, pp. 386-429
62. MacGregor, : Reinforced Concrete - Analysis and Design, Prentice-Hall, 1988
63. Paulay, T.; Loeber, P.: Shear Transfer by Aggregate Interlock, Shear in Reinforced Concrete, ACI SP-42, Vol. 1, 1974
64. CEB-MC 1990: Contribution to the Revision of The CEB-MC 1990, Comite Euro-International du Beton, Ad hoc Commission IV/VI, 1986
65. Vecchio, F.; Collins, M.: Predicting the Response fo Reinforced Concrete Beams Subjected to Shear Using Modified Compression Field Theory. ACI - Structural Journal, Vol. 85, No. 3, May-June 1988, pp. 258 - 268
66. Kaufmann, K.; Ramirez, J.: Re-evaluation of the Ultimate Shear Behavior of High-Strength Concrete Prestressed I-Beams. ACI - Structural Journal, Vol. 85, No. 3, May-June 1988, pp. 295 - 303

67. Johnson, M.; Ramirez, J.: Minimum Shear Reinforcement in Beams with Higher Strength Concrete. ACI - Structural Journal, Vol. 86, No. 4, July-August 1989, pp. 376- 382
68. Kupfer, H.; Hilsdorf, H.; Rüsck, H.: Behavior of Concrete under Biaxial Stresses. ACI-Journal, Vol. 66, No. 8, August 1969, pp. 656-666
69. Linse, D.: Festigkeits- und Verformungsverhalten von Beton unter dreiachsiger Beanspruchung (Strength- and Deformation Capacity of Concrete under triaxial Stresses). Forschungsarbeiten, Lehrstuhl und Institut für Massivbau, TU-München, 1973, pp. 25-27
70. Kotsovos, M.: A Brittle Fracturing Material, Material and Structures. RILEM, Vol. 17, No. 98, 1984
71. Stankowski, T.; Gerstle, K.: Simple Formulation of Concrete Behavior under Multiaxial Load Histories, ACI-Journal, Vol. 82, No. 2, 1985
72. Han, D.; Chen, W.: A Nonuniform Hardening Plasticity Model for Concrete Materials. Mechanics of Materials, No. 4, 1985
73. Eberhardsteiner, J.; Meschke, G.; Mang, H.: Comparison of Constitutive Models for Triaxially Loaded Concrete. In: IABSE Colloquium, Delft, 1987, pp. 197-208
74. Fardis, M.; Alibe, B.; Tassoulas, J.: Monotonic and Cyclic Constitutive Law for Concrete. Journal of Engineering Mechanics, Vol. 109, No. 2, 1983, pp. 517-536
75. Richart, F.; Brandtzaeg, A.; Brown, R.: A Study of the Failure of Concrete under Combined Compressive Stresses. Univ. of Illinois, Urbana. Bulletin No. 185, 1928. pp. 7 - 103
76. Fafitis, A.; Shah, S.: Lateral Reinforcement for High-Strength Concrete Columns. ACI, Detroit, SP-87, 1985, pp. 213-232
77. Ahmad, S.; Shah, S.: Stress-Strain Curves of Concrete Confined By Spiral Reinforcement. ACI-Journal, Vol. 79, No. 6, 1982, pp. 484-490
78. Martinez, S.; Nilson, A.; Slate, F.: Spirally-Reinforced High-Strength Concrete Columns. Research Report No. 82-10. Department of Structural Engineering, Cornell University, Ithaca, Aug. 1982
79. ACI Manual of Concrete Practice. Part1-1988, Detroit, 1988, Chapter 6

80. Billig, K.: A Proposal for a Draft Code of Practice for Prestressed Concrete. Cement and Concrete Association, London 1948
81. Komendant, A.: Prestressed Concrete Structures. Mc Graw-Hill Book company, Inc., 1952, pp. 172 - 173
82. Middendorf, K.: Anchorage Bearing Stresses in Post-tensioned Concrete. Journal of the American Concrete Institute. 1960, pp. 580- 584
83. Hawkins, N.: The Bearing Strength of Concrete Loaded through Rigid Plates. Magazine of Concrete Research, Vol. 20, No. 62, 1968, pp. 31- 40
84. Hawkins, N.: The Bearing Strength of Concrete for Strip Loadings. Magazine of Concrete Research, Vol. 22, No. 71, 1971/6
85. Nijogi, S.: Bearing Strength of Reinforced Concrete Blocks. Journal of the Structural Division, ASCE. ST5, 1975, pp. 1125 - 1137
86. Nijogi, S.: Concrete Bearing Strength - Support, Mix, Size Effect. Journal of the Structural Division, ASCE. ST8, 1974, pp. 1685 - 1702
87. Sheikh, S.: Effectiveness of Rectangular Ties as Confinement Steel in Reinforced Concrete Columns. Ph.D. - Thesis, Univ. of Toronto, 1978, 256 pp.
88. Muguruma, H.; Watanabe, F.; Iwashimizu, I.; Mitsueda, R.: Ductility Improvement of High Strength Concrete by Lateral Confinement. Reprinted from Transactions of the Japan Concrete Institute, 1983, pp. 403 - 410
89. Roberts, C.: Behavior and Design of the Local Anchorage Zone in Post-Tensioned Concrete. Master - Thesis, The University of Texas at Austin, 1990
90. Wurm, P.; Daschner, F.: Versuche über Teilflächenbelastung von Normalbeton (Tests subjected to partial area loading of concrete). Deutscher Ausschuss für Stahlbeton, Heft 286, Berlin 1977
91. Ramirez, J.; Breen, J.: Review of Design Procedures for Shear and Torsion in Reinforced and Prestressed Concrete. Research Report 248-2, Center for Transportation Research-The University of Texas at Austin, 1983, 186 pp.

92. Lin, T.Y.; Burns, N.H.: Design of Prestressed Concrete Structures. John Wiley & Sons, 1981, pp. 12 - 130
93. Libby, J. R.: Modern Prestressed Concrete. Design Principles and Construction Methods. Third edition, Princeton 1971, pp. 167 - 171
94. Leonhardt, F.: Prestressed Concrete. Design and Construction. Berlin, 1964, pp. 79 - 84
95. Hoyer, E.; Friedrich, E.: Beitrag zur Frage der Haftspannung in Eisenbeton bauteilen, (Contribution to Questions Regarding Bond Stresses in Reinforced Concrete Structural Members). Beton und Eisen, Vol. 38, No. 6, 1939, pp. 102-110.
96. Hanson, N.; Kaar, P.: Flexural Bond Tests of Pretensioned Prestressed Beams. ACI - Journal. 1959, pp. 784 - 802
97. Tepfers, R.: Lapped Tensile Reinforcement Splices. Journal of the Structural Division, ASCE, Vol. 188, No. 1, January 1982, pp. 283-301
98. Tepfers, R.: A Theory of Bond Applied Overlapped Tensile Reinforcement Splices for Deformed Bars. Chalmers Univ. of Technology, Göteborg, Publication No. 73.2, 1973, 328 pp
99. Jirsa, J.; Lutz, L.; Gergely, P.: Rationale for Suggested Development, Splice, and Standard Hook Provisions for Deformed Bars in Tension. In: Concrete International, Vol. 1, No. 7, 1979, p. 47
100. Orangun, C.; Jirsa, J.; Breen, J.: Reevaluation of Test Data on Development Length and Splices. ACI-Journal, 74, No. 3, 1977, p. 114
101. ACI 318-89: Building Code Requirements for Reinforced Concrete, Chapter 12, Detroit, 1989
102. Lormanometee, S.: Bond Strength of Deformed Reinforcing Bar under Lateral Pressure. MS - Thesis. The University of Texas at Austin, 1974 64 pp.
103. Schmidt-Thrö, G.; Stöckl, S.; Kupfer, H.: Verankerung der Bewehrung am Endauflager bei einachsiger Querpressung (Anchorage of Reinforcement at an End Bearing with Uniaxial Lateral Pressure). Deutscher Ausschuß für Stahlbeton, Heft 389, Berlin, 1988, pp.11-98

104. Kotsovos, M.: Compressive Force Path Concept: Basis for Reinforced Concrete Ultimate Limit State Design. In: ACI Structural Journal, Vol. 85, No. 1, Jan-Feb 1988, pp. 68 - 75
105. Park, R.; Paulay, T.: Reinforced Concrete Structures. Wiley—Interscience, New York, 1975, p. 671
106. Leonhardt, F.: Das Bewehren von Stahlbetontragwerken. (Reinforcing of Concrete Members) In. Beton-Kalender 1971, Berlin, pp. 303 - 398
107. PCI Design Handbook: Precast and Prestressed Concrete. Third edition. PCI, Chicago, 1985
108. Betonkalender : Taschenbuch für Beton-Stahlbeton- und Spannbetonbau sowie die verwandten Fächer. Berlin
109. Concrete Reinforced Steel Institute (CRSI) Handbook. Fourth edition. Chicago, 1984
110. El-Rahman, M., A.; Shaw, W.J.D.: Computers in Concrete Technology. In: Concrete International. 1989/8, pp. 27 - 31
111. Khana, S.: Stress-Strain Characteristics and Failure Mechanism of PIC. Master-Thesis. The University of Texas at Austin, 1981
112. Hagberg, T.: Design of Concrete Brackets: On the Application of the Truss Analogy. ACI-Journal, Proceedings V. 80, No. 1, Jan-Feb 1983, pp. 3 - 12
113. Cook, W.; Mitchell, D.: Studies of Reinforced Concrete Regions Near Discontinuities. Department of Civil Engineering and Applied Mechanics. McGill University, Structural Engineering Series Report No. 87-3, 1987. 153 pp.
114. Yong, Y.; McCloskey, D.; Nawy, E.: Reinforced Corbels of High-Strength Concrete. In: High-Strength Concrete SP-87-11. ACI, Detroit, 1985, pp. 197 - 212
115. Franz, G.; Niedenhof, H.: The Reinforcement of Brackets and Short Deep Beams. Cement and Concrete Association, Library Translation No. 114, London, 1963

116. Kriz, L.; Raths, C.: Connections in Precast Concrete Structures-Strength of Corbels. In: Journal of the Prestressed Concrete Institute. Vol. 10, No. 1, January 1965, pp. 16 - 61
117. Mattock, A.; Chen, K.; Soonswang, K.: The Behavior of Reinforced Concrete Corbels. In: PCI - Journal, V. 21, No. 3, May-June 1976, pp. 18 - 42
118. Chakrabarti, Pinaki; Farahani, Davood; Kashou, Shihadeh: Reinforced and Precompressed Concrete Corbels - An Experimental Study. In: ACI - Structural Journal. No. 86-S37, 1989, pp. 405 - 412
119. Peterson, R.: Stress Concentration Factors. New York. 1974. pp. 208
120. Chih-Bing Ling: Stresses in a Stretched Slab Having a Spherical Cavity. ASME, Vol. 81, Series E, Applied Mechanics Section, 1959, pp. 235
121. Tsuchida, E.; Nakahara, I.: Three-Dimensional Stress Concentration around a Spherical Cavity in a Semi-Infinite Elastic Body. Bull. Japan Soc. Mech. Eng., Vol. 13, 1970, pp. 499
122. Shah, S.N.: Evaluation of infill wall strengthening schemes for non-ductile reinforced concrete buildings. Master's Thesis, The University of Texas at Austin, 1989
122. Gaynor, P.: The effect of openings on the cyclic behavior of reinforced concrete shear walls. Master's Thesis, The University of Texas at Austin, 1988
124. Leonhardt, F.: Vorlesungen über Massivbau. Teil 1 bis Teil 6. Springer-Verlag, Berlin, 1984
125. Guyon, Y.: Prestressed Concrete. New York, 1953
126. Magnel, G.: Prestressed Concrete. New York, Third edition 1954, 345 pp.
127. Lenschow, R.; Sozen, M.: Practical Analysis of the Anchorage Zone Problem in Prestressed Beams. In: ACI - Journal, November 1965, pp. 1421 - 1437
128. Schlee, W.: The Stress Pattern at the Support of a Prestressed Concrete Beam. In: Beton- und Stahlbetonbau. Vol. 58, No. 7, Berlin, 1963, pp. 157 - 171

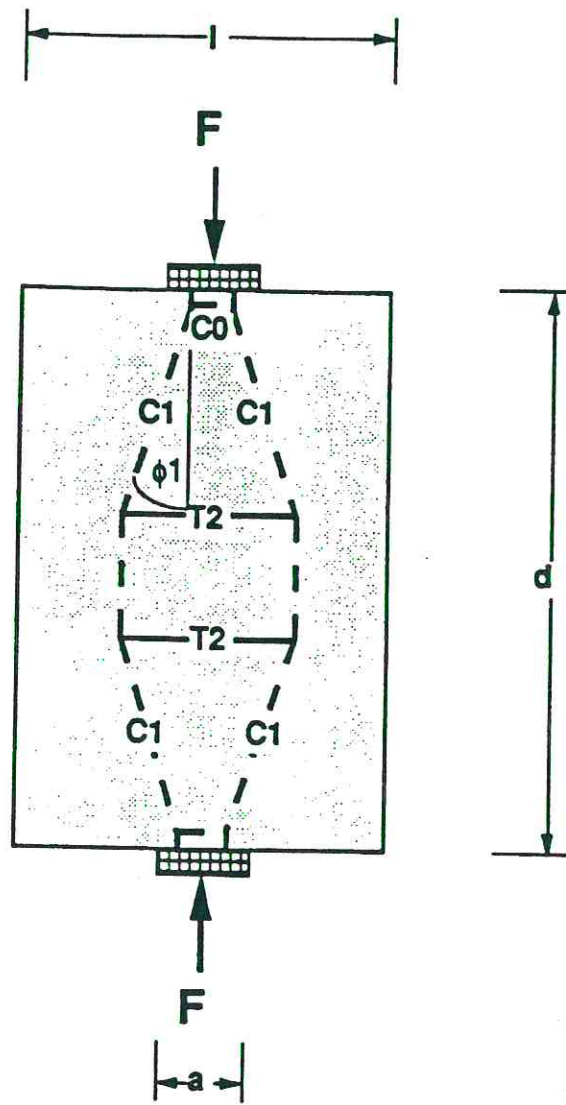
129. Leonhardt, F.: Prestressed Concrete - Design and Construction. Berlin. Second edition. 1964, 677 pp.
130. Bennet, E.W.; Abdul-Ahad, H.Y; Neville, A.: Shear Strength of Reinforced and Prestressed Concrete Beams Subject to Moving Loads. In: PCI - Journal. Nov-Dec 1972, pp. 58 - 69
131. Barton, D.L.; Anderson, R.B.; Bouadi, A.; Jirsa, J. O.; and Breen, J.E.: "An Investigation of Strut-and-Tie Models for Dapped Beam Details," Research Report 1127-1, Center for Transportation Research, The University of Texas at Austin, May 1991.

Appendix A

Detailing Aids

(from Ref. [1] and [2])

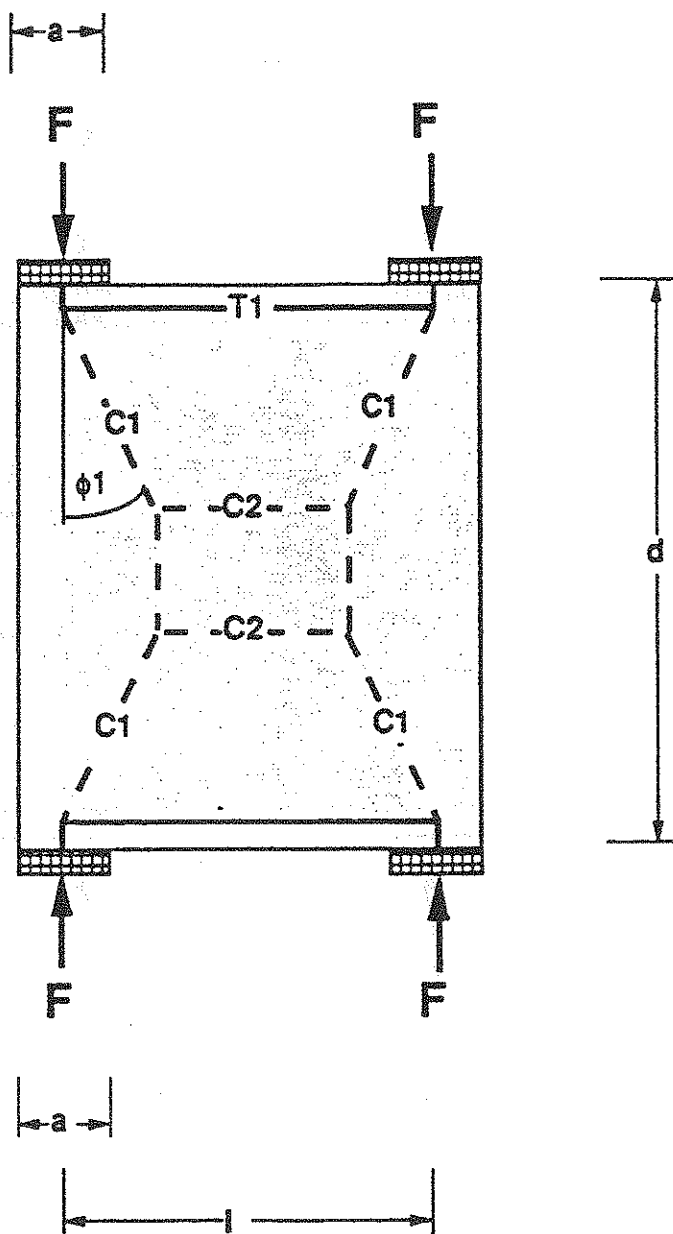
- Deep beam with one single load on both sides
- Deep beam with two single loads on both sides
- Deep beam with three single loads on both sides
- Deep beam with three single loads on one side
- Deep beam with one single load in the middle: $d \leq l$
- Deep beam with one single load in the middle: $d > l$
- Deep beam with two single loads in the middle of one side
- Deep beam with distributed compression load
- Deep beam with distributed tension load
- Cross section under torsion
- Frame corner with positive moment
- Frame corner with negative moment
- Single load in the middle of a deep beam
- Support
- The stepped beam



$$C_1 = F / (2 \cos \phi_1)$$

$$T_2 = C_0 = F / 2 \tan \phi_1$$

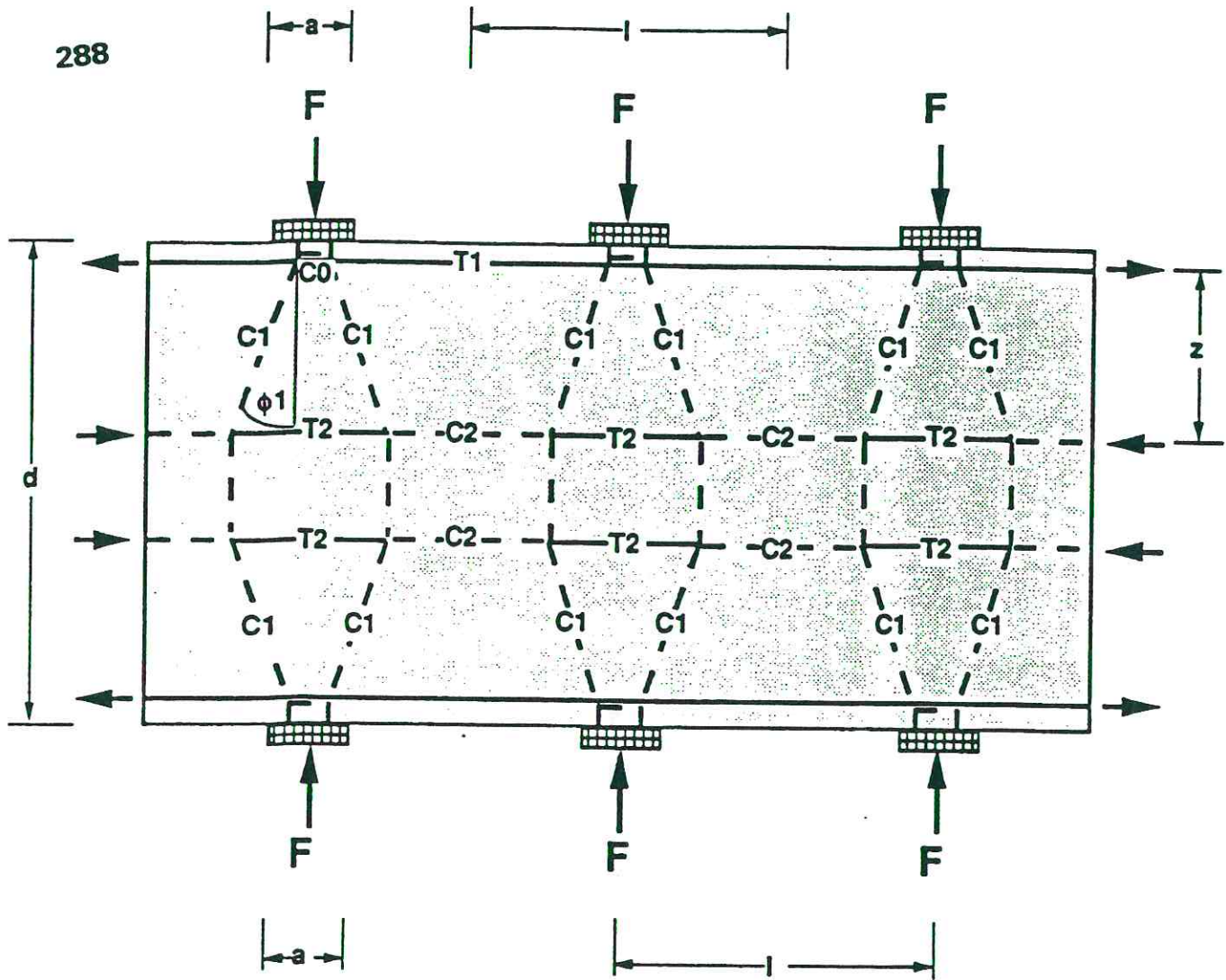
$$\phi_1 = 12 + 3 / \sqrt{(a/l)}$$



$$C_1 = F / \cos \phi_1$$

$$T_1 = C_2 = F \tan \phi_1$$

$$\phi_1 = 12 + 3 / \sqrt{(a/l)}$$



$$C1 = F / (2 \cos \phi1)$$

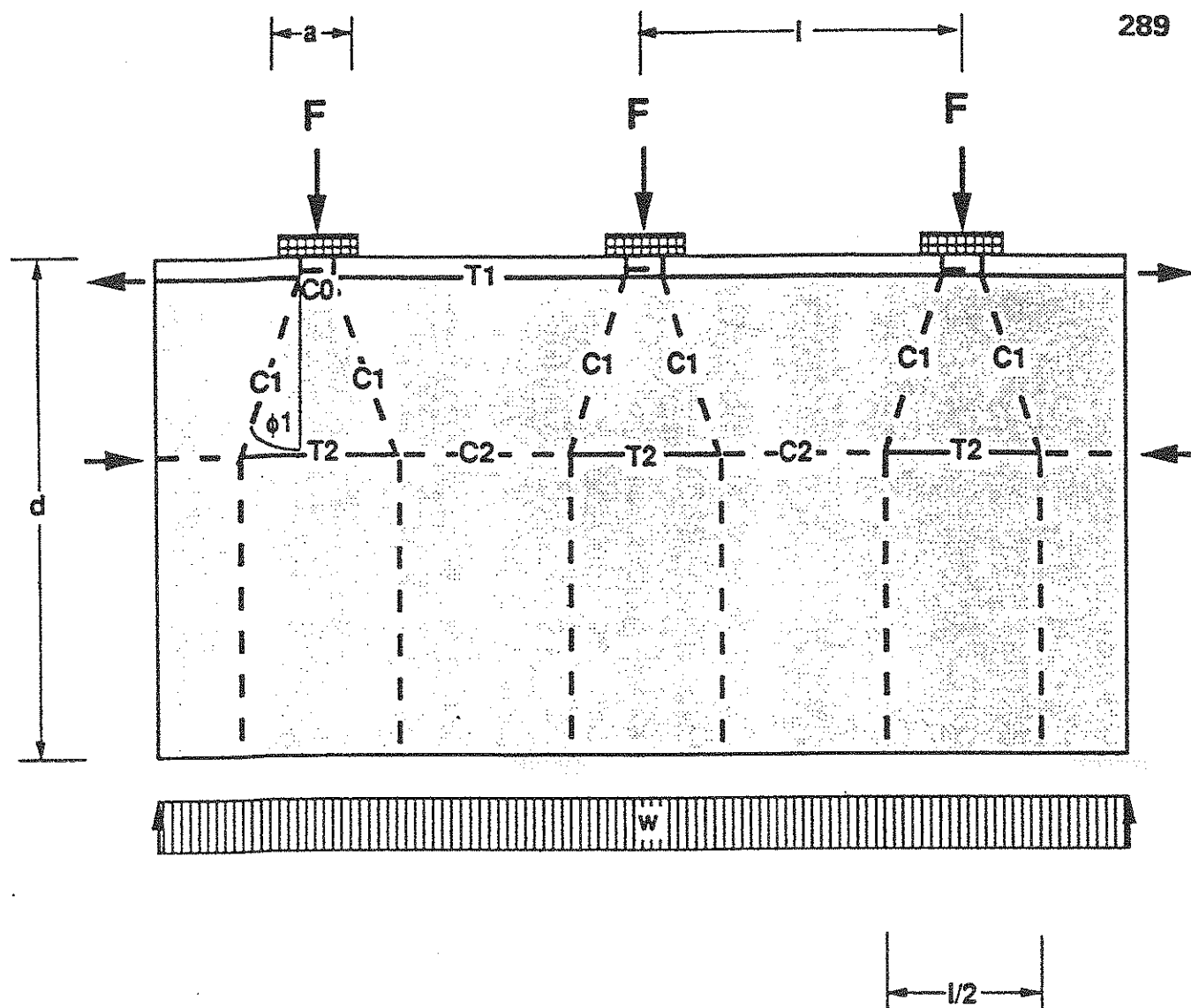
$$C0 = F / 2 \tan \phi1$$

$$T2 + C2 = F \tan \phi1$$

$$\phi1 = 12 + 3 / \sqrt{(a/l)}$$

$$\text{For } d/l \leq 1: T1 = T2 / 3$$

$$\text{For } d/l \geq 2: T1 = T2 / 2$$



$$C_1 = F / (2 \cos \phi_1)$$

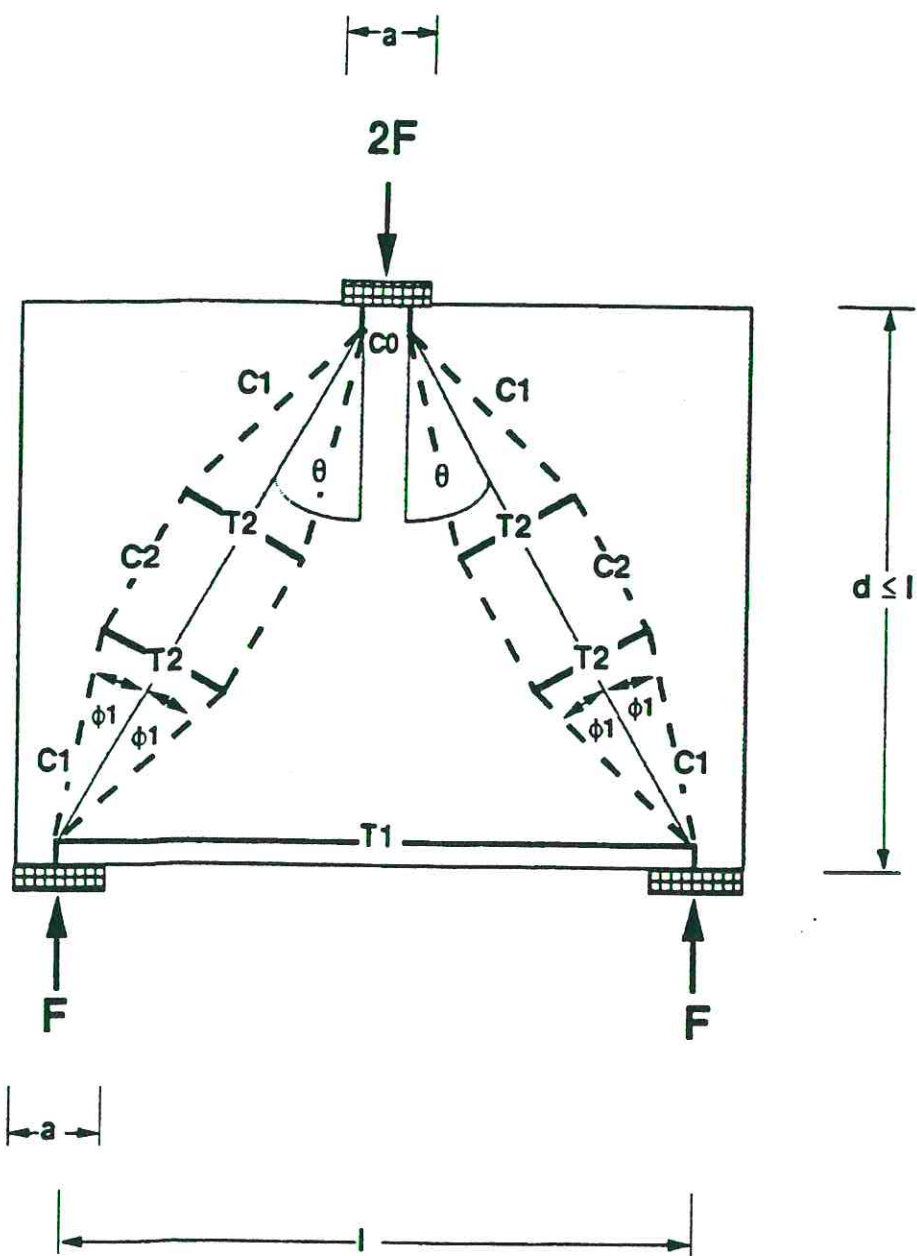
$$C_0 = F / 2 \tan \phi_1$$

$$T_2 + C_2 = F \tan \phi_1$$

$$\phi_1 = 12 + 3 / \sqrt{(a/l)}$$

$$\text{For } d/l \leq 1: T_1 = T_2 / 3$$

$$\text{For } d/l \geq 2: T_1 = T_2 / 2$$



$$C_0 = F \tan \theta$$

$$T_1 = F \tan \theta$$

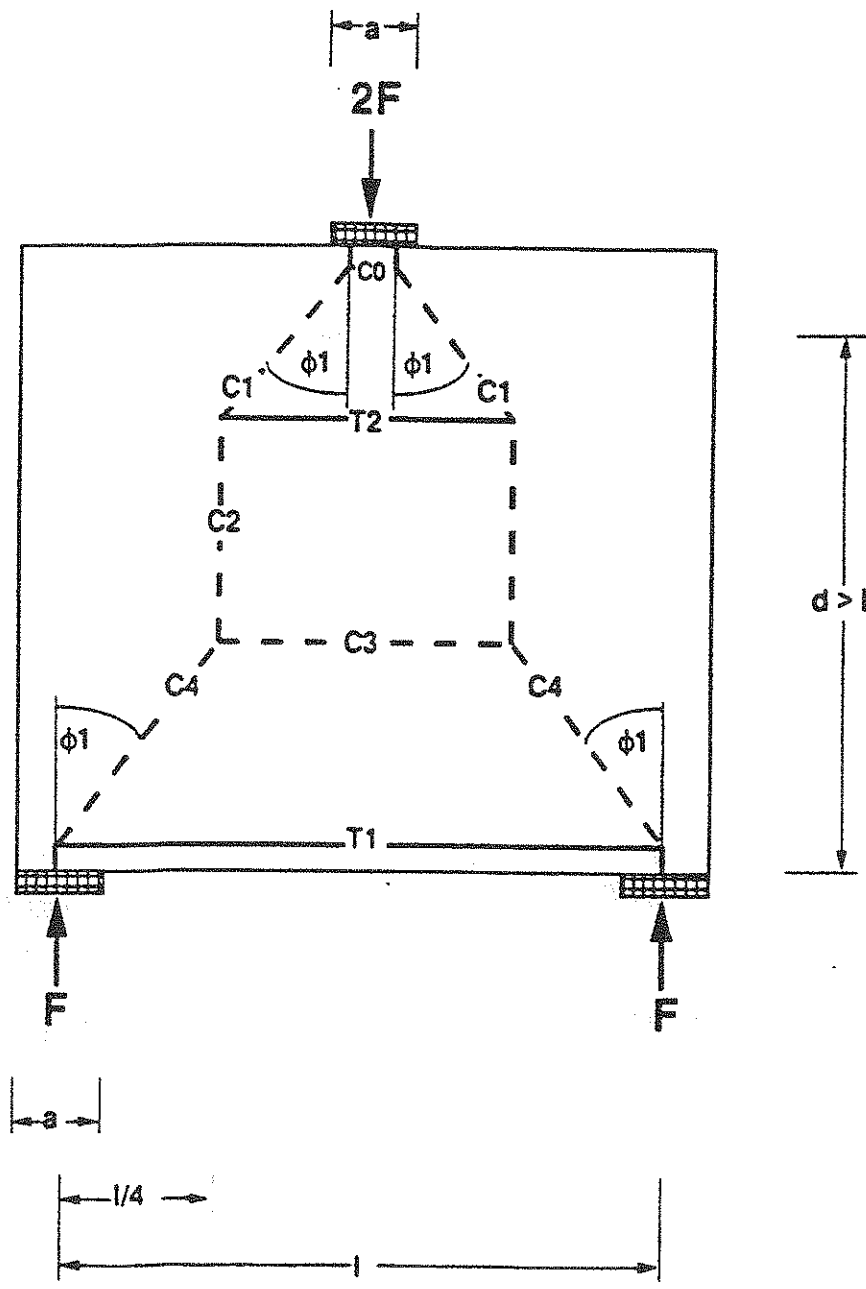
$$T_2 = F \tan \phi_1 / \cos \theta$$

$$C_1 = F / (2 \cos \phi_1 \cos \theta)$$

$$C_2 = F / (2 \cos \theta)$$

$$\phi_1 = 12 + 3 / \sqrt{(a/l)}$$

$$\theta \leq 70^\circ$$



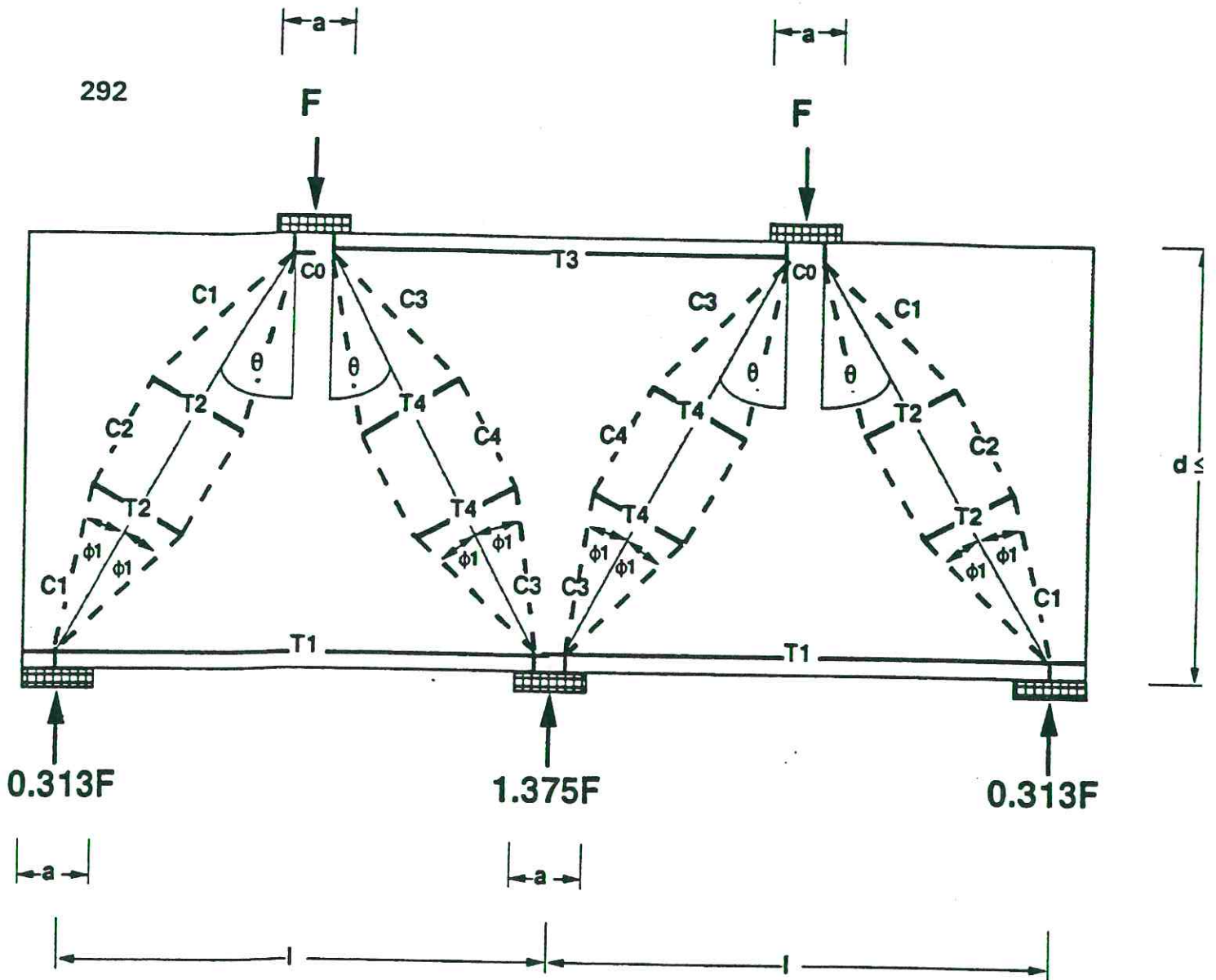
$$C_0 = C_3 = F \tan \phi_1$$

$$T_1 = T_2 = F \tan \phi_1$$

$$C_1 = C_4 = F / \cos \phi_1$$

$$C_2 = F$$

$$\phi_1 = 12 + 3 / \sqrt{al}$$



$$T1 = 1.375 F \tan \theta$$

$$C0 = 0.313 F \tan \theta$$

$$T2 = 0.313 F \tan \phi_1 / \cos \theta$$

$$C1 = 0.16 F / (\cos \phi_1 \cos \theta)$$

$$T4 = 1.375 F \tan \phi_1 / \cos \theta$$

$$C2 = 0.16 F / (\cos \theta)$$

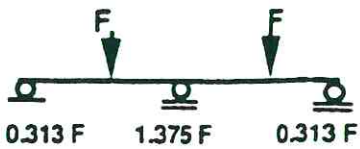
$$T3 = 1.062 F \tan \theta$$

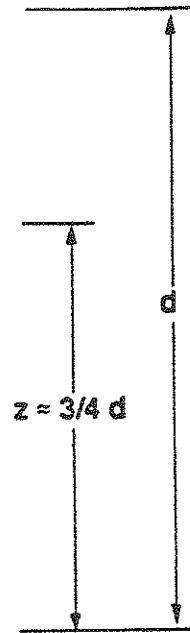
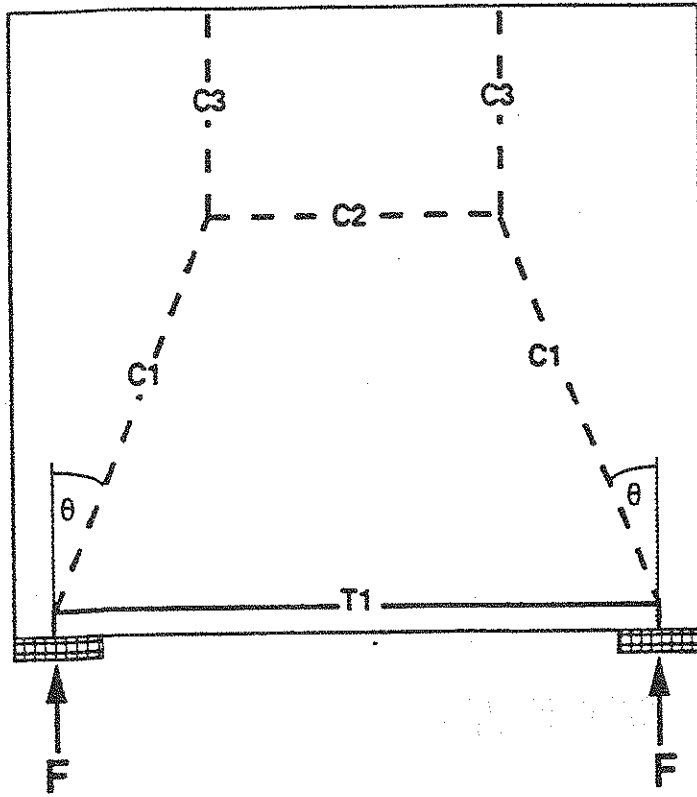
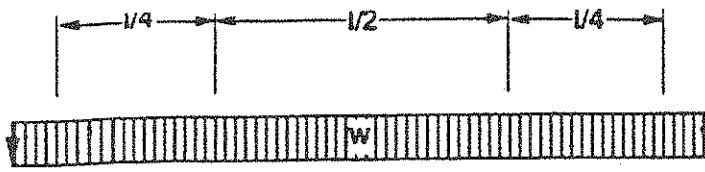
$$C3 = 0.69 F / (\cos \phi_1 \cos \theta)$$

$$C4 = 0.69 F / (\cos \theta)$$

$$\phi_1 = 12 + 3 / \sqrt{(a/L)}$$

$$\theta \leq 70^\circ$$





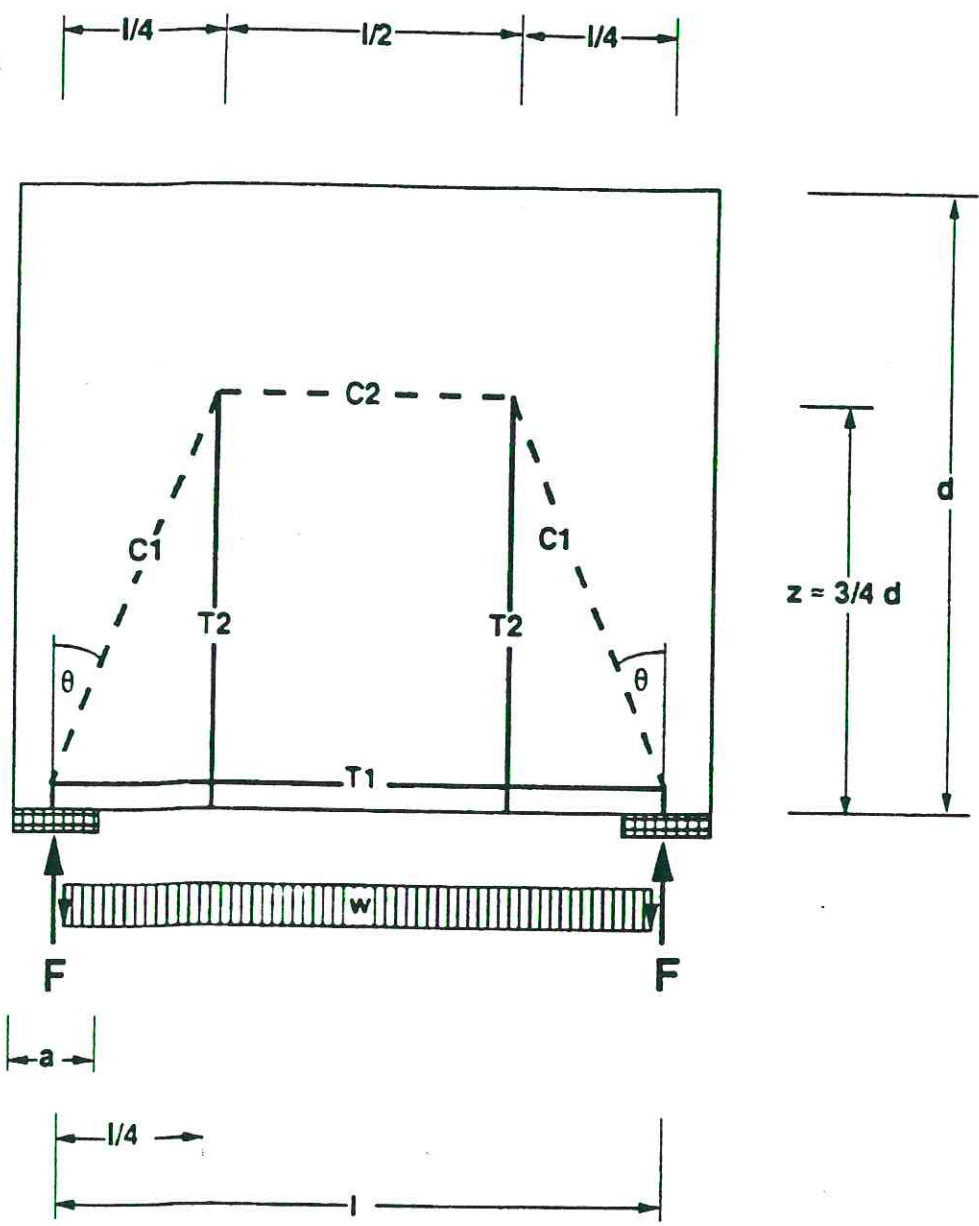
$$\arctan \theta = 1 / (4 z) = 1 / (3 d)$$

$$F = C3 = w l / 2$$

$$T1 = F \tan \theta$$

$$C1 = F / \cos \theta$$

$$C2 = T1 = F \tan \theta$$



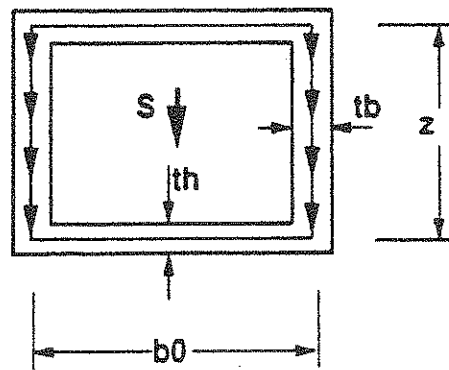
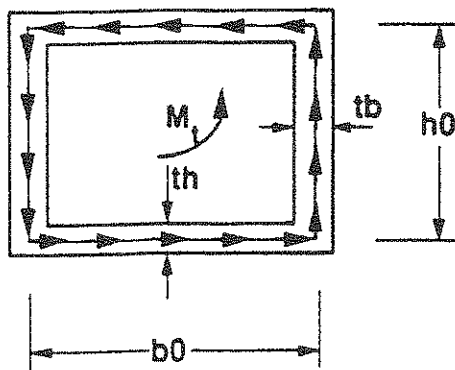
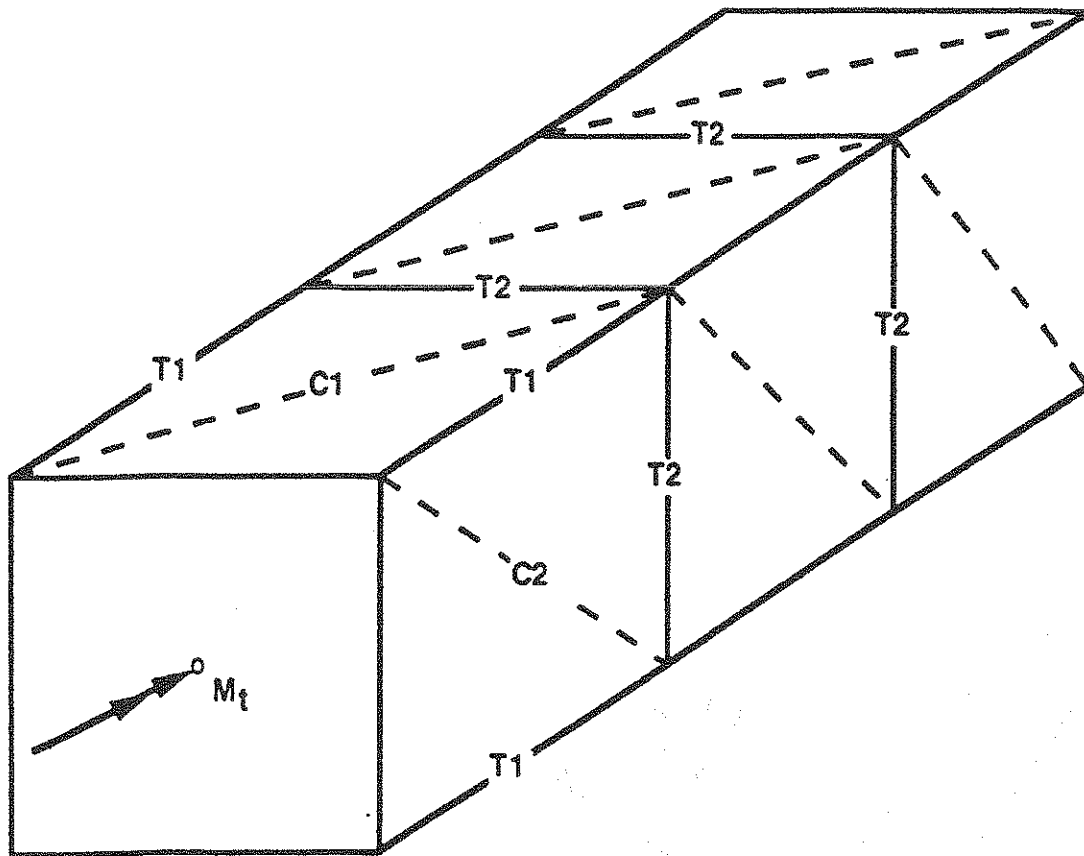
$$\arctan \theta = l / (4 z) = l / (3 d)$$

$$F = C3 = w l / 2$$

$$T1 = F \tan \theta$$

$$C1 = F / \cos \theta$$

$$T2 = F$$



$$T_t = M_t / (2 b_0 h_0)$$

$$T = T_t + T_s$$

$$T_s = S / (2 z)$$

$$th = h_0 / 6$$

$$T_1 = T / \tan \delta$$

for 45°

$$T / (b_0 \sin \delta \cos \delta) \leq v f'_c$$

$$tb = b_0 / 6$$

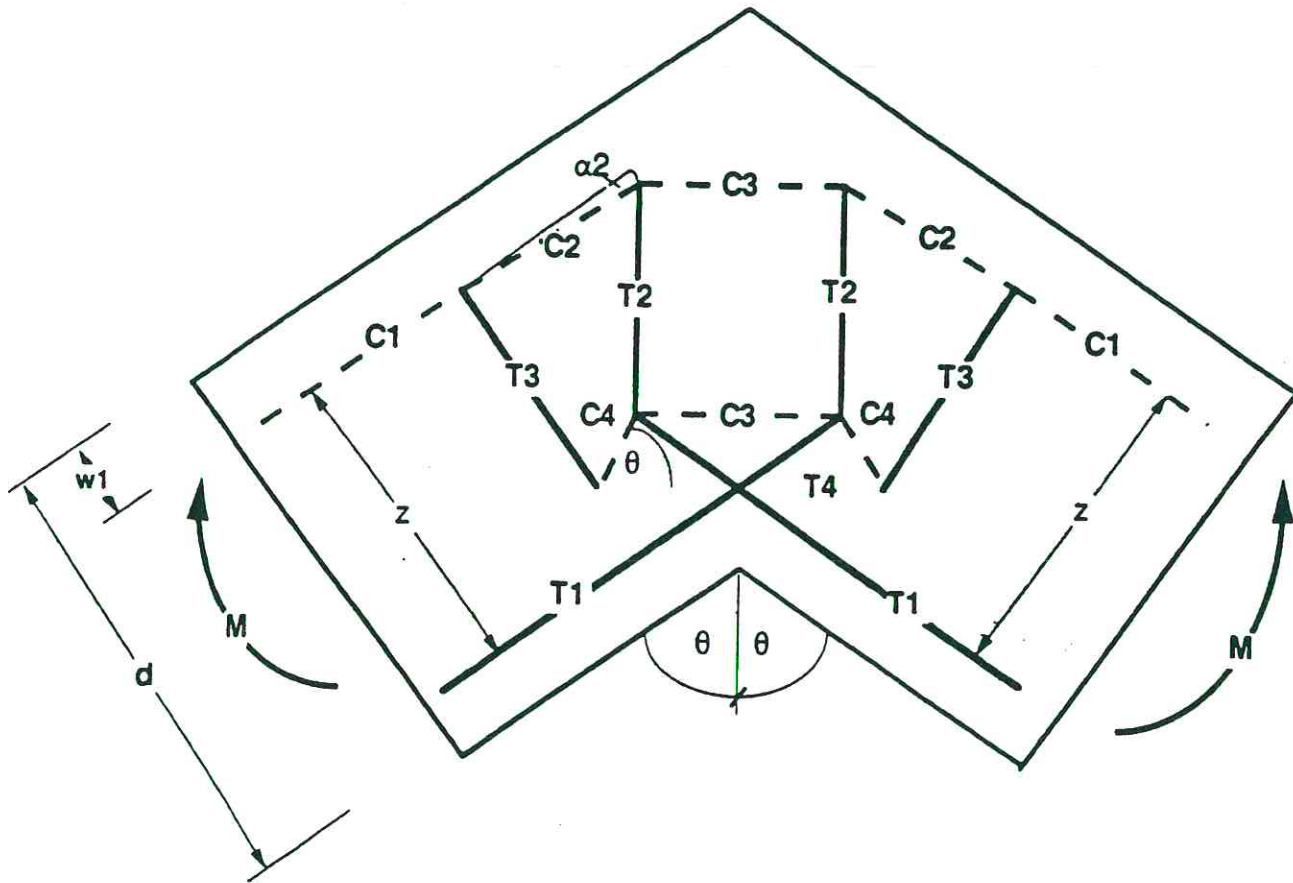
$$T_1 = T$$

$$T / (h_0 \sin \delta \cos \delta) \leq v f'_c$$

$$T_2 = T \tan \delta$$

for 45°

$$T_2 = T$$



$$M = C1 \cdot z$$

$$C1 = T1$$

$$C1 / 2 \cdot w1 \cdot b \leq v f_c$$

$$C2 = T1 / \cos \alpha2$$

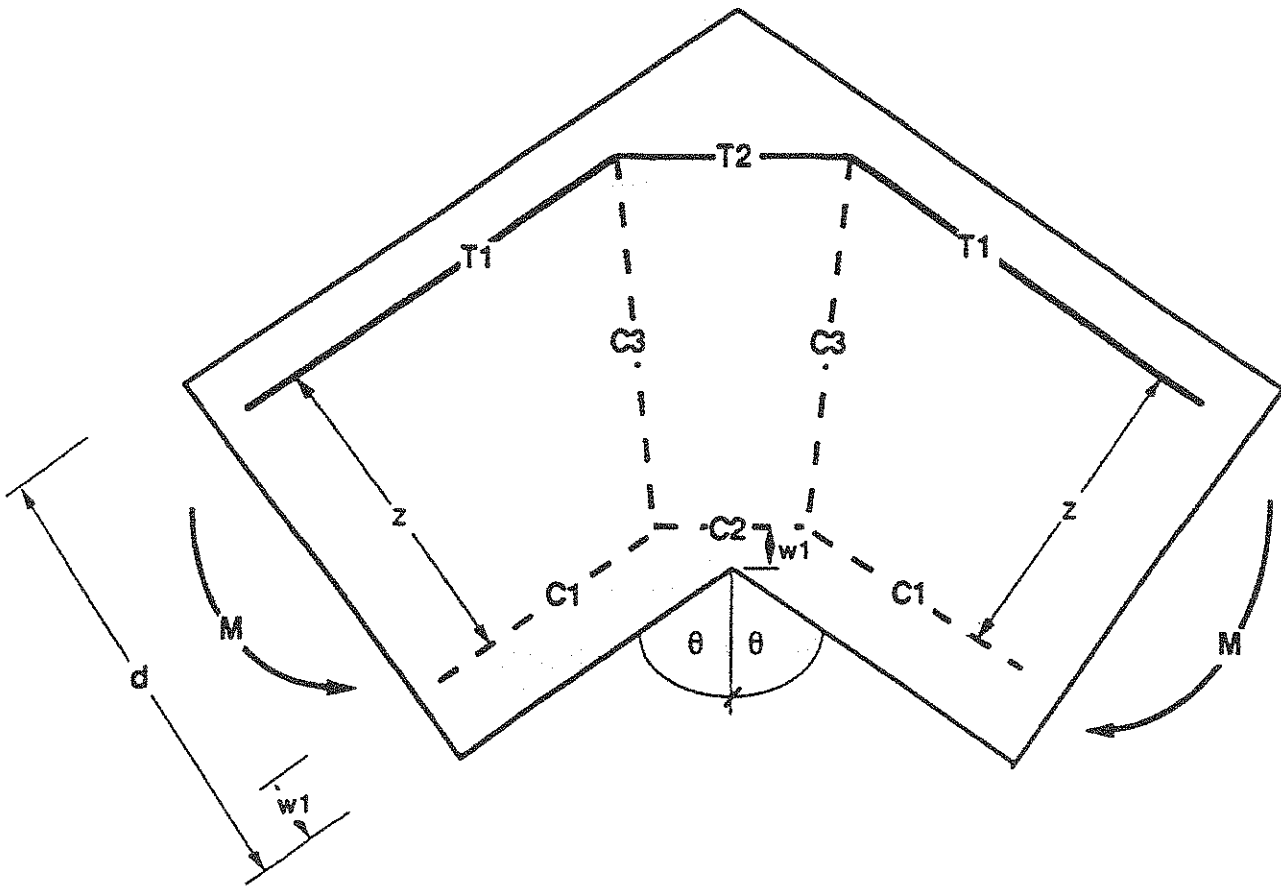
$$T2 = T1 \cdot \sin(\theta - \alpha2) / \cos \alpha2$$

$$T3 = T1 \cdot \tan \alpha2$$

$$T3 \approx 0.3 T1$$

$$T4 = T1 \cdot \tan(\alpha2) + \sin(180 - 2\theta) / \sin \theta$$

$$\alpha2 = 15 - 18^\circ$$



$$M = C1 \cdot z$$

$$C1 = T1$$

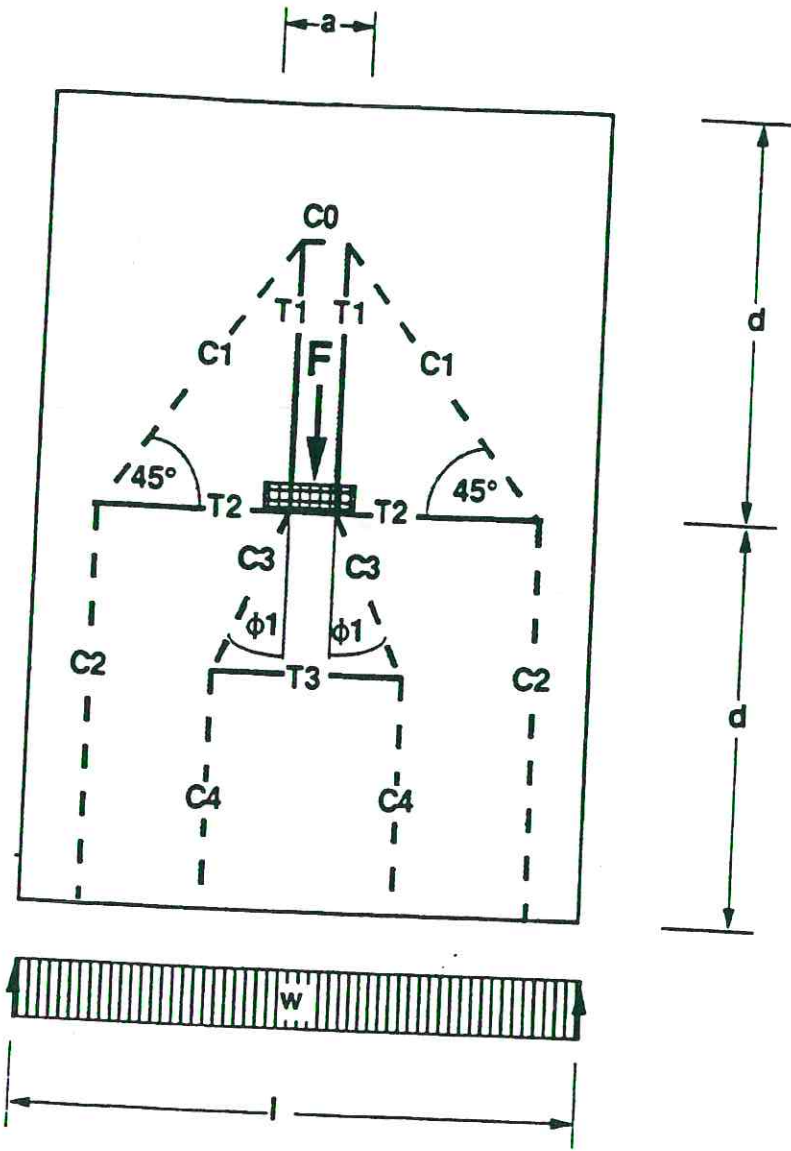
$$C1 / 2 \cdot w1 \cdot b \leq v f'_c$$

$$C2 = C1 / \sin \theta$$

$$C2 / 2 \cdot w2 \cdot b \leq v f'_c$$

$$C3 = C1 / \tan \theta$$

$$T2 = T1 / \sin \theta$$



$$T_1 = F / 4$$

$$C_0 = F / 4$$

$$T_2 = F / 4$$

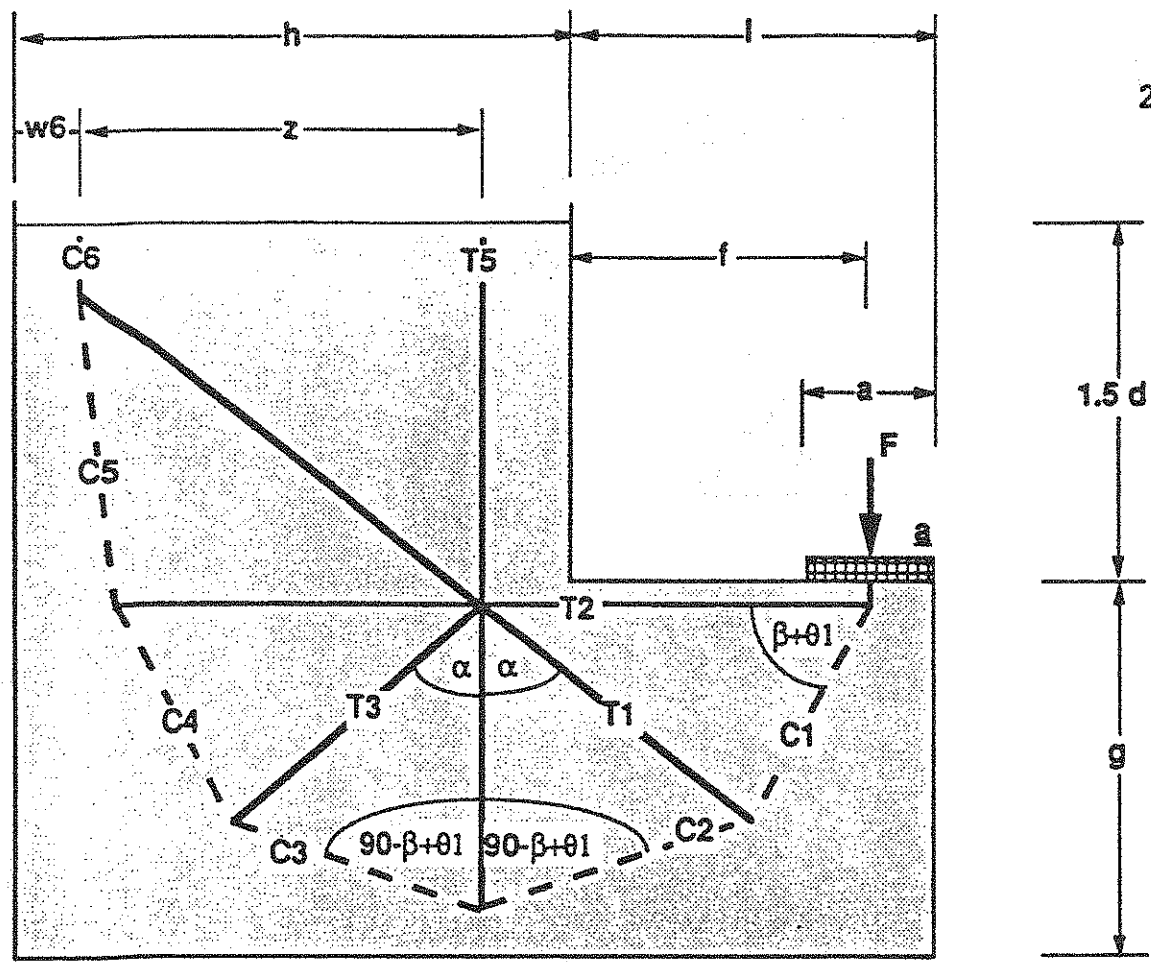
$$C_1 = 2 F / \sqrt{2}$$

$$T_3 = F / 4 \tan \phi_1$$

$$C_2 = F / 4$$

$$C_3 = F / 4 \cos \phi_1$$

$$C_4 = F / 4$$



$z = 0.75 h$

$y = 0.75 g / (2 \cos \theta_1 \sin B)$

$\arctan \beta = 0.75 g / (f + 0.25 h - w_6)$

$x = 0.75 g$

$w_6 \geq C_6 / (2 b v f_c)$

$v = [x^2 + y^2 - 2 x y \cos (90 - B + \theta_1)]^{0.5}$

$\theta_1 = 12 + 3 / \sqrt{a/f}$

$\arcsin \alpha = y \sin (90 - B + \theta_1) / v$

$T_2 = F / \tan (\beta + \theta_1)$

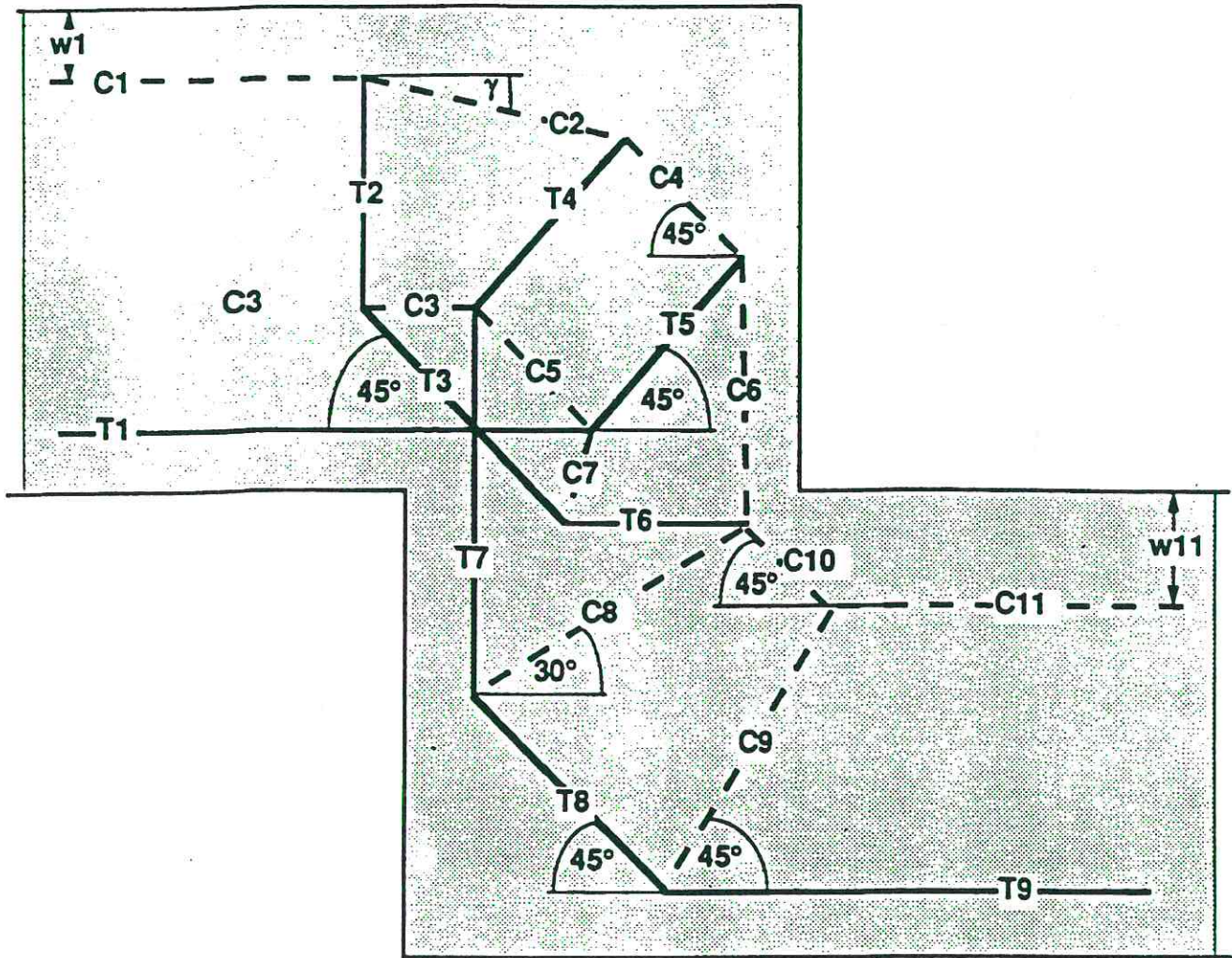
$T_1 = T_3 = C_1 \sin \theta_1 / \cos (\alpha - B)$

$C_1 = F / \sin (\beta + \theta_1)$

$C_2 = C_3 = F / \sin (\beta + \theta_1)$

$T_5 = 2 F$

$C_6 = F$



$$C1 = T1$$

$$T2 = T1 \cdot \tan \gamma$$

for $\gamma = 15^\circ$
 $T2 = T1 \cdot 0.268$

$$T3 = C1 \cdot \tan \gamma / \cos 45^\circ$$

for $\gamma = 15^\circ$
 $T3 = C1 \cdot 0.379$

$$T4 = C1 (\cos \gamma - \sin \gamma) / (2 \cos \gamma \cos 45^\circ)$$

for $\gamma = 15^\circ$
 $T4 = C1 \cdot 0.518$

$$T5 = C1 / \cos 45^\circ - T4$$

for $\gamma = 15^\circ$
 $T5 = C1 \cdot 0.896$

$$C6 = 2 C1 - 2 \cos 45^\circ T4$$

$$T6 = 1.732 C6 - 2.732 C11 - 1.366 T9$$

$$T7 = 2 C6 - 2 C11$$

$$T8 = 0.707 T9$$

$$C1 / (b \cdot 2 \cdot w1) \leq v f_c$$

$$C11 / (b \cdot 2 \cdot w11) \leq v f_c$$